

SHELF CIRCULATION PATTERNS OFF NIGERIA

A Thesis

by

KELLY ELIZABETH RIDER

Submitted to the Office of Graduate Studies of
Texas A&M University
in partial fulfillment of the requirements for the degree of

MASTER OF SCIENCE

May 2004

Major Subject: Oceanography

SHELF CIRCULATION PATTERNS OFF NIGERIA

A Thesis

by

KELLY ELIZABETH RIDER

Submitted to Texas A&M University
in partial fulfillment of the requirements
for the degree of

MASTER OF SCIENCE

Approved as to style and content by:

Worth Nowlin
(Chair of Committee)

Robert Reid
(Member)

Steven DiMarco
(Member)

Thomas Ravens
(Member)

Wilford Gardner
(Head of Department)

May 2004

Major Subject: Oceanography

ABSTRACT

Shelf Circulation Patterns off Nigeria. (May 2004)

Kelly Elizabeth Rider, B.S., The University of Texas at Austin

Chair of Advisory Committee: Dr. Worth Nowlin

Little has been published about the shelf circulation off the coast of Nigeria. Due to increased activity and associated incidents in the shallow waters offshore Nigeria, there is a need to more clearly define the near-shore circulation patterns. An oil spill occurred in January of 1998, the slick drifted in the opposite direction at twice the speed as was anticipated. It was believed that the heavy discharge from the Niger River Delta would have a strong influence on the near-shore circulation patterns and was the reason for this unexpected drift. This thesis investigates the river discharge by examining hydrographic data taken along the coastline. Using Acoustic Doppler Current Profilers, this thesis also investigates other possible forcing factors to gain an overall understanding of Nigeria's shallow water circulation. Indeed river discharge plays an important role in the near-shore circulation as the coastal waters are highly stratified; however, the coastal waters are also strongly influenced by a cross-shelf semidiurnal tide, weather events and seasonal events, such as eddies and coastal upwelling. The resulting currents are a combination of a strong bi-directional cross-shelf tidal current with a strong bi-directional alongshelf current. The waters off Nigeria are highly stratified; they have spatial coherence and a uniform vertical structure along the coastline. These coastal waters may also be influenced by a remotely forced upwelling event and by northerly drift from the Congo River. The shelf circulation is clearly a complicated system and will require further investigation to be fully defined.

ACKNOWLEDGMENTS

First of all, I would like to thank my advisors, Dr. Worth Nowlin, Dr. Robert Reid, Dr. Steven Dimarco and Dr. Thomas Ravens. I am very thankful to have worked under such a distinguished group of mentors and am very grateful for all their guidance and patience.

A special thanks to those who helped to fund my research: Thanks to Jeremy Dean for inquiring about funding, thanks to Michael Vogel for sending the inquiry over to Holland, thanks to Kevin Ewans for taking a chance on someone he hadn't heard of or met and awarding me the opportunity to complete this study, thanks to George Forristall who probably encouraged Kevin to let me do the work, thanks to Shell Nigeria for the funding and the patience, thanks to Allan Reece for allowing me to work in his group and providing me with the materials I needed to complete the job and a general thanks to the "Metocean Team" at Shell, in Houston and in Rijswijk, for being very supportive.

Last but not least, a very special thanks to Mom, Dad, Bryan, Nana, Jeremy and my wonderful friends for always being there...through good and not-so-good times.

TABLE OF CONTENTS

	Page
ABSTRACT.....	iii
ACKNOWLEDGMENTS	iv
TABLE OF CONTENTS.....	v
LIST OF FIGURES	vi
LIST OF TABLES	viii
1. INTRODUCTION	1
2. SUMMARY OF REGIONAL OCEANOGRAPHY	3
a. General Features of Atlantic Equatorial Circulation.....	3
b. Overview of Nigerian Meteorology and Near-shore Oceanography.....	7
3. DATA COLLECTION AND QUALITY CONTROL.....	11
a. Data Collected.....	11
b. Quality Control Procedures.....	13
4. FORCING FUNCTIONS.....	16
a. Time Scales of Response	16
b. Wind Fields During Field Study.....	17
c. River Discharge Rates.....	21
d. Tidal Analysis.....	27
5. WATER MASS STRATIFICATION AND GEOSTROPHIC SHEAR	37
a. Seasonal Characterization Based on Five Cruises	37
b. Inferred Geostrophic Shear.....	117
6. DESCRIPTION OF THE COASTAL CURRENT REGIME OBSERVED OFF NIGERIA	119
a. General Considerations	119
b. Horizontal Current Structure.....	127
c. Vertical Current Structures	140
7. EVIDENCE OF UPWELLING AND PRESENCE OF FORTNIGHTLY WAVE ...	156
a. Upwelling.....	156
b. Fortnightly Wave Propagation.....	162
8. CONCLUSIONS AND RECOMMENDATIONS	165
a. Major Findings.....	165
b. Recommendations for Future Work.....	168
REFERENCES	170
VITA.....	173

LIST OF FIGURES

	Page
FIG. 1. Map of study area showing major cities, rivers, locations of ADCP moorings, locations of QuikSCAT wind stations and locations of cross-shelf sections of CTD stations.	2
FIG. 2. Map of eastern equatorial Atlantic current system.....	4
FIG. 3. Monthly average rainfall for the coastal cities of Lagos, Port Harcourt and Calabar and for the interior city of Yola.....	8
FIG. 4. Map of coast of Gulf of Guinea showing volume of river inflow.....	10
FIG. 5. Daily QuikSCAT wind vectors at proposed locations of deep ADCP moorings..	18
FIG. 6. Monthly averaged mean and variance of wind speed and direction	20
FIG. 7. Map of Nigeria showing Benue River.....	22
FIG. 8. Thirty-year average of monthly average flow rates of the Benue River.	23
FIG. 9. Annual average flow rates of Benue River	24
FIG. 10. Depth contours of isohaline surfaces.....	25
FIG. 11. Percentage of water within specified salinity values.....	26
FIG. 12. Mean M_2 and S_2 tidal current ellipses	33
FIG. 13. Surface and bottom temperature contours on Cruise 1.	39
FIG. 14. Cross sections of temperature contours on Cruise 1	41
FIG. 15. Brunt Vaisala frequency for Cruise 1.....	46
FIG. 16. Surface and bottom salinity contours on Cruise 1.....	47
FIG. 17. Cross sections of salinity contours on Cruise 1.....	49
FIG. 18. Surface and bottom temperature contours for Cruise 2.....	55
FIG. 19. Cross sections of temperature contours for Cruise 2.....	57
FIG. 20. Brunt Vaisala frequency for Cruise 2.....	62
FIG. 21. Surface and bottom salinity contours for Cruise 2.	63
FIG. 22. Cross sections of salinity contours for Cruise 2	65
FIG. 23. Surface and bottom temperature contours for Cruise 3.....	71
FIG. 24. Cross sections of temperature contours for Cruise 3.....	73
FIG. 25. Brunt Vaisala frequency for Cruise 3.....	78
FIG. 26. Surface and bottom salinity contours for Cruise 3.....	79
FIG. 27. Cross sections of salinity contours for Cruise 3.....	81

	Page
FIG. 28. Surface and bottom temperature contours for Cruise 4.....	87
FIG. 29. Cross sections of temperature contours for Cruise 4.....	89
FIG. 30. Brunt Vaisala frequency for Cruise 4.....	94
FIG. 31. Surface and bottom salinity contours for Cruise 4.....	95
FIG. 32. Cross sections of salinity contours for Cruise 4.....	97
FIG. 33. Surface and bottom temperature contours for Cruise 5.....	103
FIG. 34. Cross sections of temperature contours for Cruise 5.....	105
FIG. 35. Brunt Vaisala frequency for Cruise 5.....	110
FIG. 36. Surface and bottom salinity contours for Cruise 5.....	111
FIG. 37. Cross sections of salinity contours for Cruise 5.....	113
FIG. 38. Polar plots of surface, mid-depth and bottom currents	121
FIG. 39. Power spectra from sites S2 and D5.....	125
FIG. 40. Examples of horizontal coherence, phase, gain and variance for pairs of records from the same depths at different mooring sites	129
FIG. 41. Low-passed alongshelf surface currents during deployment 1 at site S2 near the eastern end of study area and at site S5 at the western end of the study area.....	135
FIG. 42. Low-passed alongshelf surface and bottom currents at site D3	136
FIG. 43. Low-passed alongshelf mid-depth currents at site D3.	137
FIG. 44. Mean speed of 40-hr low-passed alongshelf current at site D3.	138
FIG. 45. First three vertical modes of empirical orthogonal functions (EOFs) at Sites D5, S2 and D3 and D5 combined.	141
FIG. 46. Examples of vertical coherence, phase, gain and variance between the surface and bottom currents at shallow ADCP sites in the study area.....	145
FIG. 47. Examples of vertical coherence, phase, gain and variance from deployment 1 at site D3	150
FIG. 48. Examples of vertical coherence, phase, gain and variance at site D5	153
FIG. 49. Temperature records from bottom-mounted ADCPs.....	158
FIG. 50. Comparison of current magnitude and direction to QuikSCAT winds.....	160
FIG. 51. Coherence, phase, gain and variance between the ADCP surface current and the QuikSCAT wind data at sites S2 and D3.....	161
FIG. 52. Periodogram of bottom temperature time series.	164

LIST OF TABLES

	Page
TABLE 1: Percent total variance contained in three distinct frequency bands	17
TABLE 2: Energy within mesoscale band vs. energy within weatherband.....	17
TABLE 3: Tidal current ellipses at shallow and deep ADCP mooring locations.....	29
TABLE 4: Statistics on raw and 40-hr filtered ADCP current data.....	120
TABLE 5: Summary of duration times for 40-hr low-passed alongshelf currents	139

1. INTRODUCTION

In January of 1998, oil seeped into the coastal waters off Nigeria from a pipeline belonging to Mobil Producing Nigeria Unlimited. The spill stayed off the coast and drifted along the 15- to 20-m contour paralleling the coast. The slick traveled from Qua Iboe towards the city of Lagos, on the western border of Nigeria (Fig. 1), at a speed of approximately 1.5 knots. Because of the limited knowledge of the oceanography of this region, the magnitude and direction of the drift were unexpected, hampering clean up efforts. This lack of information prompted the initiation of a joint industry project (JIP) to gain a better understanding of the shelf currents offshore Nigeria. The study area defined in the JIP includes the rivers in and near the Niger Delta and the shallow-water region (to approximately 100-m depths) off the coast of Nigeria, roughly extending from the city of Lagos to the city of Calabar (Fig. 1). Within this area, the contractor for the JIP, Evans-Hamilton Inc., carried out measurements of shelf currents and hydrography from April 2000 through May of 2001. At the same time, two local institutions, the Nigerian Institute for Oceanography and Marine Research and the University of Calabar estimated river flow of the Niger Delta's major constituents. Once properly analyzed and interpreted, these data are expected to play an important role in gaining a general understanding of the shelf circulation off Nigeria. This enhanced understanding is the objective of this thesis research, carried out with support from Shell Petroleum Development Company of Nigeria Limited (SPDC), in association with the JIP.

The information revealed by this study is expected to improve the statistics of shelf currents in the region. In turn, this will improve the reliability of engineering studies and of oil spill simulations for offshore Nigeria.

This paper is structured in the following manner. Section 2 presents a summary of the regional oceanography, Section 3 describes the oceanographic data used in this study, Section 4 describes the forcing functions driving the regional oceanography, Section 5 presents a detailed analysis of the hydrography and associated circulation, Section 6

describes the coastal current regime, Section 7 discusses upwelling and the presence of a fortnightly wave, and finally, Section 8 provides conclusions and recommendations for future work.

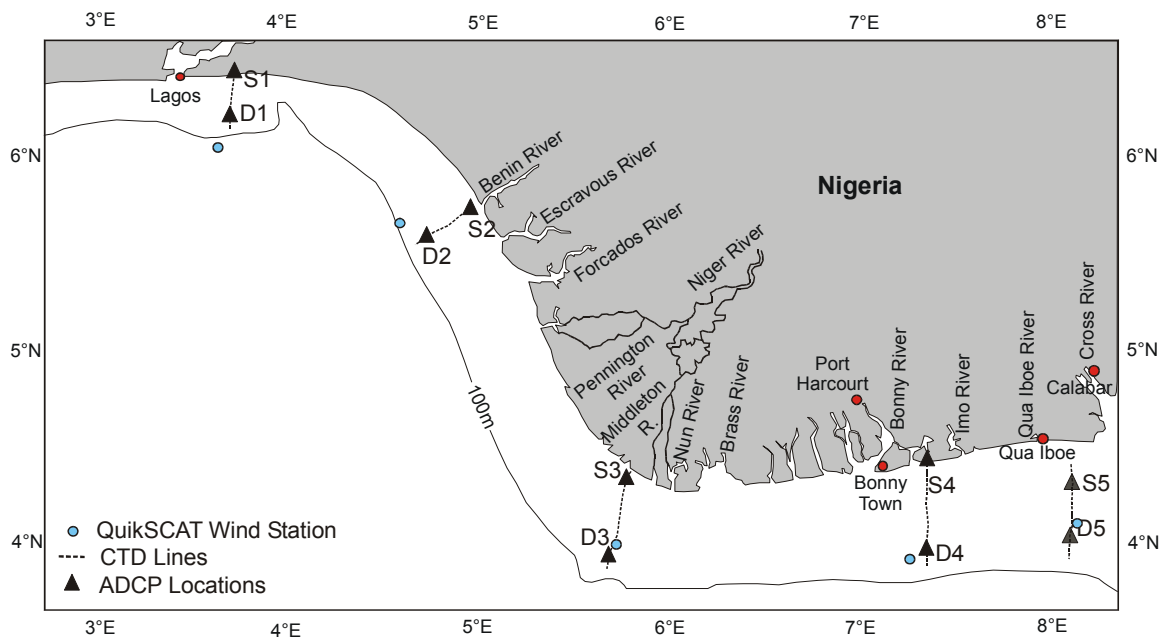


FIG. 1. Map of study area showing major cities, rivers, locations of ADCP moorings, locations of QuikSCAT wind stations and locations of cross-shelf sections of CTD stations.

2. SUMMARY OF REGIONAL OCEANOGRAPHY

a. General Features of Atlantic Equatorial Circulation

The equatorial Atlantic circulation in the Gulf of Guinea is dominated by the southeast trade winds and the eastward flowing Guinea Current (GC). Due to a meridional asymmetric distribution between the west African landmass and the ocean, the southeast trade winds are deflected as they cross the equator becoming southwesterlies in the Gulf of Guinea (Ajao and Houghton, 1998). The southwesterlies then dominate the circulation in a surface layer of 10-40 m thick (Ajao and Houghton, 1998). Illustrated in Fig. 2, the GC is an extension of both the North Equatorial Countercurrent (NECC) and the Canary Current (CC), which flows into the Gulf of Guinea from the west-northwest. All three of these currents are strongest in the northern summer months; this intensification of the current is associated with the position of the intertropical convergence. The GC varies both spatially and temporally with speeds seasonally ranging from 0.2 to 0.6 m/s, at times exceeding speeds of the NECC (Arnault, 1987). The currents in the Gulf of Guinea move towards the equator then move west to join the South Equatorial current.

There is also a westward Guinea Undercurrent (GUC), probably a branch of the Equatorial Undercurrent (EUC) which has been deflected counterclockwise by the continent (carrying with it South Atlantic Central Water), responsible for subsurface inflow to the Gulf of Guinea (Wacongne, 1988). Near the coast, the Guinea Undercurrent flows below the thermocline at half the speed of the Guinea Current. During periods of upwelling, the undercurrent may surface as the thermocline shoals, bringing with it cooler, highly saline water (Houghton, 1976).

The Gulf of Guinea has been an area of active research during the last 40 years. It has two unexplained distinguishing features: seasonal upwelling and the appearance of a strong approximately 14.7 day wave propagating in a Kelvin wave sense along the northern coast. These phenomena are described in the following subsections.

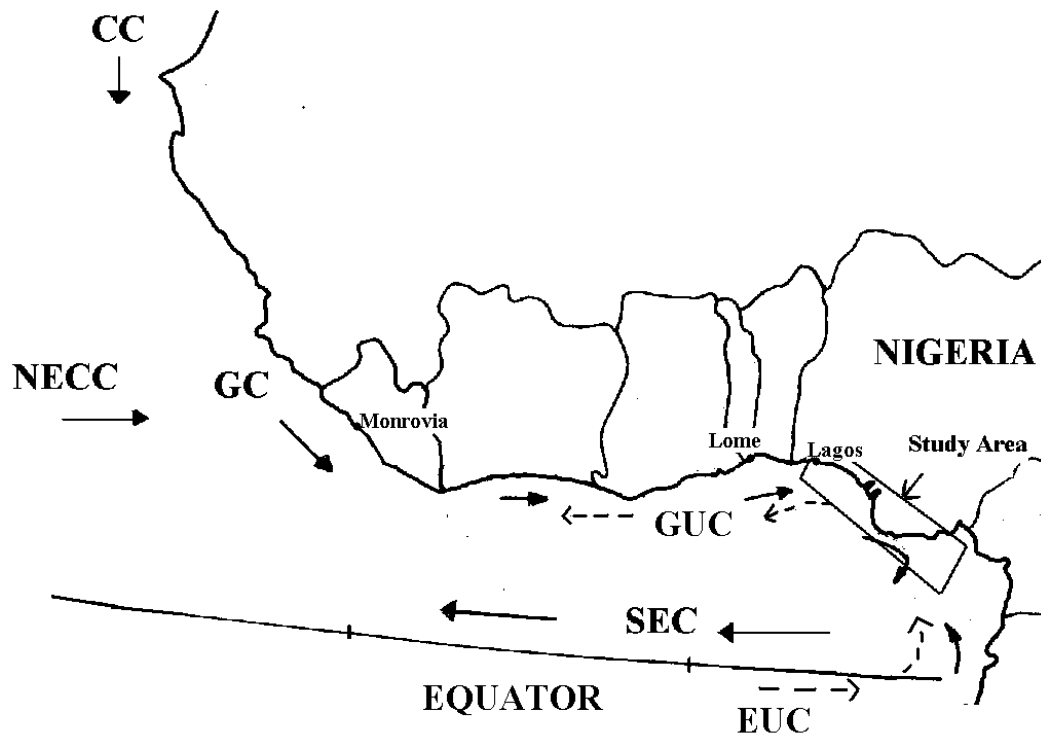


FIG. 2. Map of eastern equatorial Atlantic current system (NECC-North Equatorial Countercurrent. CC-Canary Current. GC-Guinea Current. GUC-Guinea Undercurrent. SEC-South Equatorial Current. EUC-Equatorial Undercurrent).

1) Indications of Seasonal Coastal Upwelling and Suspected Causes

From July to September (Ajao and Houghton, 1998; Clarke, 1979; Houghton, 1976; Picaut and Verstraete, 1979), unusual seasonal upwelling has been observed in the Gulf of Guinea. It is unusual because the upwelling happens very quickly (surface temperatures recorded dropping over 8°C in a single week; Clarke, 1979), the strength of the upwelling varies greatly interannually (Clarke, 1979) and, most strangely, the upwelling shows no expected correlation with direction and magnitude of the alongshore coastal wind stress (Clarke, 1979; Houghton, 1976; Picaut, 1983; Ajao and Houghton, 1998). In Houghton's study (1976), the year observed with the weakest upwelling corresponded to the year of strongest alongshore winds.

The extent of the upwelling is not conclusive. The upwelling has been seen all along the northern coast of the Gulf of Guinea, starting from Monrovia extending eastwards past Lagos (see Fig. 2 for location), where the event is seen, but is very weak (Verstraete, 1992). Ajao and Houghton (1998) point out that the upwelling of cold water offshore Nigeria is probably concealed by the sharp pycnocline formed by the surface layer of fresh river water off the Niger delta.

There have been many theories concerning this upwelling event. Verstraete clearly presents these theories in his 1992 paper, “Summary of the Seasonal Upwelling in the Gulf of Guinea”.

(a) Advection

The westward Guinea Undercurrent carries with it a well-identified South Atlantic Central Water. It has been proposed that this cold water could be advected along the northern coast; however Picaut (1983) found that the Guinea Undercurrent is not large enough, in terms of transport, to account for the upwelling by advection.

(b) Equatorial Ekman Divergence

It was proposed that the African monsoon (summertime increase in southerly wind stress) could explain both the cool waters from June to October and the strengthening of the Guinea Current. However, the monsoonal intensification of the wind stress cannot account for the coastal upwelling or the uplift of the thermocline seen throughout the Gulf of Guinea (Hastenrath and Lamb, 1977; Merle, 1978).

(c) Coastal Ekman Divergence

Local alongshore winds cannot be the force behind the upwelling either. Not only do the upwelling events show no correlation to the local wind stress, but also the cooling has been observed as deep as 500 m. Verstraete (1970) calculated velocities generated from

Ekman divergence and found them much too small to provide the vertical velocities required to displace the thermocline so drastically.

(d) Remote Forcing

Remote forcing by zonal wind stress change was first proposed by Moore, Hisar, McCreary, Merle, O'Brien, Picaut, Verstraete and Wunsch (1978). They suggested that the upwelling was forced by a rapid intensification of the easterly wind in the central-western equatorial Atlantic, around 10° to 30°W. This sudden amplification of wind stress occurs in April-May, as shown by Katz (1987), and is believed to be the catalyst of the upwelling event by generating an equatorially trapped Kelvin wave, which behaves like internal Kelvin waves trapped by a vertical wall (Allen and Romea, 1980). The wave is reflected into the Gulf of Guinea where it propagates eastward along the coast as a Kelvin wave. It then travels westward across the Atlantic as a mode 2 baroclinic Rossby waves. Remote forcing has been well received by those studying the Gulf of Guinea and has been confirmed by Philander and Pacanowski (1986) to be the driving force of the upwelling in the eastern equatorial Atlantic and a secondary force along the coasts. Upwelling along the coast is then just a consequence of equatorial adjustment responding to the change in remote wind stress.

2) Indications of a Fortnightly Wave and Suspected Causes

Houghton and Beer (1976) first noticed a westward propagating wave with a period of 14.5 days when examining the oscillations in surface temperature during the upwelling season. This meant that the rapid change in temperature at the onset of the upwelling season is due to an abrupt change in the vertical velocity of the water column (Houghton, 1976) causing the thermocline to rise and fall in synchronization with the 14-day signal. Houghton (1976) adds that this drop in temperature is also due to the evaporation of warm low salinity water from the surface. Upon plotting hydrographic data during the 1974 season, Houghton (1976) clearly presents an isostatic change in the transect propagating at a period of approximately 14 days. The signal is present throughout the

year, however it becomes more obvious during the upwelling season as the thermocline shoals, with amplitudes of surface temperature oscillations reaching 2.5°C (Picaut and Verstraete, 1979).

Picaut and Verstraete (1979) studied the wave propagating from Lome to Monrovia (see Fig. 2 for location), identifying it as a 14.77-day period wave, precisely that of the lunisolar tide (M_{sf}), traveling westward at a speed of 53 cm/s which does not vary with stratification, suggesting the wave is barotropic in nature. Only a mode 2 coastally trapped wave can travel at such a speed, however no single standing vertical wave of this type fits the observations, therefore Clarke and Battisti (1983) proposed that the wave was actually the sum of coastally trapped waves, most likely caused by some nonlinear interaction between the M_2 and S_2 tides (first suggested by Picaut and Verstraete (1979)). Because the wave is westward propagating, Clarke and Battisti (1983) suggested that the wave could be originating in the Niger Delta region, where the shelf along the northern coast of the Gulf is widest, and where semidiurnal tides should be amplified as compared to other locations along the coast. Clarke and Battisti (1983) suggest the bottom friction in the shallow water is dominantly driving the M_{sf} tide. Clarke and Battisti's theory is the latest explanation for the fortnightly wave; however, there are still discrepancies, which remain unresolved.

Not mentioned before as a possible driving force is a biweekly signal in rainfall and wind fields recently observed over West Africa based on a data set spanning from 1968-1990 (Janicot and Sultan, 2001). This biweekly oscillation in the winds was also noticed by Viltard et al. in 1997. Grodsky and Carton (2002) state that the “quasi-biweekly period is an important time scale of oscillation in the monsoon-like system that develops due to its own inherent dynamics”.

b. Overview of Nigerian Meteorology and Near-shore Oceanography

1) Summary of Meteorology

Nigeria experiences two seasons: a wet season and a dry season. Southwest winds dominate along Nigeria's coast all year long. However, due to the seasonal movement of

the intertropical convergence, southwest winds are strongest during boreal summers (approximately twice as strong as in winter (Houghton, 1976)) producing frequent rainfall. This seasonal variation is gradual and therefore it produces no significant signal to explain the rapid upwelling explained in Section 2a-1 (Ajao and Houghton, 1998). During the winter months, the Harmattan Wind¹ brings in dry dusty air as it blows from the northeast across the Sahara Desert. This is the dry season. In coastal regions, the rainy season lasts from March to November, seen in Fig. 3, producing a mean annual rainfall of 2540-4060 mm (Dublin-Green et al. 1999). Fig. 3 shows monthly average rainfall for the three major coastal cities (see Fig. 1) along with the city of Yola shown for comparison. Yola is located inland on the northeastern border of Nigeria (see figure on p. 20) and is the station location of the river data presented in Section 4b. We may note that the pattern for Yola is similar to that for the coastal area.

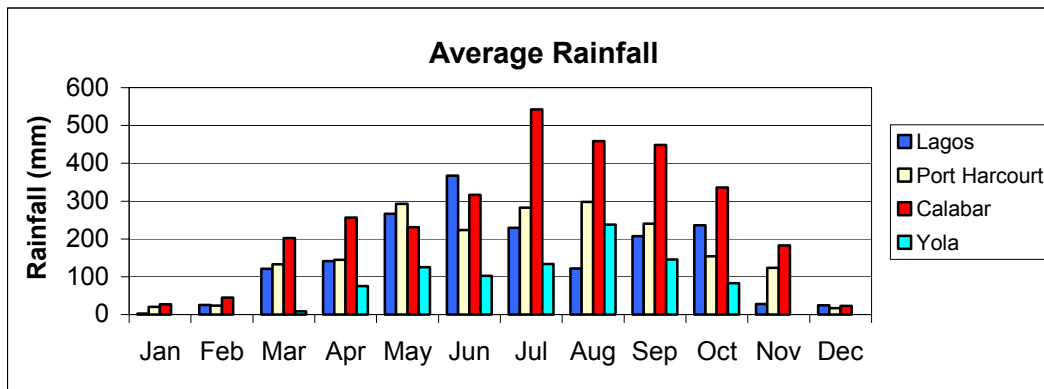


FIG. 3. Monthly average rainfall for the coastal cities of Lagos, Port Harcourt and Calabar and for the interior city of Yola. Data provided by Federal Office of Statistics, Lagos, Nigeria, via Sages Consult. Data averaged from 1993 to 1997.

¹ Harmattan Wind: “Dry, dusty, north-easterly wind which occurs in W. Africa north of the equator. Its effect extends from just north of the equator in January, almost to the northern tropics in July. In W. Africa it is known as ‘the doctor’ because of its invigorating dryness compared with humid tropical air. The harmattan wind stream occasionally extends south of the equator during the northern winter as an upper air wind over the south-westerly monsoon” (www.xrefer.com).

2) Nigeria's Rivers

It is thought that Nigeria's rivers play an important role in the coastal circulation as the Gulf of Guinea receives approximately 2.4×10^{12} m³/yr of fresh water (Adegbie et al, 1996) from two major rivers, the Niger and the Congo. The Niger River is the third longest river in Africa, draining 190×10^9 m³/yr (River Systems of the World, 2002) of freshwater into the Niger Delta each year from a basin covering most of equatorial Africa. The Congo River discharging in the ocean further south at Banana, Congo is the second longest river in Africa carrying with it the second highest volume of water in the world. The discharge from the Congo drifts along the coast northwards until it reaches Calabar estuary (Awosika and Ibe, 1994), located off the city of Calabar in the eastern end of the study area (Fig. 1).

Other important rivers in Nigeria are the Niger's tributaries the Benue, Sokoto, Kaduna and Anambra rivers, as well as the Benue, Escravos, Sombreiro, Bonny, Cross, Imo, Ogun and Osun rivers. Exact outflows of each river were not found. However, as part of JGOFS-LOICZ, Awosika and Ibe (1994) published a diagram providing statistics for three circulation cells along the Gulf of Guinea's coast. This was done as part of a water and salt budgeting effort and included total river discharge flowing into each cell with a warning that the figures for freshwater inflow are preliminary estimates. A modified version of Awosika and Ibe's diagram is presented as Fig. 4, illustrating general estimates of freshwater entering each region. Regions A and B receive water from the Niger River Delta. What is interesting about this figure is not the outflow estimates but rather the idea that the large amount of freshwater entering region C on Nigeria's eastern coast results from northerly drift from the Congo River, which has an annual discharge rate of 1300×10^9 m³ (River Systems of the World, 2002). If this is the case, the Congo River plays an important role in near-shore circulation off Nigeria.

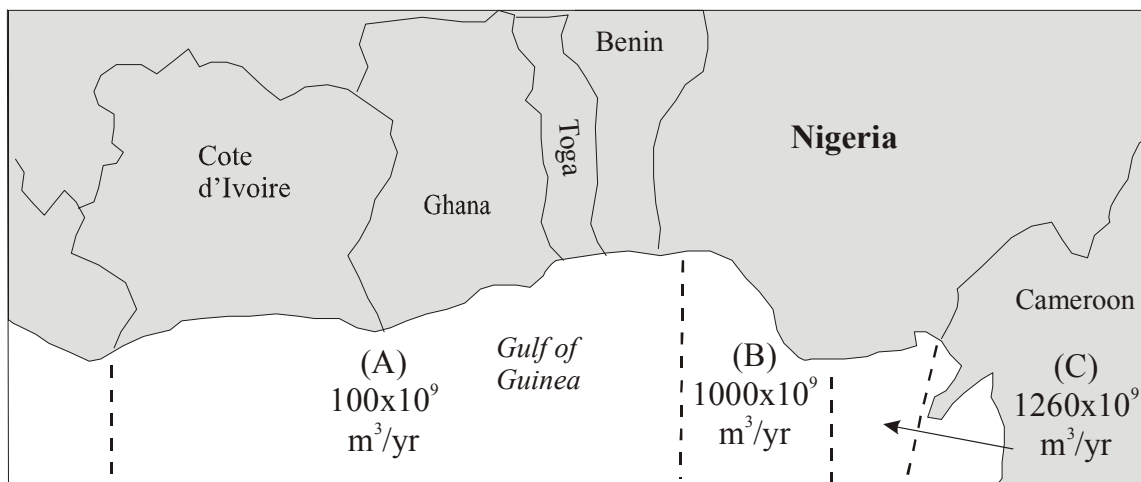


FIG. 4. Map of coast of Gulf of Guinea showing volume of river (freshwater) inflow. Inflow into 3 circulation regions is shown as defined by Awosika and Ibe (in press). Regions A and B receive drifts from the Niger delta and region C receives the northward drift from the Congo River.

3) Features of Nigerian Near-shore Oceanography

No detailed analysis of the physical oceanography of the Niger Delta region was found; however the following general descriptive features were summarized by Dublin-Green et al. (1999). The entire Gulf of Guinea is highly stratified with a warm fresh surface layer over high salinity subtropical water. Offshore Nigeria, the upper limit of the thermocline is at 12-15 m increasing with distance from shore. Sea surface temperatures remain warm at 27°-28°C from October to May and 24°-25°C from February to November. Surface salinity is generally less than 35— less than 30 off the Niger Delta. The dominant current affecting offshore Nigeria is the Guinea current strongest in the northern summer months. Tides and tidal currents offshore Nigeria are semidiurnal in nature with amplitudes increasing from west to east along the coast. Large swells from the persistent southwesterlies intersect Nigeria's coastline from the southwest. Storm surges are characteristic of April and August causing high tides and rough seas.

3. DATA COLLECTION AND QUALITY CONTROL

a. Data Collected

A JIP survey (managed by ExxonMobil) was designed to provide data for investigating the physical oceanography of the Nigerian shelf, including the fresh water discharge from the rivers in the Niger Delta region. The 12-month measurement program was executed from April of 2000 to May of 2001. Data obtained were of four types as described below. Additionally, wind data were obtained from NASA's satellite scatterometer measurements.

1) Current Measurements

Moorings with RD Instruments (RDI) 300 kHz Workhorse acoustic Doppler current profilers (ADCP) were deployed and maintained along five cross-shelf transects at locations shown in Fig. 1. Two ADCP units were placed along each transect, one in shallow water (15 to 20 m, designated by the letter "S") and one in deeper water (40 to 70 m, designated with the letter "D"). Information on these ADCP units can be found at RDI's website (Workhorse ADCP Series). The data were collected using 20-minute ensembles in bins evenly spaced along the water column from approximately 2-m off the seafloor to the sea-surface. For the type of ADCP used, the bins of data within a below-surface depth equal to 6% of the total depth will be ignored, as the data will be contaminated by side-lobe interferences. The averaging bins were 1-m in vertical extent at deep-water locations and 0.5-m in extent at shallow-water locations. The moorings were deployed, collected and serviced during a series of five cruises.

Of the ten initial ADCP site deployments, only D3 and S5 yielded measurements for the entire survey period. Moorings D5, S2, S3 and S4 yielded measurements for at least nine months. The remaining ADCPs either have not been located or have been located but not recovered.

2) Surface Drifter Measurements

Drifters from Metocean Data Systems Limited were deployed to obtain estimates of near-surface (within 1 m of the surface) currents of the coastal water. These units provided positioning data via System Argos.

Thirty-six drifters were deployed, but few survived the first week at sea. Many drifters were collected by local fishermen and many simply stopped transmitting, perhaps due to collisions with vessels or internal failures. The few drifters that survived to produce data gave some limited information on the surface currents.

3) CTD Profiles

Vertical profiles of Conductivity-Temperature-Depth (CTD) were made along each of the 5 cross-shelf transects during deployment, servicing and retrieval of the ADCP moorings. Along each transect, profiles were made at 10-m intervals of bottom depth, from 5- 10-m water depth to approximately 75- 95-m water depth, depending on the shelf width at the transect location. CTD data along each transect were successfully obtained during each of the five cruises.

4) River Surveys

Discharge rates of eleven rivers, shown in Fig. 1, were intended to be estimated using a RDI 600 kHz Rio Grande River ADCP. This unit was mounted on a small boat for estimating river outflow as the vessel traversed the river. Information on this ADCP unit is available at RDI's website (ChannelMaster H-ADCP). Measurements were made monthly over the survey year. The Nigerian Institute for Oceanography and Marine Research (NIOMR) staff collected discharge data from the Benin, Escravous, Forcados, Pennington, Middleton and Nun rivers. Rivers.

5) Wind Data

Daily wind data was downloaded from Remote Sensing System's website (ftp.ssmi.com). The website stores QuikSCAT Level 3 daily gridded ocean wind vectors from NASA's satellite scatterometer (SeaWinds on QuickSCAT, 2001). The data are available on a $0.25^\circ \times 0.25^\circ$ grid. Data from the grid points most closely corresponding to each of the five deep ADCP mooring locations (Fig. 1) were analyzed. Data obtained include the magnitude and direction of the wind data, times of the orbital passes and formation on whether rain was detected at the time of measurement.

b. Quality Control Procedures

1) ADCP Current Measurements

MATLAB was used for all calculations described in this section. Time series of the raw velocity components were plotted for selected depths for each deployment period. Then, the velocity components were rotated into along- and across-isobath components at each mooring site and examined visually.

A 40-hr low-pass cosine-Lanczos filter was applied to the data (Emery and Thompson, 2001). The rotated, filtered velocities were plotted as line plots showing each component and as stick plots, showing both magnitude and direction versus time. The stick plots were made using a MATLAB routine designed by D. Rudnick (1996) and modified by Steve DiMarco (1997). Compass plots also were made of the low passed, rotated data to more easily identify dominant current directions. These will be discussed in Section 6a.

Spectra of the filtered data were constructed and energy associated with the weatherband (2-10 day period) and with mesoscale (10-100 day period) events were calculated. Results are presented in Section 4a.

Spectra were constructed from the raw current data for each deployment of each instrument to identify dominant frequencies. To increase confidence, a block average of

the spectra was taken, dividing the time series into 30 days and averaging the spectra of each. The block-averaged spectra will be discussed in Section 6a.

Major, energetic tidal components were determined from examination of power spectra. The amplitudes of the energetic tidal signals were determined using the method of cyclic descent, based on Bloomfield (1976). The tidal analysis is presented in Section 4d.

To examine vertical structure of the current fields, coherences were determined between the surface, mid and bottom depth bins for sites D3 and D5 and coherences between the surface and bottom depths were determined for the shallow sites S2, S3, S4 and S5. The vertical coherences at the shallow and deep sites will be discussed in Section 6c.

In addition, empirical orthogonal functions (EOFs) were calculated to examine modes of vertical variability at each site. These results will be discussed in Section 6c.

In an attempt to identify and estimate any wave propagation, coherence and phase between current records at various locations were examined; these results are discussed in Section 6b.

2) CTD Measurements

The temperature and salinity data were smoothed by averaging measurements over 2-m depth intervals and assigning the average temperature or salinity values to the mean depth in each interval.

The density data were calculated from conductivity, pressure and temperature. A routine, “sw_pen.m” obtained from the SEA-MAT CSIRO Seawater Toolkit webpage (1998) was used to calculate the potential density from the smoothed temperature, salinity and pressure data.

To examine the stability of the water column at each CTD site, the Brunt-Vaisala frequency was calculated using a MATLAB code, “sw-bfrq.m” provided by the SEA-MAT CSIRO Seawater Toolkit webpage (1998).

To visualize the variability between CTD stations, which may be caused by seasonal or shorter term forcing factors or differences in locations, vertical profiles of temperature

and salinity were plotted. Vertical sections of contoured salinity and temperature were made along each cross-shelf section for each of the five cruises. Likewise, areal contoured fields of surface and bottom salinity, temperature and potential density were constructed for each cruise. These vertical and areal contour maps are presented in Section 5a.

The vertical shear of geostrophic currents was estimated by application of the methodology of Sverdrup, Helland-Hansen, Csanady and others (as reviewed in Wang, 2002) along each cross-shelf transect for each cruise. The relative geostrophic currents will be presented in Section 5b.

3) Surface Drifter Observations

Raw satellite tracked drifter fixes were obtained via Service Argos. Many of the recovered drifters transmitted very short records for various reasons. Because of confusion as to the validity of these short records it was determined to examine only those records longer than two weeks. This left only three records, which were compared to moored current measurements that were nearly coincident in both space and time, but are not discussed in this report as they provide very limited information.

4) Wind Measurements

Time series of the QuikSCAT winds were plotted as stick plots to show magnitude and direction. At the grid points closest to each of the five deep ADCP moorings. In tropical regions with low mean winds, such as offshore Nigeria, the rain causes the scatterometer to estimate higher winds than exist, therefore all measurements taken while rain was detected were deleted. In addition, any wind vectors with magnitude or direction greater than three standard deviations from the mean of the time series were removed. The wind data will be presented in Section 4b. Coherence between the winds and currents were calculated to provide useful information concerning potential wind-induced upwelling, and is presented in Section 7a.

4. FORCING FUNCTIONS

a. Time Scales of Response

To separate the responses of coastal circulation offshore Nigeria into classes depending on different types of forcing, time series of currents were divided into three bands: a high-frequency band, a weather band and a mesoscale band. The high-frequency band consists of events with periods less than 40 hr. Because most energy in this band is due to tides, the energy within the band will be referred to as tidal energy. The weatherband consists of events with 2- to 10-day periods and the mesoscale band, including events such as eddies, consists of events with 10- to 100-day periods. The percentages of the total variance within each frequency band was calculated for surface and bottom bins from each current time series and are presented in Table 1.

Table 1 shows that in general more energy is found in the tidal and mesoscale bands than in the weather band. The amount of tidal energy is highest in the eastern end of the study area (sites S4, S5 and D5) and is generally significantly higher at the bottom than at the surface. The amount of variance within the mesoscale frequency band is highest in the surface currents as compared to the bottom; mesoscale events generally contribute about half the total variance within the surface currents except at site S5. Energy within the weather band is usually highest in the surface currents, which may be expected for wind-forced events. Ratios of energy within the weather band (E_w) to that within the mesoscale band (E_m) were calculated and are presented in Table 2. Generally there was more energy within the mesoscale band; however, the energy in the weather band became more dominant in the eastern end of the study area. There were several cases, mainly at sites S5 and D5, where the bottom current contains more weather band variance than the surface current during the same deployment at the same site. This is counterintuitive; however, it should be noted that at sites S5 and D5, the bottom currents were largely (up to 80%) tidal and therefore, the actual amount of energy within the weatherband is still relatively small, remaining consistent throughout the study area.

The ratios presented in Table 2 suggest that the longer time scale events such as seasonal weather changes, river discharge and eddies have more influence on the current regime than shorter scale weather events.

TABLE 1. Percent of total variance contained in three distinct frequency bands.

		Deployment	D3		D5		S2		S3		S4		S5	
			Surface	Bottom	Surface	Bottom	Surface	Bottom	Surface	Bottom	Surface	Bottom	Surface	Bottom
Frequency Band	Tidal	1	63	51	-	-	26	32	19	38	-	-	51	53
		2	17	42	-	-	23	32	-	-	-	-	37	50
		3	21	43	46	77	35	44	-	-	33	63	46	56
		4	22	51	29	80	-	-	15	19	-	-	45	51
	Weather	1	14	16	-	-	25	19	23	26	-	-	28	22
		2	19	13	-	-	32	25	-	-	-	-	24	22
		3	18	23	12	17	22	21	-	-	15	15	24	25
		4	29	8	16	10	-	-	20	23	-	-	26	18
	Mesoscale	1	23	33	-	-	49	49	58	36	-	-	21	25
		2	64	45	-	-	45	43	-	-	-	-	39	28
		3	61	34	42	6	43	35	-	-	52	22	30	19
		4	49	41	55	10	-	-	65	58	-	-	29	31

TABLE 2. Energy within mesoscale band vs. energy within weatherband.

		D3		D5		S2		S3		S4		S5	
		E_w/E_m		E_w/E_m		E_w/E_m		E_w/E_m		E_w/E_m		E_w/E_m	
Deployment		Surface	Bottom	Surface	Bottom	Surface	Bottom	Surface	Bottom	Surface	Bottom	Surface	Bottom
1		0.2	0.5	-	-	0.5	0.4	0.4	0.7	-	-	1.3	0.9
2		0.3	0.3	-	-	0.7	0.6	-	-	-	-	0.6	0.8
3		0.3	0.7	0.3	3.0	0.5	0.6	-	-	0.3	0.7	0.8	1.3
4		0.6	0.2	0.3	1.1	-	-	0.3	0.4	-	-	0.9	0.6

b. Wind Fields During Field Study

NASA's QuikSCAT Level 3 daily gridded ocean wind vectors were plotted for the duration of the study period at locations corresponding to each proposed deep ADCP location (Fig. 5). The dots appearing at the -5 m/s level indicate days at which rain was detected by the scatterometer. The gaps appear where rain was detected, where values

were not recorded by the scatterometer and where wind speeds exceeded acceptable quality control parameters, as described in Section 3.

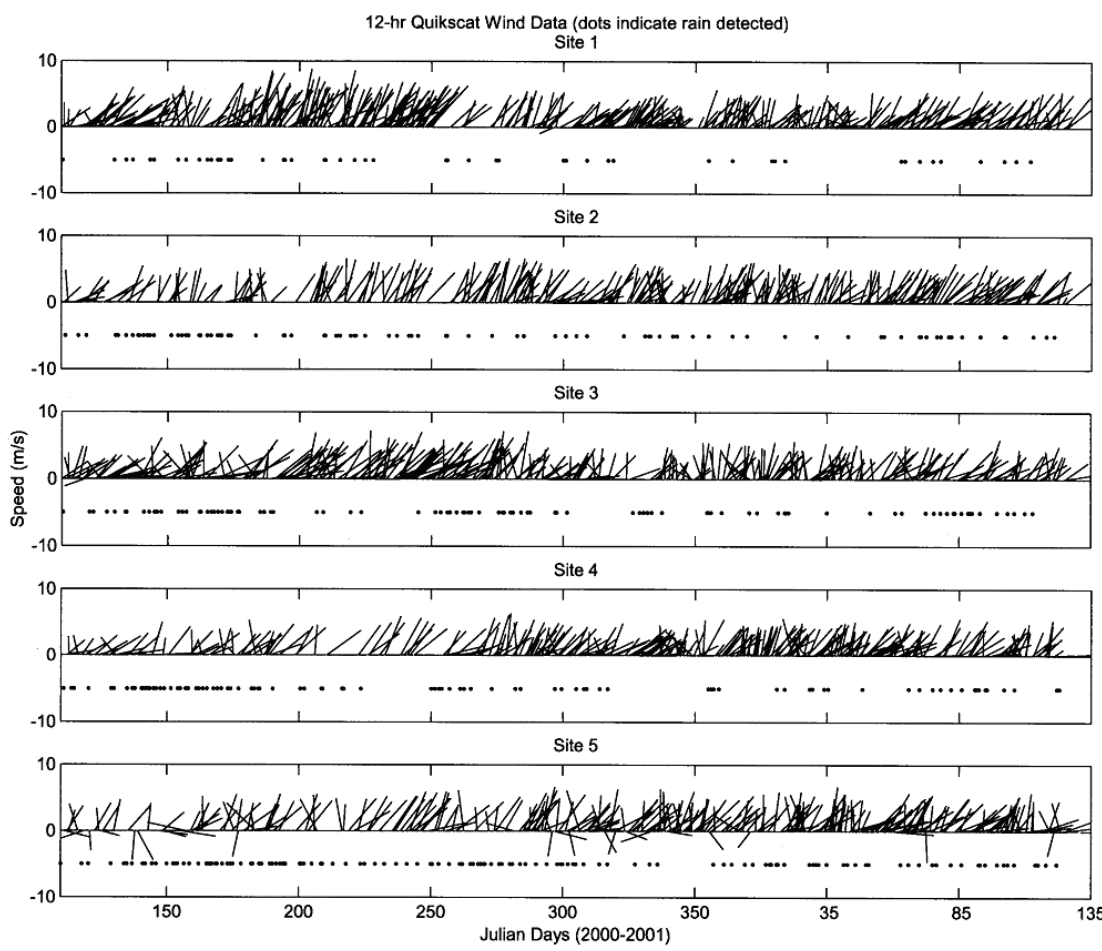


FIG. 5. Daily QuikSCAT wind vectors at proposed locations of deep ADCP moorings (Fig. 1). North is up in the vector plots. Dots indicate times during which rain was detected and wind vectors were deleted.

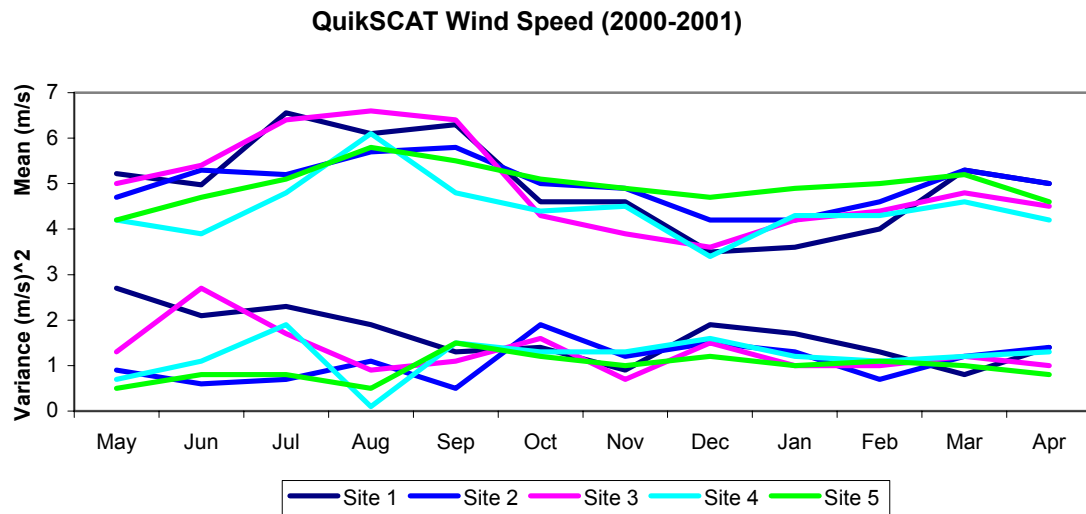
Fig. 5 clearly shows a predominately steady southwesterly wind that is strongest in the boreal summer months, in agreement with Houghton’s (1976) earlier observations. With the exception of site 5, there were no reversals in wind direction. The frequency of

rain detected increases significantly from site 1 to site 5, or eastward along the coast, consequently decreasing the continuity of the time series.

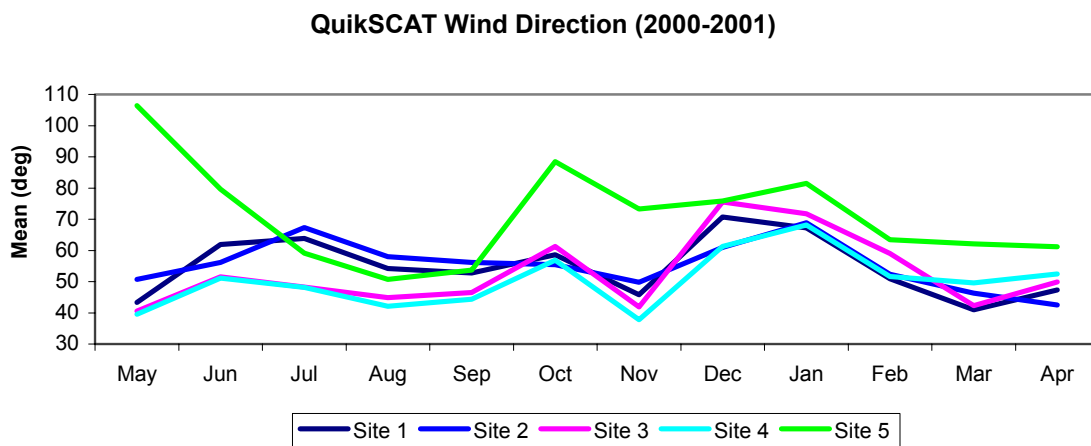
To more clearly illustrate the annual pattern, the monthly means and variances of the wind speed and the mean directions were calculated (Fig. 6). The mean wind speeds (Fig. 6a) vary little, ranging between 4 and 7 m/s with low variance. The wind speeds from June through September are approximately 50% higher than the rest of the year, as expected (Section 2b). The weakest mean speeds occur in December for sites 1-4. Upon examination of the shift in mean wind direction (Fig. 6b) in December, it can be inferred that this decrease in wind speed is probably due to the monsoonal winds, as the steady wind direction slowly rotates 20-30° clockwise from September to December, when the Harmattan Wind sweeps off the desert, opposing the ever-present southwesterlies.

The findings agree with those presented in Houghton's 1976 study. He showed a very steady wind speed, varying approximately 2 m/s over the year, however the magnitudes range from 2 to 4 m/s, half of what is seen from the QuikSCAT data, a difference that could easily be due to instrumental advancements and interannual variation in equatorial wind strength. He also showed the prevailing southwesterly wind with mean direction varying annually by 40° similar to the variance in direction shown below in Fig. 6b, with the exception of site 5.

Site 5 consistently shows patterns that differ from sites 1-4. Site 5 showed occasional wind reversals, increased rainfall, less variance in mean speed and greater variance in direction. As seen in the overview of meteorology (see Average Rainfall chart for Calabar (site 5) compared to Lagos (site 1) and Port Harcourt (site 4) (Fig. 3)) and confirmed by the QuikSCAT data, site 5 also experiences a significantly higher amount rainfall as compared to the rest of Nigeria's coastline.



(a)



(b)

FIG. 6. Monthly averaged (a) mean and variance of wind speed and (b) direction. (b) indicates direction toward which wind was blowing from QuikSCAT wind vectors shown in Fig. 4.

c. River Discharge Rates

As part of the field study, river discharge data were collected at the mouths of the various rivers, at different times during different stages of the tidal cycle. The results are unclear and do not provide reliable river discharge rates. Therefore, they were not used.

In this section river discharge information presented in Section 2b is studied along with an historical set of river flow data. The historical discharge data are examined as a proxy to the pattern of seasonal and interannual river discharge rates into the study area. Then, the volume of low salinity water observed during the different cruises of field study is examined briefly.

1) A Historical Record of Benue River Flow Rates

Various global repositories of data on river flow rates were contacted. The only discharge data located from Nigerian rivers were held by the Global Runoff Data Center (GRDC) for a station positioned on the Benue River in the city of Yola located near the mountainous eastern border of Nigeria (Fig. 7). The Benue River is the chief tributary to the Niger River and the second longest river in Nigeria. Although the Benue does not directly enter the Gulf of Guinea, and Yola is located more than 600 km northeast of the study area, it is believed that the Benue River should exhibit patterns of variability very similar to other rivers discharging into the study area. Thus, the annual and interannual patterns should provide proxies for the variations of river discharge affecting the near-shore circulation of the study area.



FIG. 7. Map of Nigeria showing Benue River. Yola is the location of the river gauging station for which data are available.

The GRDC provided monthly average flow rates of the Benue River at Yola for the thirty years 1960-1989. Thirty-year monthly averages (Fig. 8) and annual averages (Fig. 8) were calculated from these data for examination of annual and interannual patterns.

Seen in Fig. 8 is the very large range in flow during the annual cycle, with the peak flow rate occurring in September. There is very little flow from January to June. The flow rate then increases by tenfold from June to September, where river discharge peaks. The flow rates remain significant but decreasing November through December. The annual cycle of river discharge matches fairly well with the annual cycle of rainfall in Nigeria's coastal cities (Fig. 3), indicating the annual pattern of the Benue River should provide a fairly reliable representation of river discharge patterns around the Niger Delta. It should be noted that the year-to-year differences from this average annual cycle are much larger during the periods of high flow than during low flow, indicating substantial interannual variance to be seen directly in Fig. 9.

There is significant interannual variability in river flow rates (Fig. 9). Yearly average discharge rates range from 8.5 to 46 m^3/s with a variance of 78 $(\text{m}^3/\text{s})^2$. There is some hint of a long-term trend toward lower flow rates, however, the record is much too short to be draw convincing conclusions.

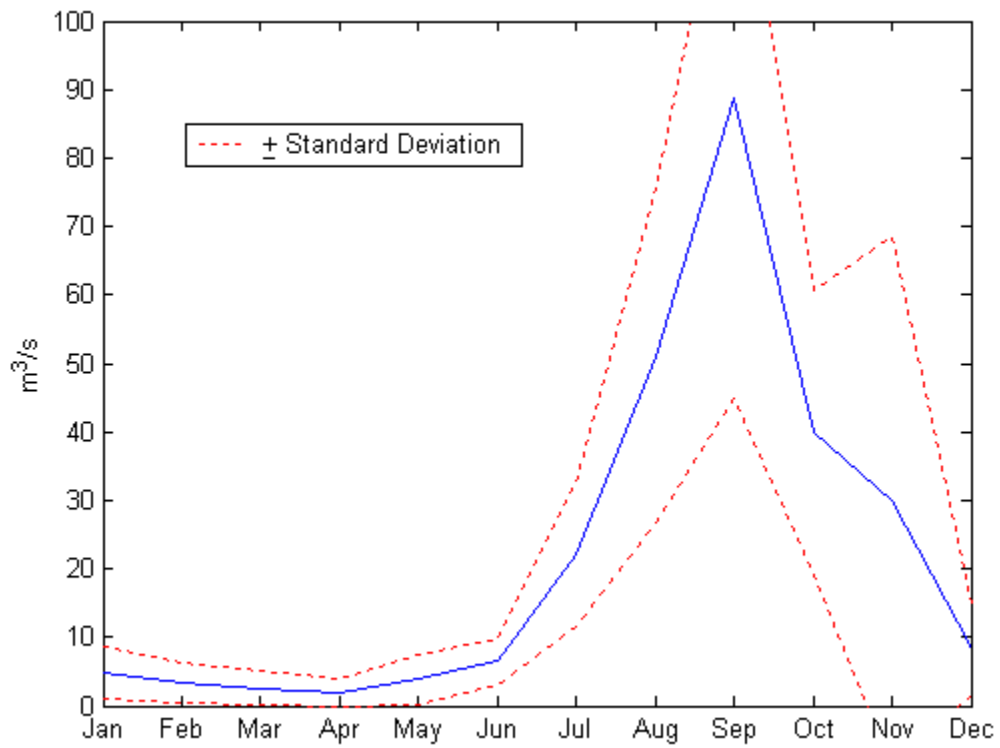


FIG. 8. Thirty-year average of monthly average flow rates of the Benue River (as measured at Yola, Nigeria). Data provided by the Global Runoff Data Center.

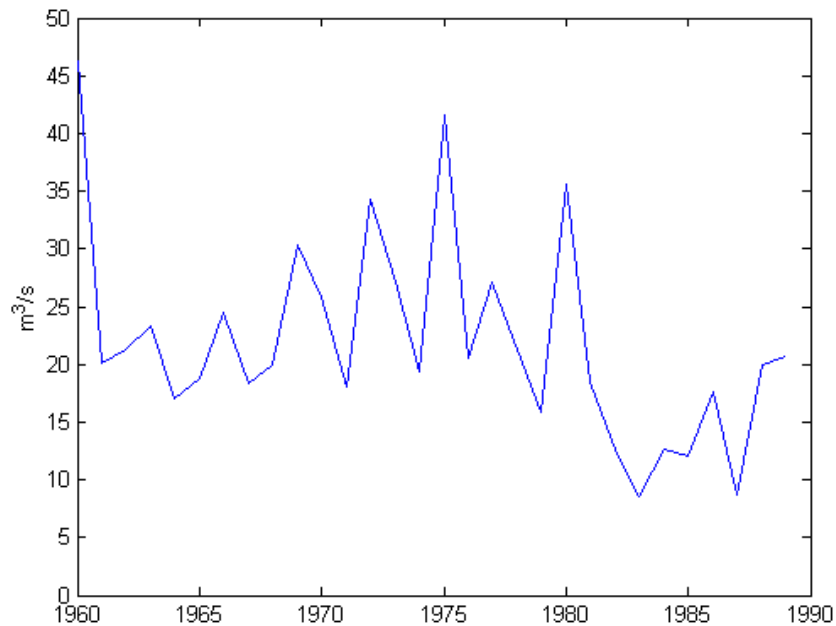


FIG. 9. Annual average flow rates of Benue River (as measured at Yola, Nigeria). Averages based on average flow rates for each month in the year. Data provided by the Global Runoff Data Center.

2) Significance of Freshwater to Study Area

Fig.10 shows areal distributions of depths of selected isohalines to indicate the volume of low salinity water present throughout the study area. The vertical migration from cruise to cruise of isohaline surfaces can be indicative of seasonal variation of freshwater entering the study area through river discharge, rainfall and by surface currents. Fig. 10a-e documents changes in depth of the 32 isohaline throughout the year. A salinity of 32 was chosen as a reference point as it is consistently present throughout the field program. The depths of the 32 isohaline illustrate a higher volume of fresh water in lines 4 and 5 than elsewhere throughout the year. Fig. 10f shows the depth of the 24 isohaline, which appeared only during Cruise 3, in October, just after the season of historically highest river discharge. Again, the 24 isohaline shows the larger volume of fresh water present in lines 4 and 5.

In an effort to quantify the amount of river water seen across the study area, the percentage of water within specified salinity ranges was calculated along each line and is shown in Fig. 11a-e. The amount of freshwater entering the coastal waters is again strongest around lines 4 and 5. Upon examining the percentages, the effects of the river system (a lowering of salinities) can be seen from July to February, but most definitively in October, as expected from the monthly average flow rate pattern (Fig. 8). In Fig. 8, the high discharge lasts only to November, but both Figs. 10 and 11 show the high discharge rates from July to November affect the hydrographic characteristics all the way through February.

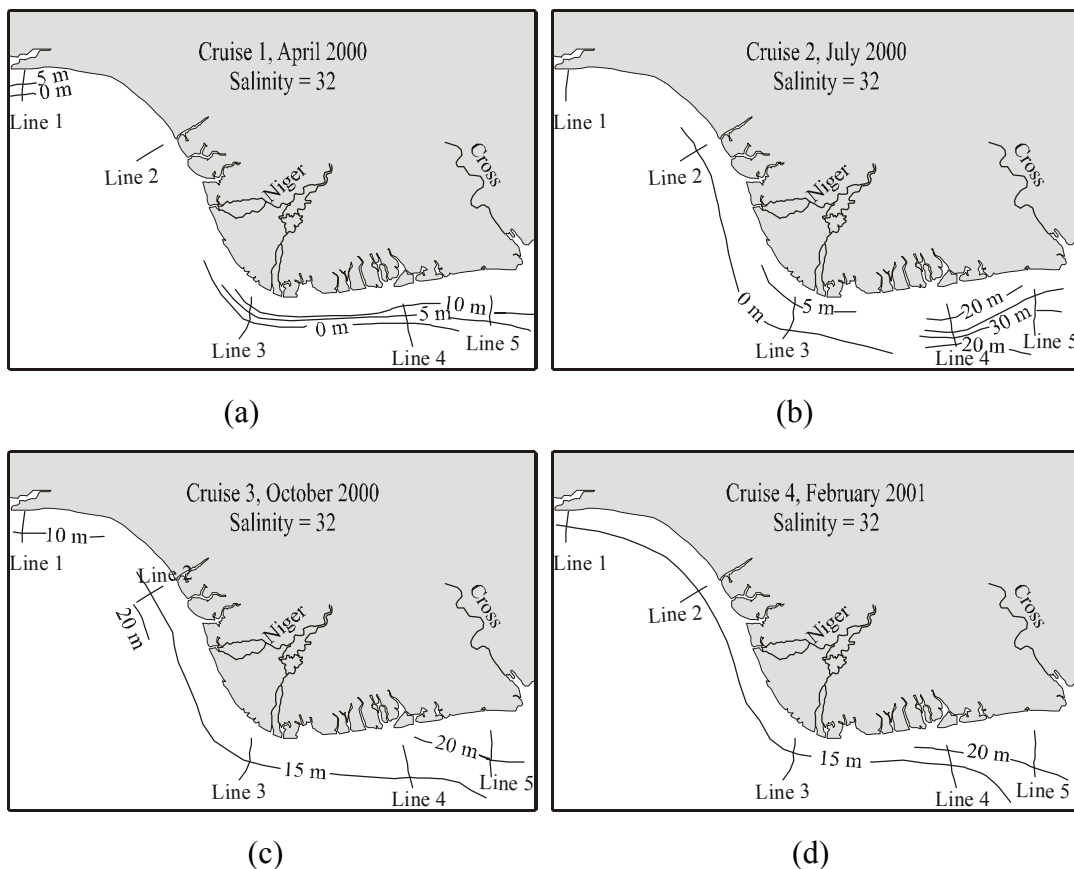


FIG. 10. Depth contours of isohaline surfaces (to illustrate amount of fresh water present in the study area during each cruise). (a)-(e) Depth contours for salinity equals 32. (f) Depth contour for salinity equals 24.

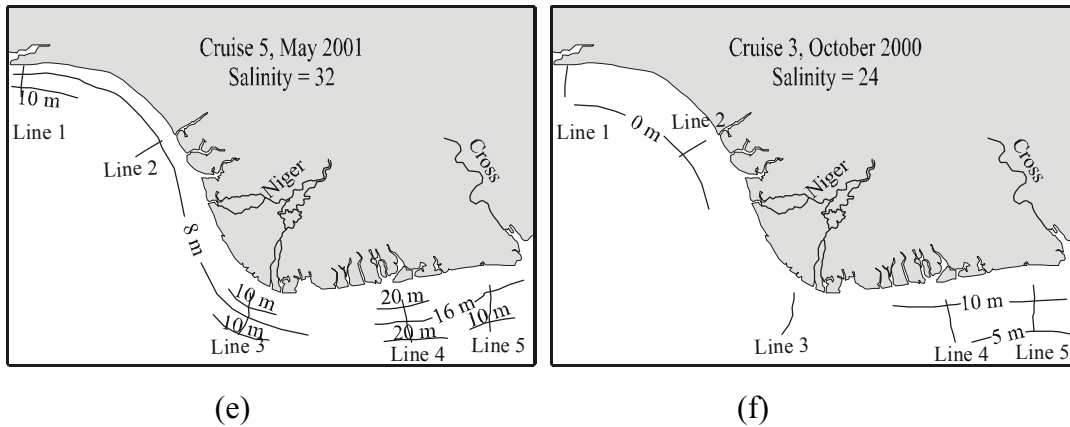


FIG. 10. Continued.

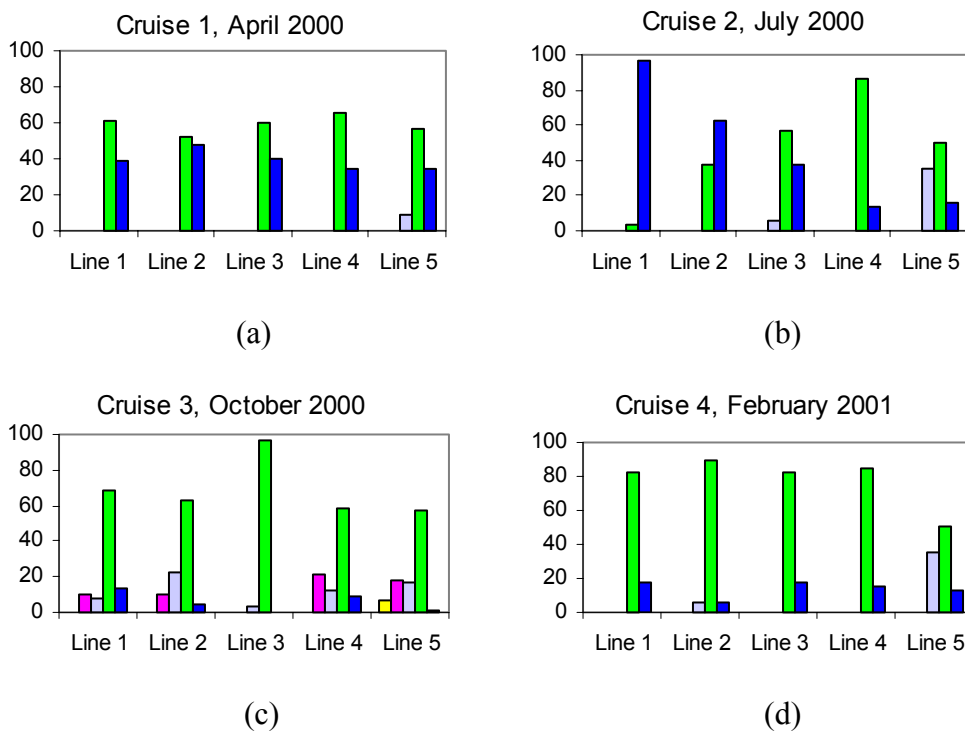
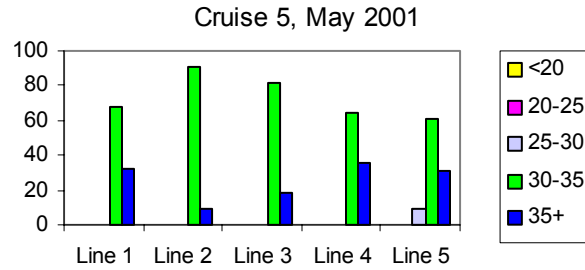


FIG. 11. Percentage of water within specified salinity values (during each cruise calculated along each line).



(e)

FIG. 11. Continued.

d. Tidal Analysis

Because tides result in very energetic events in the study area, the full analysis of tidal currents based on the study data is presented in this subsection of forcing functions.

The method of cyclic descent (MCD), based on Bloomfield (1976), was used to extract energetic tidal signals from the ADCP velocity time series. For this research, a MATLAB program designed by Steven DiMarco (1995) was used to run the MCD analysis. The MCD is a form of harmonic analysis, which uses an iterative least squares approach to solve for amplitudes and phases of specified frequencies. In this case the frequencies were those of the M_2 , S_2 , N_2 , K_2 , K_1 , O_1 , P_1 , Q_1 , M_4 and M_6 tidal constituents. These frequencies were decided upon after examining the raw spectra, shown later in Section 6a. Although there was very little indication of a diurnal signal, the 4 main constituents were included. The compound tides, M_4 and M_6 , which can be expected in shallower water, were seen on the spectra and included in the MCD analysis. The MCD allows for data gaps, therefore all deployments were combined and analyzed as a continuous times series by filling in any time gaps with extraneous values (-999). The analysis was carried out on a near-surface and a near-bottom bin for all mooring sites and additionally at a mid-depth bin for sites D3 and D5. The MCD solves for two unknowns, a and b , which are related to the amplitude and phase of the tidal constituent by: $a = A \cos \phi$ and $b = -A \sin \phi$.

Tidal ellipses were constructed from the amplitude and phase of each tidal constituent, calculated from the north-south (v) and east-west (u) current components using a MATLAB program designed by Xu (2002). The major (M) and minor (m) axes of each tidal current ellipse were calculated using the following definitions (Foreman, 1977):

$$\begin{aligned} M &= \text{abs}^{1/2}(u + iv) + \text{abs}^{1/2} \text{conj}(u - iv), \text{ and} \\ m &= \text{abs}^{1/2}(u + iv) - \text{abs}^{1/2} \text{conj}(u - iv), \text{ where} \\ u &= \text{Amp}_u (e^{-i\phi(u)}), \text{ and} \\ v &= \text{Amp}_v (e^{-i\phi(v)}). \end{aligned}$$

The angle of the major axis relative to the east-west axis is:

$$\begin{aligned} \alpha &= 1/2 (\alpha_1 + \alpha_2), \text{ where} \\ \alpha_1 &= \text{ang}^{1/2}(u + iv), \text{ and} \\ \alpha_2 &= \text{ang}^{1/2} \text{conj}(u - iv). \end{aligned}$$

In the above equations, Amp is the amplitude of the tidal constituent, ϕ is the phase of the tidal constituent and i is $\sqrt{-1}$.

To correct for the 18.6-year lunar orbital tilt, the astronomical phase modulation (v) and the nodal amplitude correction (f) were calculated from the latitude and center time of the time series using a MATLAB program created by Pawlowicz (2000) based on tidal theory described in Pawlowicz et al. (2002). The amplitudes obtained from the MCD analysis were then divided by f to correct for nodal modulation. The Greenwich phase lag was determined using the following relation: $G_i = v_i - 0.5 (\alpha_1 + \alpha_2)$.

Table 3 presents the magnitudes of the major and minor axis (corrected by f), the orientation of the major axis relative to the east-west axis (+ is counterclockwise, cc) and the Greenwich phase lag for each MCD tidal analysis. The rotation of the tidal current vector is indicated by the sign of the minor axis (positive for cyclonic rotation and negative for anti-cyclonic rotation). A value for each parameter shown is given at a near-surface depth and a near-seafloor depth.

Table 3. Tidal current ellipses at shallow and deep ADCP mooring locations.

(a) Site S2 tidal current ellipses at surface and near-bottom locations. Total water depth ranged from 14-15 m during deployments 1, 2 and 3.

Tidal Component	Period (h)	Major Axis (cm/s)		Minor Axis (cm/s)		Theta (deg) CC of E-W axis		G (deg)	
		surface	bottom	surface	bottom	surface	bottom	surface	bottom
M ₂	12.421	6.1	7.3	-2.0	-1.9	28.6	26.4	335.2	330.2
S ₂	12	2.5	2.4	0.3	-0.5	16.7	23.1	345.9	348.2
N ₂	12.66	1.8	1.7	-0.3	-0.4	47.6	35.4	148.7	153.6
K ₂	11.97	1.0	1.6	-0.1	0.2	46.2	31.6	177.9	179.0
K ₁	23.93	1.8	1.7	0.2	-0.3	25.2	19.5	359.7	303.5
O ₁	25.82	0.9	0.7	-0.1	-0.1	96.3	57.5	321.7	305.4
P ₁	24.01	1.7	0.9	-0.4	0.3	77.3	48.9	353.8	346.0
Q ₁	26.87	0.8	0.9	0.2	0.2	51.4	66.3	181.2	169.9
M ₄	6	0.6	0.9	0.1	0.2	23.9	39.9	269.2	260.4
M ₆	4	0.9	1.0	-0.1	0.0	39.7	47.7	276.5	278.0

(b) Site S3 tidal current ellipses at surface and near-bottom locations. Total water depth ranged from 14-15 m during deployments 1 and 4.

Tidal Component	Period (h)	Major Axis (cm/s)		Minor Axis (cm/s)		Theta (deg) CC of E-W axis		G (deg)	
		surface	bottom	surface	bottom	surface	bottom	surface	bottom
M ₂	12.421	8.1	8.0	1.3	1.1	46.4	42.7	257.1	263.1
S ₂	12	2.1	2.3	0.5	0.7	43.3	57.5	291.2	290.3
N ₂	12.66	1.7	1.6	0.3	0.4	50.6	41.8	169.8	185.8
K ₂	11.97	0.4	0.6	-0.1	0.3	19.8	97.6	199.6	104.7
K ₁	23.93	1.0	0.8	0.8	-0.7	37.6	-35.4	306.4	271.6
O ₁	25.82	0.3	0.7	0.3	0.2	107.0	18.2	282.2	297.7
P ₁	24.01	0.9	0.9	0.8	0.6	31.5	-32.4	13.9	289.7
Q ₁	26.87	0.3	0.2	0.0	0.1	4.1	28.6	184.7	251.4
M ₄	6	0.9	0.9	-0.1	-0.1	49.2	51.9	313.3	284.6
M ₆	4	0.4	0.3	-0.2	-0.1	87.8	73.8	250.9	230.2

Table 3. Continued.

(c) Site D3 tidal current ellipses at surface, mid-depth and near-bottom locations. Total water depth ranged from 50-51 m during deployments 1, 2, 3 and 4.

Tidal Component	Period (h)	Major Axis (cm/s)		Minor Axis (cm/s)		Theta (deg) CC of E-W axis		G (deg)	
		surface	bottom	surface	bottom	surface	bottom	surface	bottom
M ₂	12.421	8.2	6.2	-2.8	2.1	41.8	82.5	352.1	319.1
S ₂	12	2.0	2.9	0.5	1.0	3.4	91.6	9.9	11.0
N ₂	12.66	1.6	1.2	-0.6	0.2	21.7	60.0	140.2	154.7
K ₂	11.97	1.2	0.8	0.7	-0.3	-66.2	71.9	92.3	161.9
K ₁	23.93	0.8	0.6	-0.2	-0.1	73.2	28.4	24.5	312.5
O ₁	25.82	0.6	0.4	0.0	0.0	36.6	77.5	343.3	6.8
P ₁	24.01	0.9	0.2	-0.2	0.2	-21.5	55.0	63.4	38.9
Q ₁	26.87	0.1	0.1	0.0	0.1	-67.7	85.7	250.5	213.7
M ₄	6	0.8	0.3	0.0	0.1	79.3	95.8	317.8	263.3
M ₆	4	0.3	0.2	0.0	0.0	71.7	-85.8	276.0	214.9

(d) Site S4 tidal current ellipses at surface and near-bottom locations. Total water depth was 20 m during deployment 3.

Tidal Component	Period (h)	Major Axis (cm/s)		Minor Axis (cm/s)		Theta (deg) CC of E-W axis		G (deg)	
		surface	bottom	surface	bottom	surface	bottom	surface	bottom
M ₂	12.421	11.6	15.2	3.3	0.1	86.8	88.8	349.7	362.5
S ₂	12	2.7	7.6	0.1	0.9	77.6	89.7	339.9	342.6
N ₂	12.66	5.1	2.5	0.8	-0.7	77.1	91.4	210.0	174.3
K ₂	11.97	1.1	3.0	-0.4	0.1	88.3	87.4	124.1	159.4
K ₁	23.93	0.6	1.1	0.3	0.7	29.6	93.8	2.5	357.9
O ₁	25.82	0.7	1.1	-0.4	-0.1	24.7	93.6	346.6	2.7
P ₁	24.01	2.8	1.0	-1.1	0.2	54.5	66.6	36.4	337.2
Q ₁	26.87	0.9	1.0	-0.7	-0.5	64.9	71.9	195.8	198.7
M ₄	6	1.9	1.8	0.4	0.7	85.4	102.1	252.2	331.8
M ₆	4	0.5	0.3	-0.1	0.0	79.2	61.8	290.5	281.6

Table 3. Continued.

(e) Site S5 tidal current ellipses at surface and near-bottom locations. Total water depth ranged from 15-20 m during deployments 1, 2, 3 and 4.

Tidal Component	Period (h)	Major Axis (cm/s)		Minor Axis (cm/s)		Theta (deg) CC of E-W axis		G (deg)	
		surface	bottom	surface	bottom	surface	bottom	surface	bottom
M ₂	12.421	12.0	12.2	-1.3	-2.2	78.9	74.6	182.7	181.3
S ₂	12	3.7	4.1	-1.2	-0.9	98.0	98.7	330.6	329.8
N ₂	12.66	2.5	2.2	-0.4	-0.3	90.8	103.8	150.8	149.9
K ₂	11.97	1.3	0.7	-0.4	0.0	109.2	83.8	357.6	338.2
K ₁	23.93	1.7	1.2	-0.4	0.1	88.9	81.8	343.5	166.5
O ₁	25.82	0.9	0.4	0.1	-0.2	171.9	130.1	285.3	290.1
P ₁	24.01	2.6	1.7	-0.8	-0.4	78.6	80.8	216.6	4.7
Q ₁	26.87	0.3	0.2	0.0	0.0	135.9	14.8	146.4	56.4
M ₄	6	1.6	1.7	0.0	-0.4	86.5	88.9	264.6	262.1
M ₆	4	0.7	0.8	0.2	-0.1	104.9	98.2	117.8	117.4

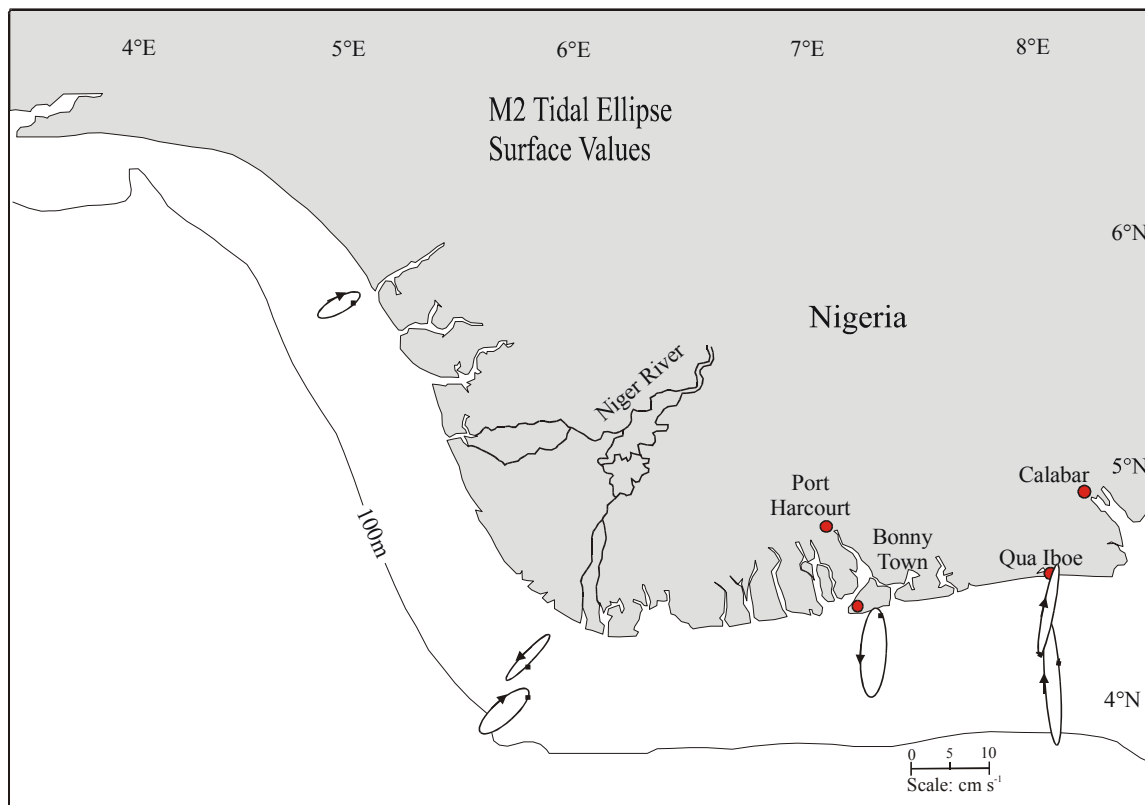
(f) Site D5 tidal current ellipses at surface, mid depth and near bottom locations. Total water depth ranged from 44-49 m during deployments 1, 3 and 4.

Tidal Component	Period (h)	Major Axis (cm/s)		Minor Axis (cm/s)		Theta (deg) CC of E-W axis		G (deg)	
		surface	bottom	surface	bottom	surface	bottom	surface	bottom
M ₂	12.421	16.4	12.5	-2.0	-1.6	94.1	82.3	295.2	319.7
S ₂	12	4.5	4.2	-0.6	-0.8	88.5	84.1	359.9	0.3
N ₂	12.66	4.1	1.6	-0.7	0.0	81.1	75.7	168.0	4.2
K ₂	11.97	1.3	1.3	0.1	-0.4	61.4	47.3	344.0	140.6
K ₁	23.93	1.5	1.3	0.0	-0.6	31.9	103.4	314.6	183.3
O ₁	25.82	0.4	0.5	0.1	-0.1	56.8	74.2	170.2	166.3
P ₁	24.01	0.6	0.9	-0.3	-0.2	79.3	57.7	224.0	343.7
Q ₁	26.87	0.5	0.4	0.1	0.1	140.6	93.3	61.1	35.2
M ₄	6	1.3	2.2	-0.3	0.1	97.0	91.5	264.5	135.2
M ₆	4	0.8	0.8	0.0	-0.1	91.6	98.7	233.0	217.8

As shown in Table 3, and later in Section 6, the tides are strongly dominated by the semidiurnal signals, which account for 95 percent of the total tidal energy, averaged over the six ADCP locations. In fact, the semidiurnal signal is so strong in the study region,

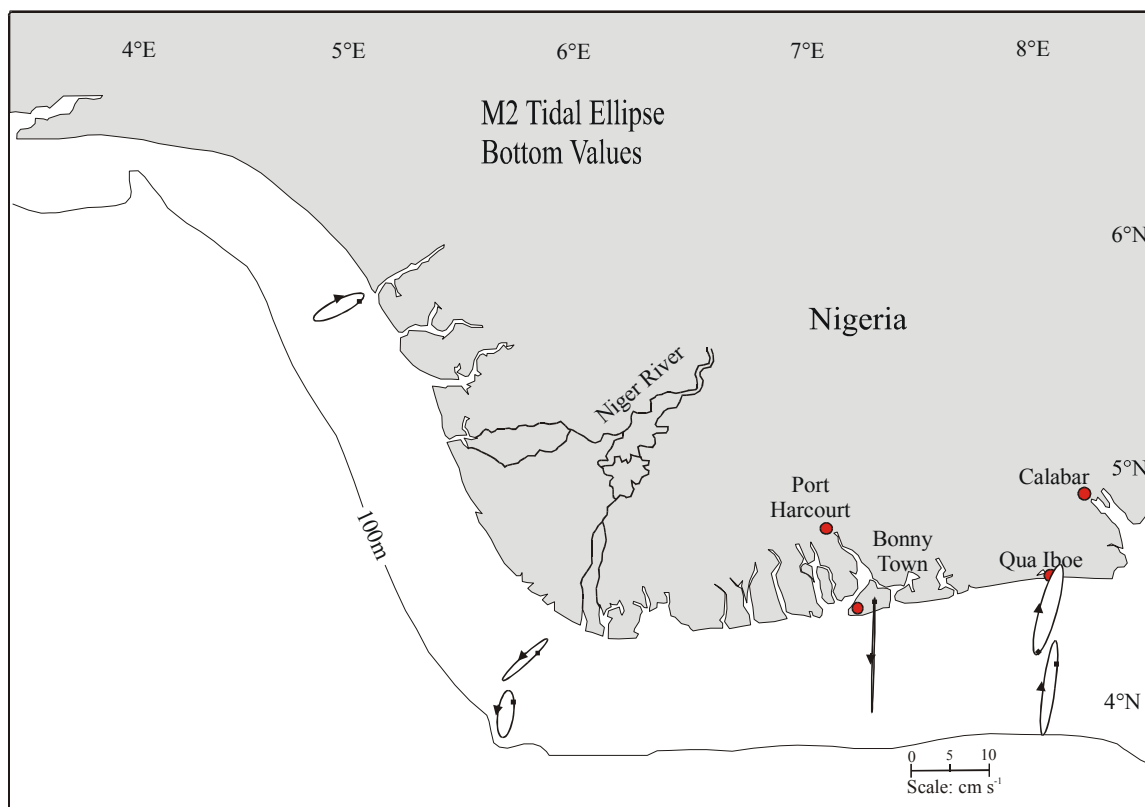
they overpower the typical solar diurnal heating cycle and induce a semidiurnal cycle in temperature (see Section 7) throughout the region. The M_2 alone contributes 68-86 percent of the total tidal energy and together the M_2 and S_2 tides contain an average of 90% of the total tidal energy. The diurnal tides contain an average of 5% of the total tidal energy, with the shallow ADCP locations averaging slightly higher at 6%, and the deeper ADCP location averaging slightly lower at 3%. This intensification of the diurnal tides seen in the shallow locations, especially in the P_1 tide, is expected as the diurnal tides are amplified in shallow water, especially on wide shelves (Clarke and Battisti, 1977). There is also an amplification of the M_4 tide in the shallow water at all locations excluding site S2.

The tides are generally barotropic meaning the amplitudes of the tidal constituents are generally independent of depth and stratification. In several cases the tidal components seem to be bottom-intensified presumably due to friction. Areal views of the M_2 and S_2 surface and bottom tidal ellipses are shown in Fig. 12. The alignment of the ellipses is strongly cross-shelf. It can be easily seen that the semi-diurnal tides are amplified as the shelf widens to the eastern part of the study area, a pattern that is rarely seen (Clarke and Battisti, 1977). There is little or no relationship between distance from shore and strength of the semidiurnal tides; however, with only two deep sites, this conclusion is speculative.



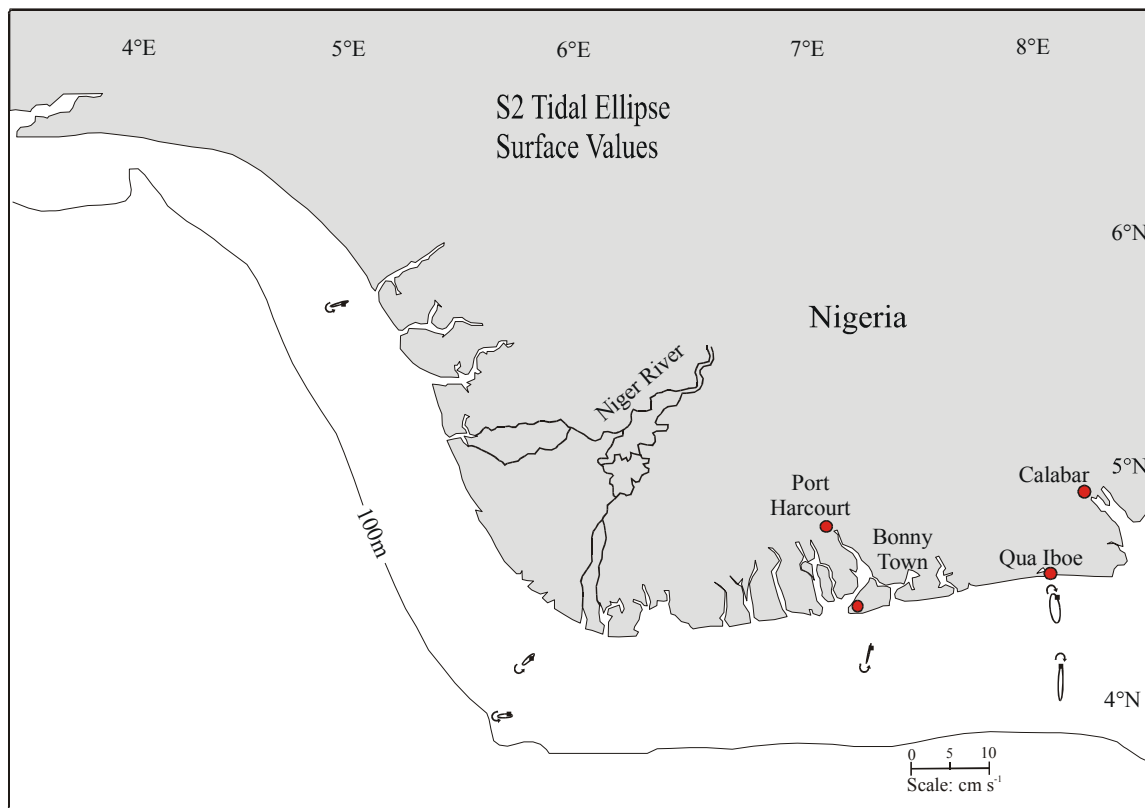
(a)

FIG. 12. (a)-(d) Mean M_2 and S_2 tidal current ellipses (from near-surface and bottom current records during the period from April 2000 to May 2001). The circles show the orientation of the tidal current vectors at 0000 UTC, October 28, 2000, the mid date of data collection. The arrows show the rotational direction of the tidal current vectors.



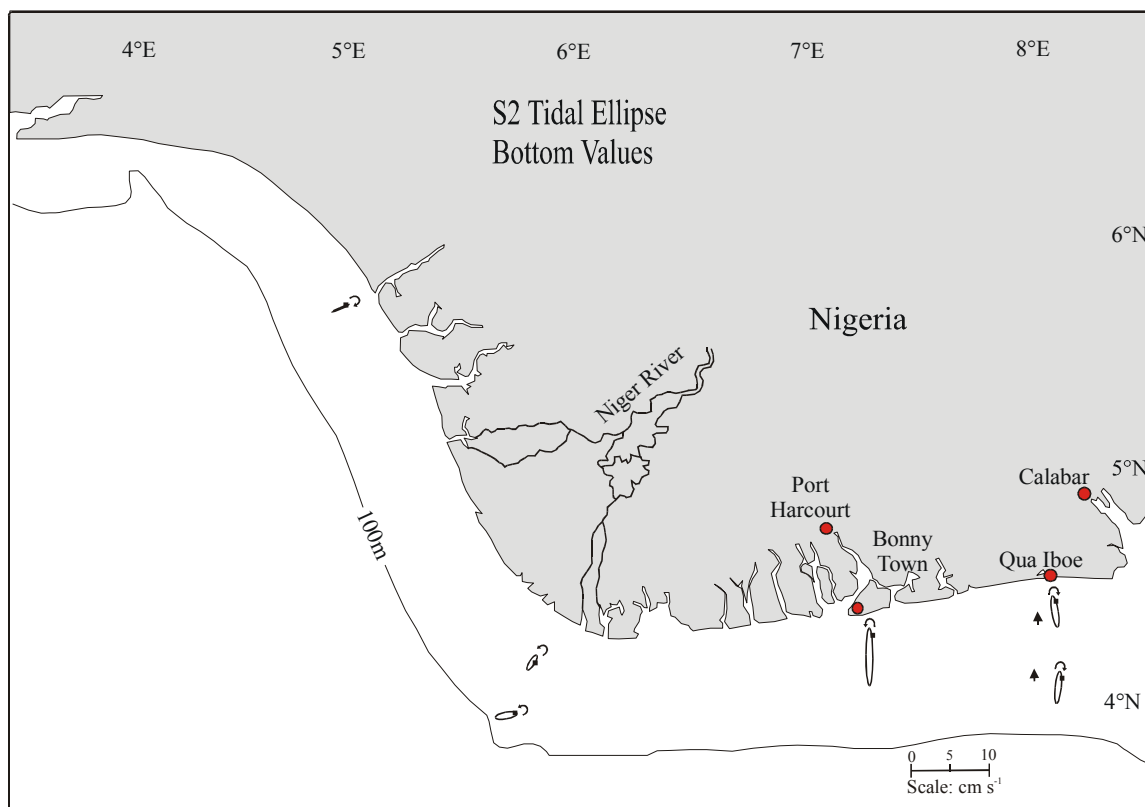
(b)

FIG. 12. Continued.



(c)

FIG. 12. Continued.



(d)

FIG. 12. Continued.

5. WATER MASS STRATIFICATION AND GEOSTROPHIC SHEAR

a. Seasonal Characterization Based on Five Cruises

In this section the water mass stratification observed during each of the five cruises of the field study is described and examined for indications of the circulation, including upwelling, and for influences of forcing by wind and river discharge. Cruises 1 and 5 were carried out in April and May, respectively, and are taken as indicative of conditions in spring. Cruises 2, 3 and 4 were made in July, October and February, respectively, and are taken as representative of summer, fall and winter.

For each cruise the following materials were prepared and examined, though not all are shown here:

Plots of T, S and sigma-t versus depth (pressure) for each CTD station,

Cross-shelf vertical sections of T and S,

Areal distributions of surface and bottom T, S and sigma-t.

Areal distributions of depths of selected isohalines (indicative of the amount of low salinity river water present) and

Vertical distribution of Brunt-Vaisala frequency for each CTD station.

Throughout the study period, lower salinities are seen in the eastern end of the study area. It was shown in Fig. 3 that the eastern end of the study region receives a higher amount of rainfall, which would account for the very low surface salinities. It was also shown in figs. 9 and 10 that line 5, on the eastern edge of the study region, receives a significantly higher amount of fresh water than the rest of the study area. From this it can be inferred that a higher amount of river discharge enters the eastern end of the study area, peaking in the fall; however the exact amount or source of the river discharge cannot be determined. It seems likely that drift from the Congo River could be responsible for the high volume of very low salinity water seen along lines 4 and 5. The following discussion of hydrography closely examines the effects of the river discharge

and rainfall on study area, giving insight into the spatial distribution of the fresh water and its sources.

1) April 2000; Cruise 1

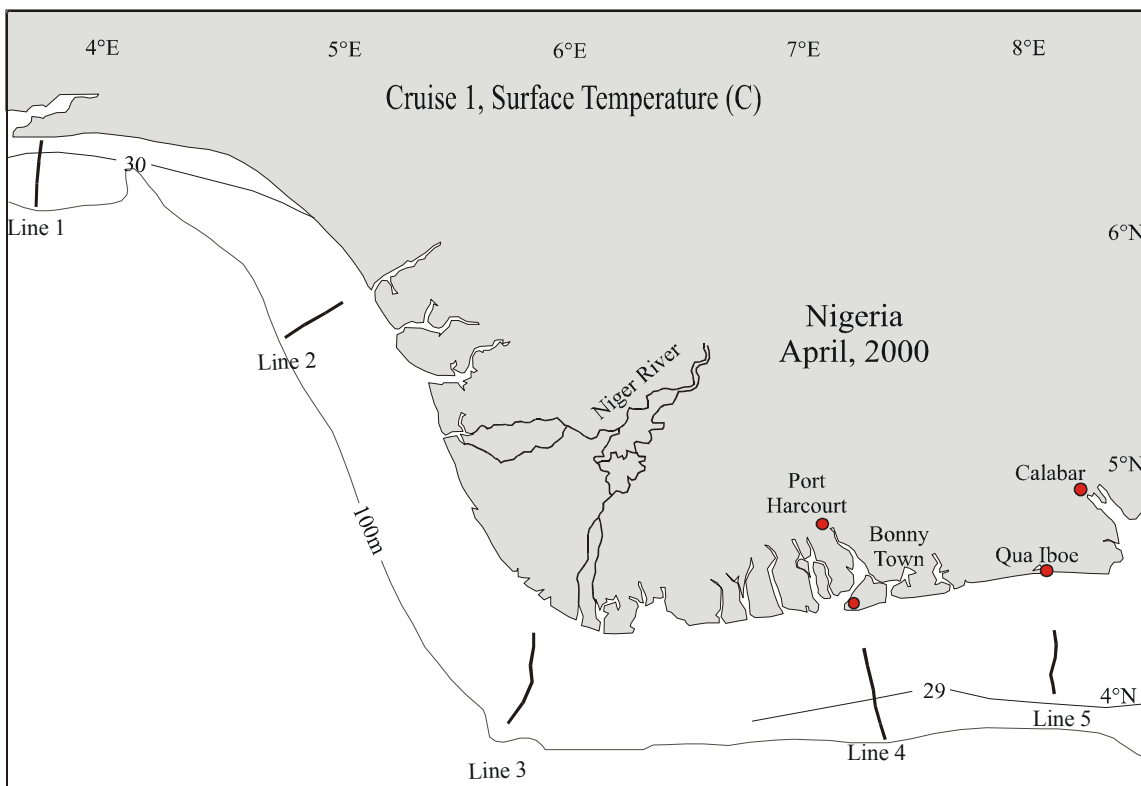
Cruise 1 was carried out 18-22 April 2000. The surface temperature distribution (Fig. 13) shows a homogenous surface layer with temperatures of 29°-30°C. Vertical sections of temperature on lines 1 through 5 are shown in Fig. 14. There was a layer of relatively uniform temperature (greater than 29°C) down to depths of 20-30 m throughout the study region. That the thermocline near 20-30 m corresponded to the seasonal pycnocline is seen by examination of vertical distributions of Vaisala frequency (Fig. 15). The general distribution and ranges of temperature are similar on all lines except 4, where colder water (less than 17°C) occurred at the bottom of the deepest section and the 29° isotherm was found above 10 m at the shallowest station. The bottom temperature distribution (Fig. 13) shows near-shore values greater than 29°C (27° on line 3), decreasing offshore with increasing depth to less than 19°C (17° on line 4).

The surface salinity distribution from Cruise 1 (Fig. 16) shows lower salinity water nearer the coast. Near-shore values increase westward from less than 29.5 on line 5 to near 32.5 on line 2; between line 2 and line 1, nearshore surface salinity decreased to less than 31. Fresh water sources appear to be the Cross and Qua Iboe rivers and Lagos Lagoon or rivers to the east.

Vertical cross-shelf sections of salinity are shown in Fig. 17, for lines 1 through 5. On all five lines there was a slight halocline near the thermocline, contributing to the seasonal pycnocline. On lines 1, 4, 5 and to lesser extent on line 3, a near surface halocline at the base of the lower salinity surface water was clearly present (see also Fig. 15 showing secondary pycnoclines in the vertical distributions of Viasala frequency). Salinity values in the deeper portions of each section are between 35.5 and 36, except for line 2 where two regions having $S > 36$ are seen. Salinities values on line 2 are generally greater than on the other lines. Moreover, the lower salinity surface waters on line 2 are confined to very near-shore, resulting in a nearly horizontal halocline within the surface layers; consequently there is no salinity contribution to a vertical pycnocline (Fig. 15).

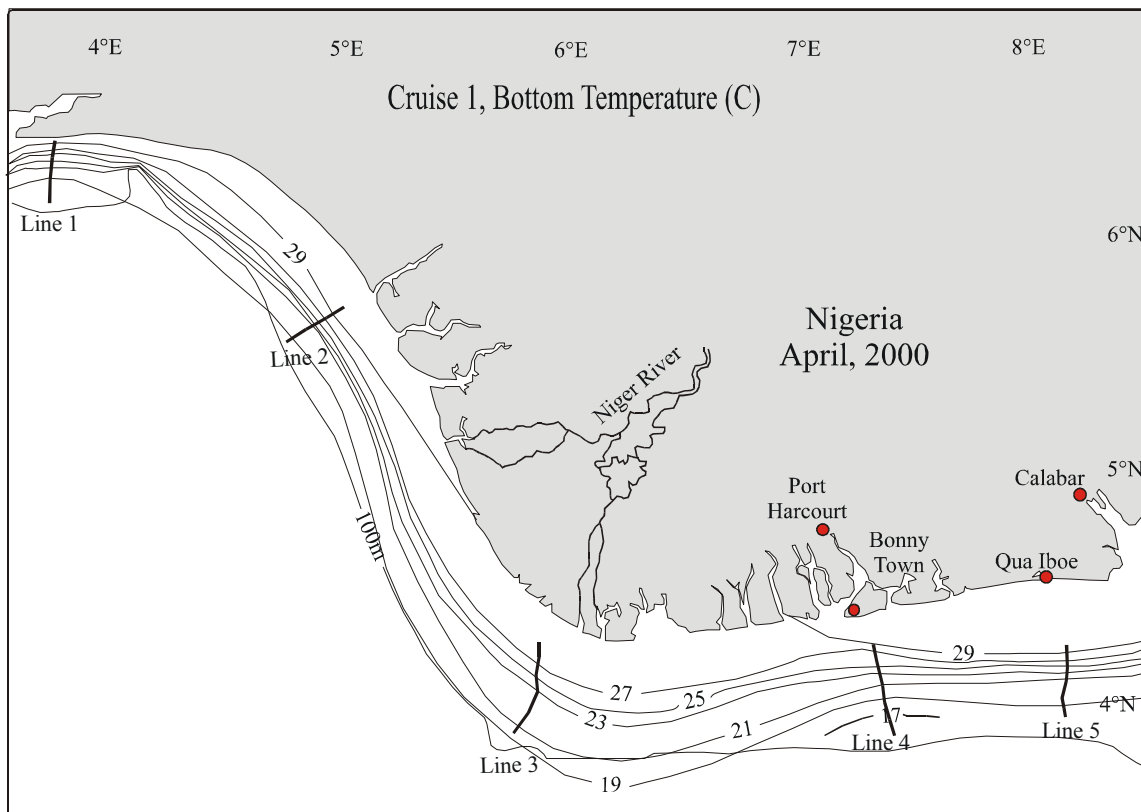
The bottom salinity distribution (Fig. 16) shows near-shore values greater than 32, except at line 5, where slightly lower values are seen.

It should be noted that the strength of the stratification (seen in Fig. 15 and in Brunt-Vaisala Frequency plots shown later in Section 5) indicated by the Brunt-Vaisala Frequency (N^2) is phenomenal. An N^2 value of 0.01, seen throughout the study area and throughout the year, corresponds to an oscillation with a period of about 10 seconds. To gain an appreciation for the strength of this stratification, the deep ocean has N^2 values corresponding to periods of 3-5 hours, and textbook guidelines indicate that the shortest periods are at about 1 minute for large density gradients.



(a)

FIG. 13. Surface and bottom temperature contours (from CTD measurements) on Cruise 1.



(b)

FIG. 13. Continued.

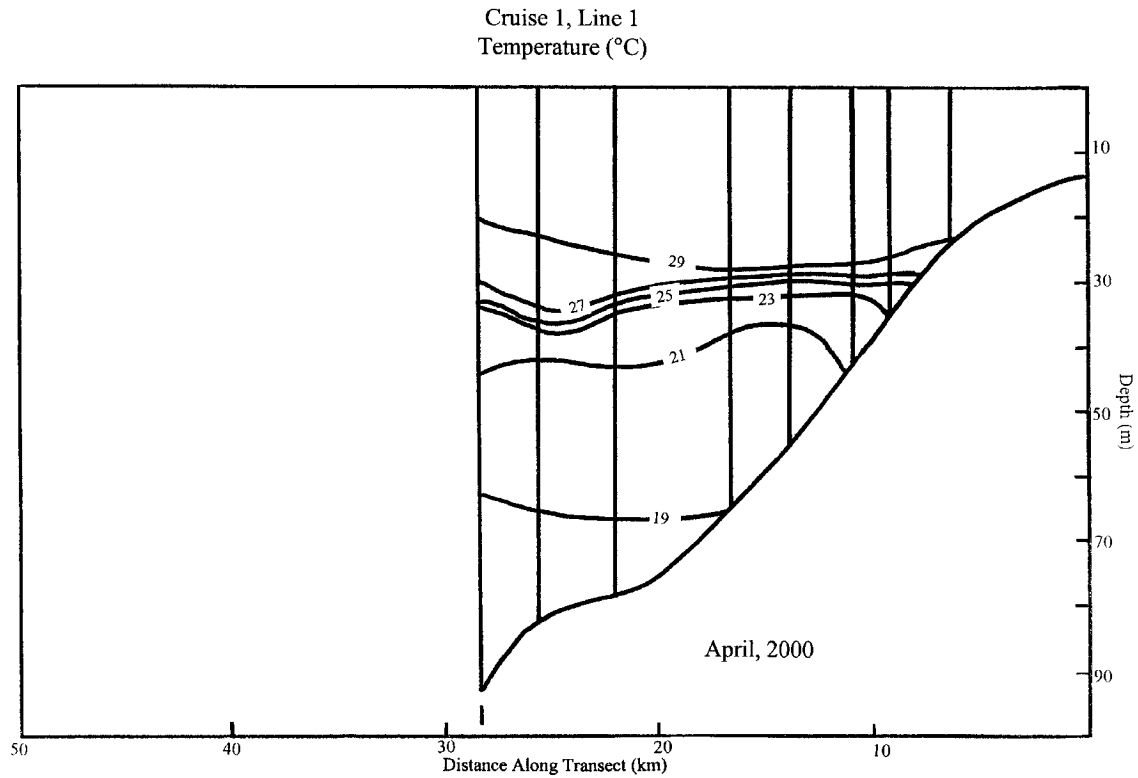
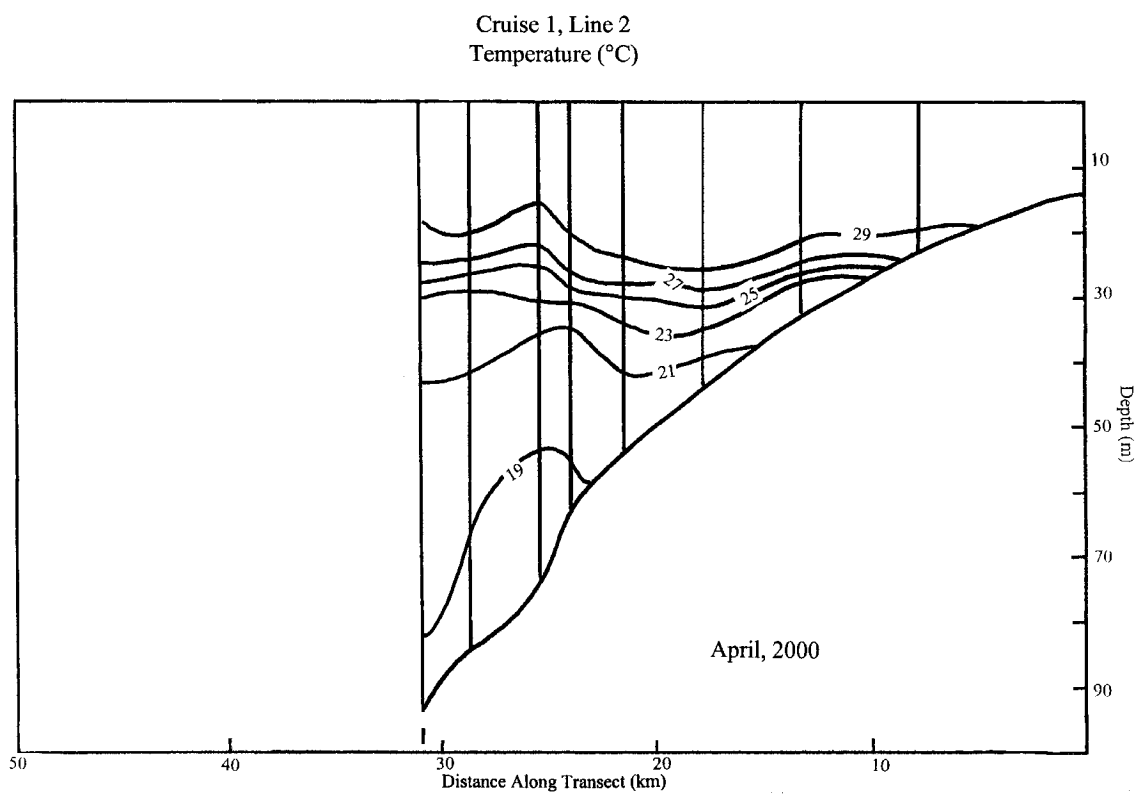
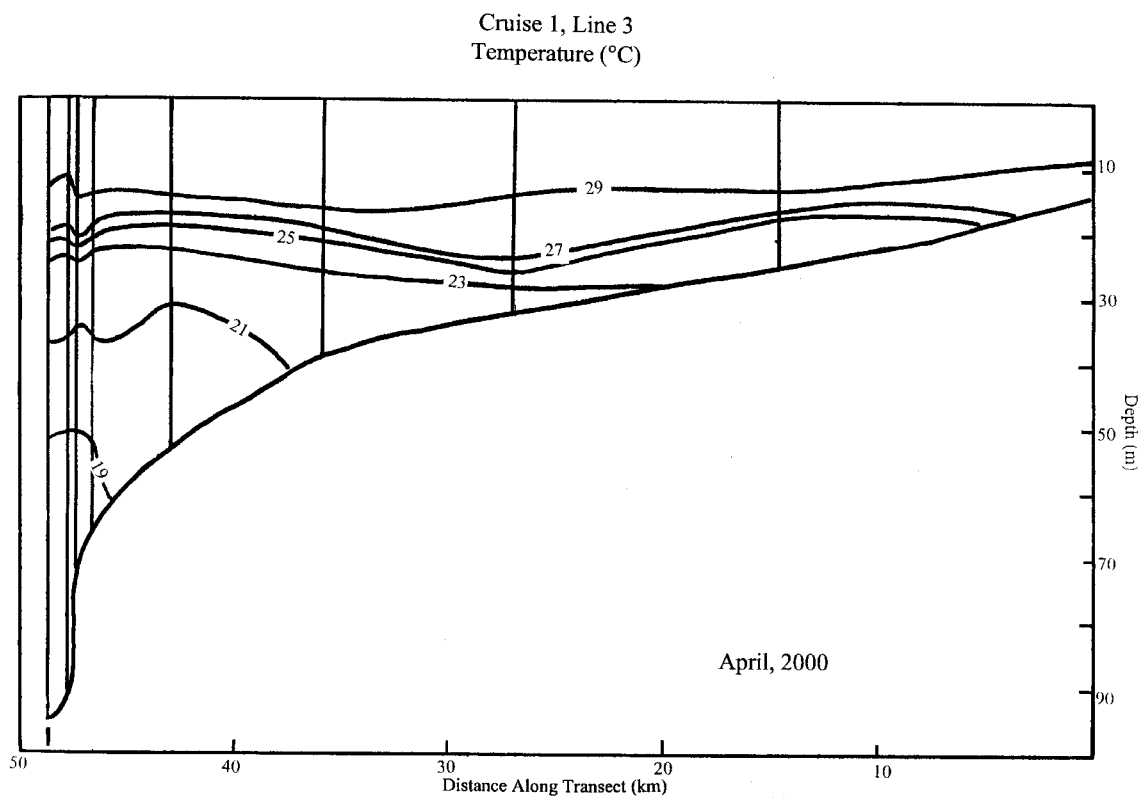


FIG. 14. (a)-(e) Cross sections of temperature contours (from CTD measurements along lines 1-5) on Cruise 1. Vertical lines represent sites of measurements on each line.



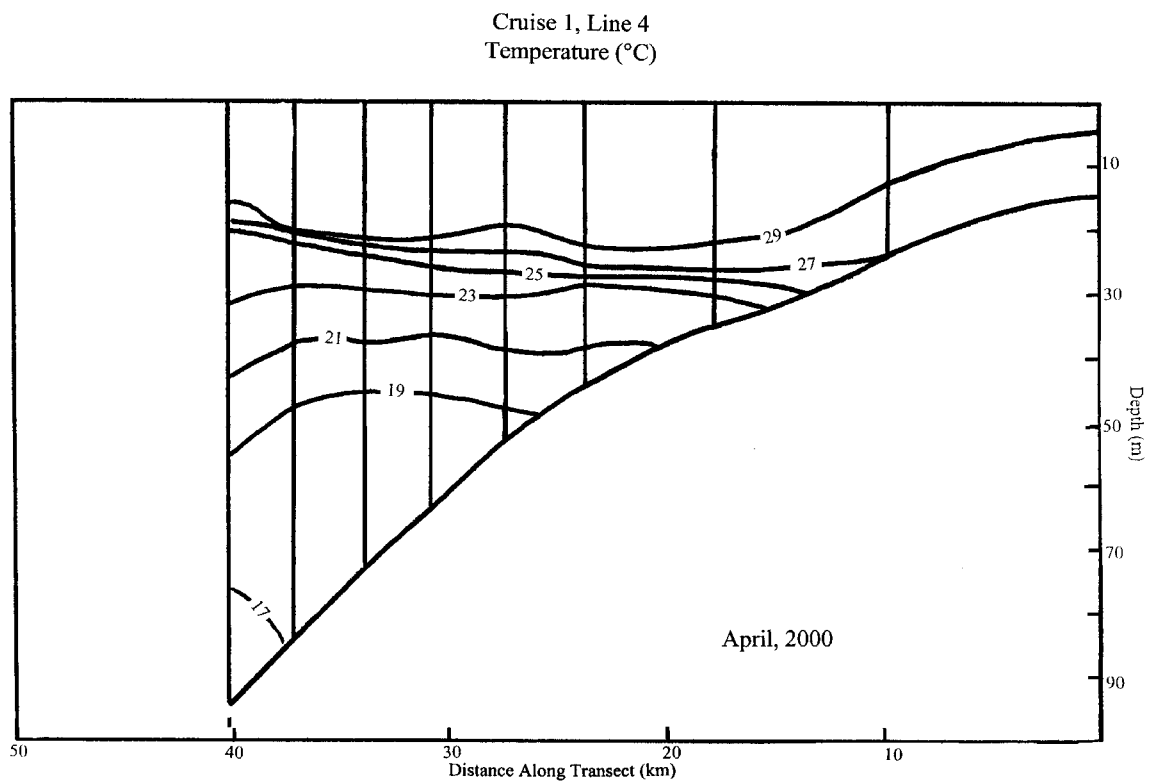
(b)

FIG. 14. Continued.



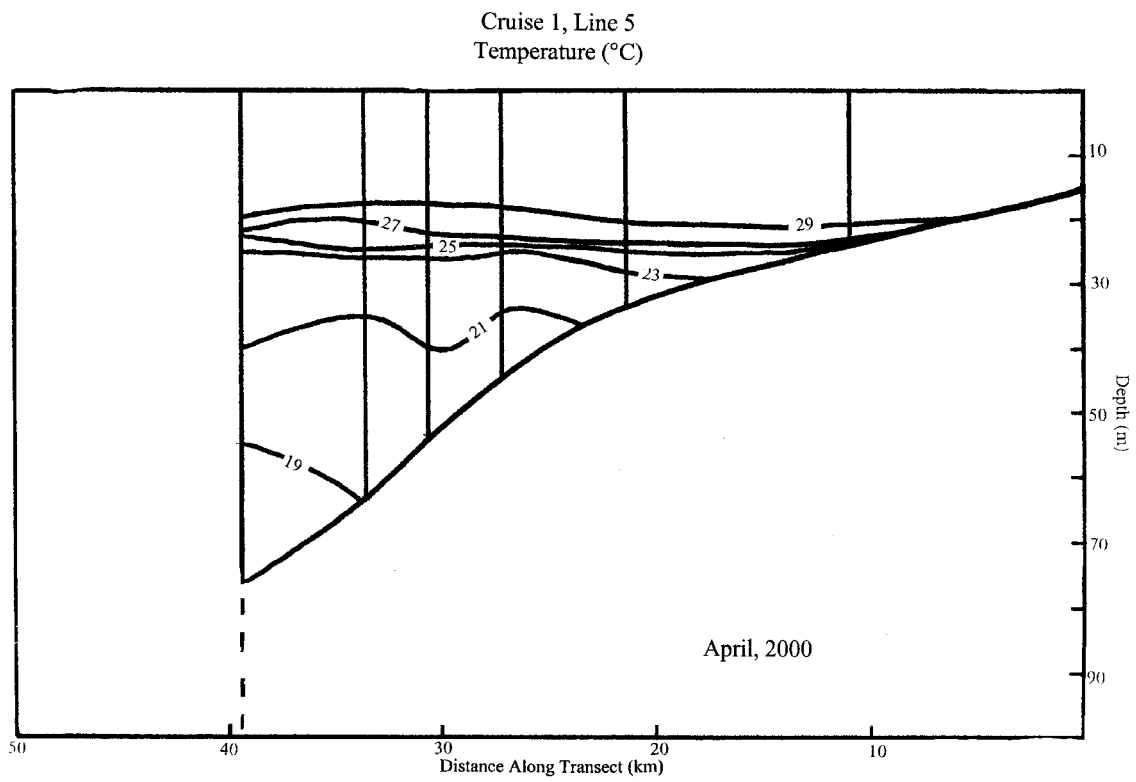
(c)

FIG. 14. Continued.



(d)

FIG. 14. Continued.



(e)

FIG. 14. Continued.

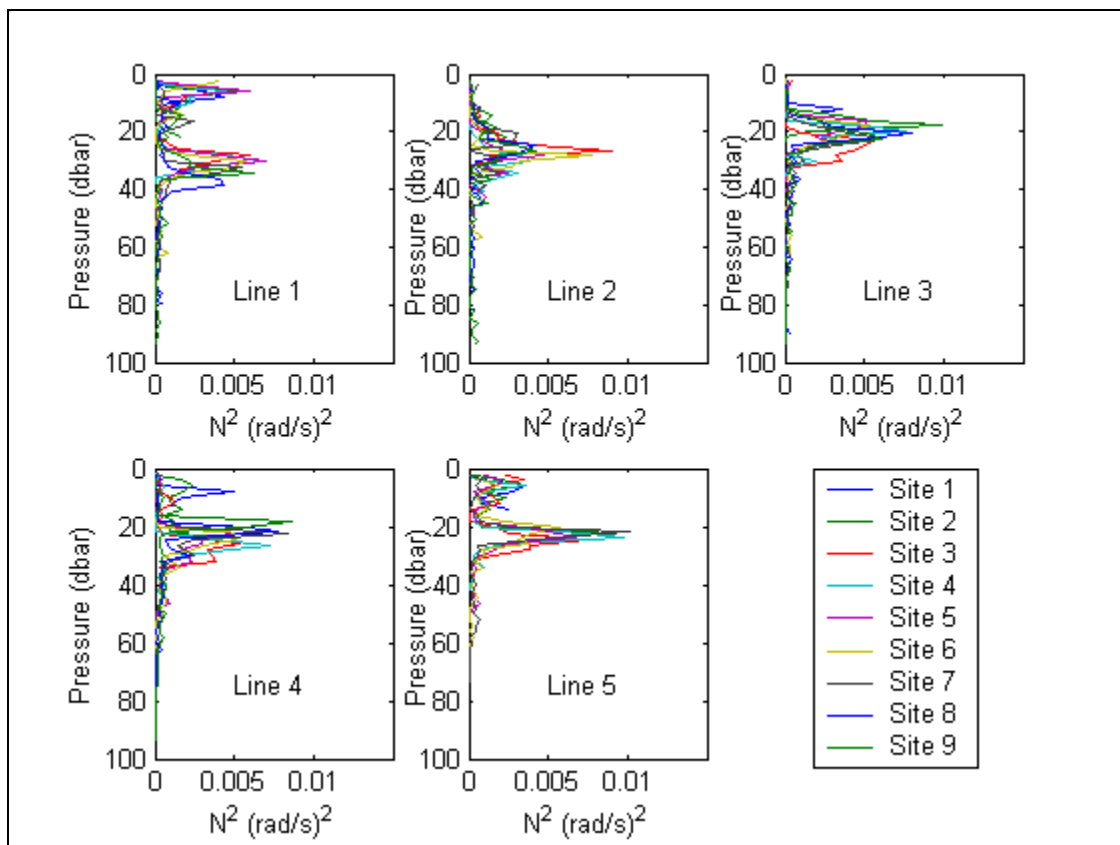
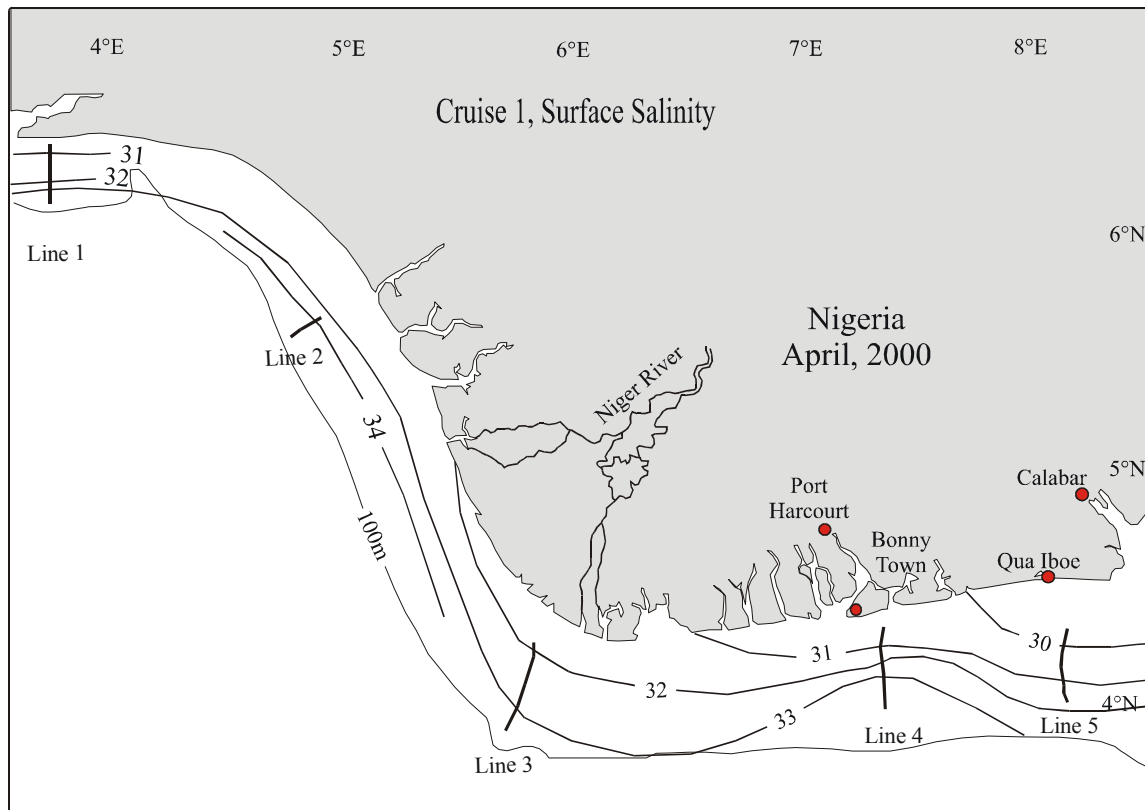
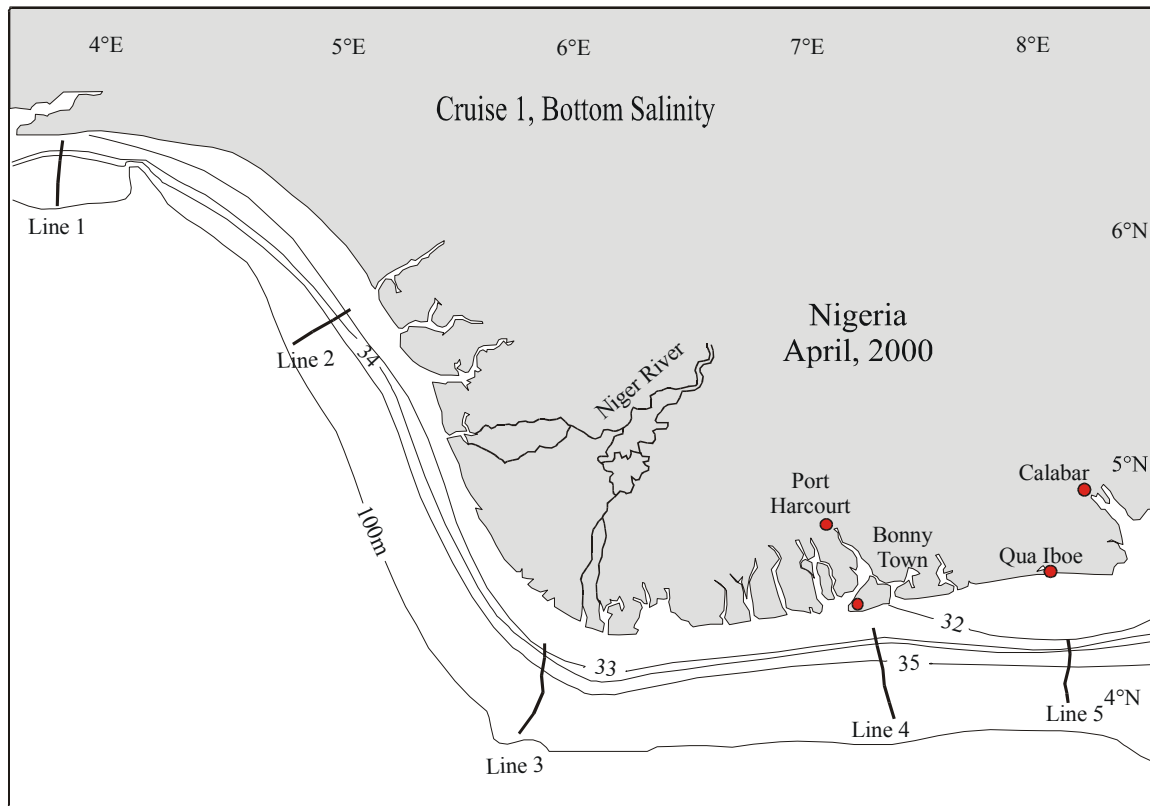


FIG. 15. Brunt Vaisala frequency for Cruise 1 (calculated from CTD measurements).



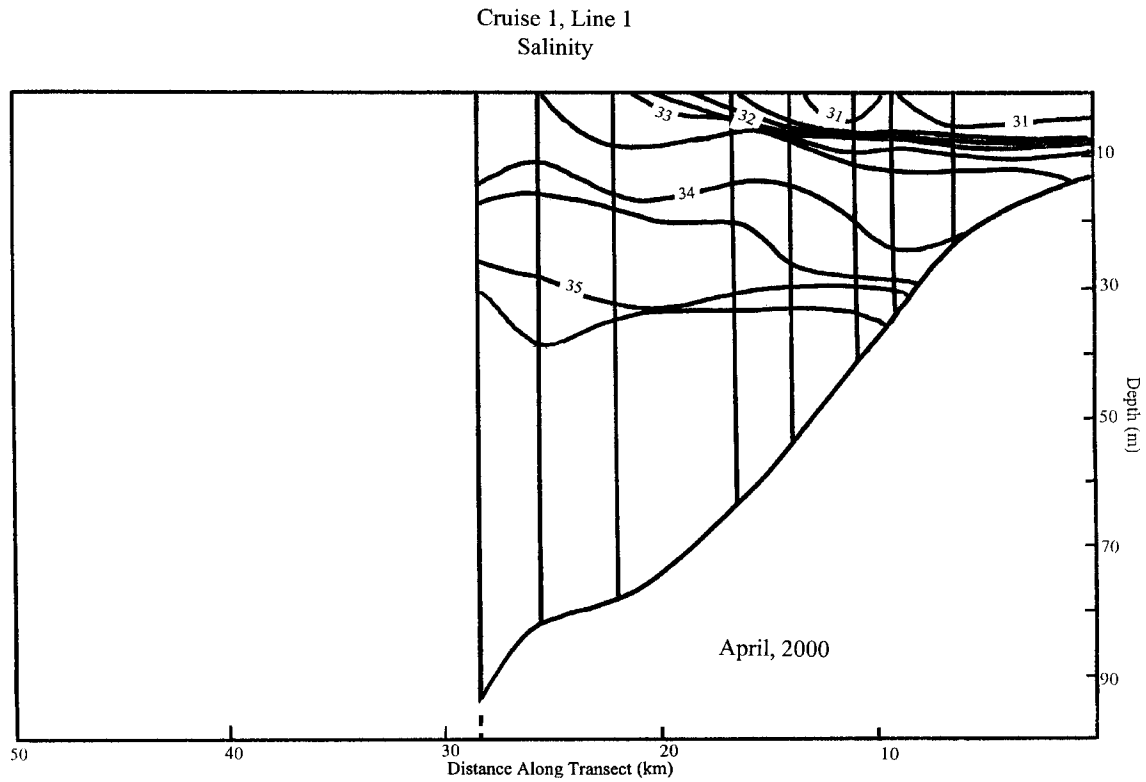
(a)

FIG. 16. Surface and bottom salinity contours (from CTD measurements) on Cruise 1.



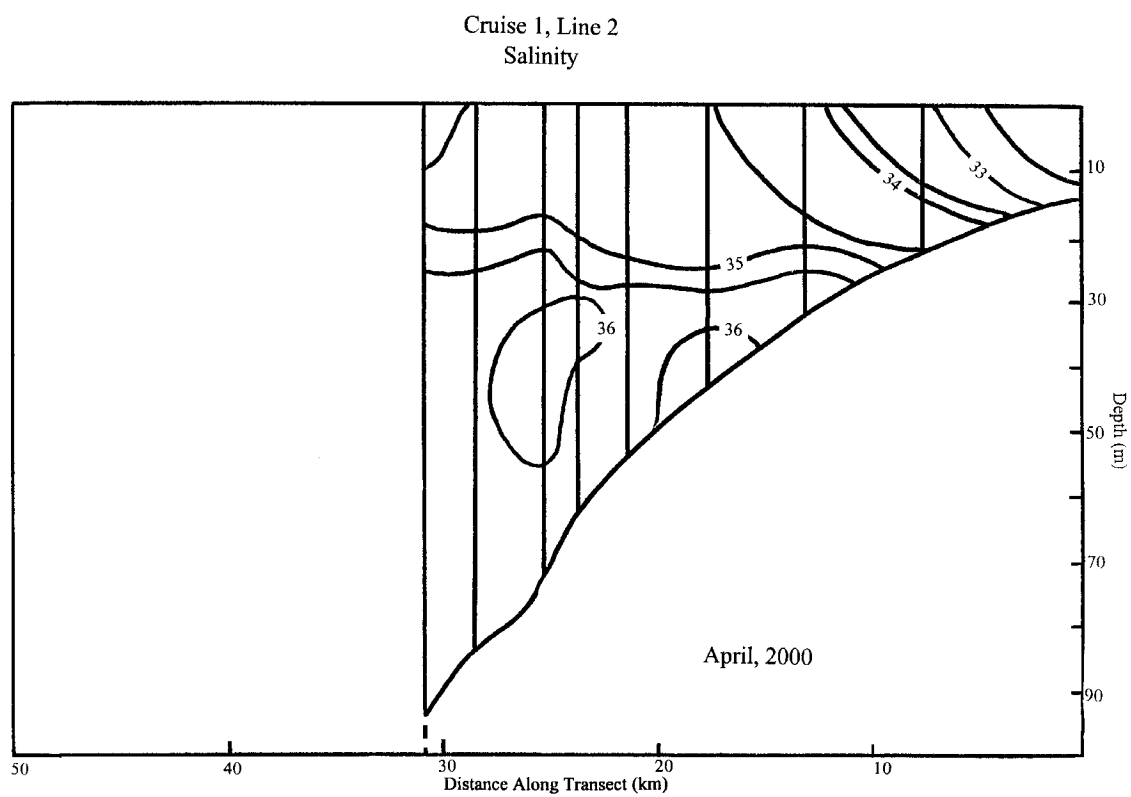
(b)

FIG. 16. Continued.



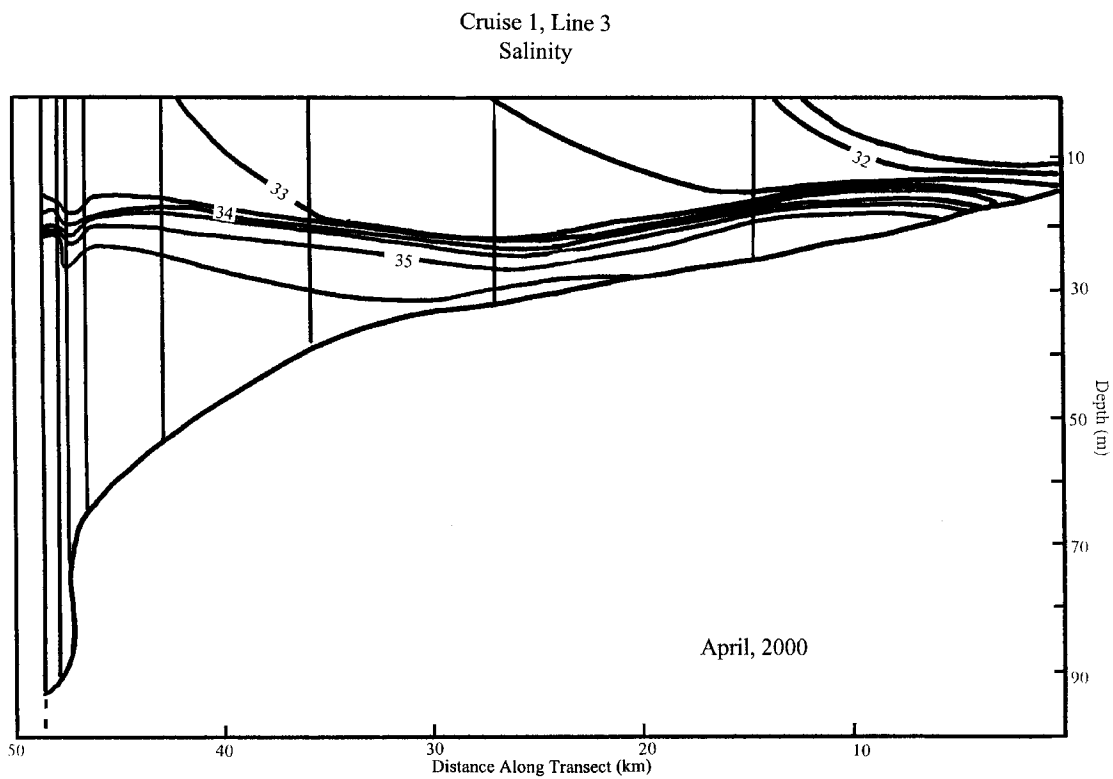
(a)

FIG. 17. (a)-(e) Cross sections of salinity contours (from CTD measurements along lines 1-5) on Cruise 1. Vertical lines represent sites of measurements on each line.



(b)

FIG. 17. Continued.



(c)

FIG. 17. Continued.

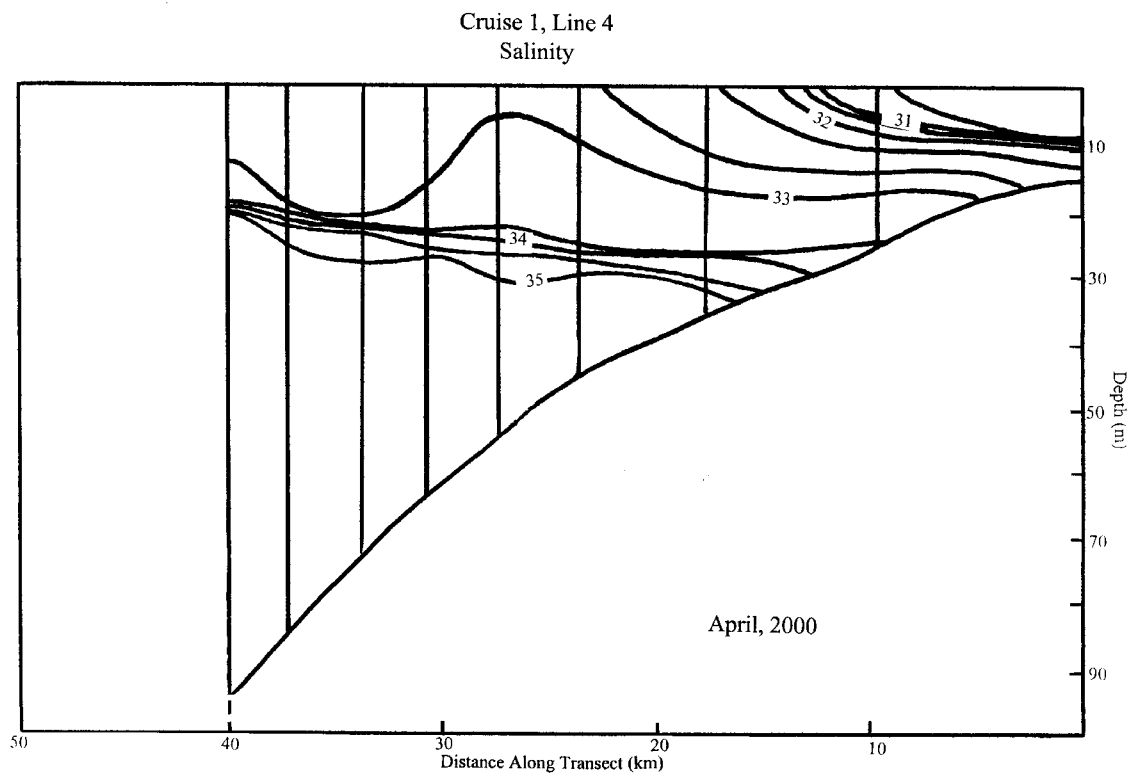
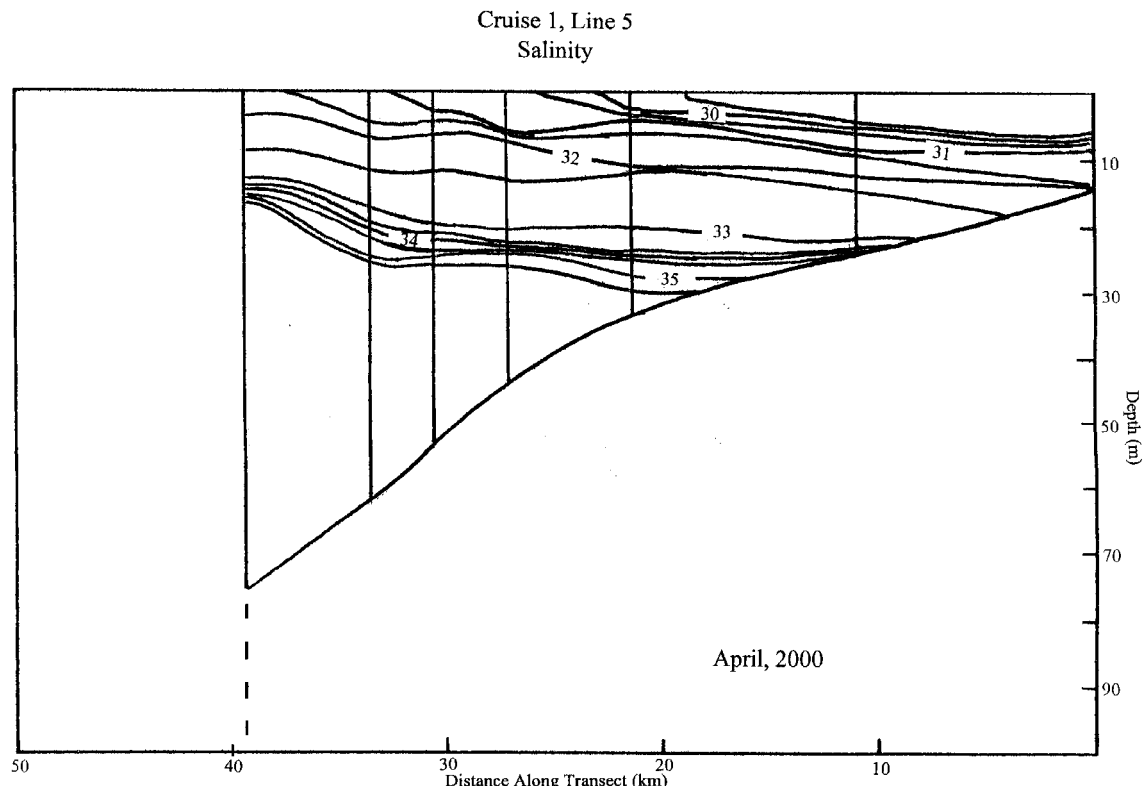


FIG. 17. Continued.



(e)

FIG. 17. Continued.

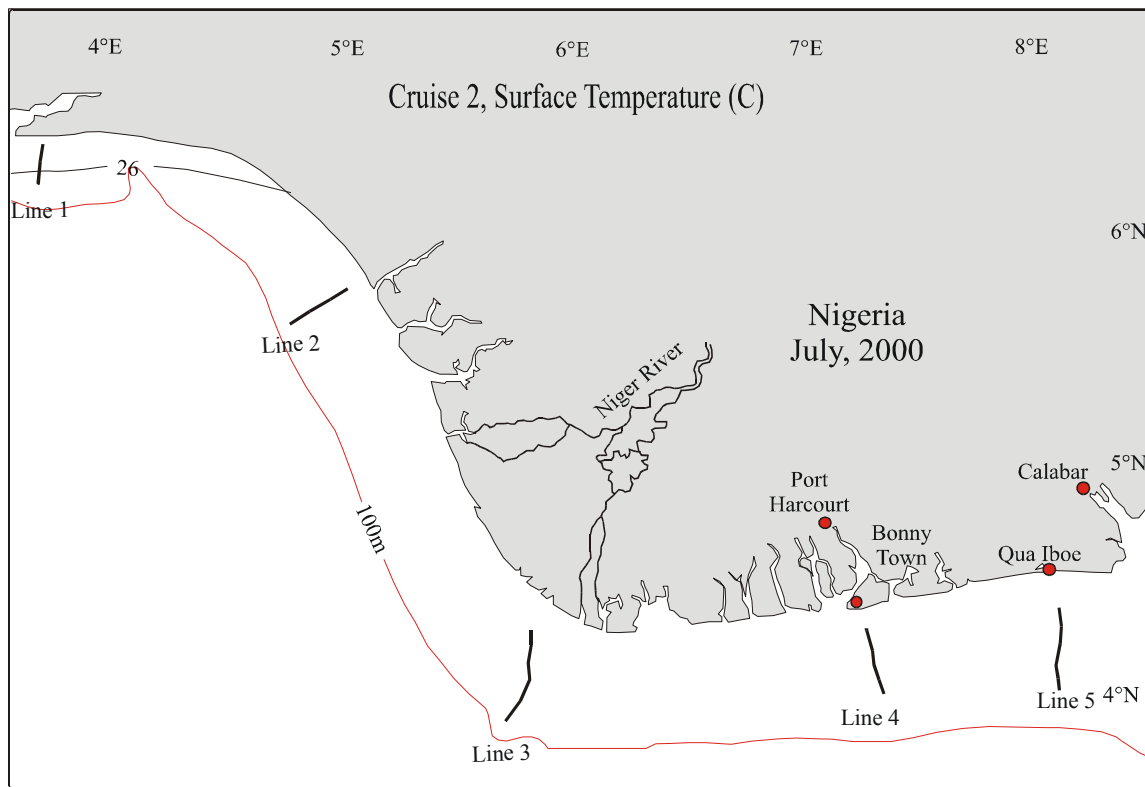
2) July 2000; Cruise 2

Cruise 2 was carried out 22-26 July 2000. The surface temperature distribution (Fig. 18) shows a homogenous surface layer with temperatures between 25° and 26°C , except near the coast on line 5 where $T > 26^{\circ}\text{C}$. Vertical sections of temperature on lines 1 through 5 are shown in Fig. 19. There was a layer of relatively uniform temperatures $> 25^{\circ}\text{C}$ down to depths of 25-35 m throughout the study region, with the exception of the minor appearance of water warmer than 27°C in lines 4 and 5 at the deeper stations. The thermocline is at 35 m depth along line 5, rising westward to 25 m at line 1. The ranges of temperature are similar on all lines (17° - 25°C); however, the thermocline generally weakens westward from line 5. These features are reflected in the depth and strength of the main pycnocline seen in the vertical distributions of Brunt-Vaisala frequency for lines

1-5 (Fig. 20). The bottom temperature distribution (Fig. 18b) shows near-shore values between 26° and 27°C, decreasing as depth increases to less than 17°C.

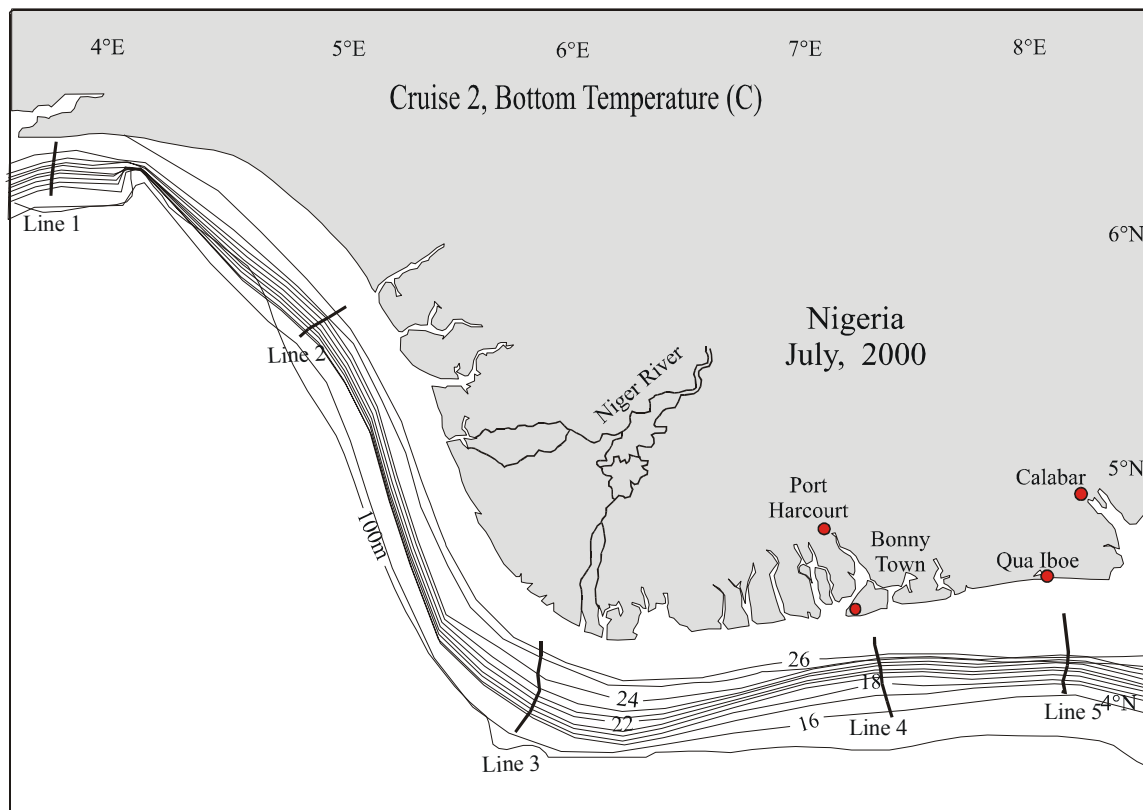
The surface salinity distribution from Cruise 2 (Fig. 21a) shows lower salinity water near the coast except on line 1. Low-salinity water is concentrated in the eastern end of the study area extending seaward over line 5 nearly to the 100 m isobath. The freshest near-shore surface water was observed on line 3. Vertical cross-shelf sections of salinity are shown in Fig. 22 for lines 1 through 5. Line 1 has no halocline, with salinities ranging from 35-36 throughout the section. On lines 2-5 there was a slight halocline near the thermocline, contributing to the seasonal pycnocline. On lines 2, 3 and 5 a near-surface halocline at the base of the lower salinity surface water was clearly present (also seen in Fig. 20 showing vertical distributions of Viasala frequency). The lower salinity surface waters on line 4 are confined to very near-shore, resulting in a nearly horizontal salinity gradient near shore; consequently there is no salinity contribution to a vertical pycnocline (Fig. 20). Salinity values in the deeper portions of each section are between 35.5 and 36. The 35 m isohaline rises (moving westward) from 40 m on line 5 to 5 m on line 1. The waters become more saline east to west, from line 5 to line 1. The bottom salinity distribution (Fig. 21b) shows near-shore values ranging from greater than 30 to greater than 35 generally increasing westward from line 5.

The water mass as a whole is 2- to 4°C cooler than in April. There is evidence of upwelling on line 1: the salinity is high and homogenous. Upwelling could be occurring in lines 2-5 as well; however, positive evidence is masked by the westward near-shore flow of river discharge strongly influencing the hydrographic characteristics on these lines. The river discharge is much higher than it was in April with the eastern end of the study region receiving the greatest amount of fresh-water inflow.



(a)

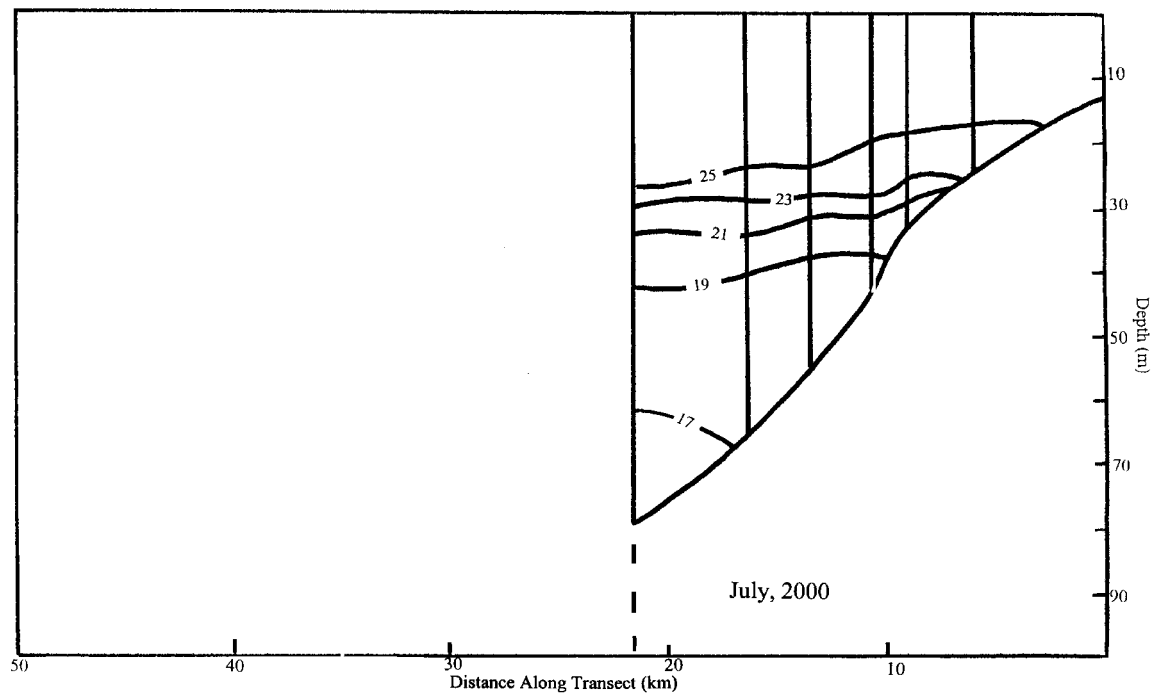
FIG. 18. Surface and bottom temperature contours (from CTD measurements) for Cruise 2.



(b)

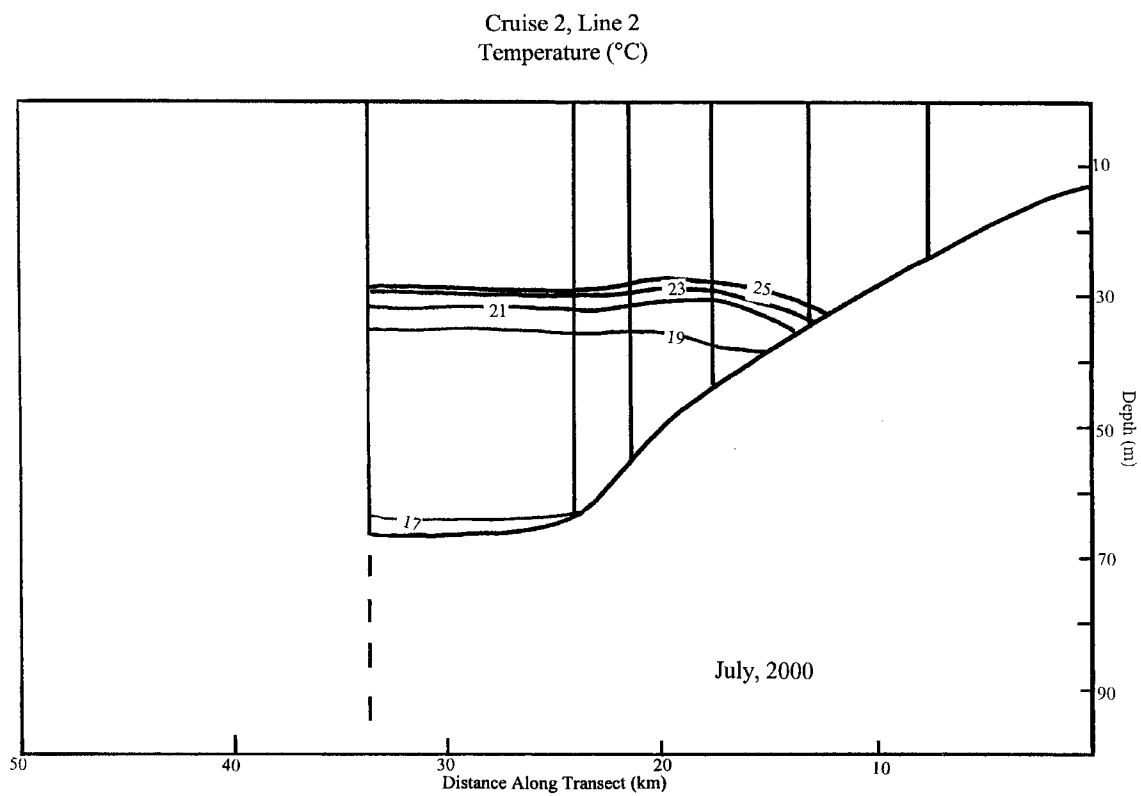
FIG. 18. Continued.

Cruise 2, Line 1
Temperature (°C)



(a)

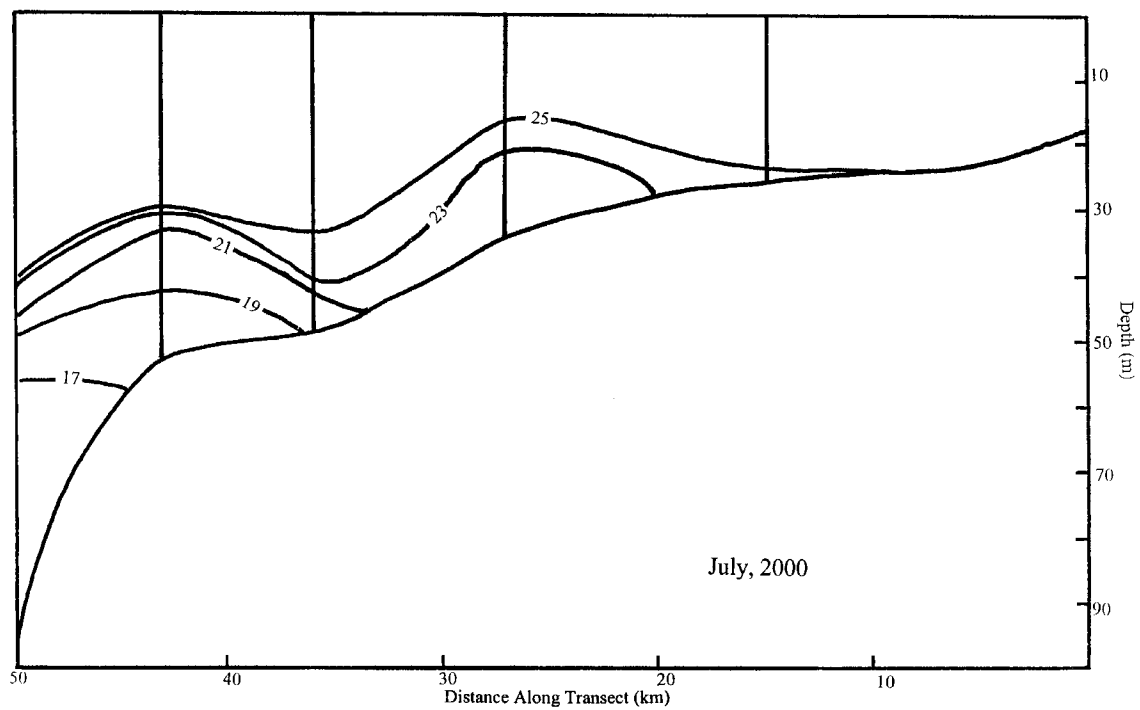
FIG. 19. (a)-(e) Cross sections of temperature contours (from CTD measurements along lines 1-5) for Cruise 2. Vertical lines represent sites of measurements on each line.



(b)

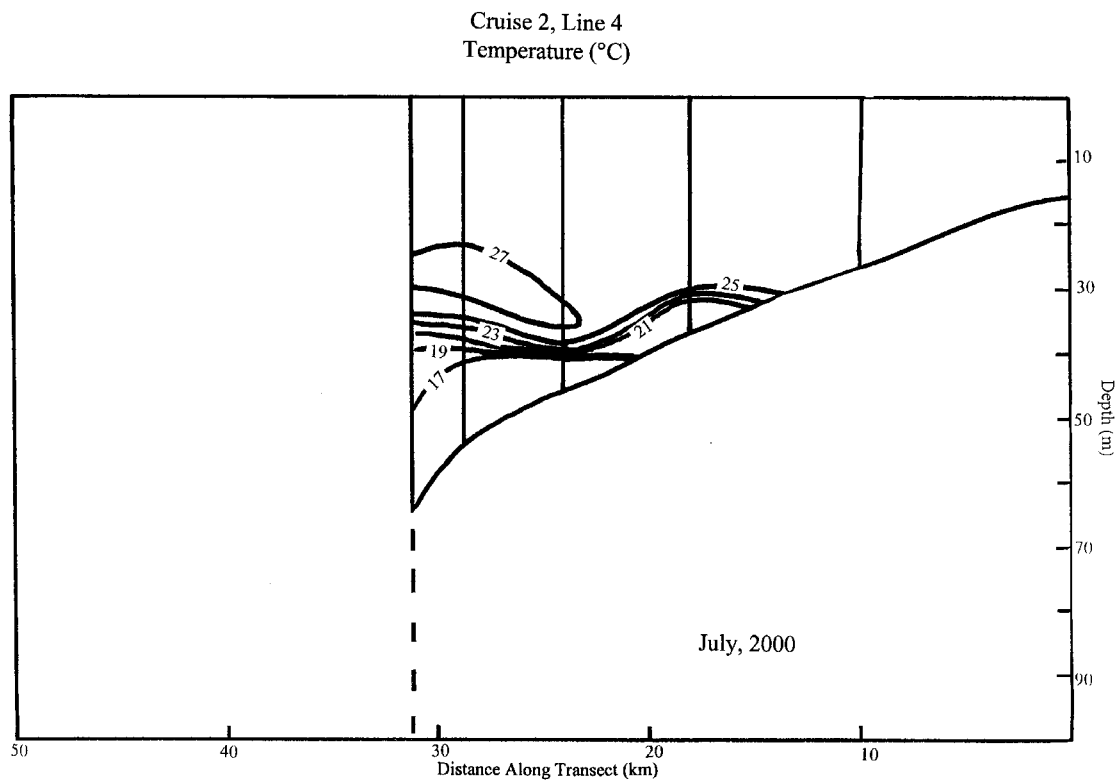
FIG. 19. Continued.

Cruise 2, Line 3
Temperature (°C)



(c)

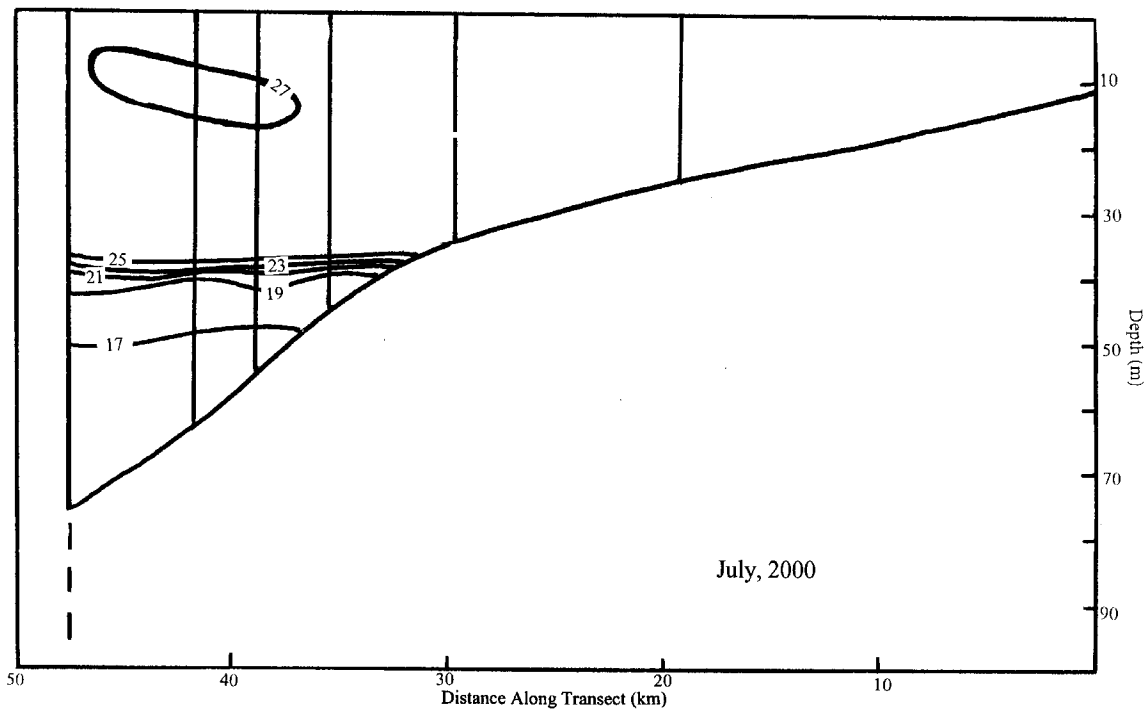
FIG. 19. Continued.



(d)

FIG. 19. Continued.

Cruise 2, Line 5
Temperature (°C)



(e)

FIG. 19. Continued.

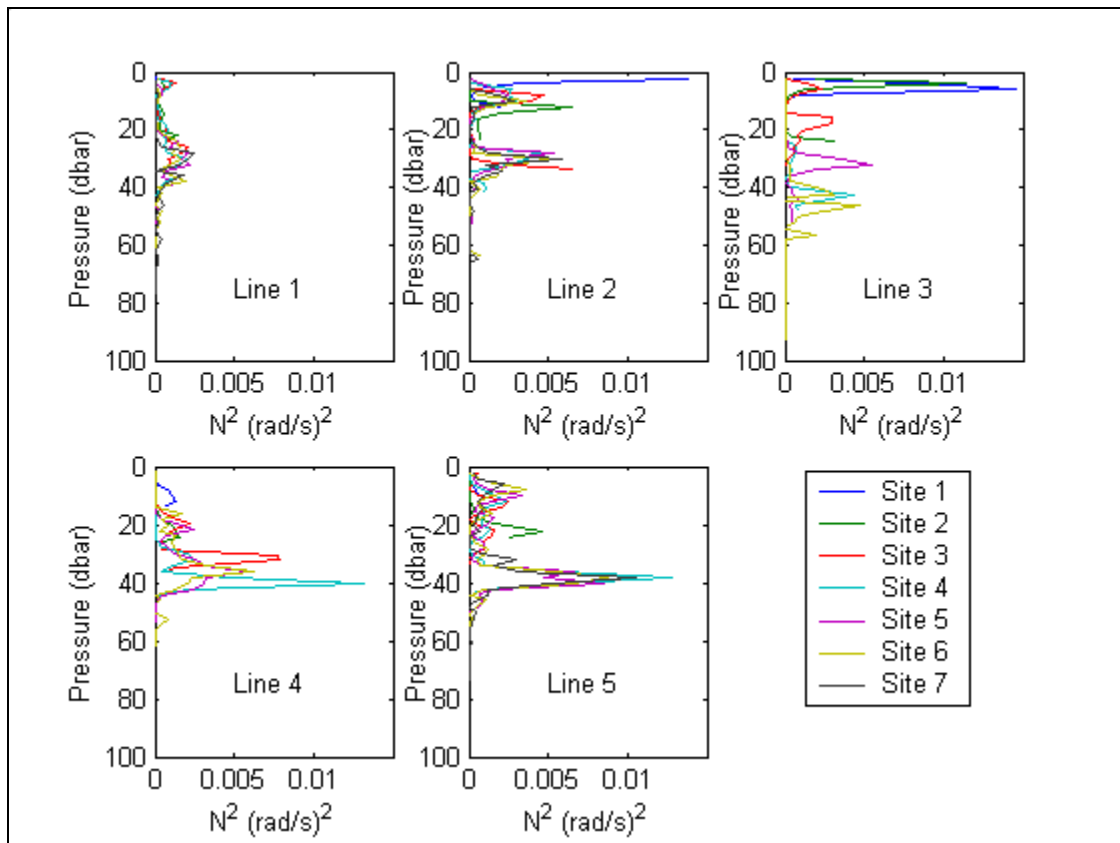
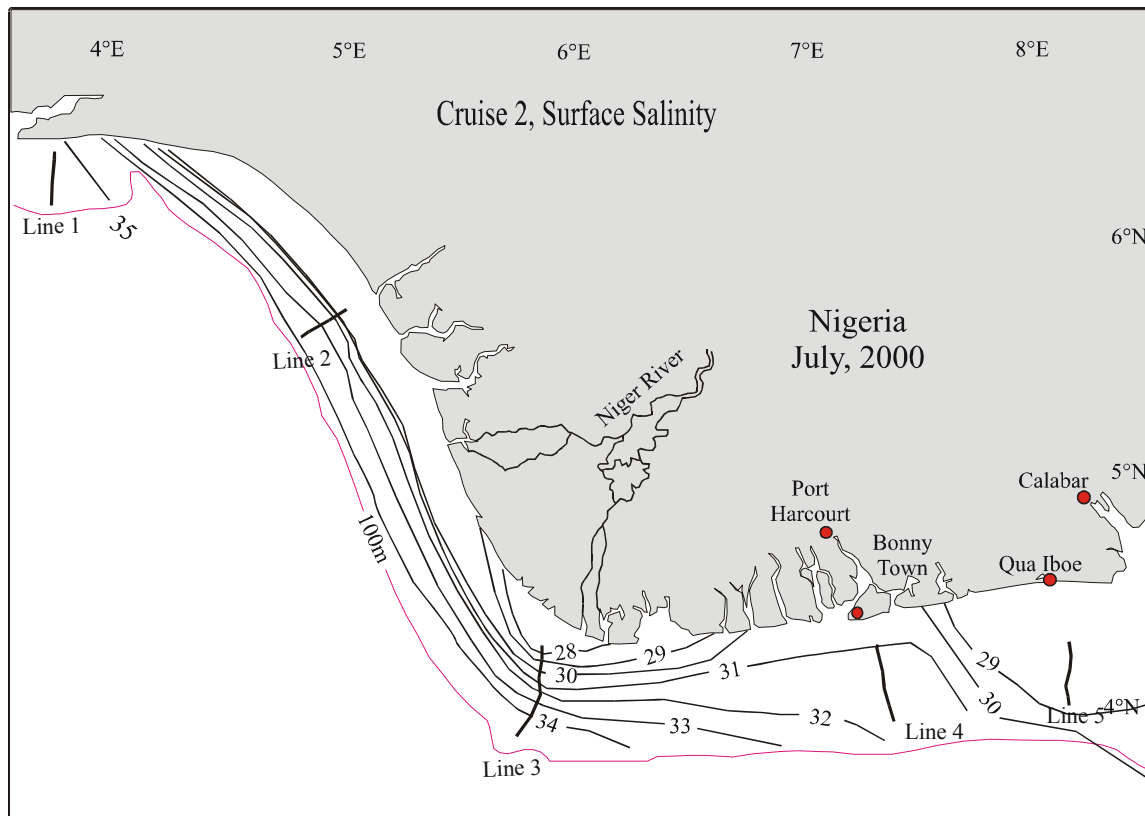
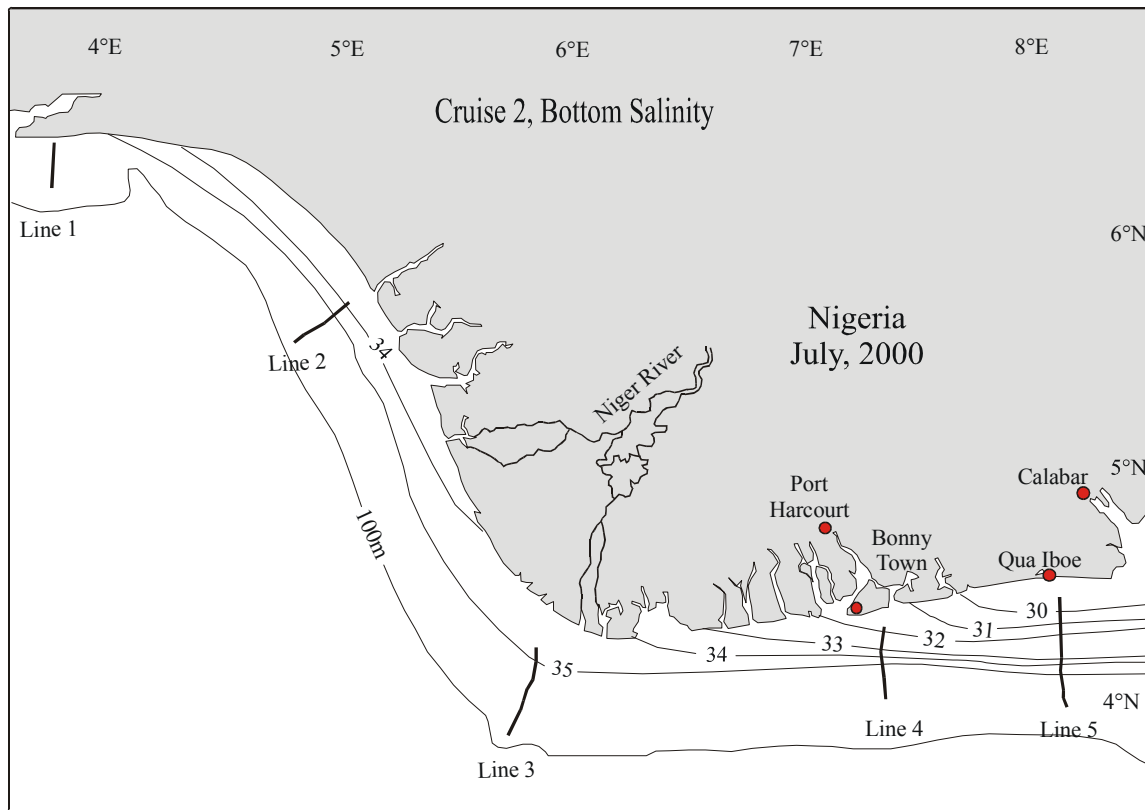


FIG. 20. Brunt Vaisala frequency for Cruise 2 (calculated from CTD measurements).



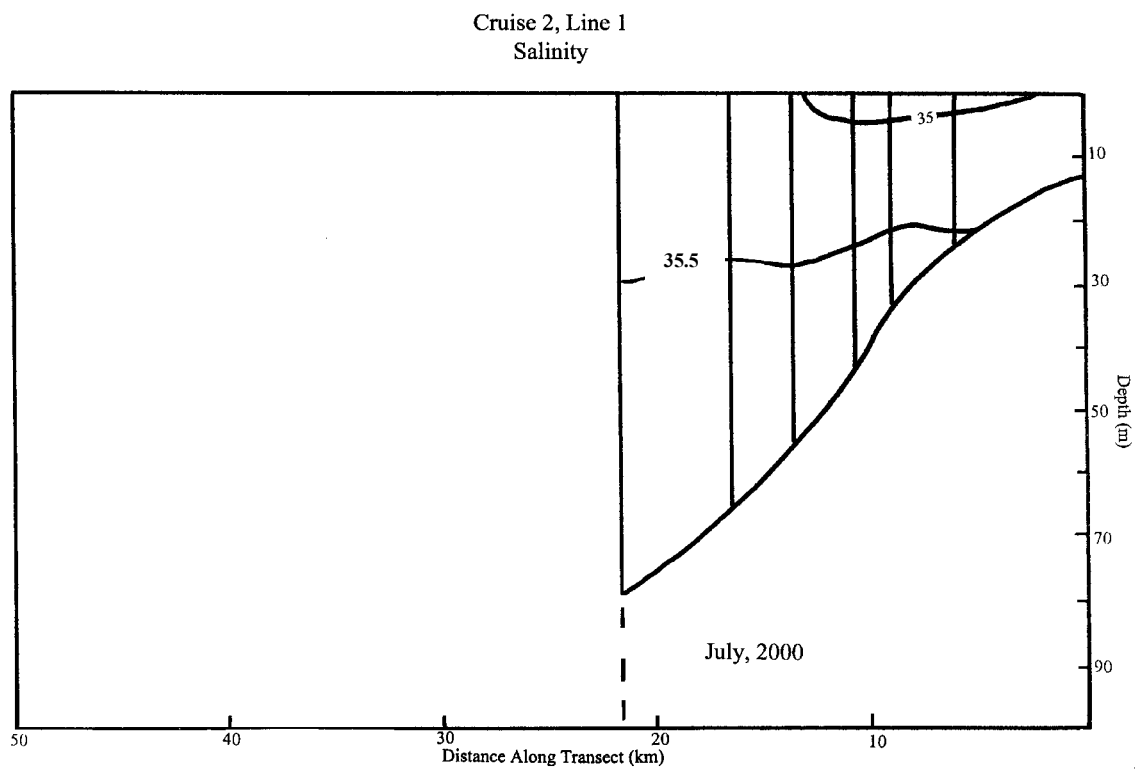
(a)

FIG. 21. Surface and bottom salinity contours (from CTD measurements) for Cruise 2.



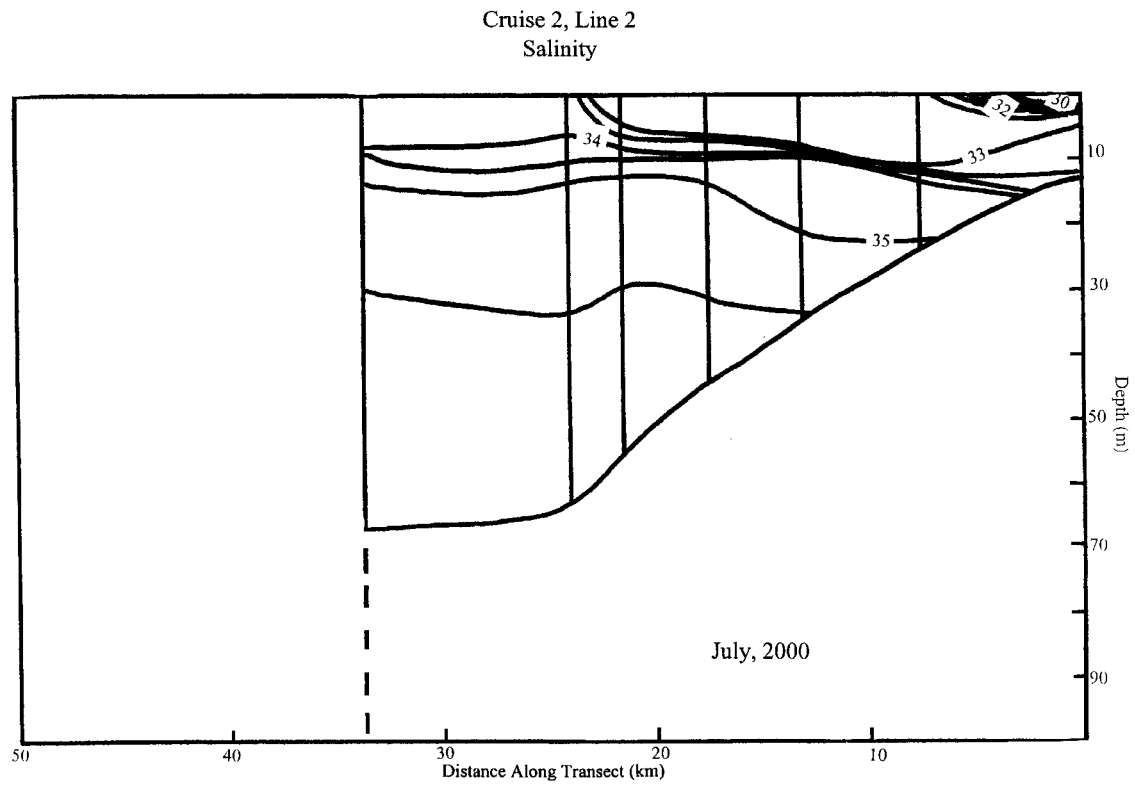
(b)

FIG. 21. Continued.



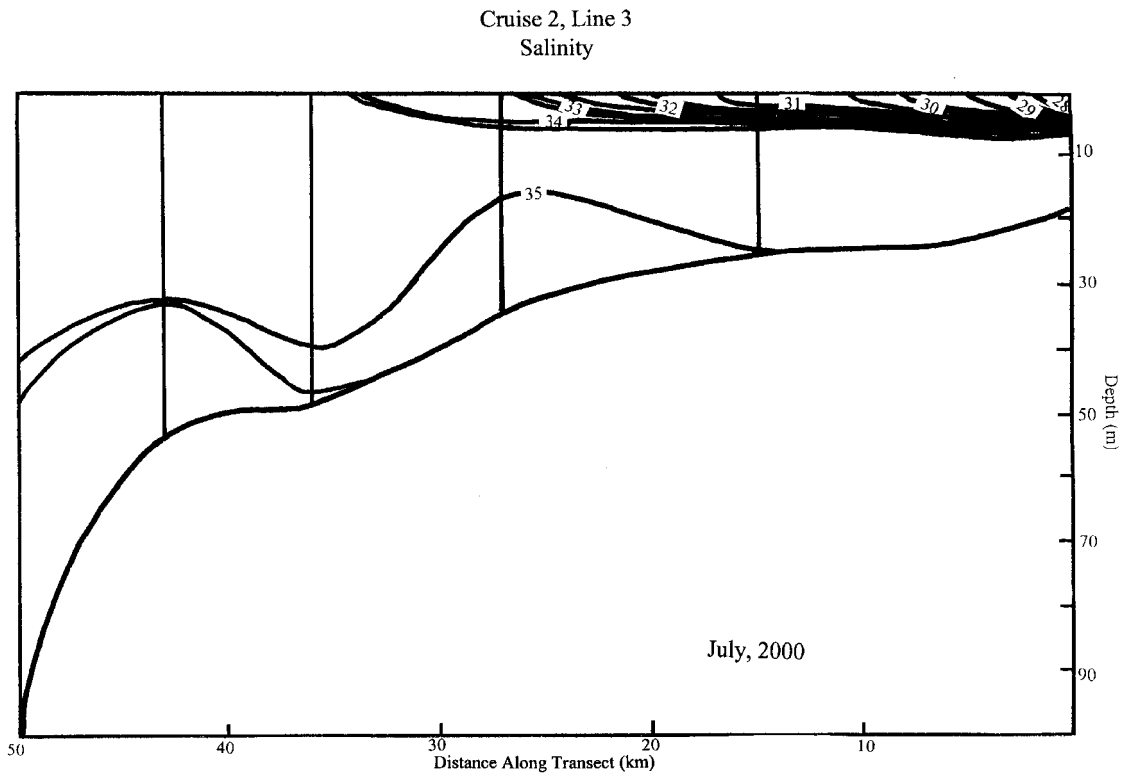
(a)

FIG. 22. (a)-(e) Cross sections of salinity contours (from CTD measurements along lines 1-5) for Cruise 2. Vertical lines represent sites of measurements on each line.



(b)

FIG. 22. Continued.



(c)

FIG. 22. Continued.

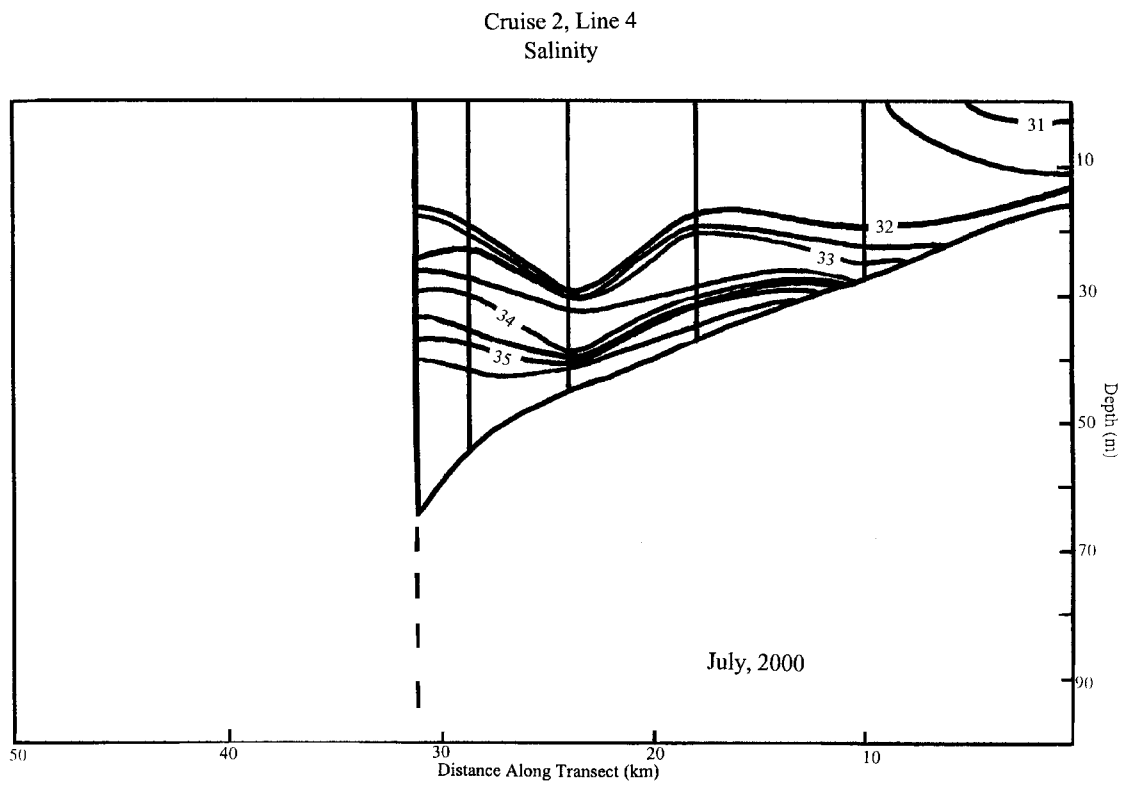
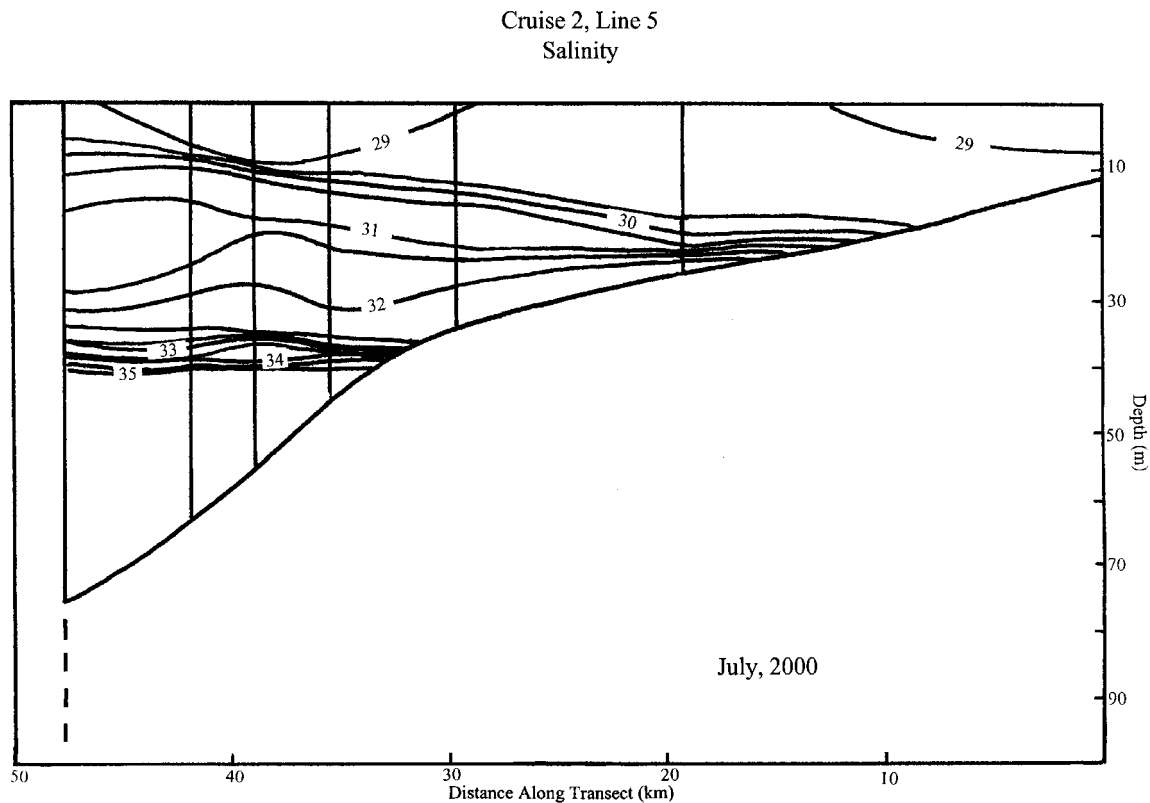


FIG. 22. Continued.



(e)

FIG. 22. Continued.

3) October 2000; Cruise 3

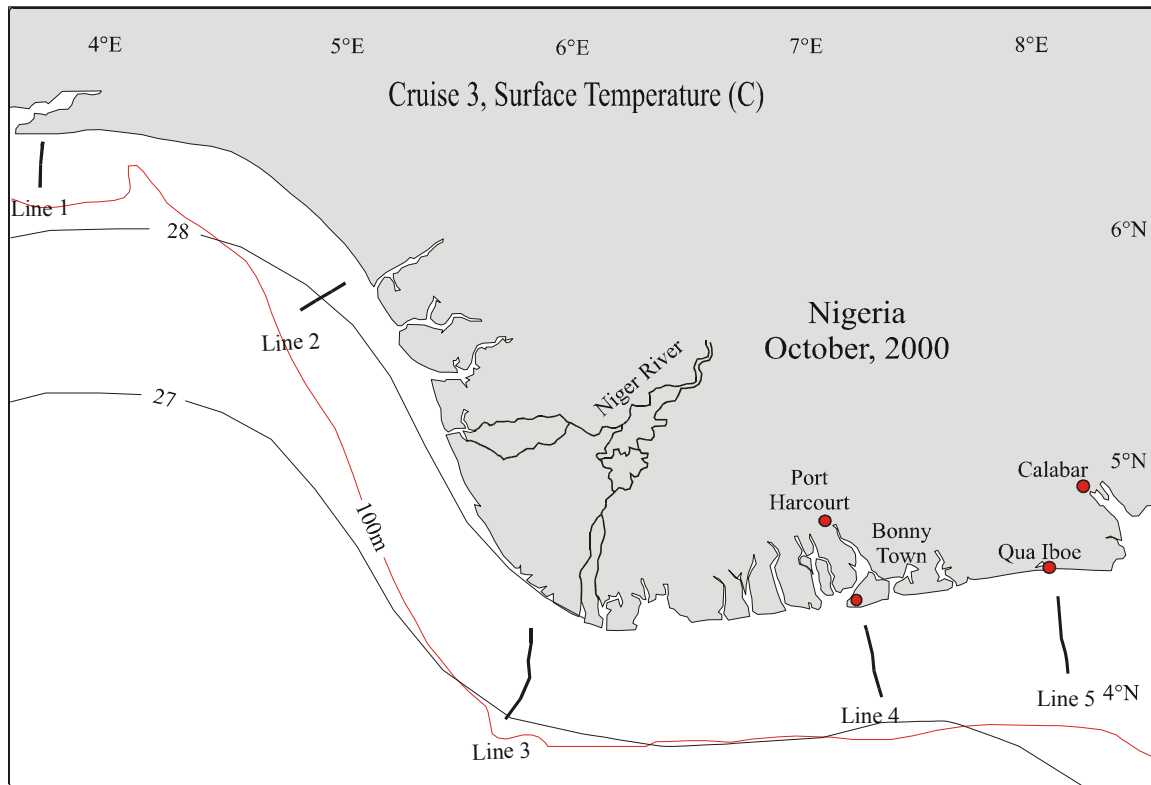
Cruise 3 was carried out 27-30 October 2002. The surface temperature distribution (Fig. 23a) shows a homogenous surface layer with temperatures of 27°-28°C, warming slightly westward. Vertical sections of temperature on lines 1 through 5 are shown in Fig. 24. There was a layer of relatively uniform temperature (greater than 27°C) down to depths of 15 m throughout the study region, except for line 3 where the 27° isotherm was found near 40 m. This marks the bottom of the surface layer, and corresponds to a weak pycnocline as seen in the Vaisala frequency (Fig. 25). From those depths there is little change in temperature (25° and 27°C) down to the thermocline near 60-70 m. This corresponded to the seasonal pycnocline as seen by examination of vertical distributions of Vaisala frequency (Fig. 25). The general distribution and ranges of temperature are

similar on all lines except line 2, where warmer water (greater than 19°C) occurred at the bottom of the deepest section. The bottom temperature distribution (Fig. 23b) shows near-shore values around 26°C for lines 4 and 5 increasing westward to 28°C at line 1. Temperature decreased with depth to less than 18°C.

The surface salinity distribution from Cruise 3 (Fig. 26a) shows lower salinity water nearer the coast. Near-shore values increase westward from less than 19 on line 5 to near 26 on line 3 then decreases to less than 24 on line 1. It appears that fresh water is entering the study region most heavily in the east. There may be an additional source of low salinity near-shore water west of line 1.

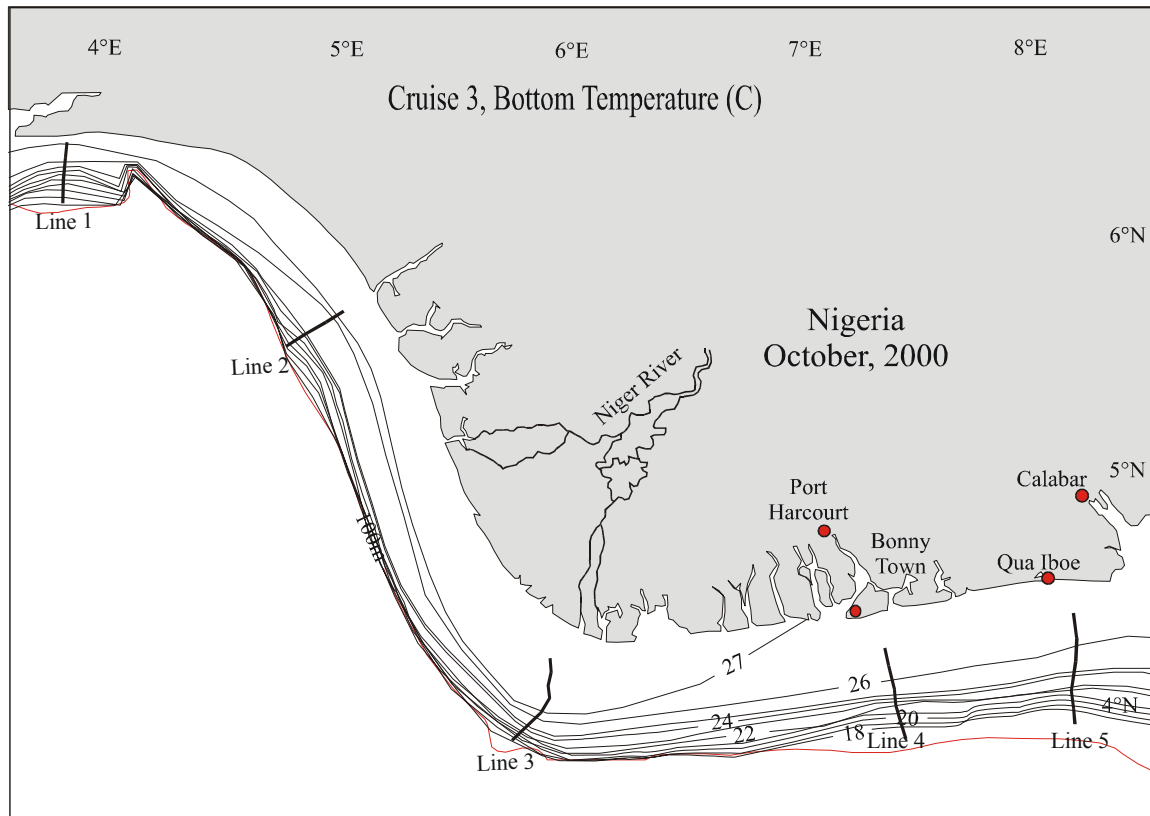
Vertical cross-shelf sections of salinity are shown in Fig. 27 for lines 1 through 5. On lines 1, 2, 4, 5 and to lesser extent on line 3 strong, near-surface haloclines at the base of the lower salinity surface water were clearly present. These were less deep on lines 2 and 3; on line 3 the upper halocline was present only at the inner station. On lines 2, and to some extent on line 5, a second halocline was found somewhat deeper in the water column. These features gave rise to strong pycnoclines as seen in Fig. 25 in the vertical distributions of Viasala frequency. The bottom salinity distribution (Fig. 26b) shows near-shore values less than 32 on line 5 decreasing westward to less than 30 on line 1.

The water mass as a whole was some 2°C warmer and less saline on Cruise 3 in October than on Cruise 2 in July. There is clear indication that a large volume of fresh water had entered the eastern end of the study area with low salinity water extending more than 100 km offshore. The westward near-shore flow of river discharge is strongly influencing the hydrographic characteristics of the entire study area. In addition, there seems to be a source of fresh water closer to Lagos.



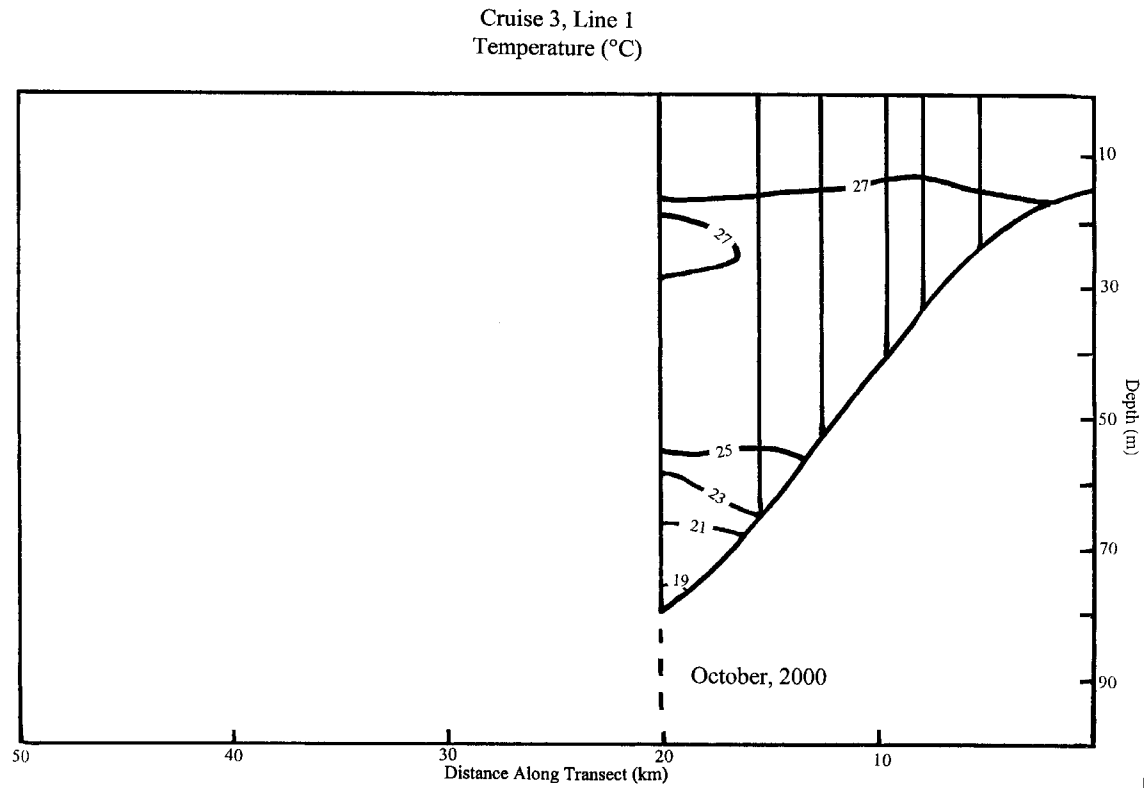
(a)

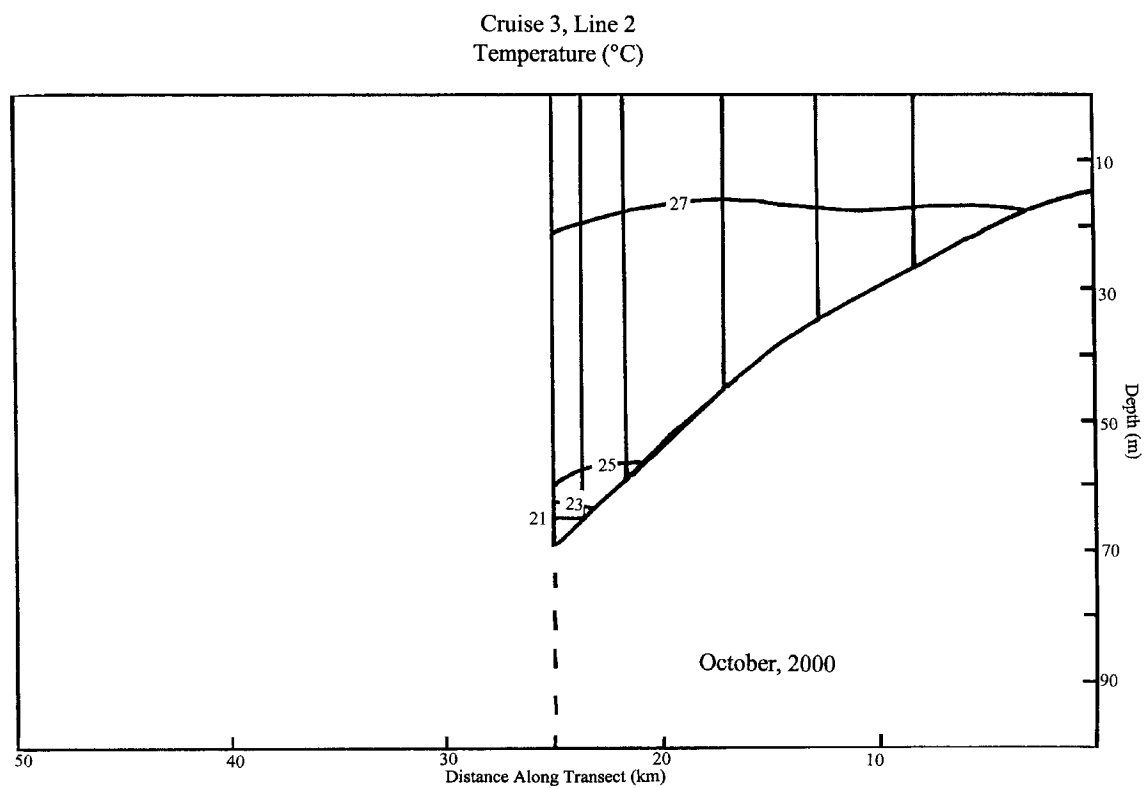
FIG. 23. Surface and bottom temperature contours (from CTD measurements) for Cruise 3.



(b)

FIG. 23. Continued.

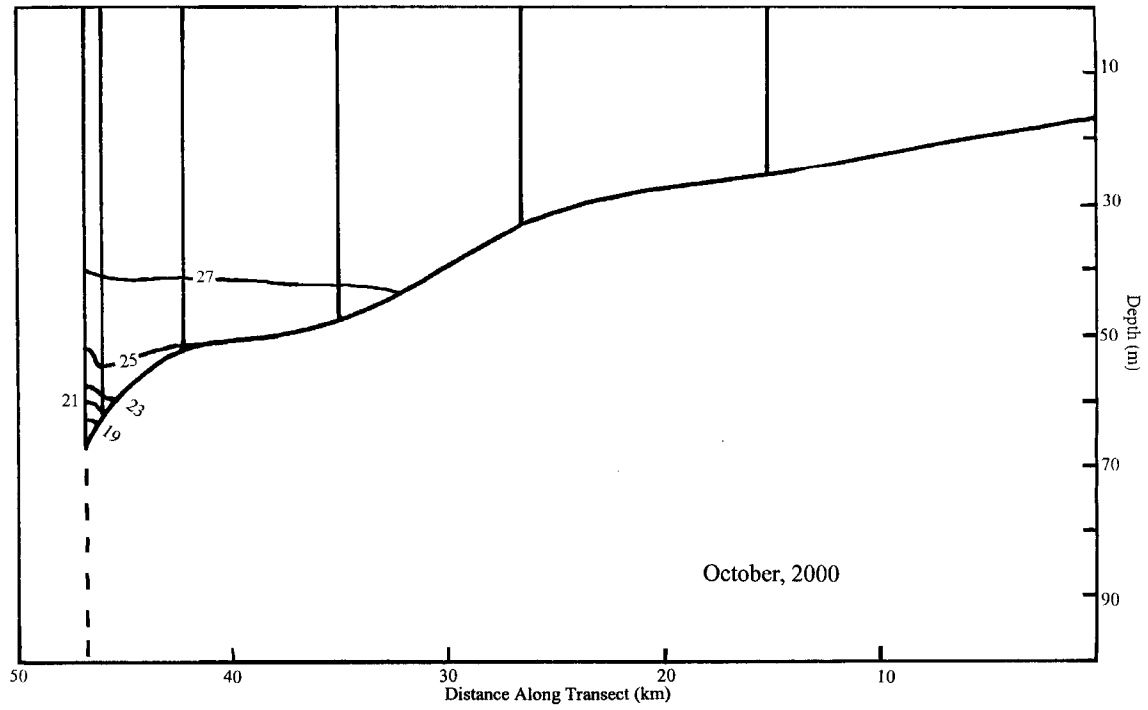




(b)

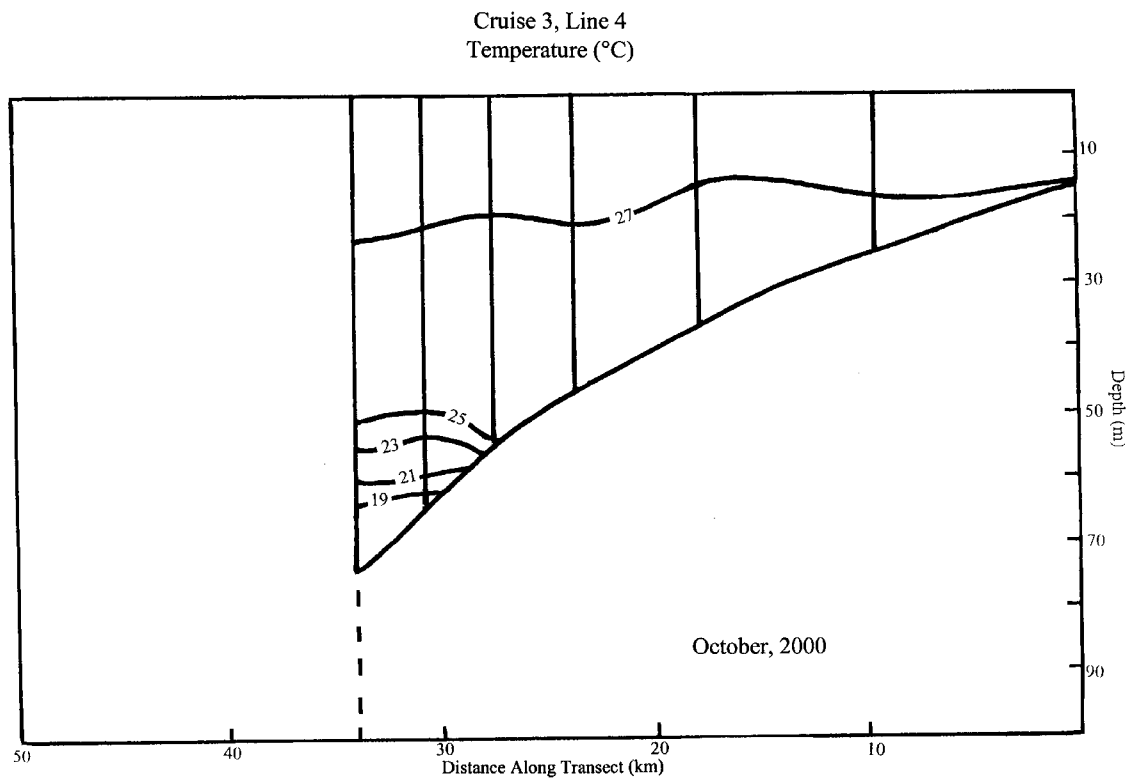
FIG. 24. Continued.

Cruise 3, Line 3
Temperature (°C)



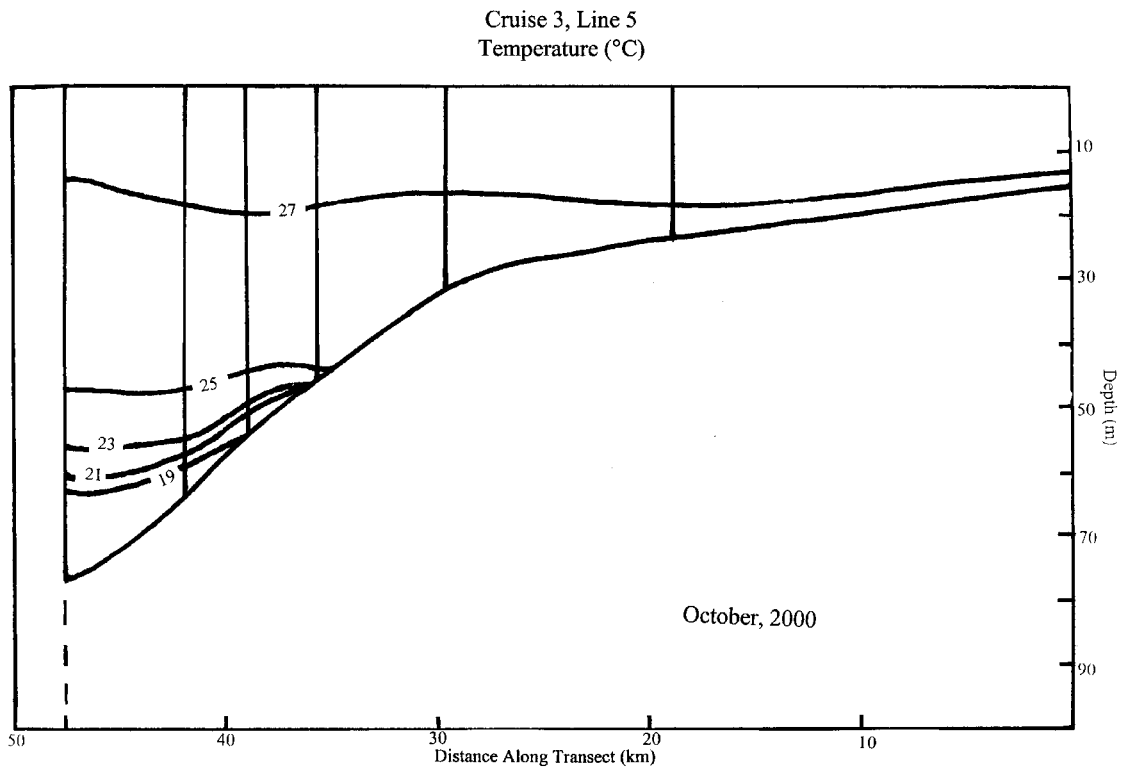
(c)

FIG. 24. Continued.



(d)

FIG. 24. Continued.



(e)

FIG. 24. Continued.

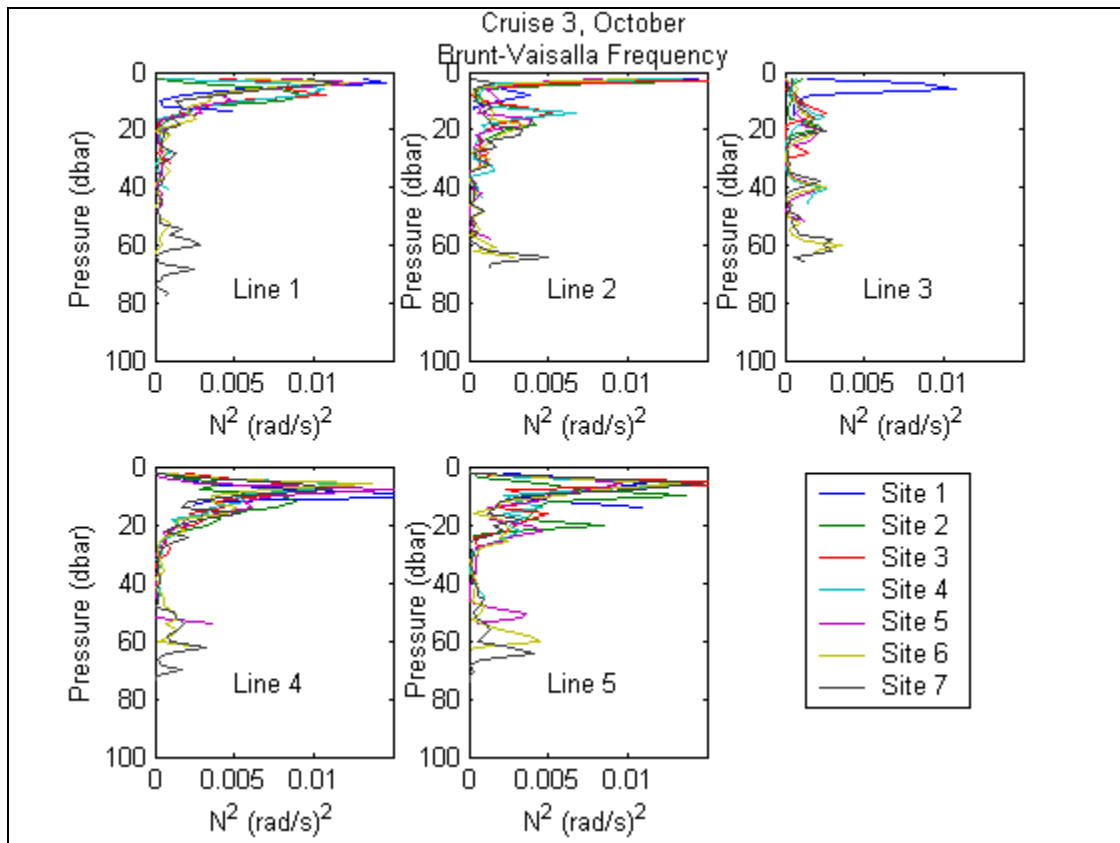
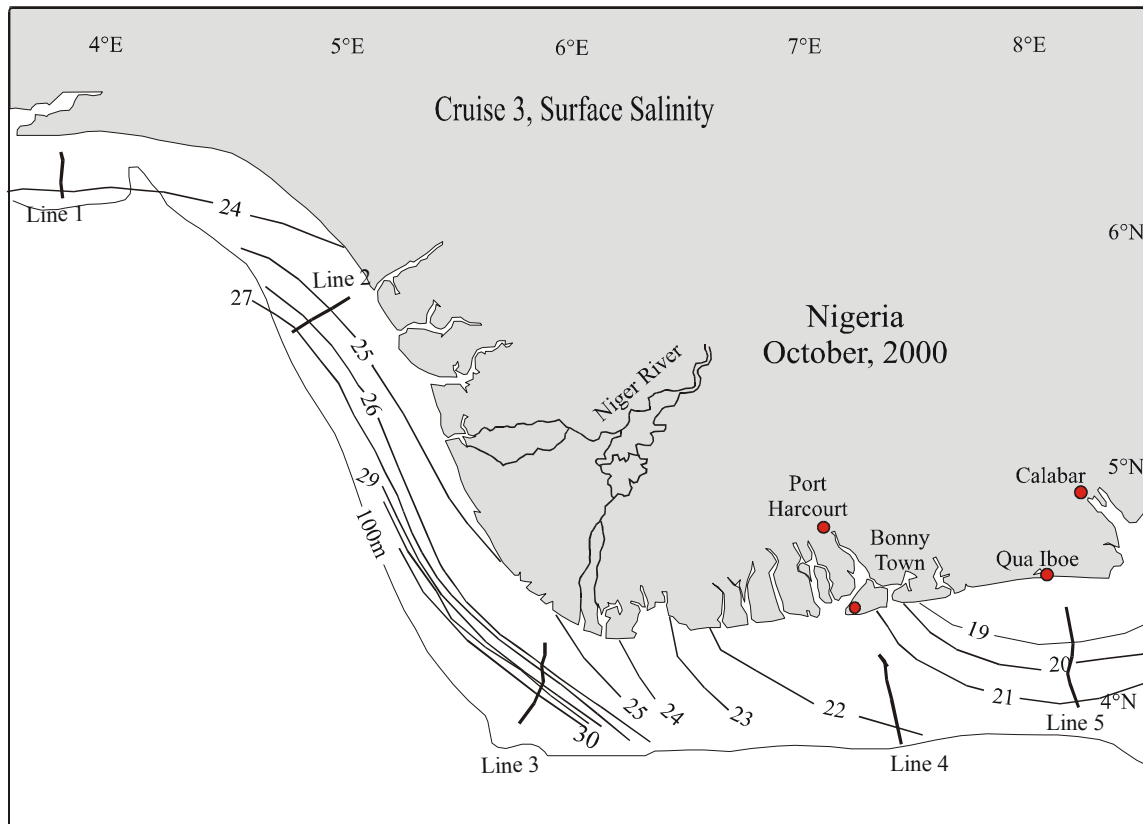
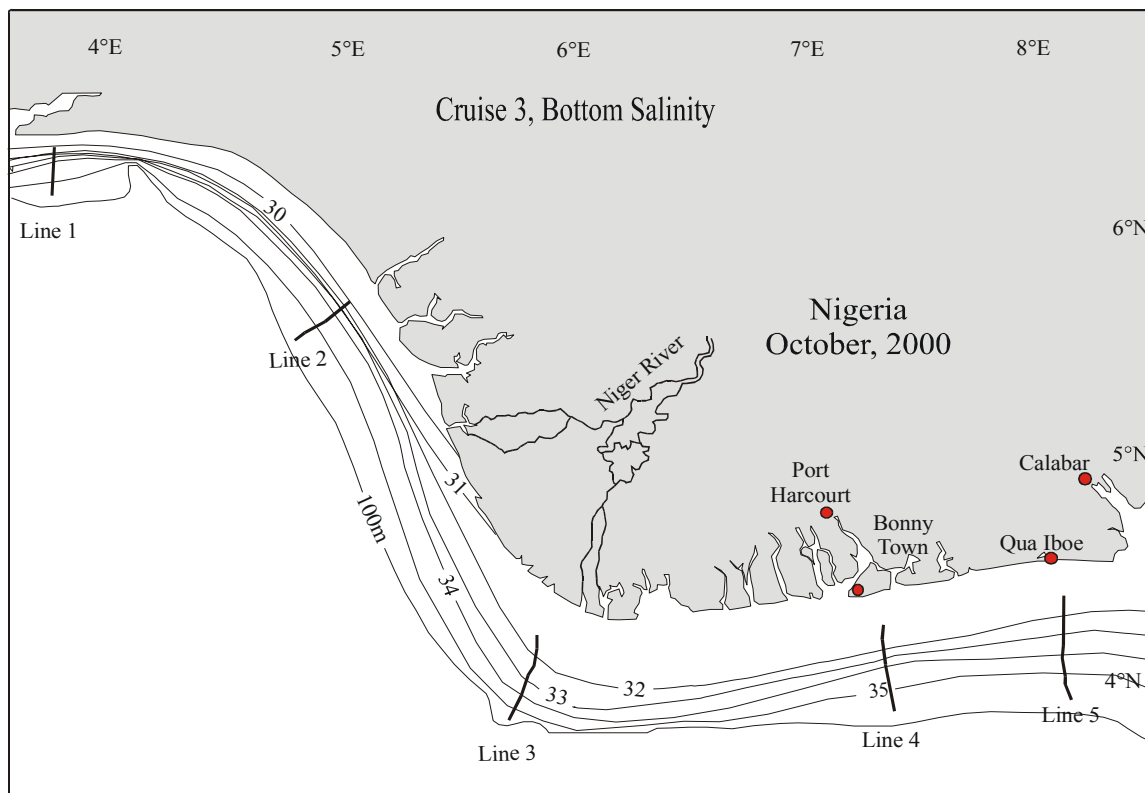


FIG. 25. Brunt Vaisala frequency for Cruise 3 (calculated from CTD measurements).



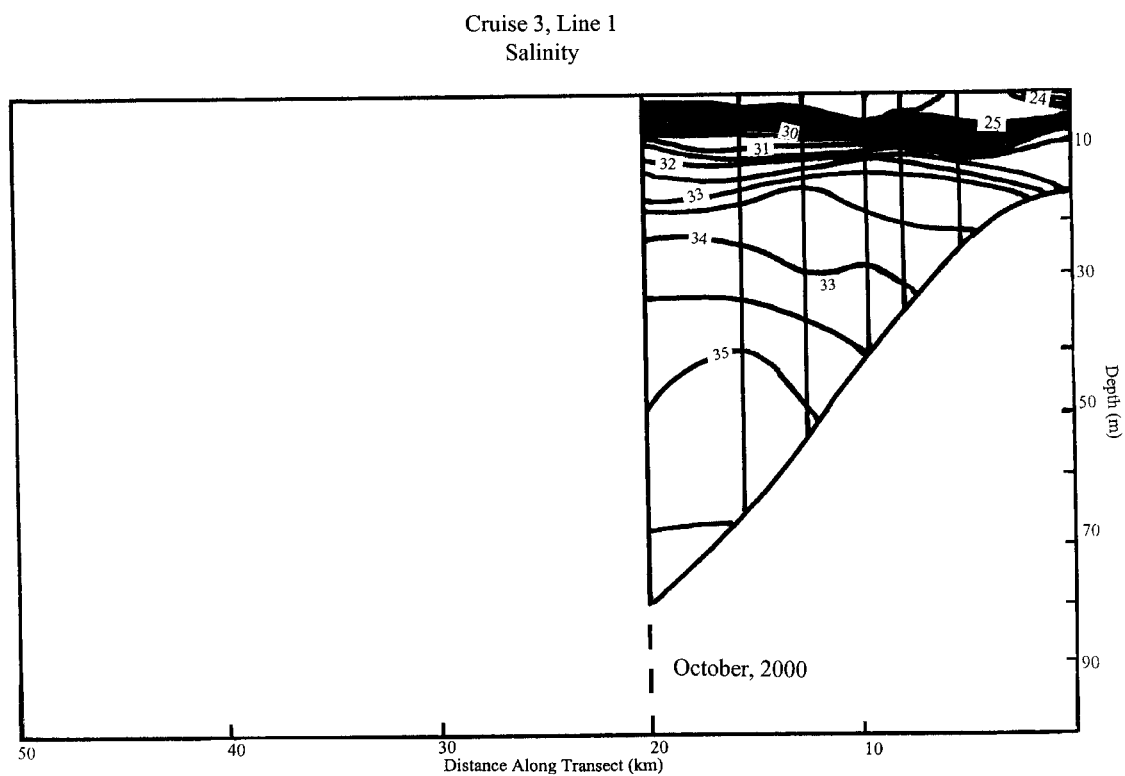
(a)

FIG. 26. Surface and bottom salinity contours (from CTD measurements) for Cruise 3.



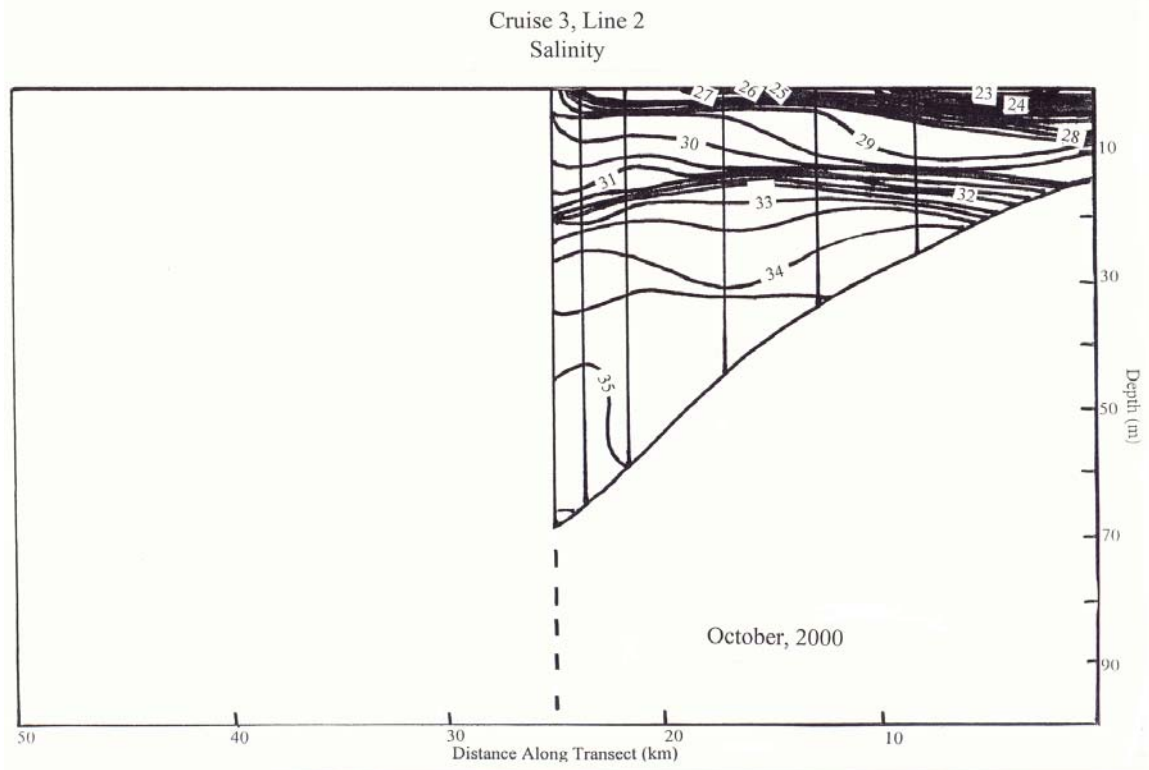
(b)

FIG. 26. Continued.



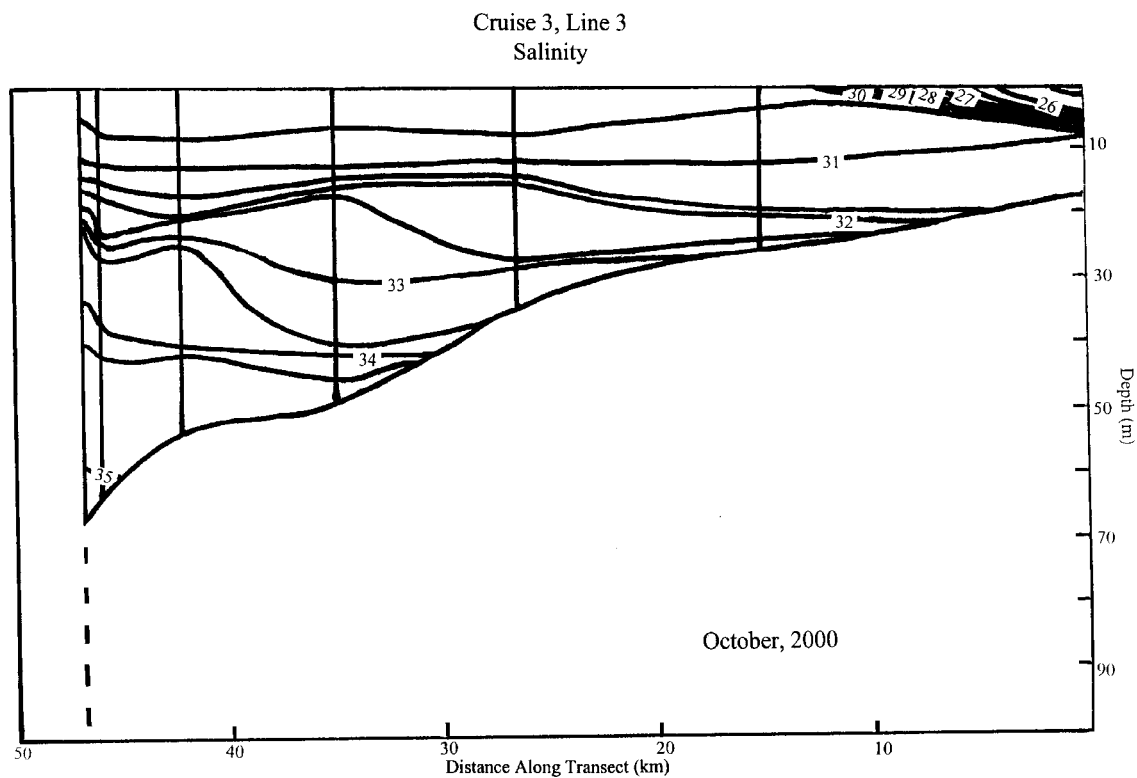
(a)

FIG. 27. (a)-(e) Cross sections of salinity contours (from CTD measurements along lines 1-5) for Cruise 3. Vertical lines represent sites of measurements on each line.



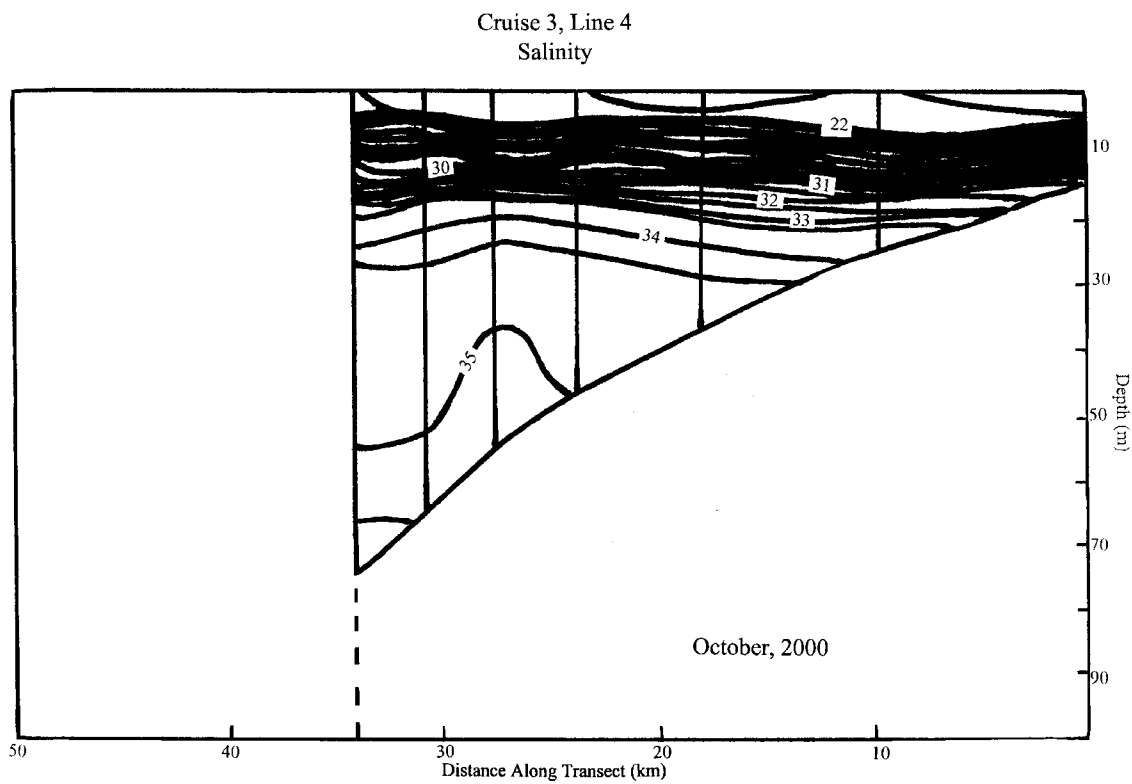
(b)

FIG. 27. Continued.



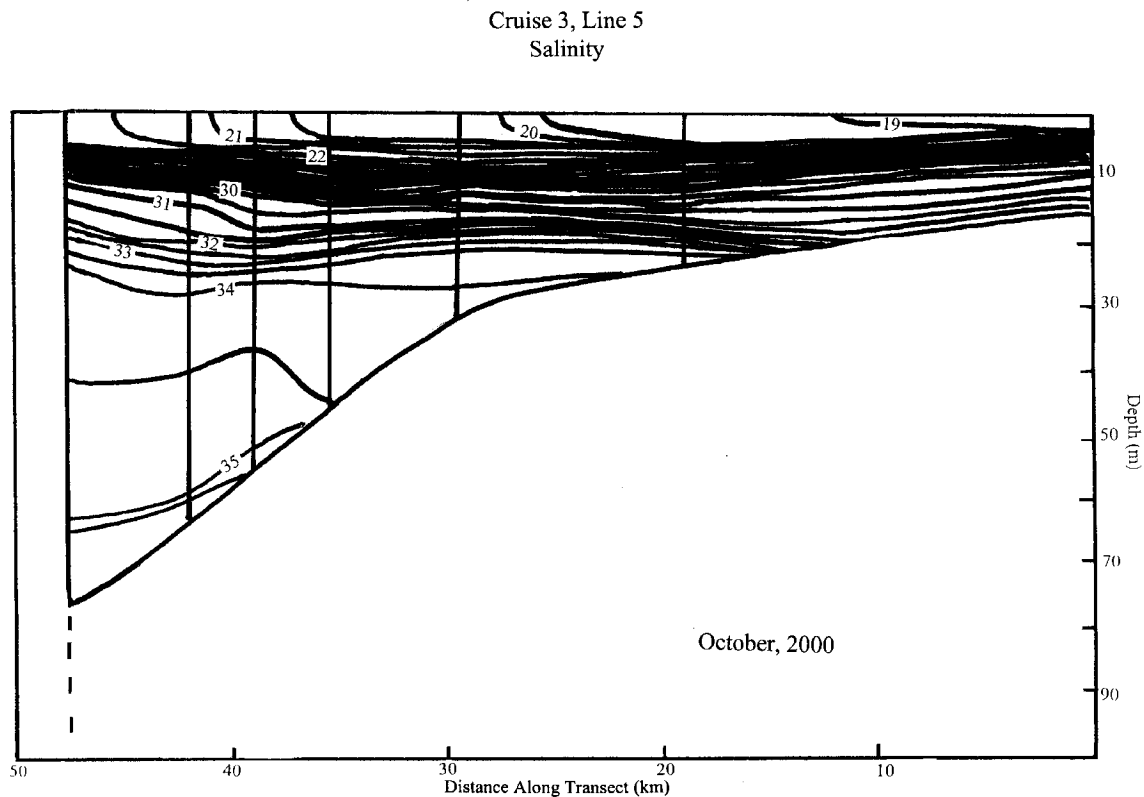
(c)

FIG. 27. Continued.



(d)

FIG. 27. Continued.



(e)

FIG. 27. Continued.

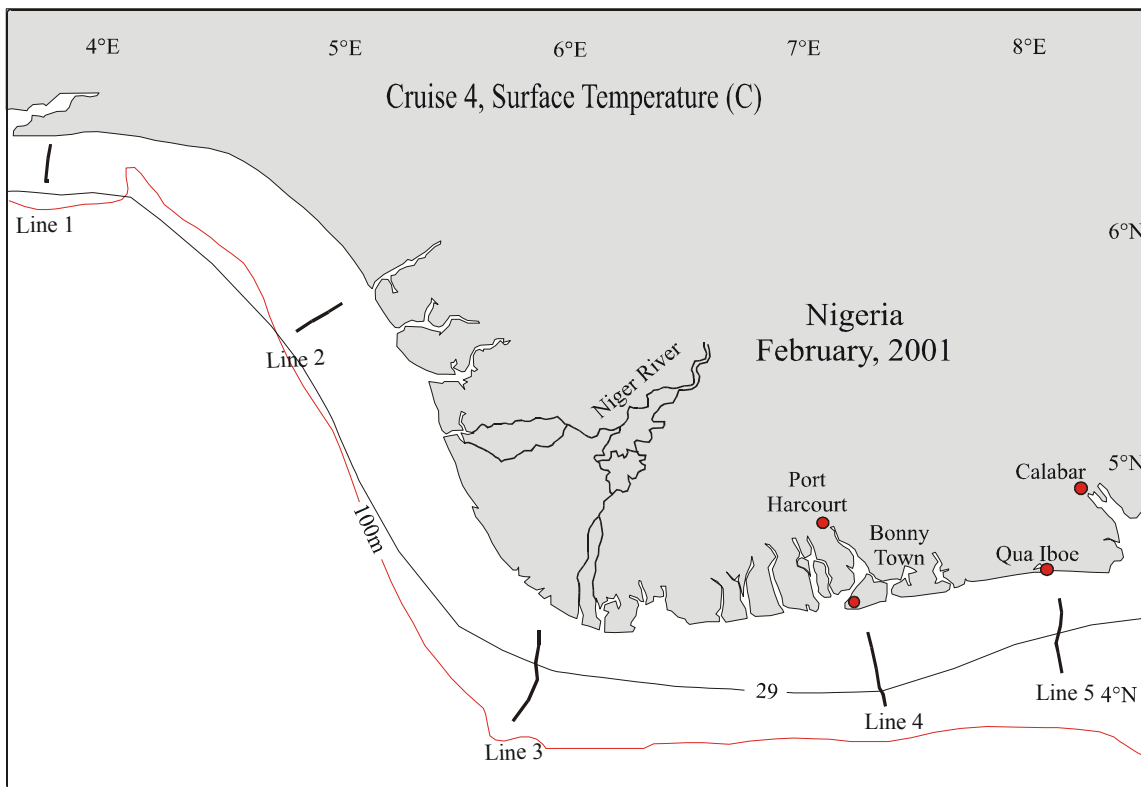
4) February 2001; Cruise 4

Cruise 4 was carried out 1-5 February 2001. The surface temperature distribution (Fig. 28a) shows a homogenous surface layer with temperatures near 29°C . Vertical sections of temperature on lines 1 through 5 are shown in Fig. 29. Surface temperatures were greater than 27°C down to depths of 30-40 m throughout the study region, except for layers greater than 29°C surface water on the offshore end of lines 3 and 5. The thermocline centered near 40-50 m corresponded to the seasonal pycnocline as seen by

examination of vertical distributions of Vaisala frequency (Fig. 30). The bottom temperature distribution (Fig. 28) shows near-shore values of 29°C, decreasing as depth increases to less than 20°C, to less than 18°C on line 1 because that line extends to greater depths than the other lines.

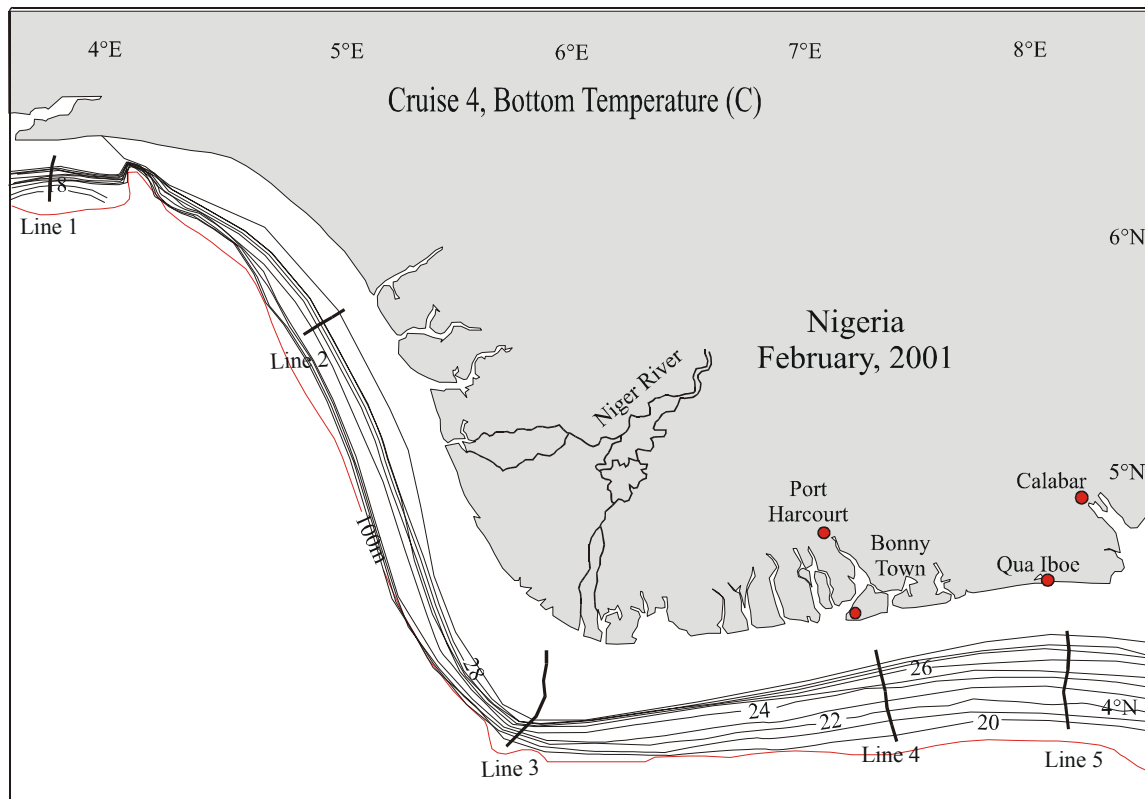
The surface salinity distribution from Cruise 5 (Fig. 31) shows values increasing westward from less than 29 on line 5 to near 31 on line 1. These values were similar to those on Cruise 1 and much larger than those found on Cruise 3, indicating little influence of river discharge.

Vertical cross-shelf sections of salinity are shown in Fig. 32 for lines 1 through 5. Lines 2-5 have strong haloclines at the base of shallow mixed surface layers of 10-15 m in depth. On line 1 the halocline with similar salinity values is not as strong and was found centered near 40 m, thus contributing to the seasonal pycnocline. These features are seen clearly in vertical distributions of Viasala frequency (Fig. 30). A peculiar feature is seen in the salinity distribution at station 4 on line 2; it is not reflected in the temperature distribution, so it may be an error in the data at that station. Salinity values in the deeper portions of each section are between 35.5 and 36. The bottom salinity distribution (Fig. 29) shows near-shore values of less than 32 to less than 34, with lower values at lines 4 and 5.



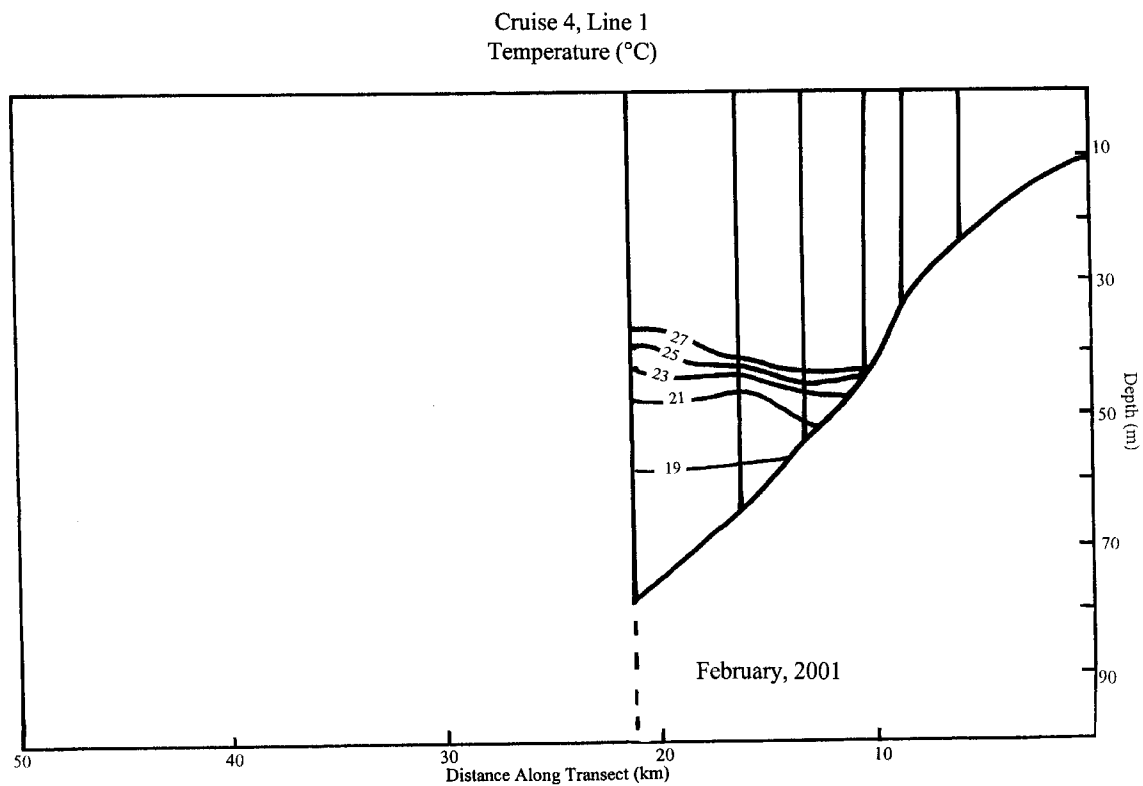
(a)

FIG. 28. Surface and bottom temperature contours (from CTD measurements) for Cruise 4.



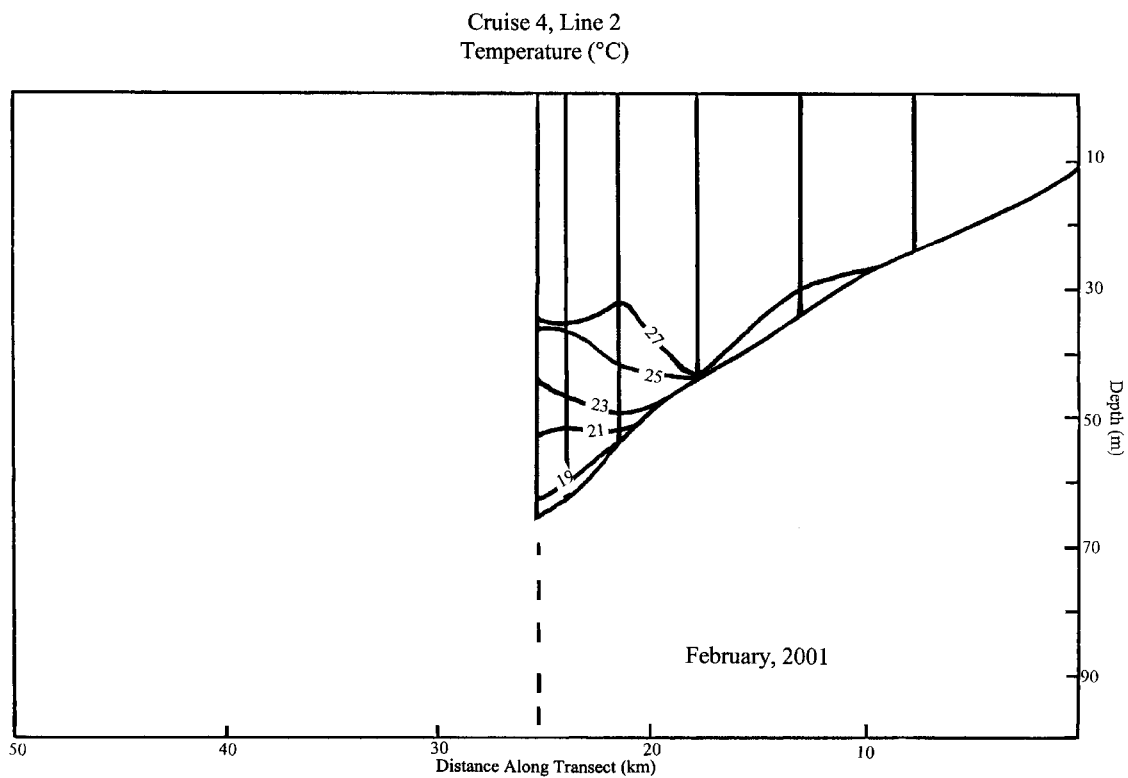
(b)

FIG. 28. Continued.



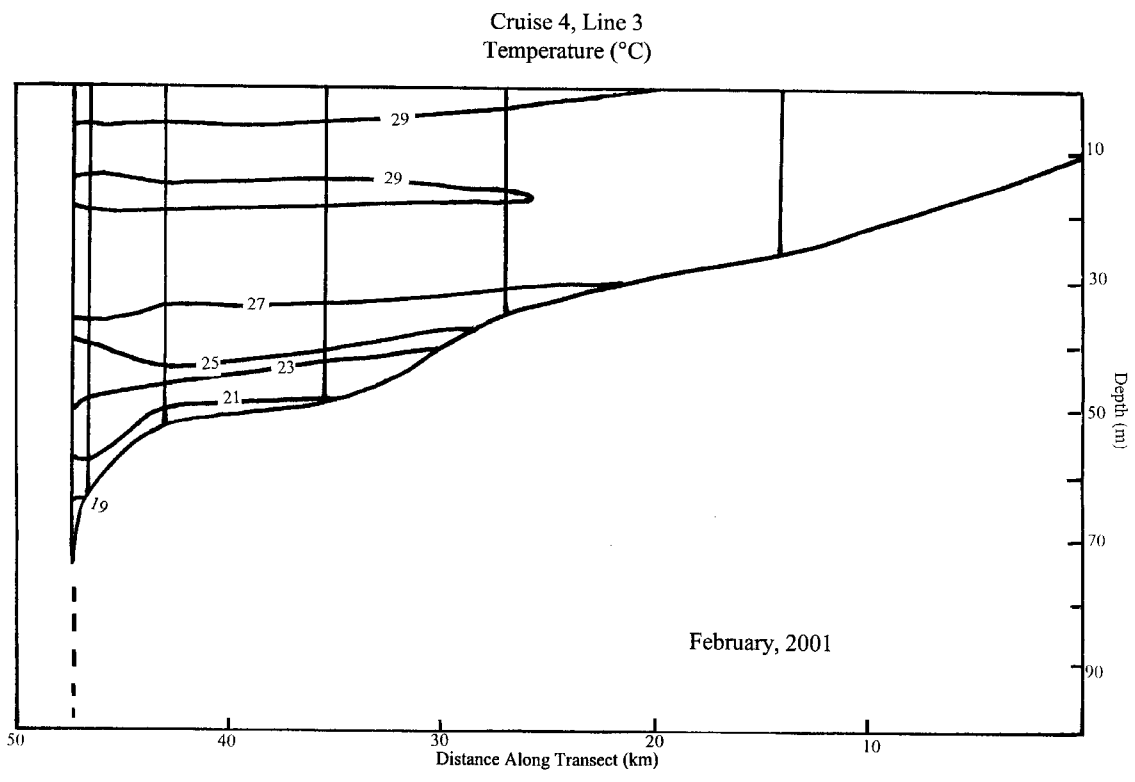
(a)

FIG. 29. (a)-(e) Cross sections of temperature contours (from CTD measurements along lines 1-5) for Cruise 4. Vertical lines represent sites of measurements on each line.



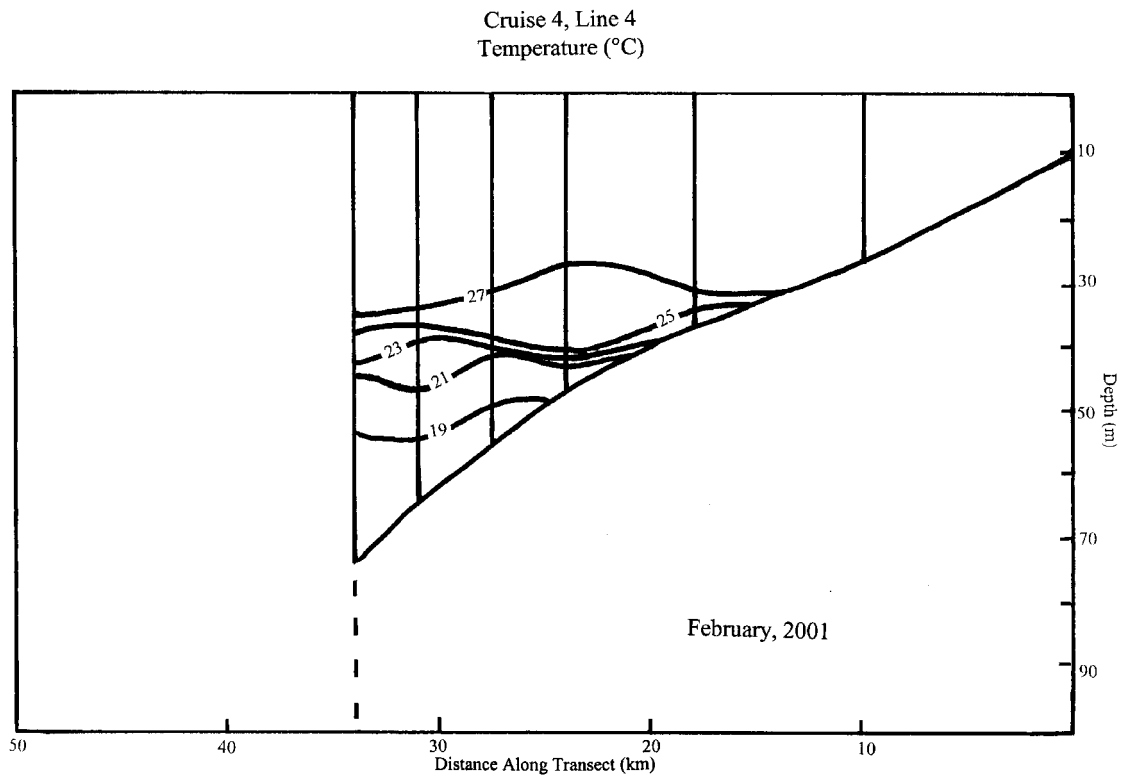
(b)

FIG. 29. Continued.



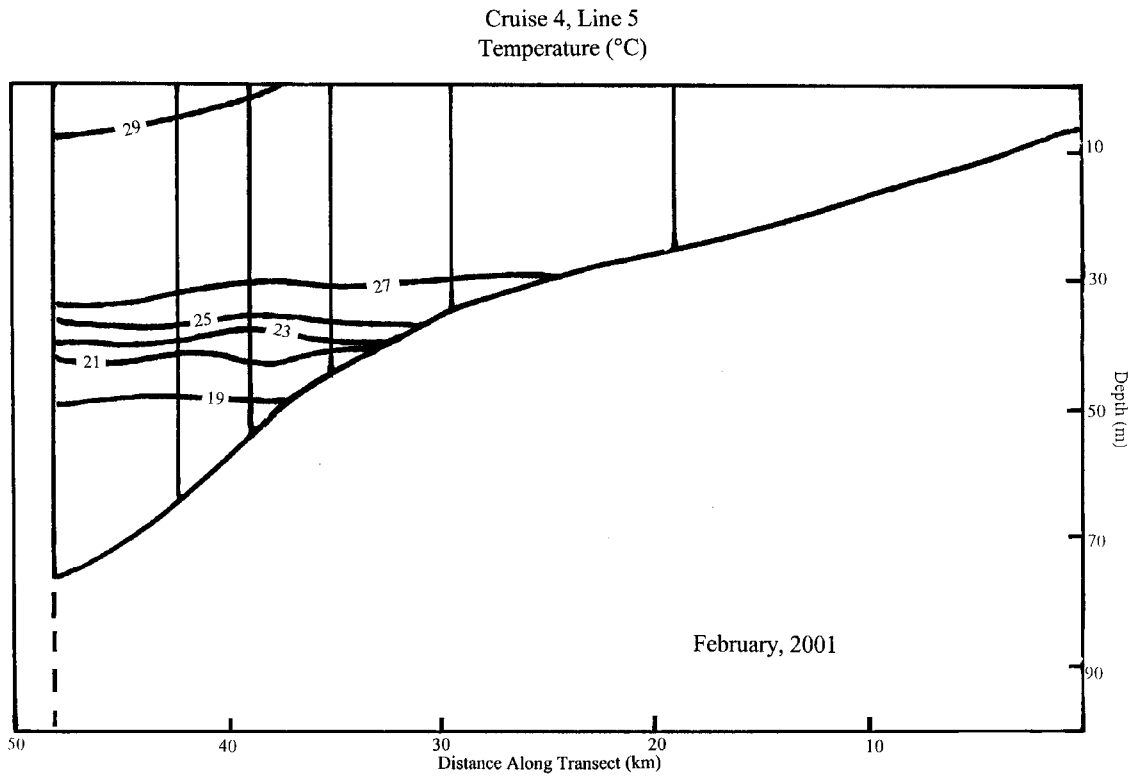
(c)

FIG. 29. Continued.



(d)

FIG. 29. Continued.



(e)

FIG. 29. Continued.

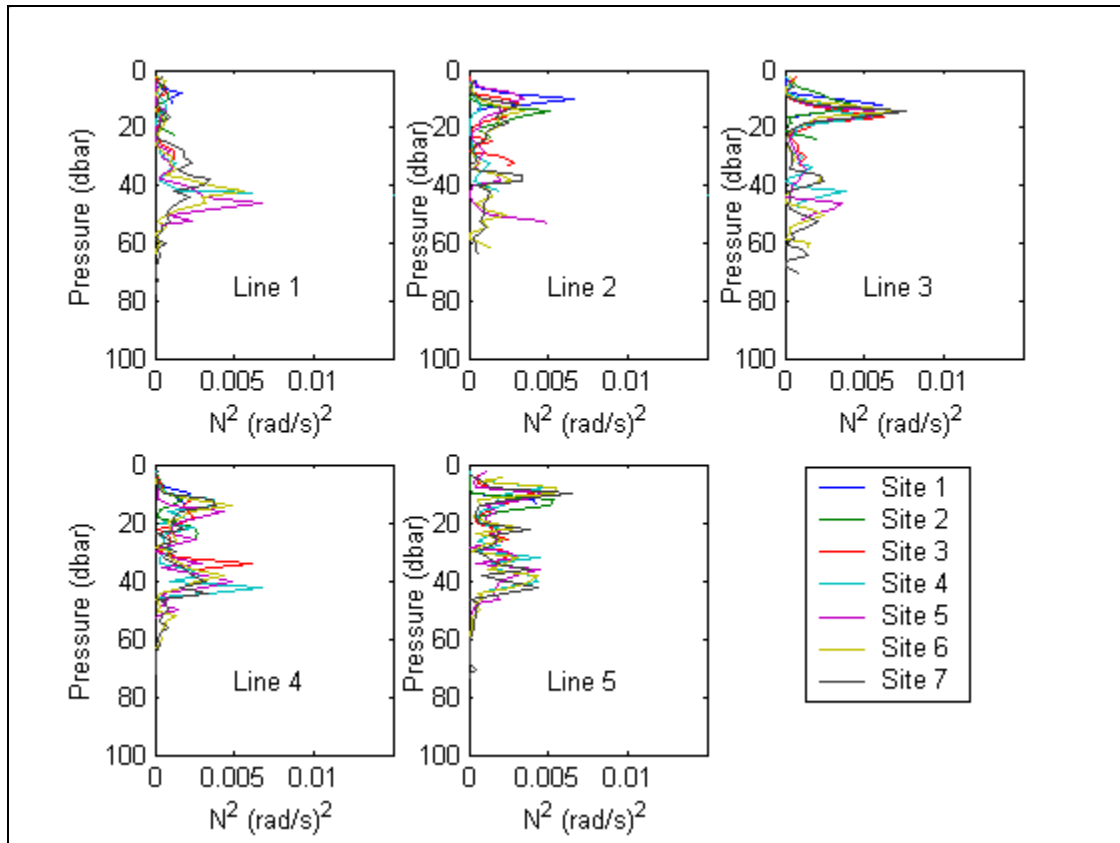
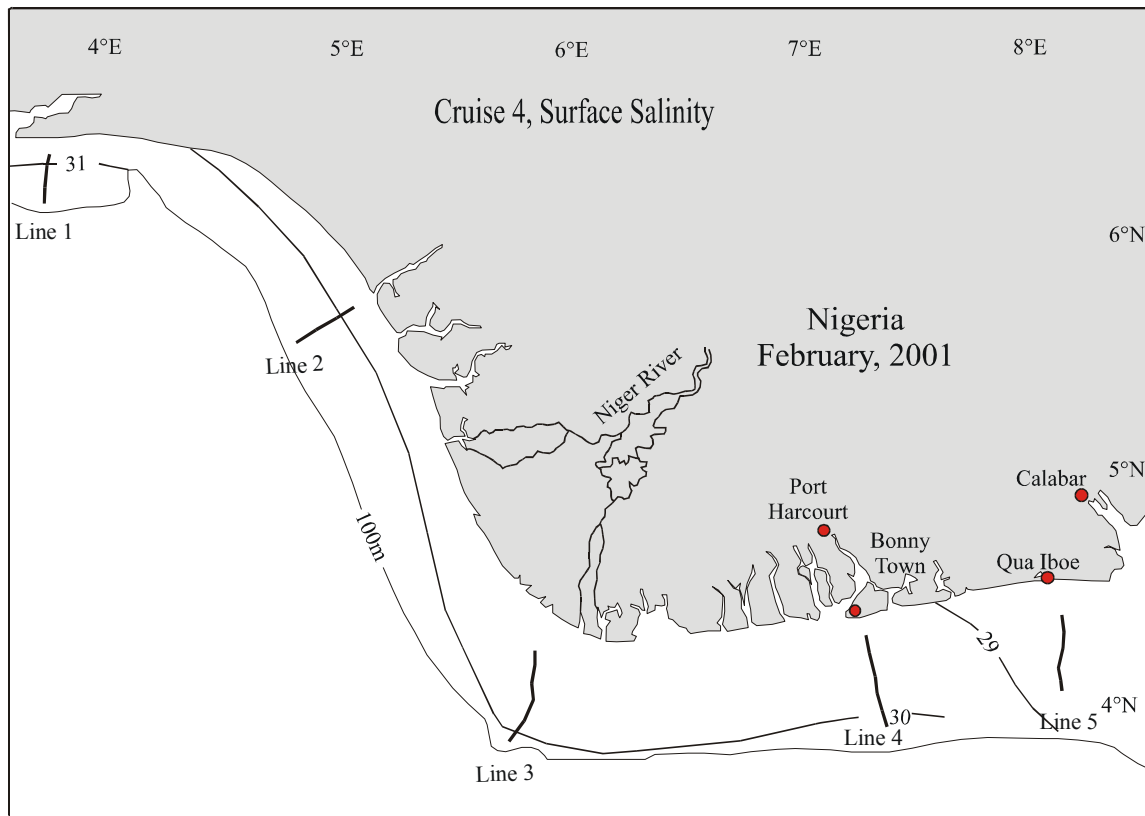
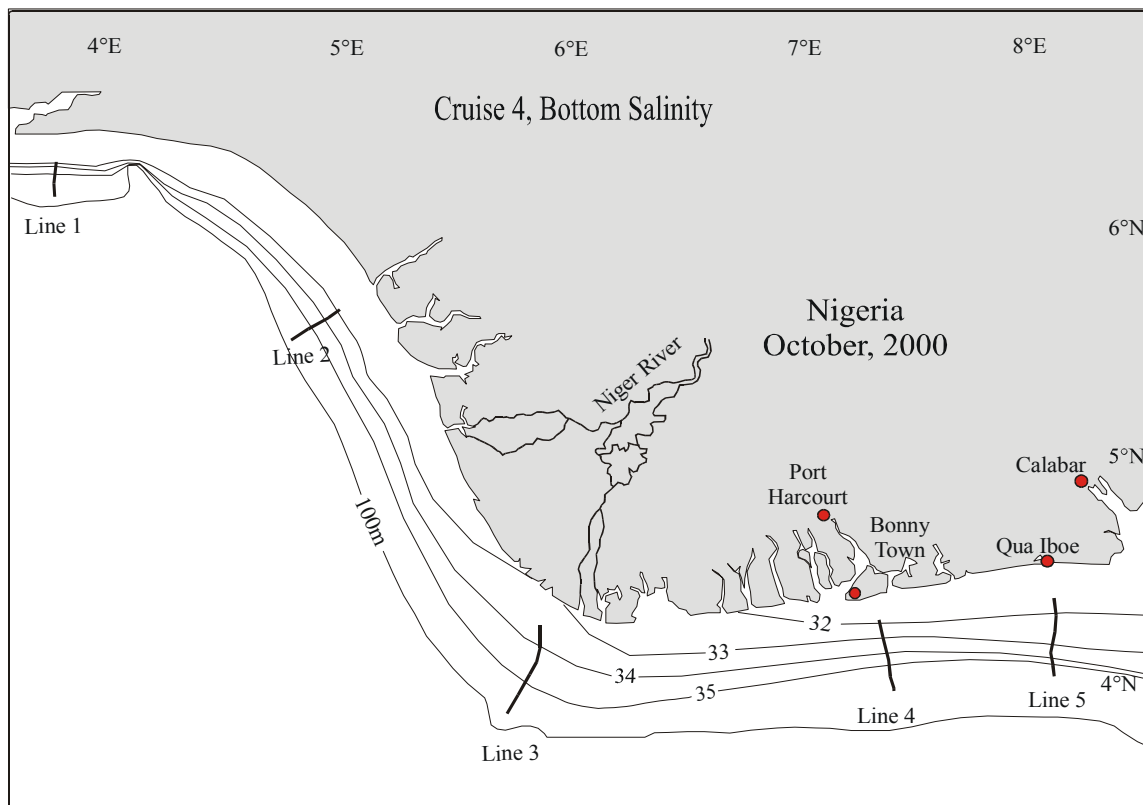


FIG. 30. Brunt Vaisala frequency for Cruise 4 (calculated from CTD measurements).



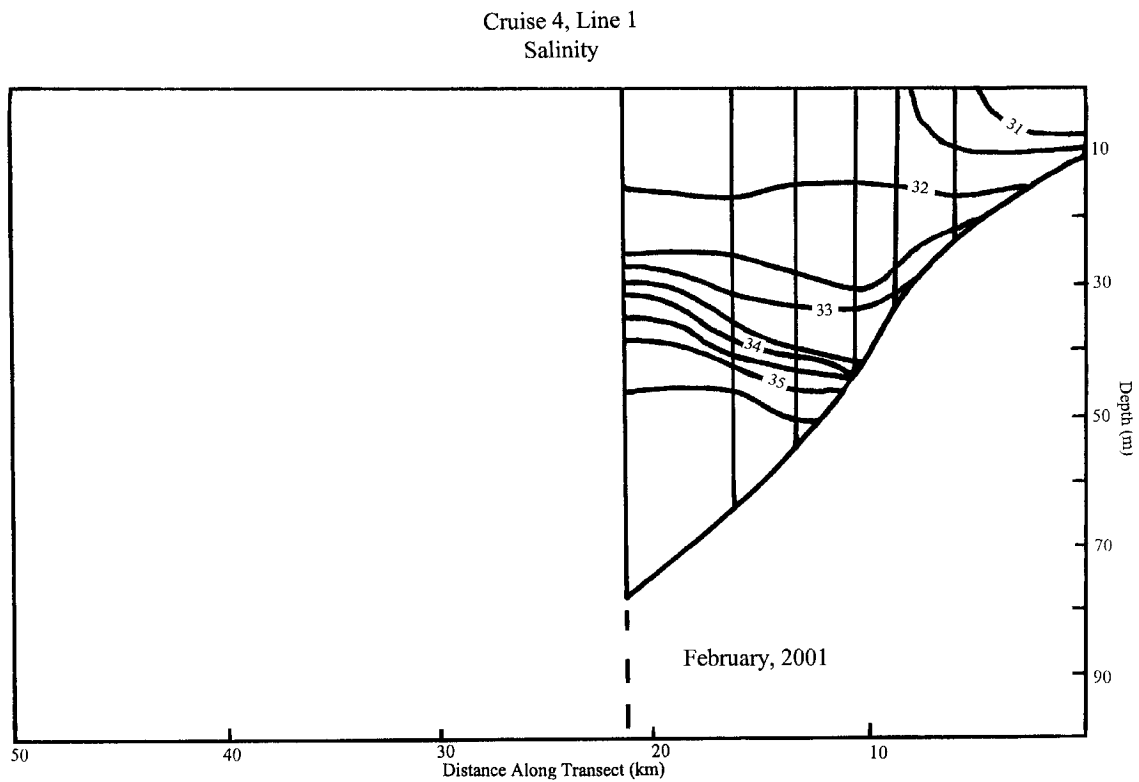
(a)

FIG. 31. Surface and bottom salinity contours (from CTD measurements) for Cruise 4.



(b)

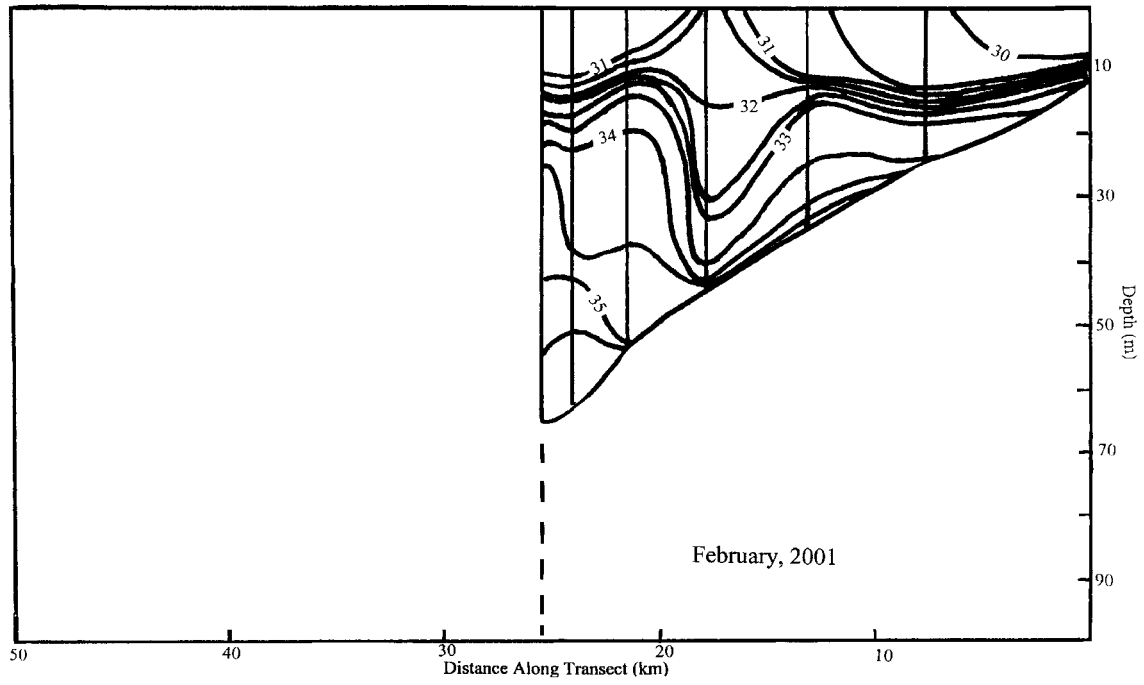
FIG. 31. Continued.



(a)

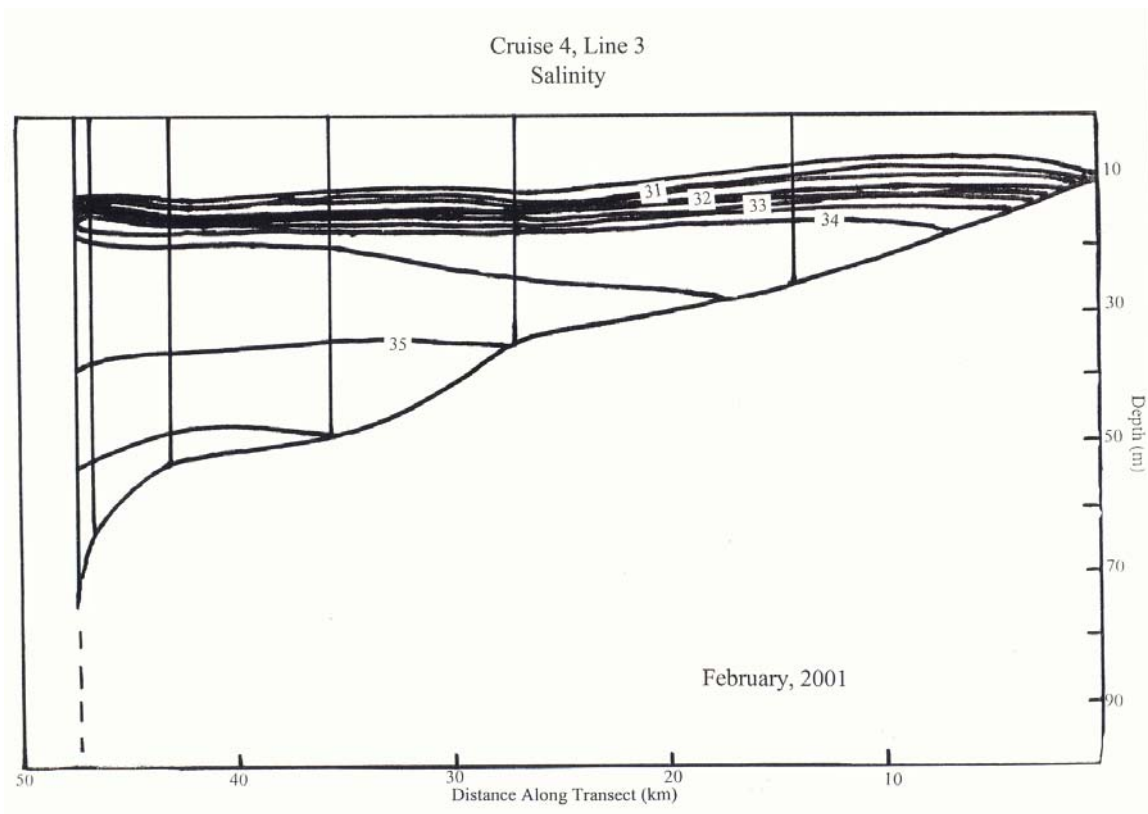
FIG. 32. (a)-(e) Cross sections of salinity contours (from CTD measurements along lines 1-5) for Cruise 4. Vertical lines represent sites of measurements on each line.

Cruise 4, Line 2
Salinity



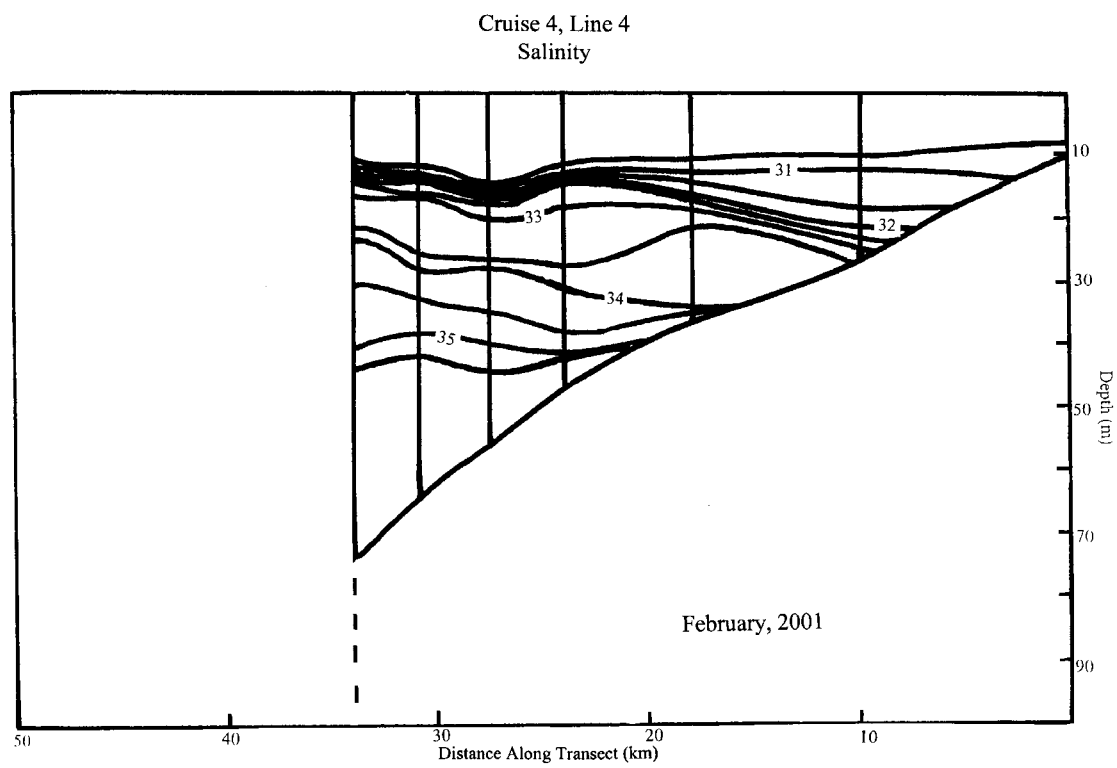
(b)

FIG. 32. Continued.



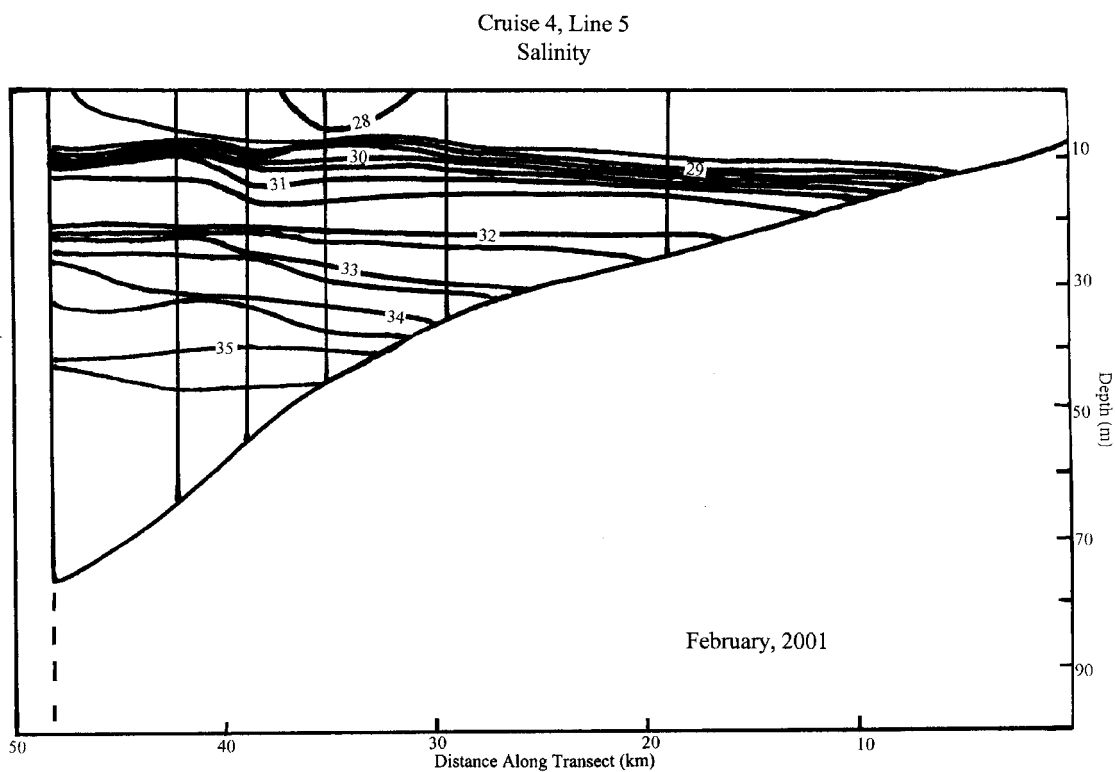
(c)

FIG. 32. Continued.



(d)

FIG. 32. Continued.



(e)

FIG. 32. Continued.

5) May 2001; Cruise 5

Cruise 5 was carried out 5-9 May 2001. The surface temperature distribution (Fig. 33a) shows temperatures between 29° and 30°C, with warmer waters on lines 2, 3 and 4. Vertical sections of temperature on lines 1 through 5 are shown in Fig. 34. There was a layer of relatively uniform temperature (greater than 29°C) down to the top of the thermocline. The thermocline was centered near 20 m on line 5; near 30 m on lines 1, 3 and 4; and near 40 m on line 1. This is reflected in the vertical distributions of Vaisala frequency (Fig. 35). The bottom temperature distribution (Fig. 33b) shows near-shore values of 29°C, decreasing as depth increases to below 20°C, except in line 1 which extends to greater depths and temperatures less than 19°C.

The surface salinity distribution from Cruise 5 (Fig. 36) shows slightly lower salinity water nearer the coast. Near-shore values generally increase westward from less than 30 on line 5 to near 32 on line 1. The low salinity water (less than 31) seen on line 2 could reflect discharge from any of the nearby rivers (Benin, Escravous, Forcados, or the Ramos) or increased rainfall. Otherwise, the eastern end of the study region still seems to receive the largest amount of fresh water.

Vertical cross-shelf sections of salinity are shown in Fig. 37 for lines 1 through 5. The distribution of low salinity waters near shore is very prominent on lines 5, 2 and to lesser extent on 4; on those lines there was a horizontal salinity gradient in the surface waters. On lines 4 and 5 the main halocline corresponded in depth with the thermocline, increasing the vertical pycnocline. Vertical sections for lines 1 and 3 show two weak haloclines; one near the depth of the thermocline and one above that depth near 10 m. These features are seen in the vertical distributions of Vaisala frequency (Fig. 35). No clear halocline was present on line 2. Salinity values in the deeper portions of each section are between 35.5 and 36. The 35.5 isohaline deepens from 30 to 50 m moving westwards from line 1 to line 4 and then rises back to 40 m on line 5. The bottom salinity distribution (Fig. 36) shows near-shore values greater than 32 to greater than 34. Line 4 has the lowest bottom salinity at 32. Lines 2 and 3 have bottom salinities near 34 and lines 1 and 5 have bottom salinities of 33.

As for other cruises, the eastern end of the study area received the greater amount of fresh water; however there is some evidence of discharge from the Benin, Escravous, Forcados, or Ramos rivers affecting line 2. As a whole the water mass in May was about 2° warmer and more saline than it was in February. There seemed to be very little influence of river discharge as compared to July or October. Conditions were very similar to those in April 2000.

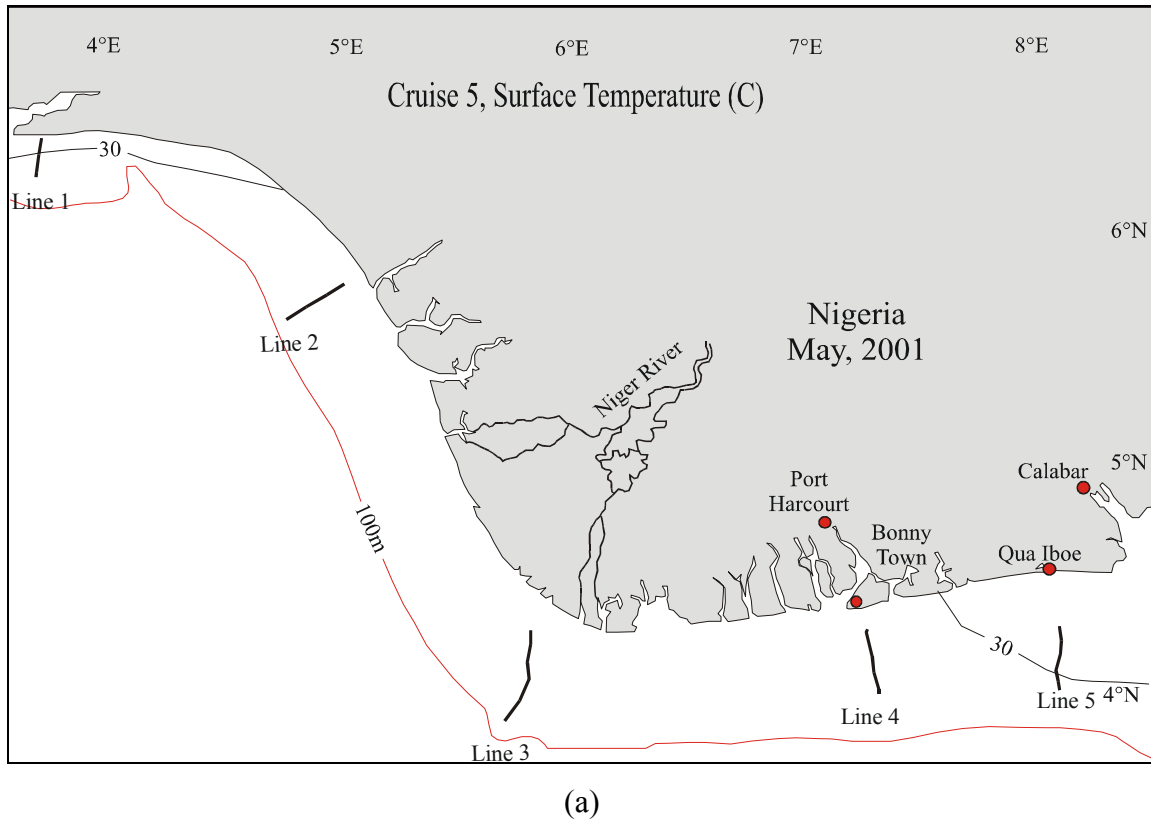
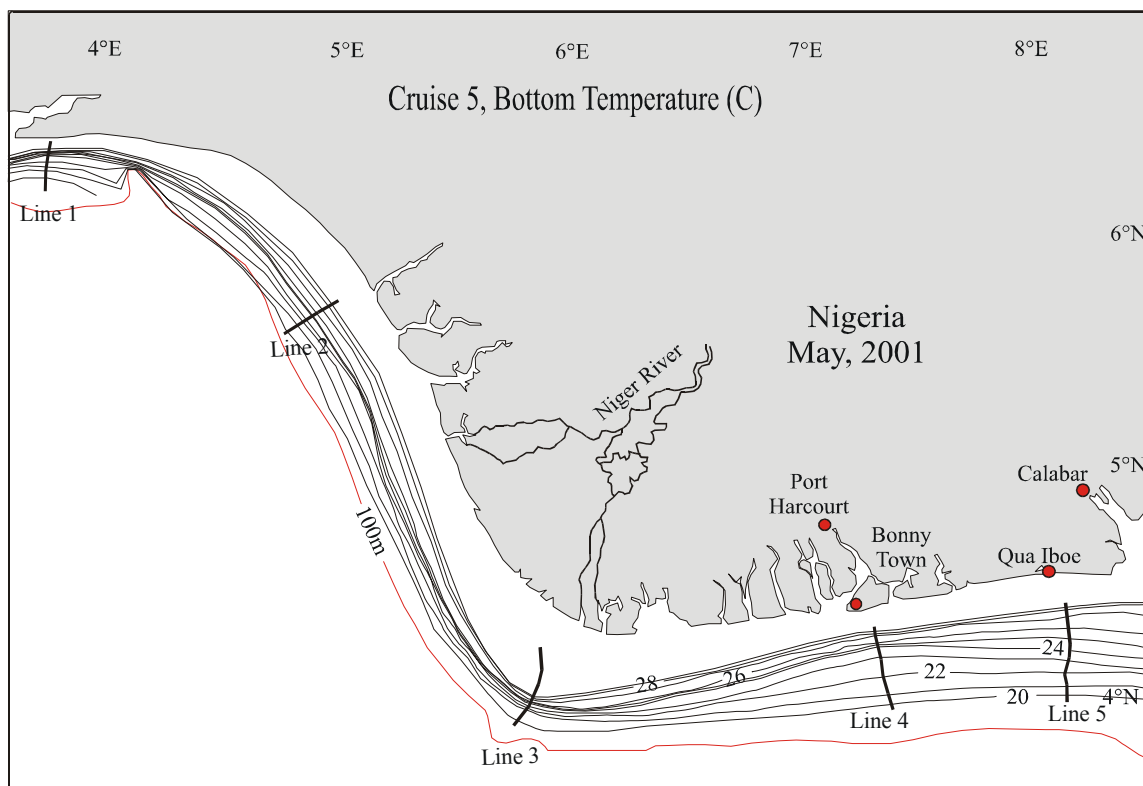


FIG. 33. Surface and bottom temperature contours (from CTD measurements) for Cruise 5.



(b)

FIG. 33. Continued.

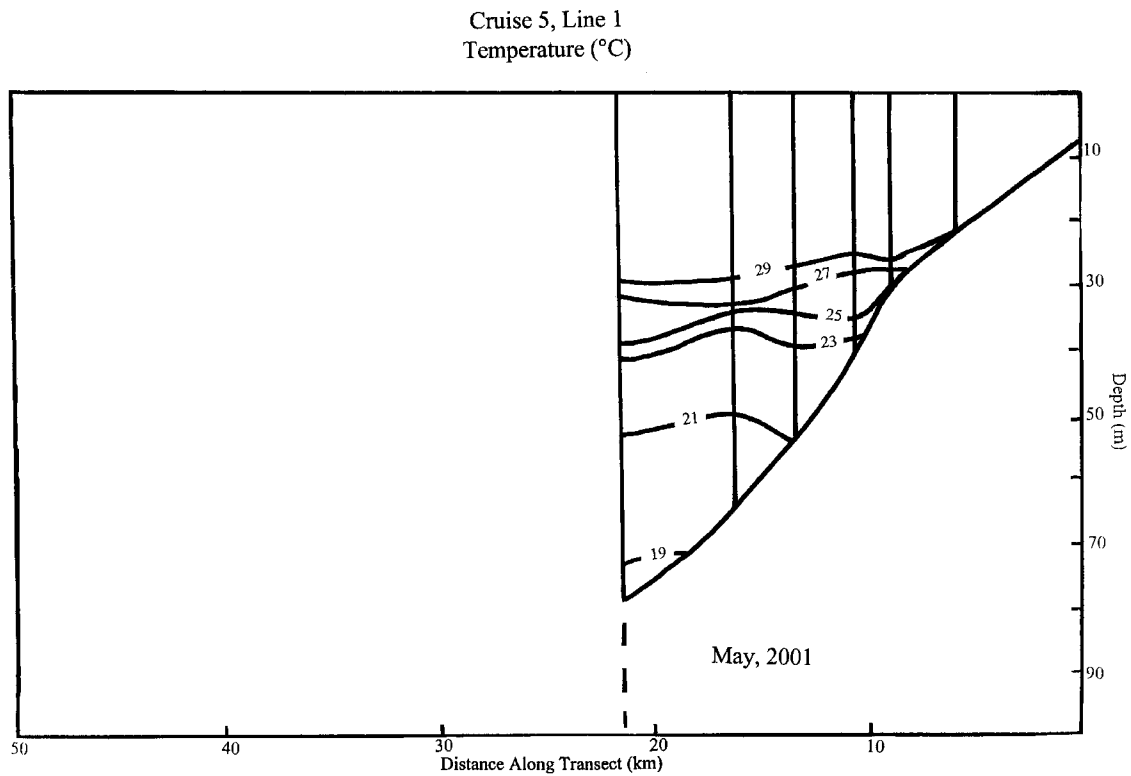
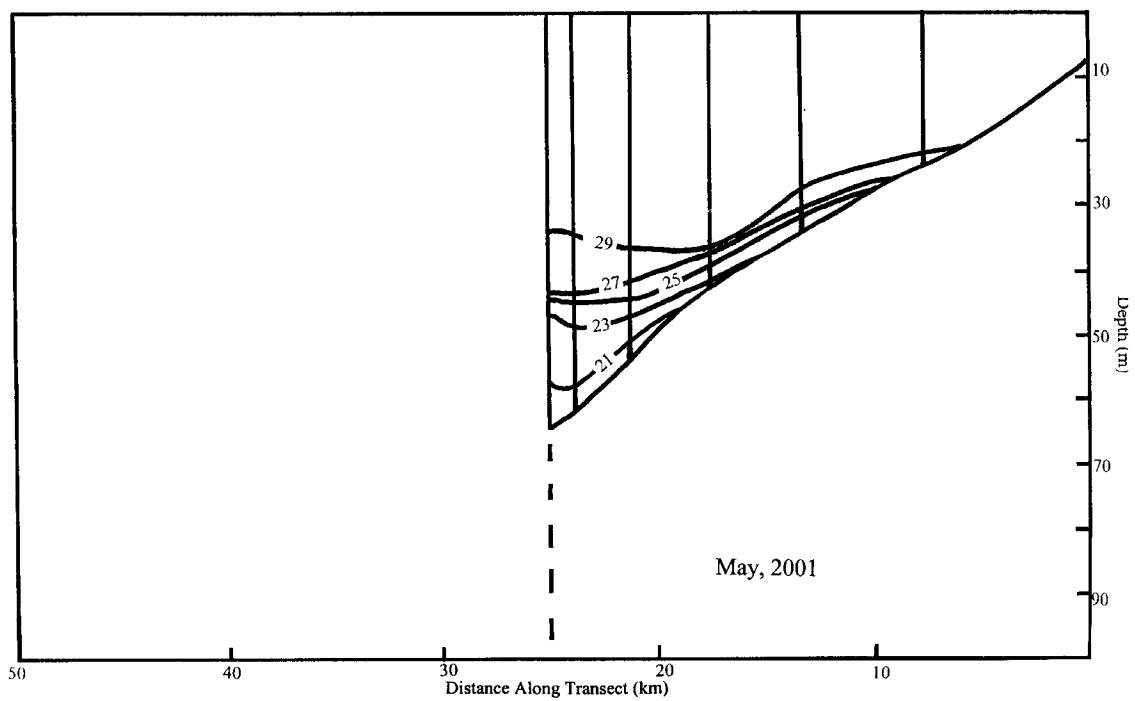


FIG. 34. (a)-(e) Cross sections of temperature contours (from CTD measurements along lines 1-5) for Cruise 5. Vertical lines represent sites of measurements on each line.

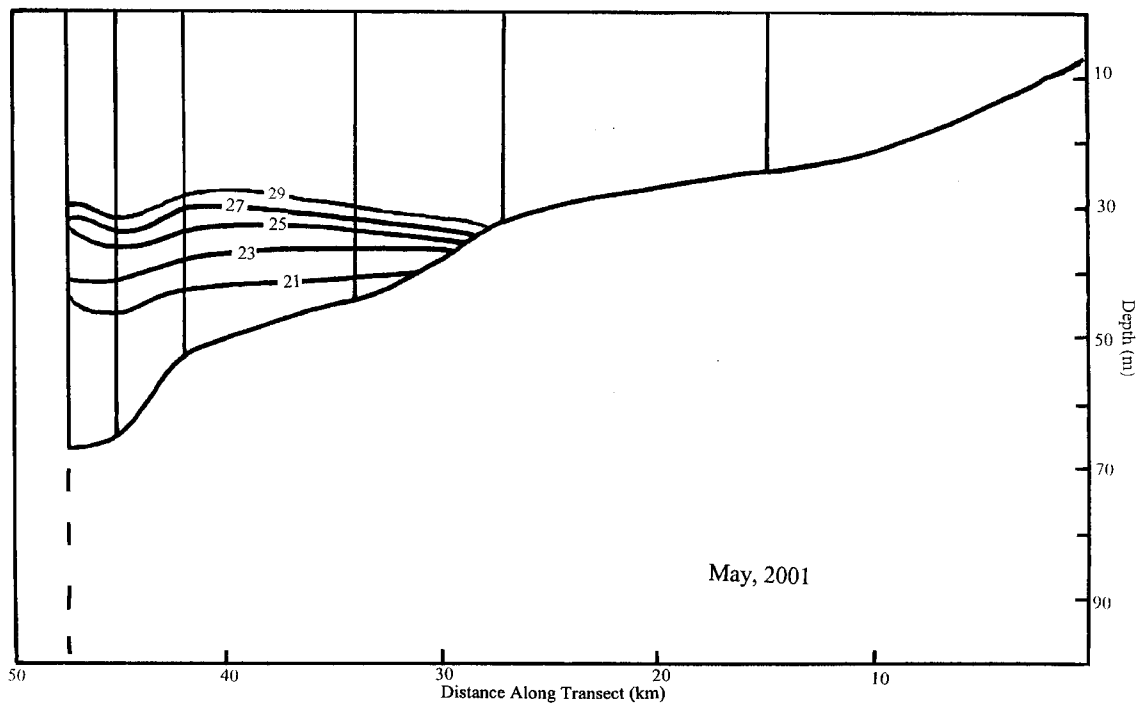
Cruise 5, Line 2
Temperature (°C)



(b)

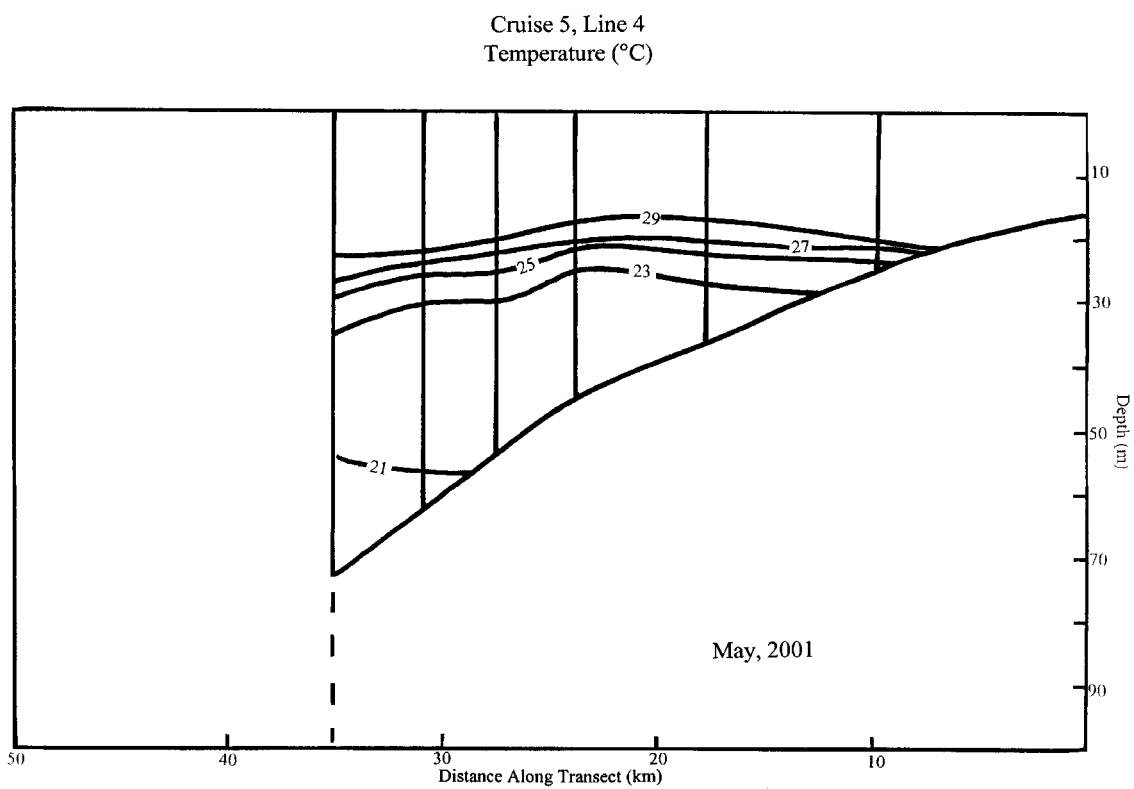
FIG. 34. Continued.

Cruise 5, Line 3
Temperature (°C)



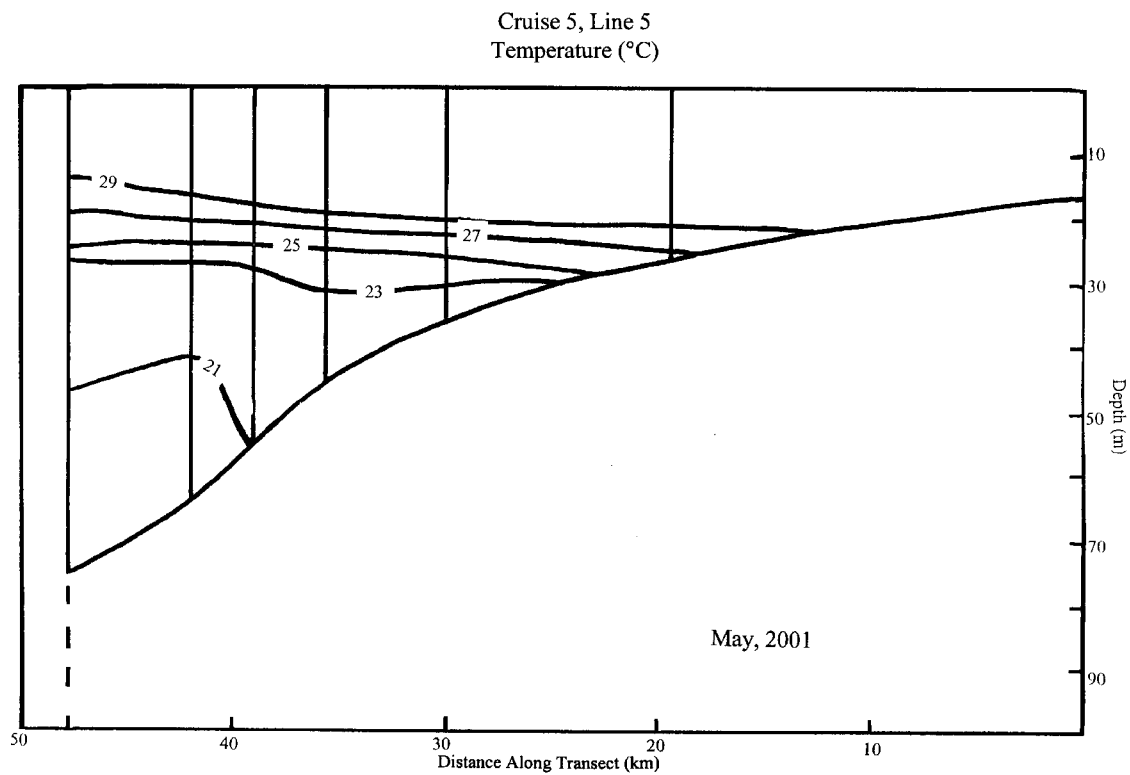
(c)

FIG. 34. Continued.



(d)

FIG. 34. Continued.



(e)

FIG. 34. Continued.

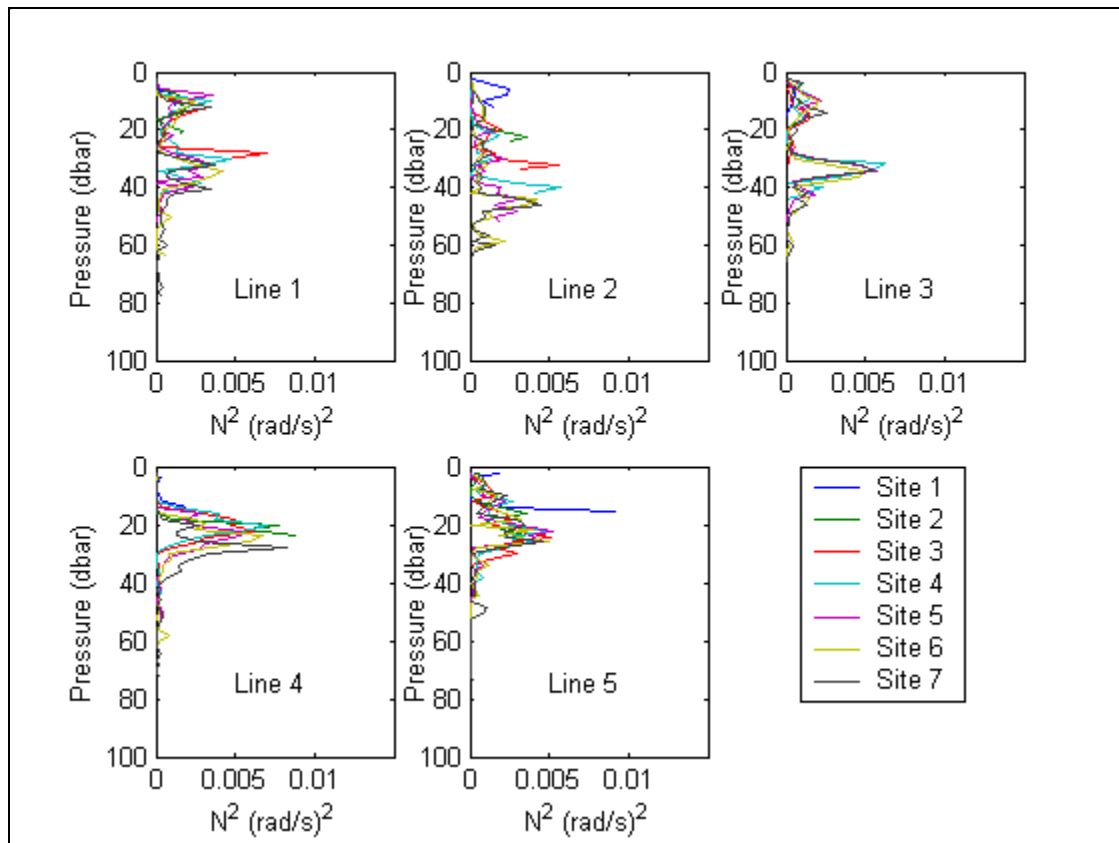
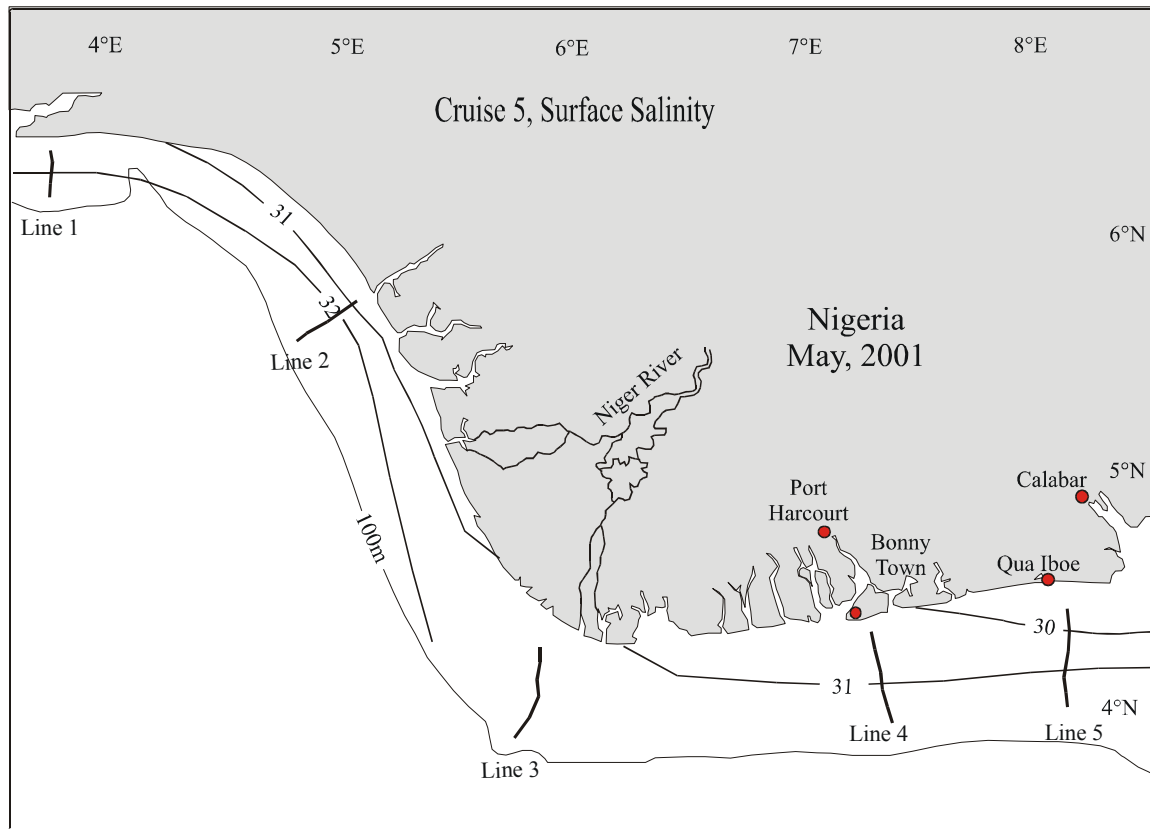
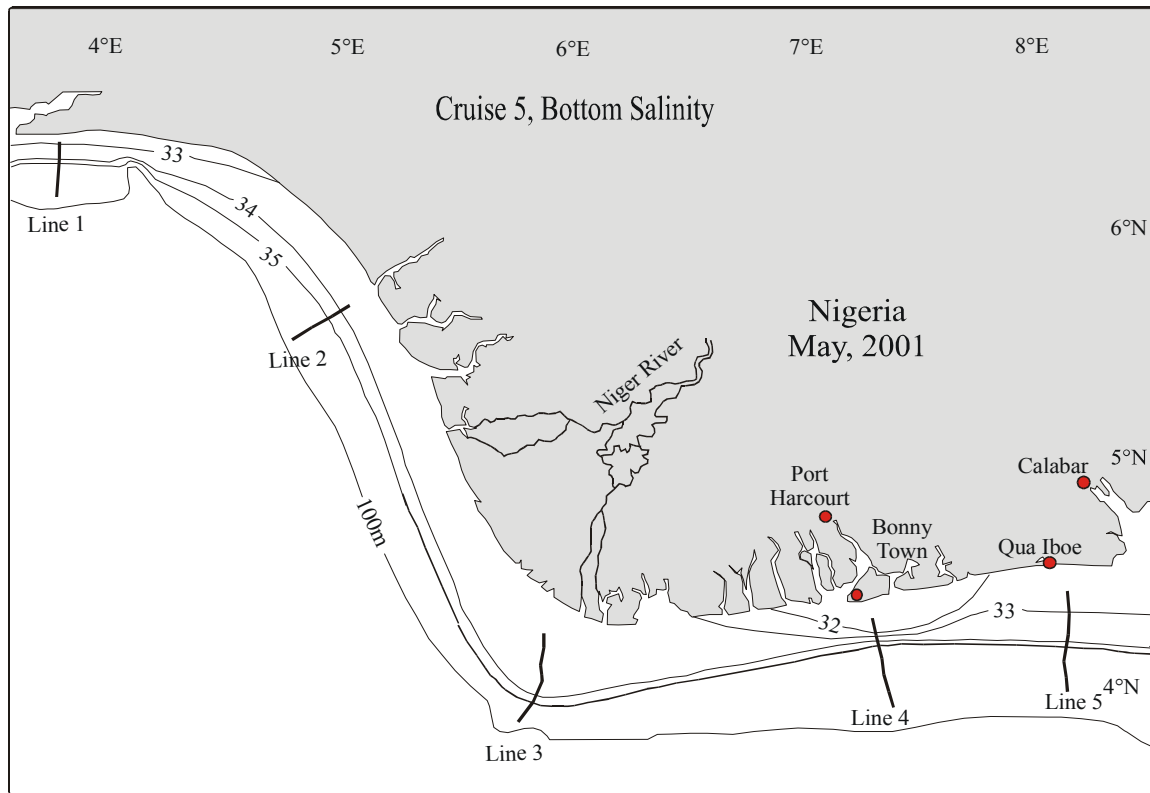


FIG. 35. Brunt Vaisala frequency for Cruise 5 (calculated from CTD measurements).



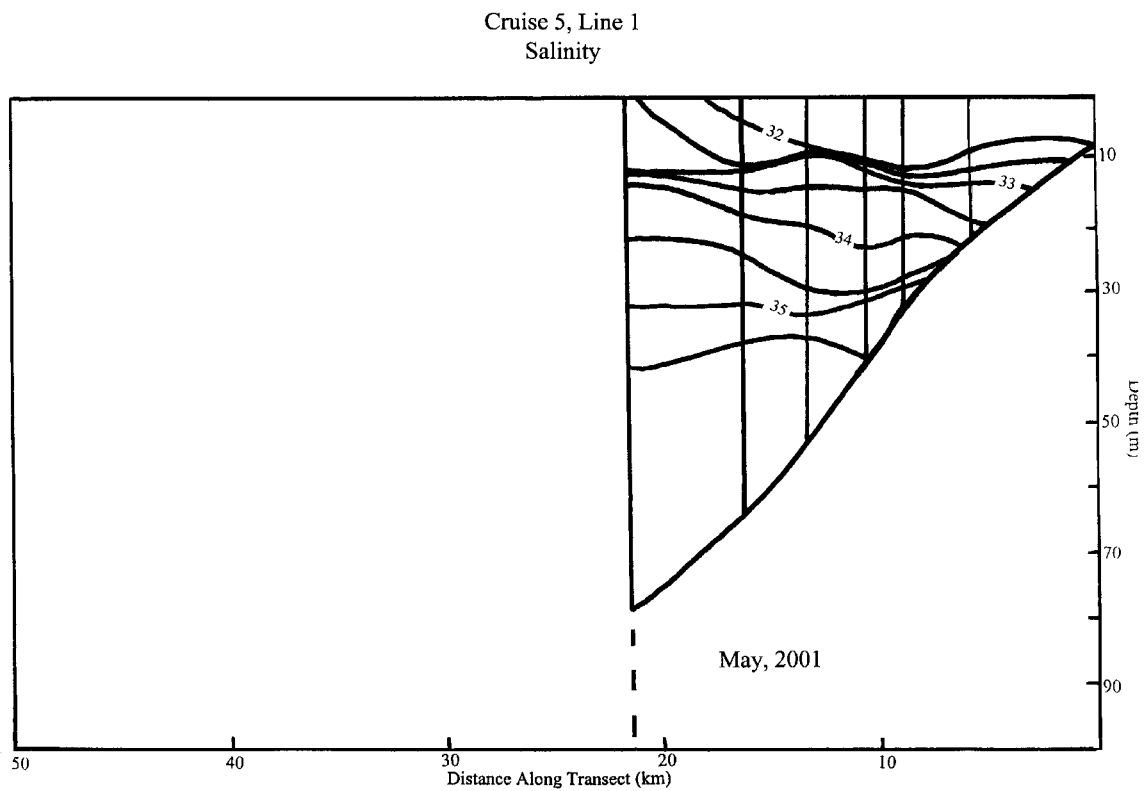
(a)

FIG. 36. Surface and bottom salinity contours (from CTD measurements) for Cruise 5.



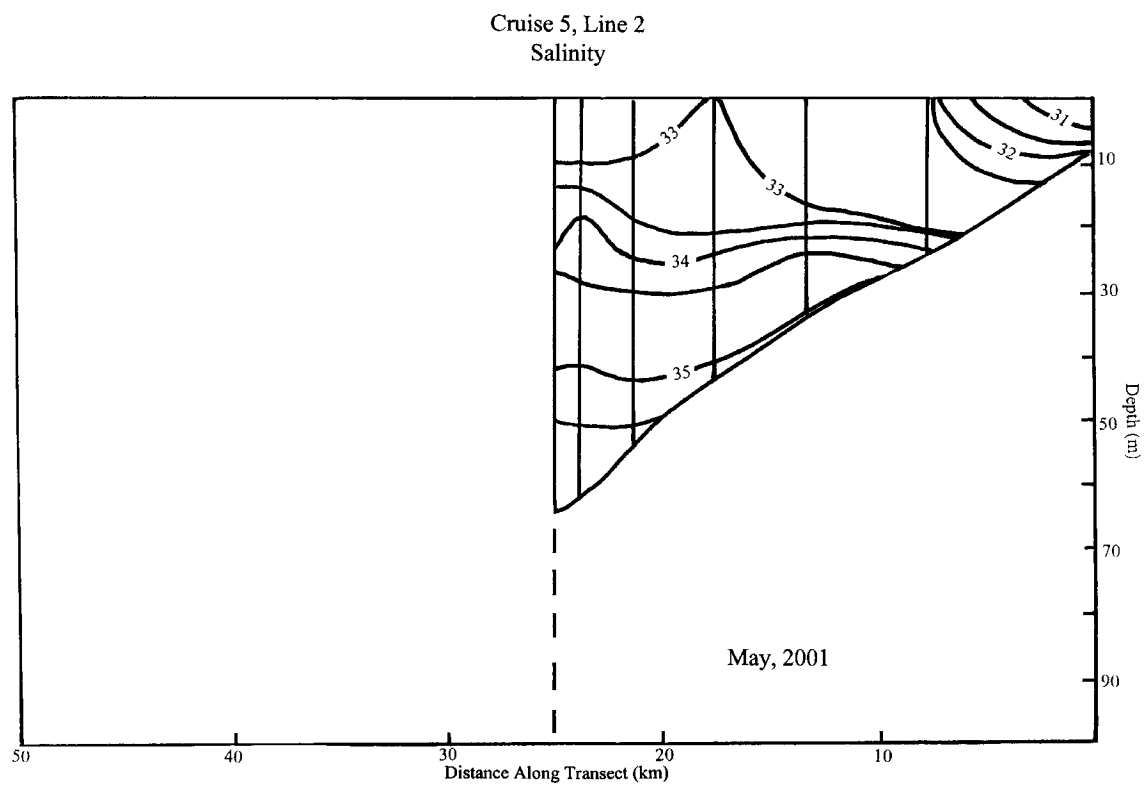
(b)

FIG. 36. Continued.



(a)

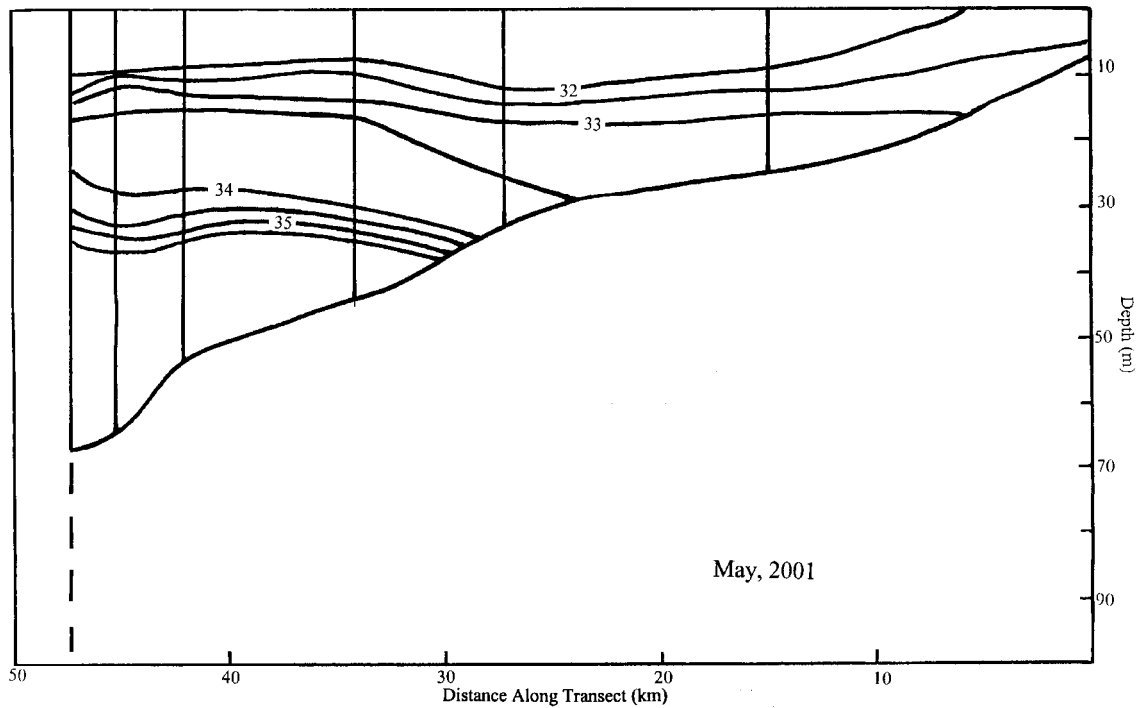
FIG. 37. (a)-(e) Cross sections of salinity contours (from CTD measurements along lines 1-5) for Cruise 5. Vertical lines represent sites of measurements on each line.



(b)

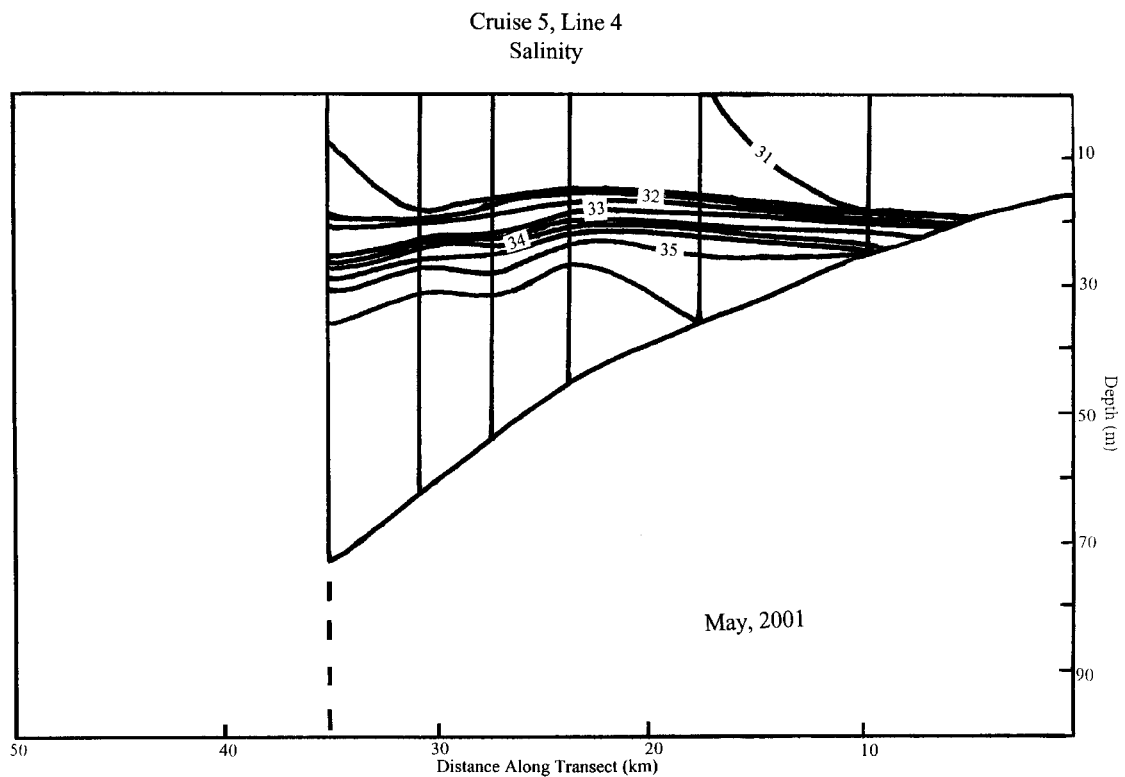
FIG. 37. Continued.

Cruise 5, Line 3
Salinity



(c)

FIG. 37. Continued.



(d)

FIG. 37. Continued.

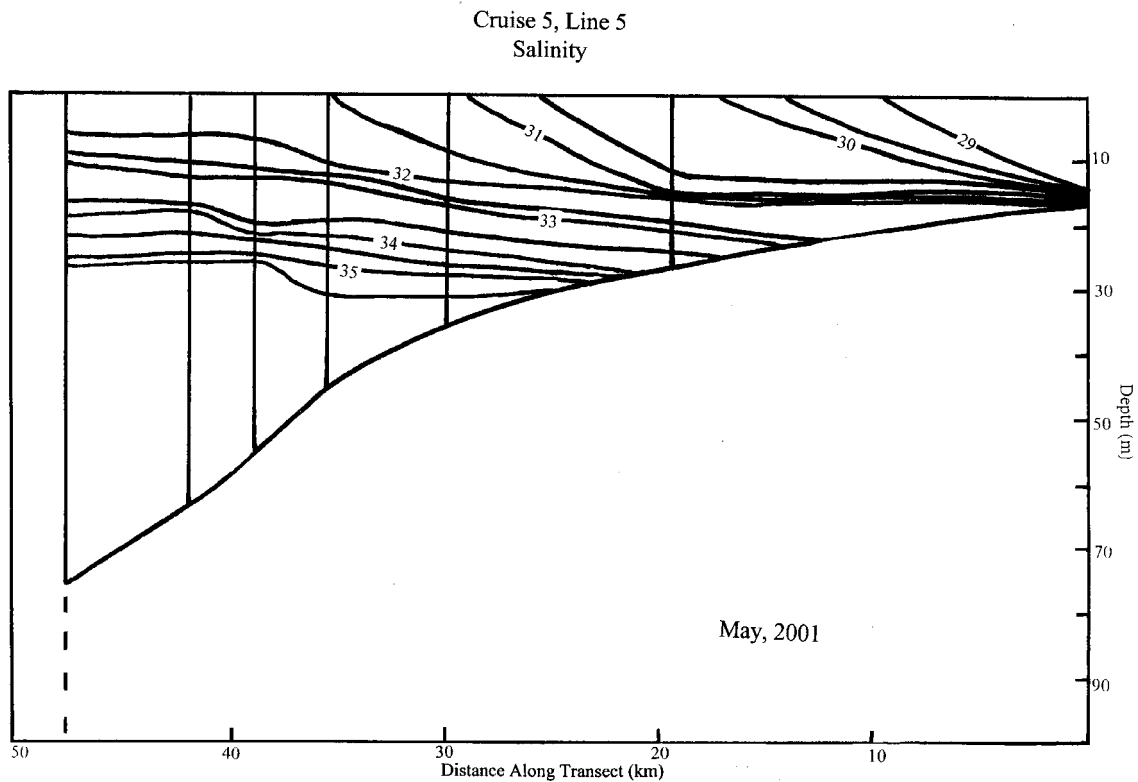


FIG. 37. Continued.

b. Inferred Geostrophic Shear

To obtain the geostrophic shear, first the specific volume anomaly was determined from the temperature, salinity and pressure measurements at each CTD station. The specific volume anomaly was then averaged between isobaric surfaces (in this case, every 2 decibars) and multiplied by the change in pressure between the isobaric surfaces to obtain a dynamic height for the interval. The dynamic heights were then summed from the reference level of 60 decibars (db) up to 5 db to obtain the dynamic height (DH) of 5 db relative to 60 db. Because the water depths vary from station to station along each CTD line, the contribution of DH from the deeper water column at one site had to be added to the total DH of the shallower site (done for all sites along the line reaching depths less than 60 db) in order carry out an even comparison along the cross-shelf

transect. This means the DH of site 1 (the site nearest to shore and therefore shallowest) contains contributions from the deeper water column (up to 60 db) of all other sites along the CTD transect. The DH contributions from the deeper sites were added to the shallow sites by integrating values along the seafloor slope according to methodology developed by Sverdrup, Helland-Hansen, Csanady and others (as reviewed in Wang, 2002). Once a DH was obtained from each station along the five transects during each cruise, the geostrophic speeds normal to the transects were determined between each pair of adjacent stations using the following equation:

$$V_g = \Delta DH / fL,$$

where $f = 2\Omega \sin(\theta)$, the Coriolis parameter, with Ω the rotation period of the earth and θ the latitude. L is the length of between sites.

The resulting geostrophic calculations produced frequent reversals along the transect providing no useful information concerning the geostrophic flow field. This is most likely because the bottom density was not uniform along isobaths resulting in pycnobathic flow which is not reflected using this methodology.

6. DESCRIPTION OF THE COASTAL CURRENT REGIME OBSERVED OFF NIGERIA

a. General Considerations

The currents present offshore Nigeria are the result of several forces and appear very complicated. It was shown in Section 4a that anywhere from 20 to 80% of the energy of those currents is tidal. The remaining energy may be divided between weather scale events and mesoscale events, with slightly more energy seen in mesoscale events as shown in Section 4a. To describe the current regime, a number of analysis techniques were applied to the ADCP current data and examined, including:

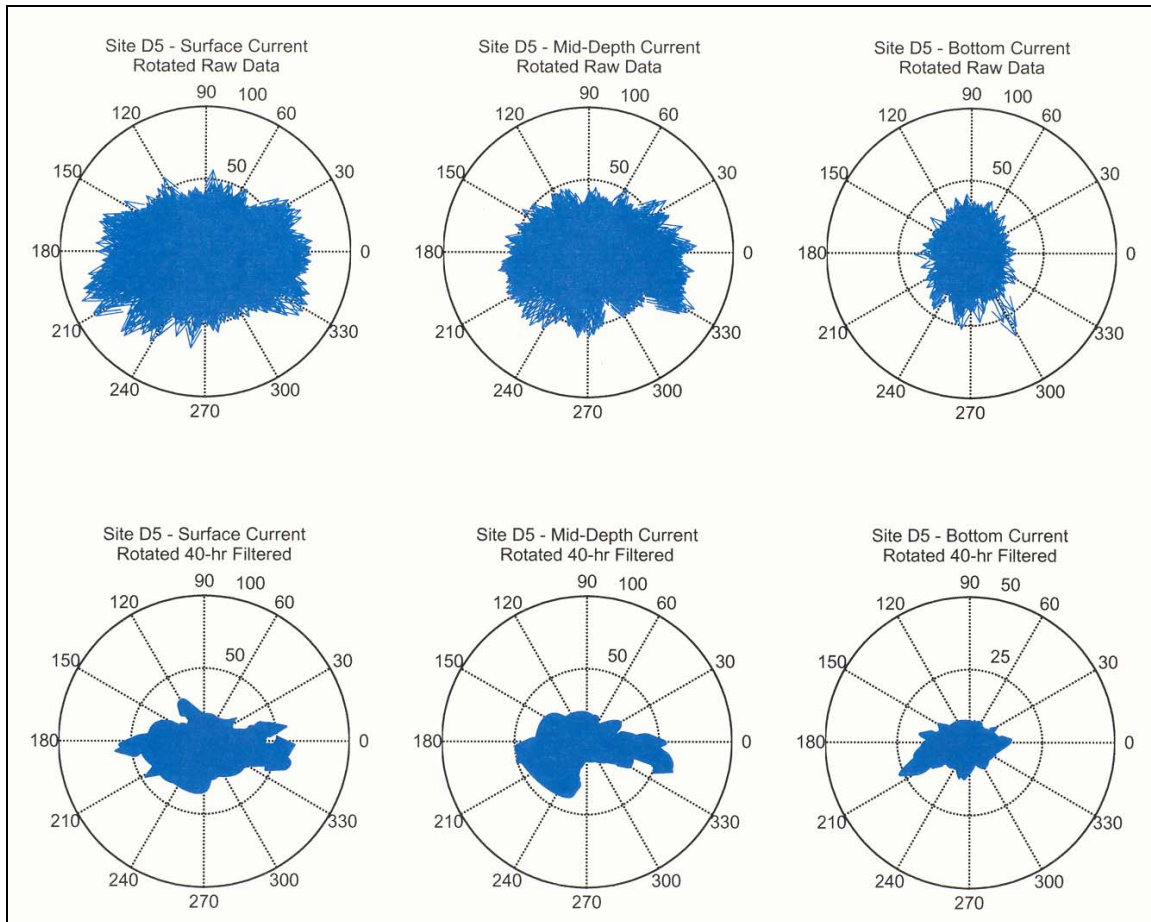
Plots of raw and 40-hr, low-passed time series of current vectors and components,
Compass plots of the raw and 40-hr low-passed currents,
Spectra of the raw current data,
Horizontal coherence of currents between sites,
Time series and persistence vs duration for low-passed alongshelf currents,
Vertical empirical orthogonal function (EOF) analysis of currents at each ADCP location
and
Vertical coherence of horizontal currents at different sites.

Statistics of the raw and 40-hr low-passed current speeds are presented in Table 4. Unfiltered maximum speeds are 72-121 cm/s at surface and 52-74 cm/s at bottom. The largest values are found to the west for both surface and bottom records. Mean currents are 19-33 cm/s at the surface and 13-20 cm/s at the bottom. The means are consistently larger than the standard deviations. Note there is little difference between mean bottom currents at shallow moorings and those at deep moorings. The instrument depths for the shallow moorings are 2 m below the sea surface and 3 m above the seafloor. The instrument depths for the deep moorings are 3-4 m below the sea surface, 22-25 m below the sea surface and 6 m above the seafloor for surface, mid-depth and bottom instruments, respectively.

TABLE 4. Statistics on raw and 40-hr low-passed ADCP current data (units are cm/s). WD indicates water depth at the ADCP mooring location.

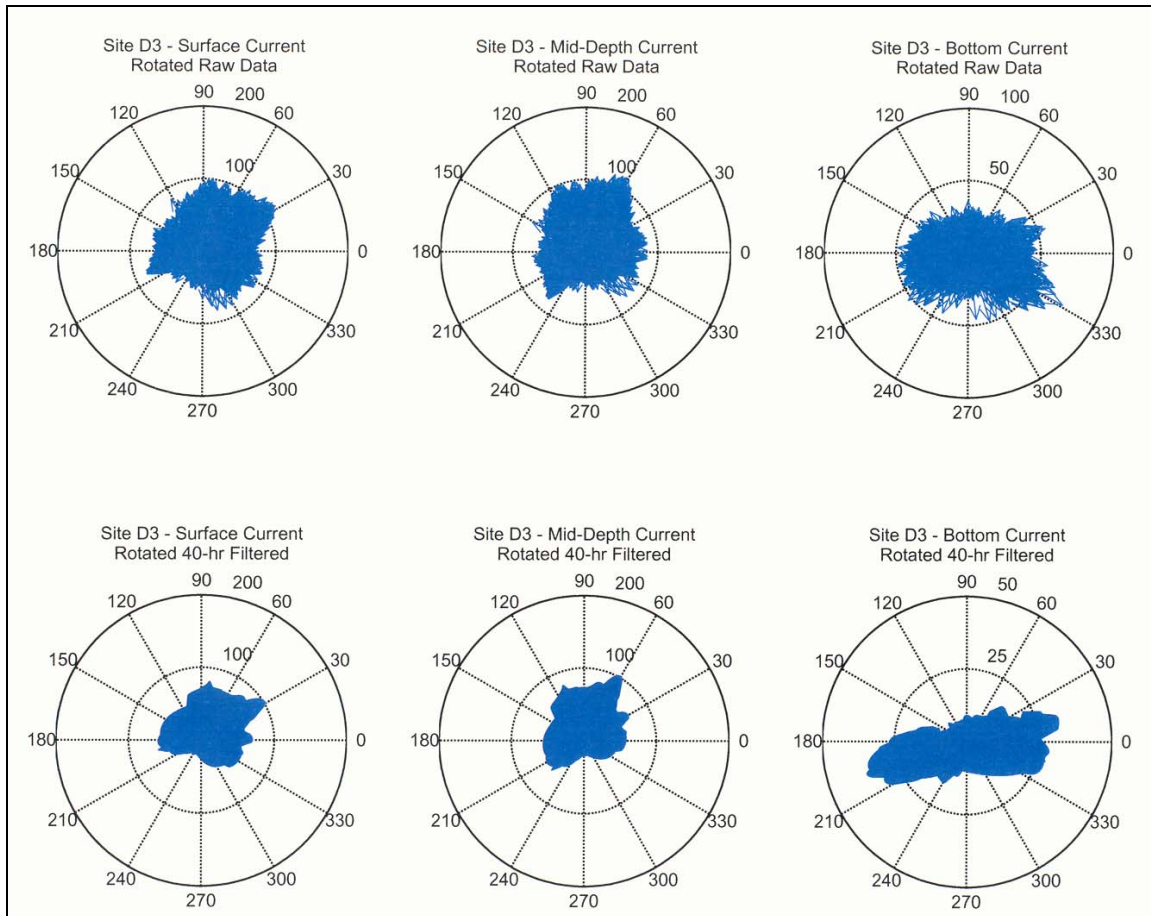
			D3		D5		S2		S3		S4		S5	
			WD = 50-51 m		WD = 44-49 m		WD = 14 - 15 m		WD = 15 - 25 m		Wd = 20 m		WD = 15 - 19 m	
			Raw	Filtered	Raw	Filtered	Raw	Filtered	Raw	Filtered	Raw	Filtered	Raw	Filtered
Current Speeds (cm/s)	Surface	Mean	33	30	26	21	23	19	29	27	23	19	19	14
		Std	19	18	14	12	14	13	17	16	12	10	11	13
		Max	118	102	92	63	121	81	94	73	72	44	100	46
	Mid-depth	Mean	22	20	21	17	-	-	-	-	-	-	-	-
		Std	13	12	14	13	-	-	-	-	-	-	-	-
		Max	88	67	83	63	-	-	-	-	-	-	-	-
	Bottom	Mean	17	13	13	6	17	13	20	17	17	10	15	10
		Std	9	7	7	4	9	8	10	9	9	5	8	6
		Max	74	36	65	27	60	40	58	41	52	23	54	30

Several conclusions can be drawn from examination of the compass plots of the raw and 40-hr, low-passed data. Such plots for sites D3, D5 and S2 are shown as Fig. 38 for currents rotated so that 0° is alongshelf in the direction counter to the direction of propagation of a shelf wave (referred to as the upcoast direction). (A shelf wave would be expected to propagate from Qua Iboe toward Lagos, i.e., downcoast, along the shelf under study.) The onshore, cross-shelf direction is then 90° in the rotated coordinates. Site D5 (Fig. 38a) illustrates directional characteristics at the eastern end of the study area (sites S4, S5 and D5). Site D3 (Fig. 38b) represents both S3 and D3. Site S2 (Fig. 38c)



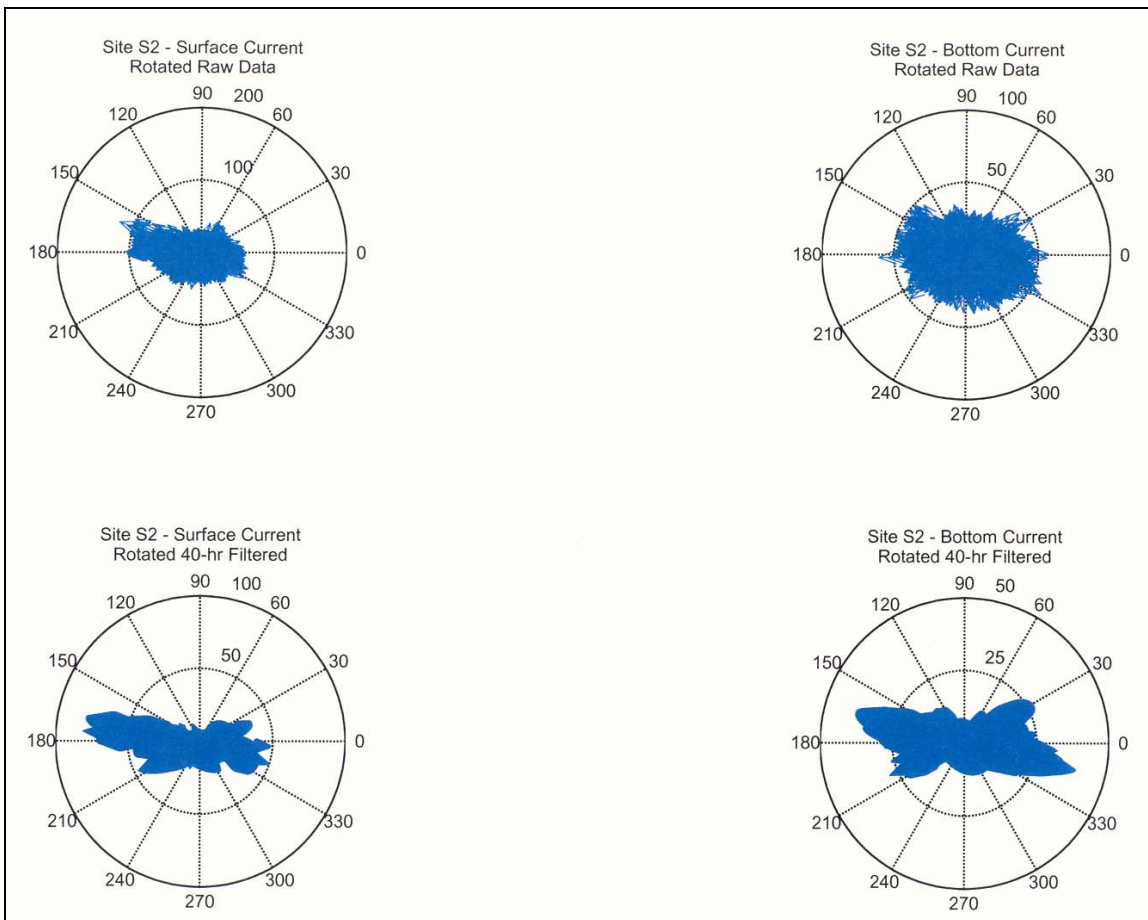
(a)

FIG. 38. (a) – (c): Polar plots of surface, mid-depth (for D3 and D5) and bottom currents. Downcoast in the sense of a propagating Kelvin wave is toward 180° . Current speeds are in cm/s. Both raw and 40-hour filtered data are shown at each site.



(b)

FIG. 38. Continued.



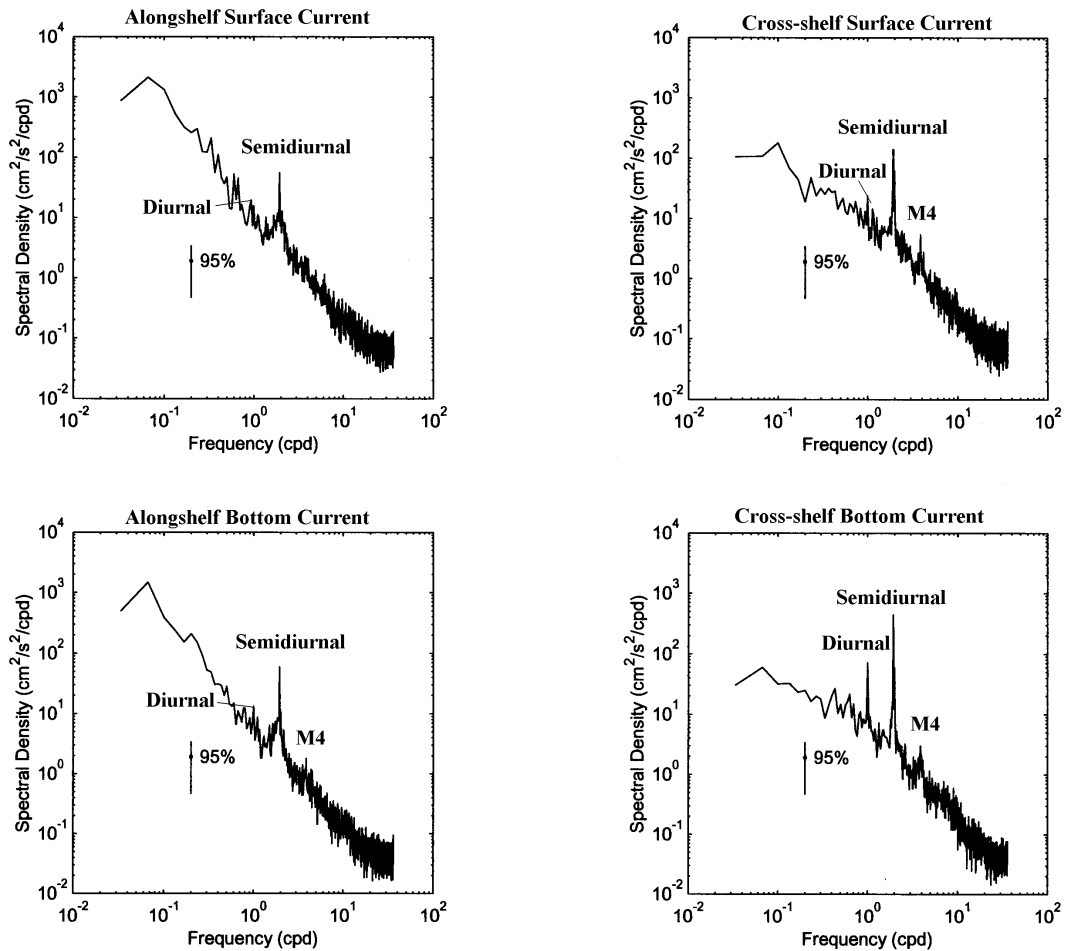
(c)

FIG. 38. Continued.

represents the western part of the study region. Raw and low-passed surface currents are aligned alongshelf in the eastern end of the study area (S4, S5 and D5), strongly alongshelf at site S2 and have no preferred direction at sites S3 and D3. The raw bottom currents show a slight bi-directional cross-shelf preference in the east at site D5, where the tides are strongest, and show a slightly alongshelf direction elsewhere. The low-passed currents show a bi-directional alongshelf current in all depths of the water column except for the surface currents at site D3 and S3 previously mentioned.

Powerspectra (Fig. 39) were calculated for each of the sites over the four deployment periods for the alongshelf and cross-shelf surface and bottom currents. The spectra were calculated using 30-day segments of record and the resulting spectra were averaged to increase the degrees of freedom and obtain a confidence limit while still retaining appropriate resolution (Welch, 1967). The spectra are shown at two sites to represent the study area: one shallow site on the western edge of the study (Fig. 39a) and one deep site in the eastern end of the study (Fig. 39b). (Note that there are some differences from location to location, mainly in the strength of the semidiurnal signal.), The spectra clearly show that the currents are dominated by a semidiurnal signal, strongest in the cross-shelf directional component, with only a slight diurnal signal present, stronger in the bottom currents. More dominant than the diurnal signals are the M_4 and M_6 signals in the cross-shelf components, site S2 being an exception. There is slightly more energy in the surface currents than in the bottom currents over the entire spectra and within periods greater than 1 day. There is significantly more energy in the alongshelf currents than in the cross-shelf currents.

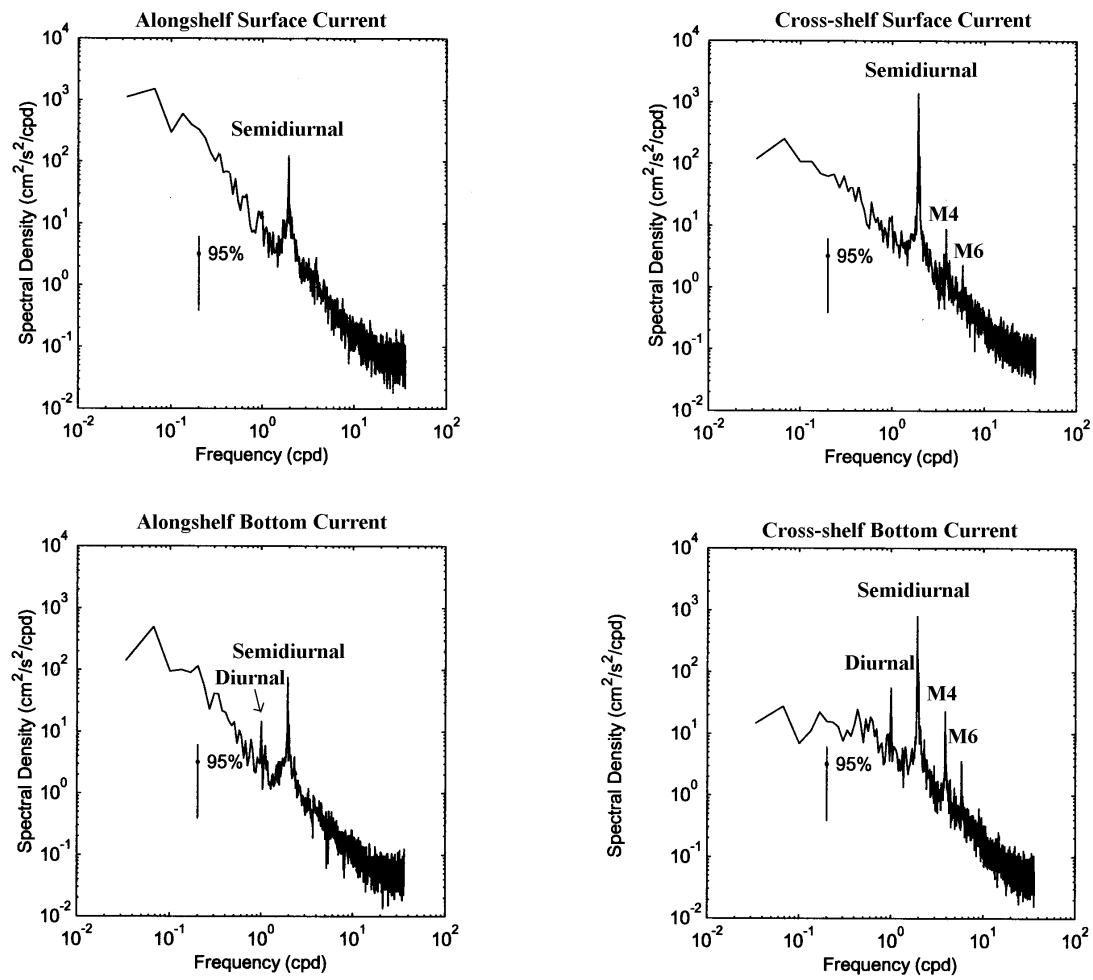
Site S2 Spectra



(a)

FIG. 39. Power spectra from sites (a) S2 and (b) D5. Power spectra obtained by block averaging spectra calculated using 30-day segments of record, taken to represent the study area. Vertical line indicates 95% confidence intervals determined from degrees of freedom.

Site D5 Spectra



(b)

FIG. 39. Continued.

b. Horizontal Current Structure

1) Horizontal Coherence²

Horizontal coherence was calculated between surface currents at shallow and deep ADCP locations (cross-shelf) and for both surface and bottom currents at neighboring pairs of alongshelf ADCP locations.

The coherence has peaks at tidal frequencies, mainly the semidiurnal frequency, in both alongshelf and cross-shelf current components. Additionally, peaks in coherence occur at some periods > 40 hrs between alongshelf current components. Within the frequency range above the tides some peaks in coherence occur, but they are rarely significant and not consistent from one pair of moorings to another. The results are illustrated in Fig. 40, where (a) – (d) illustrate both surface and bottom coherence between alongshelf adjacent sites and (e) – (f) illustrate the surface coherence between cross-shelf sites.

Coherence within the semi-diurnal bandwidth ranged from 0.4 to 0.9, increasing eastward along the study area. Semidiurnal coherence is most significant for the cross-shelf components; however coherence between the alongshelf semidiurnal currents is quite large between the shallow sites (pair S2 and S3 and pair S4 and S5). Coherence within the M_4 tidal frequency is seen east of the Niger Delta (e.g., between sites D3 and D5) and coherence within the M_6 tidal frequency is seen between D5 and S5. The phase between sites was small for semidiurnal frequencies with virtually no phase lag in the cross-shelf direction except between sites S2 and S3, which have a cross-shelf phase lag of about 6 hours from S2 to S3 at the surface and from S3 to S2 at the bottom. There is also a slight cross-shelf phase lag at the semidiurnal frequency of about $1 \frac{1}{2}$ hours from D5 to D3.

Coherence at periods >40 hrs is significant between pairs of alongshelf currents from cross-shelf locations (e.g., pair D3 and S3 and pair D5 and S5). It should be noted that between sites D3 and S3 the coherence at periods > 40 hrs is greater than the coherence

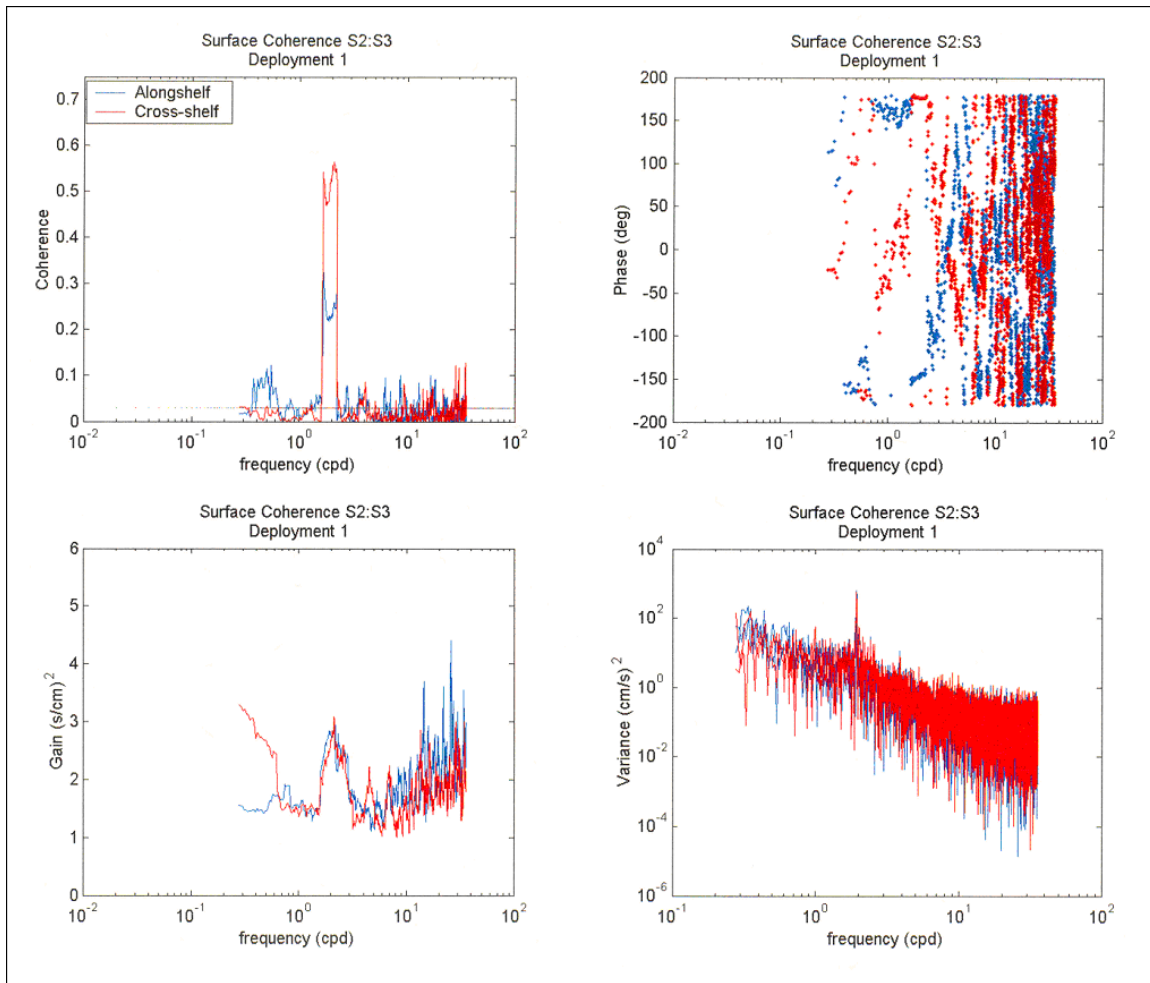
² Throughout the coherence analyses, the word “significant” is used to describe values that fall above the confidence limit (γ) obtained using the following equation from Emery and Thompson (2001): $\gamma = 1 - \alpha[2/DOF - 2]$, where $\alpha = 1 - CI$, and CI = specified confidence interval.

within tidal frequencies. The coherence between low-passed currents between alongshelf sites is lower than between sites located across the shelf, but still significant where values range from 0.1 to 0.3 between surface values. Coherence between the current for periods >40 hr in the alongshelf direction (such as between site pair S2 and S3 and pair D3 and D5) differed greatly by deployment and by site. The phase between such long-period currents from sites located both alongshelf and cross-shelf is not steady and varies greatly from site to site and by deployment.

The relatively high coherence between spatially separated ADCP locations for periods greater than 40 hrs give a strong indication that alongshelf currents dominate at low frequencies. This is consistent with conclusions from the polar plots shown in Section 6a, and it will be seen more clearly in the following Section, 6b-2.

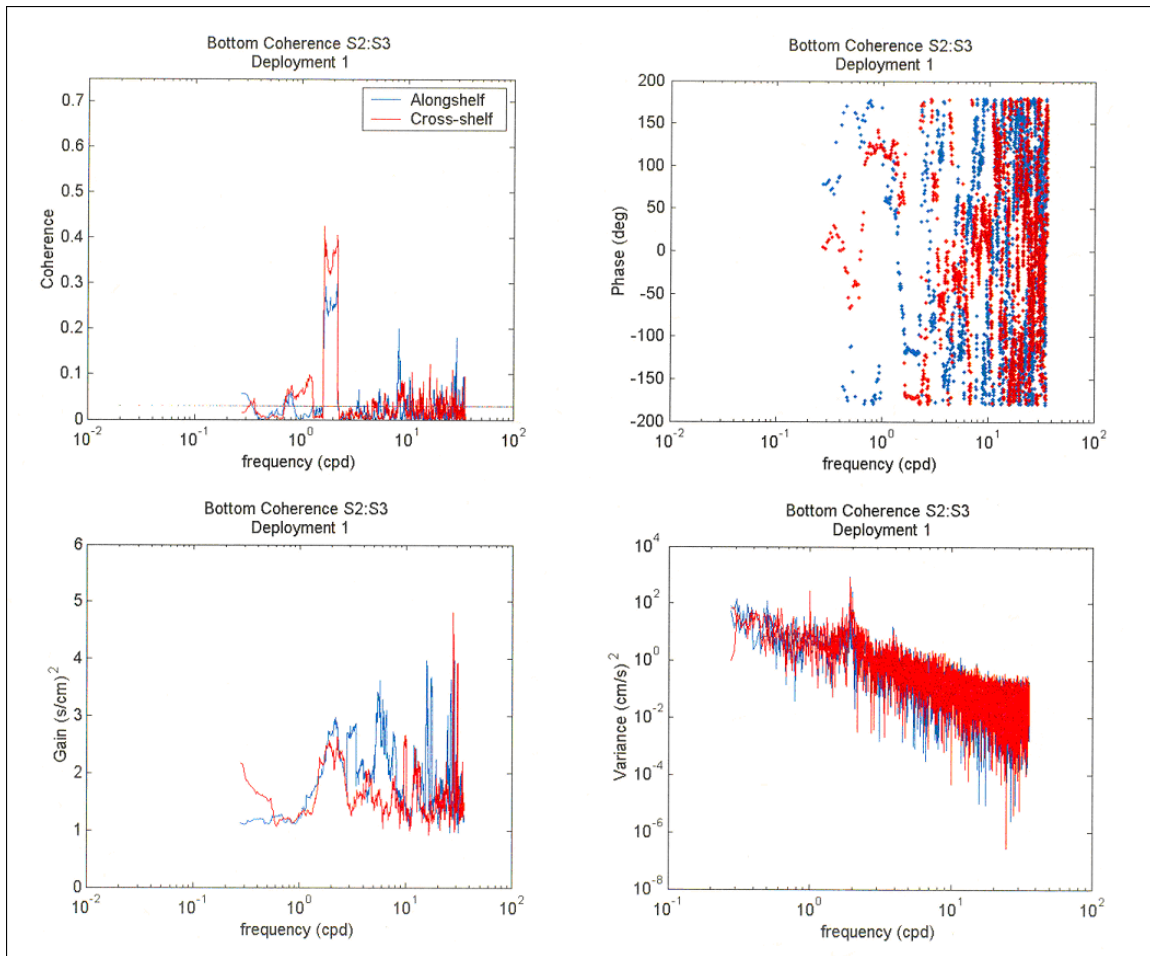
2) Alongshelf, low-passed currents

As shown in Fig. 38, once the tides are removed, or the current time series has been low-pass filtered, the remaining current is strongly oriented in the alongshelf direction, generally preferring neither upcoast nor downcoast flow. The term “downcoast” refers to the along-isobath direction a Kelvin wave would travel along the shelf—from east to west in the study region. The absence of a dominant current direction can be seen by the frequent reversals in the low-passed alongshelf current seen in Figs. 41 and 42. Fig. 41 illustrates the frequent reversals at inconsistent intervals in the low-passed alongshelf



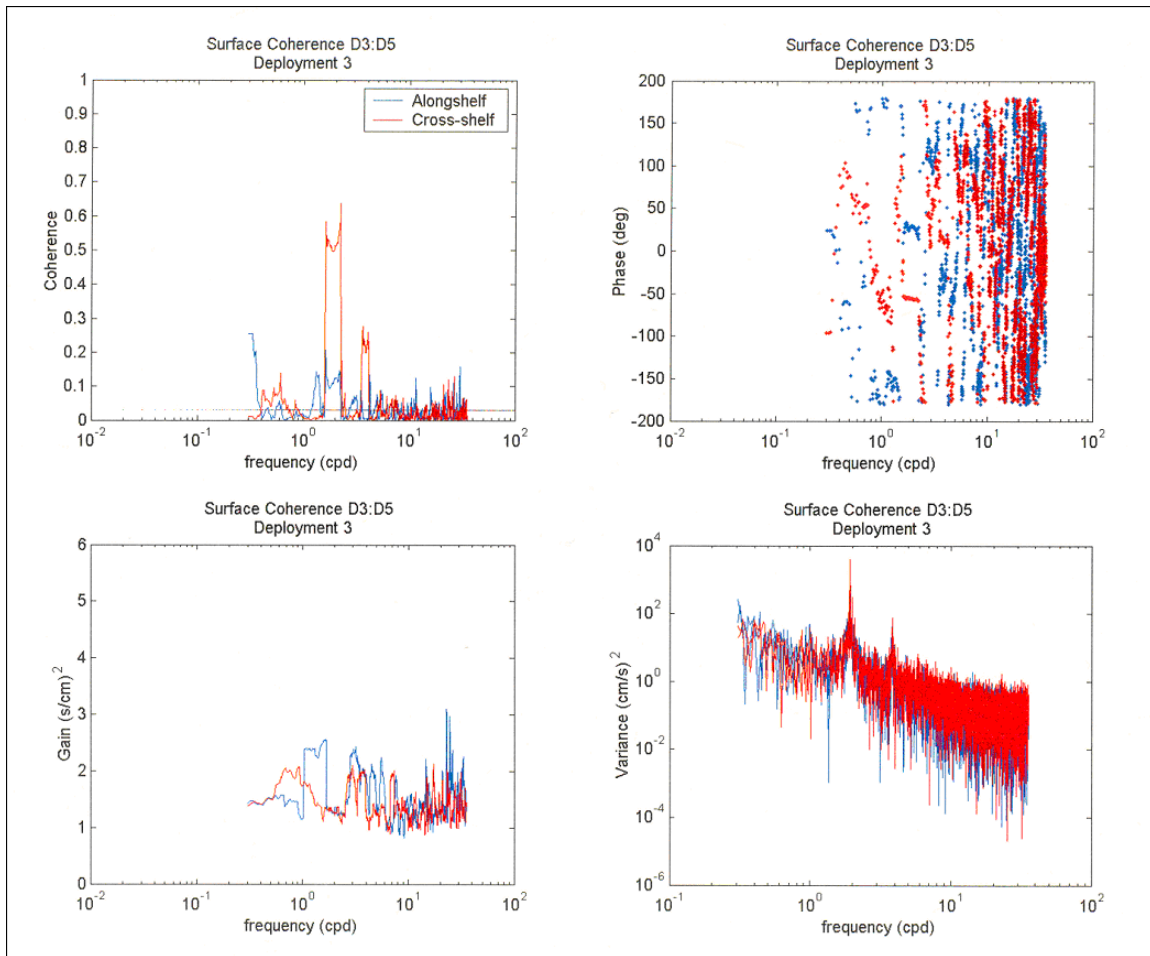
(a)

FIG. 40. (a) – (f) Examples of horizontal coherence, phase, gain and variance for pairs of records from the same depths at different mooring sites. Horizontal lines on coherence spectra indicate the significance level representing a 95% confidence interval. Red represents the cross-shelf current component and blue represents the alongshelf current component. (a) – (d) illustrate coherence between pairs of alongshelf sites S2 and S3, and D3 and D5. (e) and (f) illustrate coherence between pairs of cross-shelf sites D3 and S3 and D5 and S5.



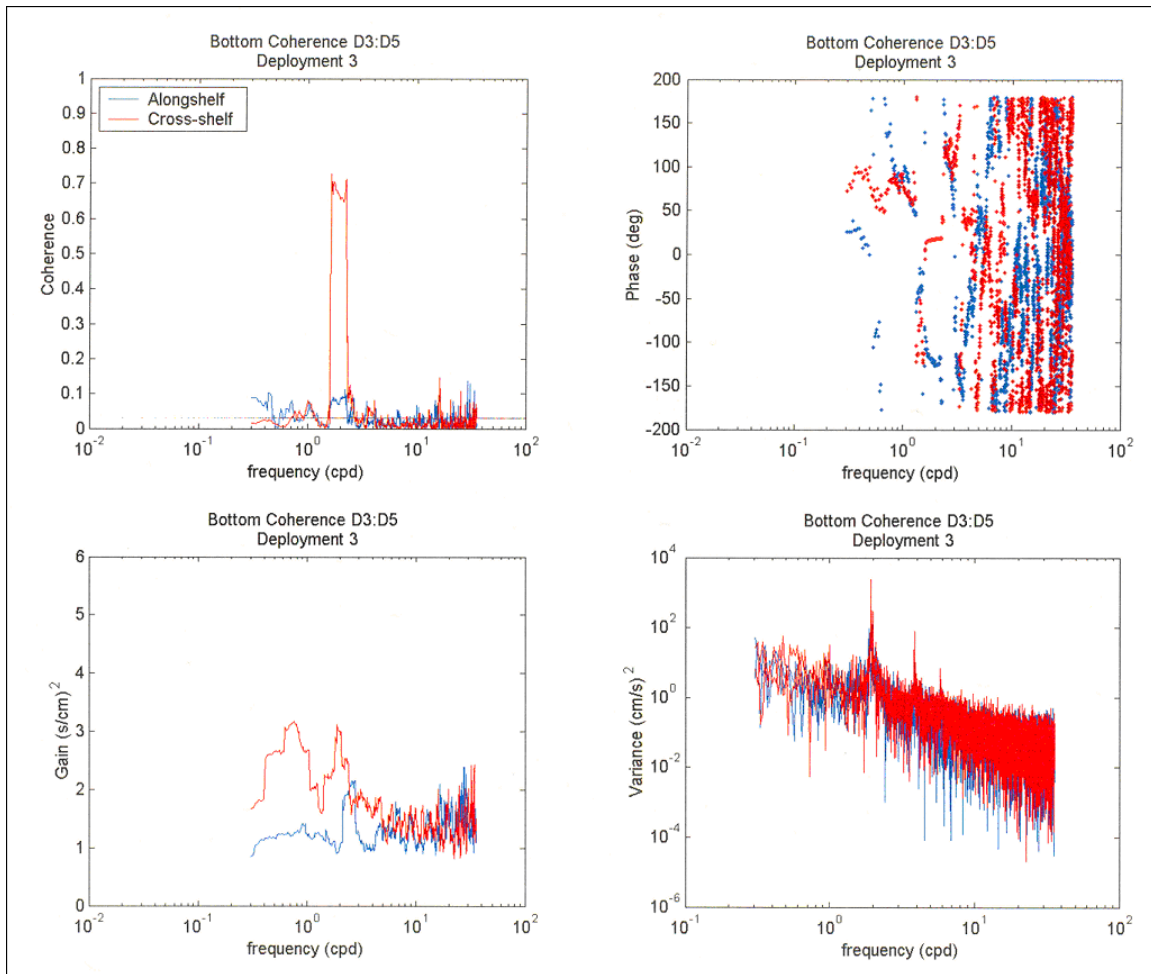
(b)

FIG. 40. Continued.



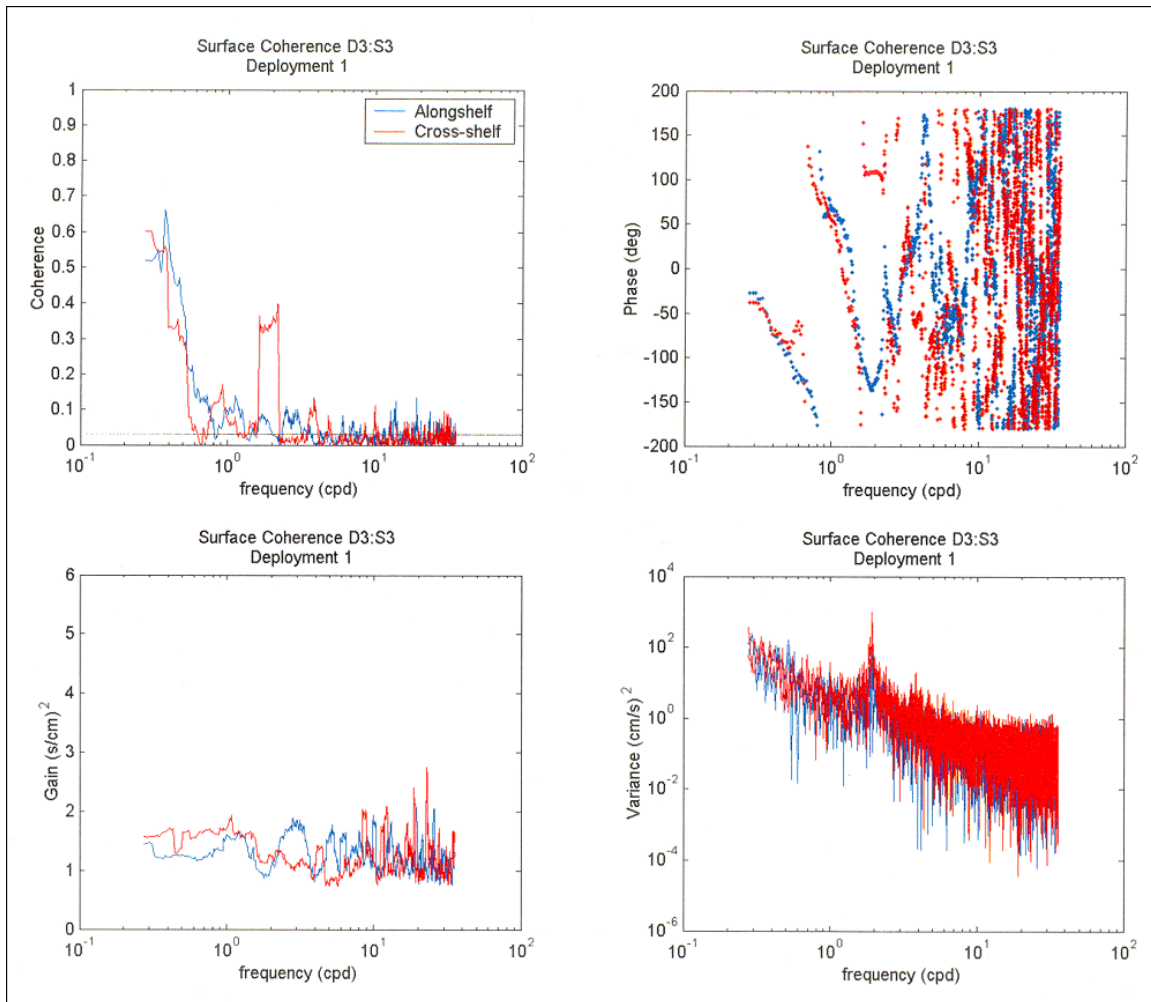
(c)

FIG. 40. Continued.



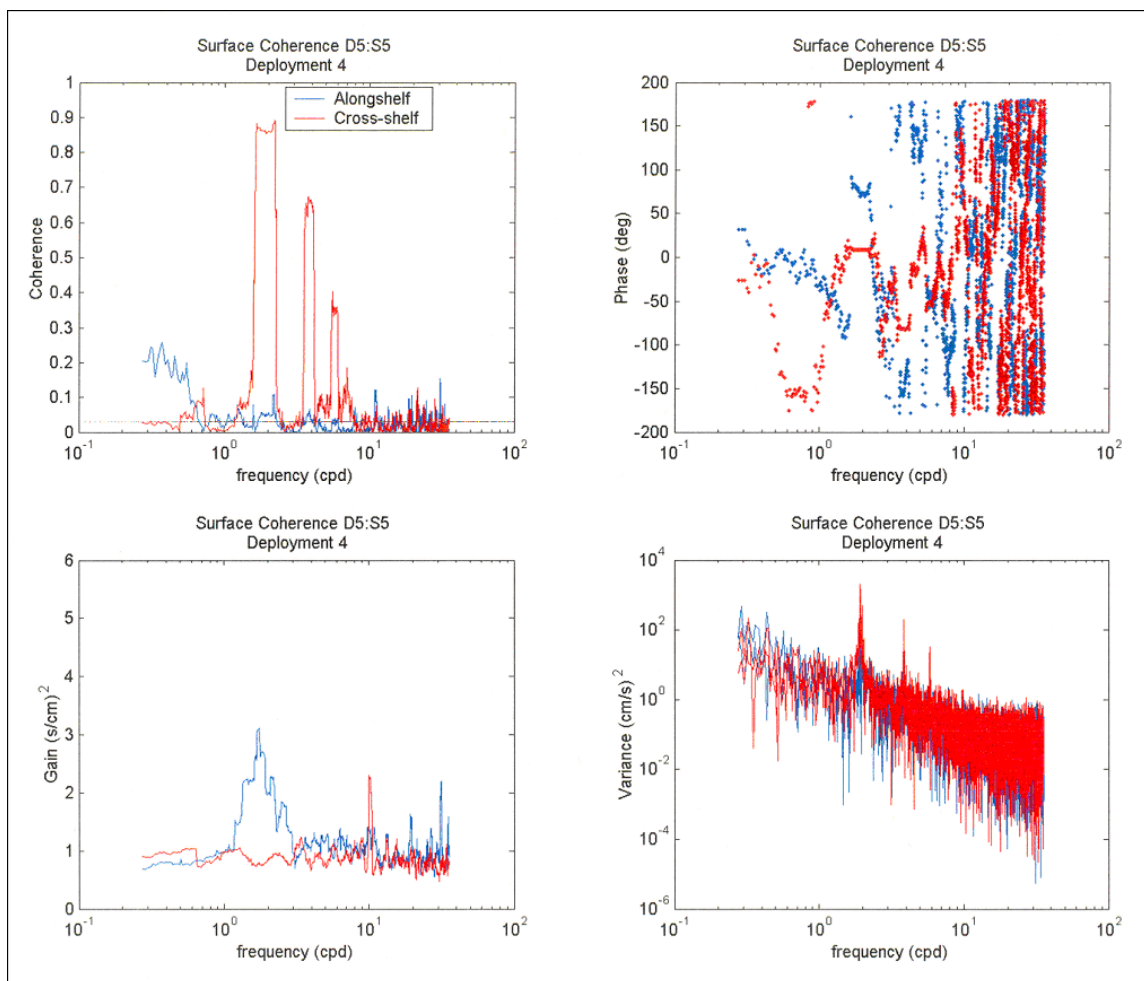
(d)

FIG. 40. Continued.



(e)

FIG. 40. Continued.



(f)

FIG. 40. Continued.

currents at sites S2 and S5, located at opposite ends of the study area. Fig. 41 also seems to indicate more current reversals in the western than in the eastern part of the study area. Fig. 42 shows the surface and bottom low-passed alongshelf time series for site D3, located between the sites shown in Fig. 41. It is seen that the alongshelf current frequently reverses throughout the water column. The surface currents seem to exhibit longer durations in a given direction than the bottom currents. To illustrate that the patterns of reversals continued throughout the year, Fig. 43 shows mid-depth alongshelf currents for all four deployment periods at site D3.

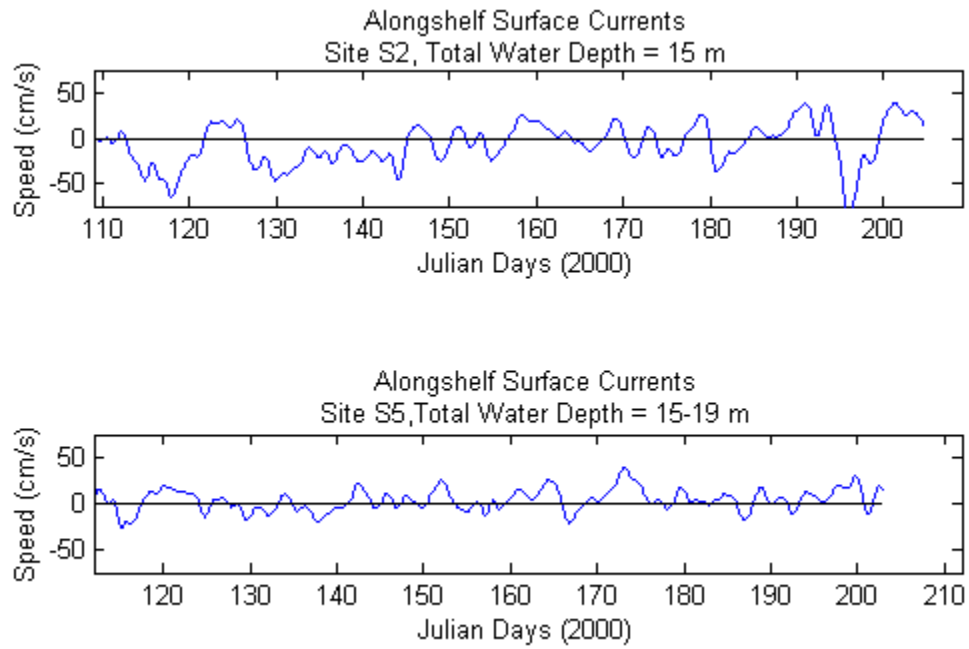


FIG. 41. Low-passed alongshelf surface currents (~ 2 m depth) during deployment 1 at site S2 (top) near the eastern end of study area and at site S5 (bottom) at the western end of the study area. A positive speed indicates upcoast flow.

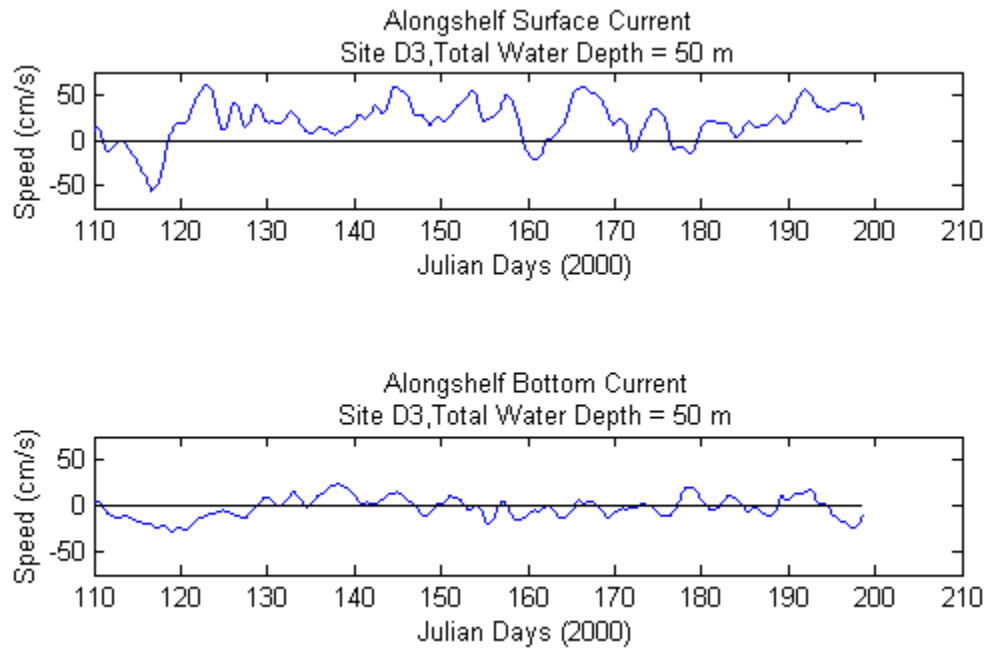


FIG. 42. Low-passed alongshelf surface (top) and bottom (bottom) currents at site D3 (in the central study area). A positive speed indicates upcoast flow.

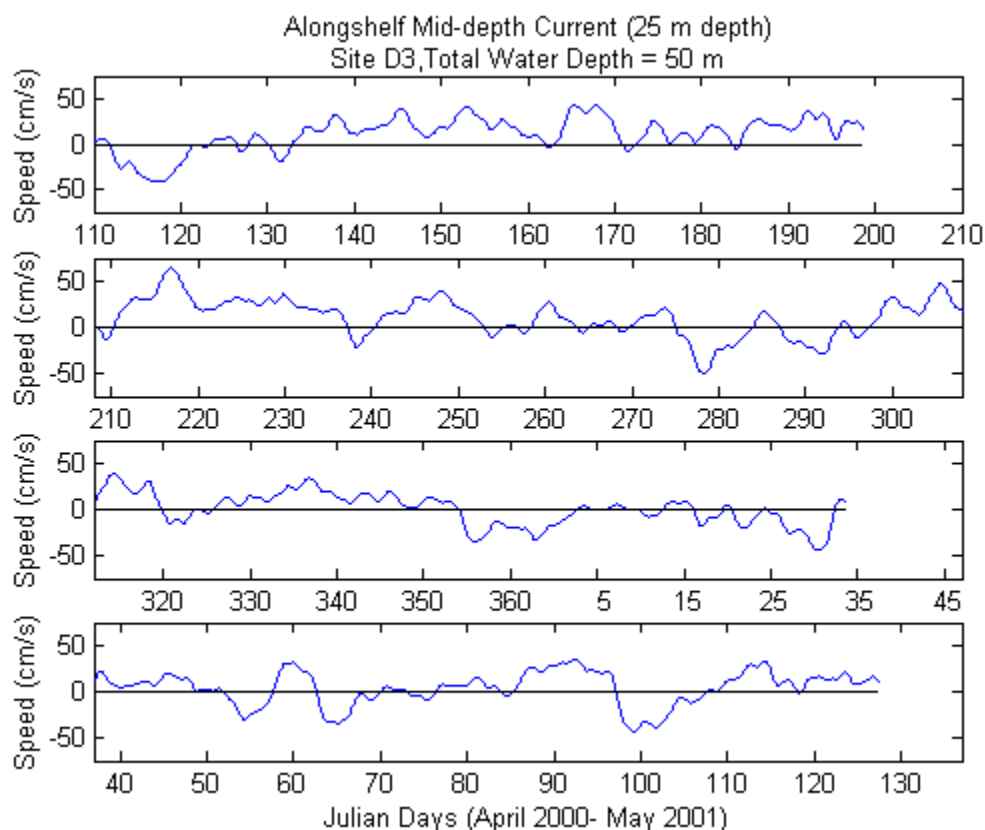
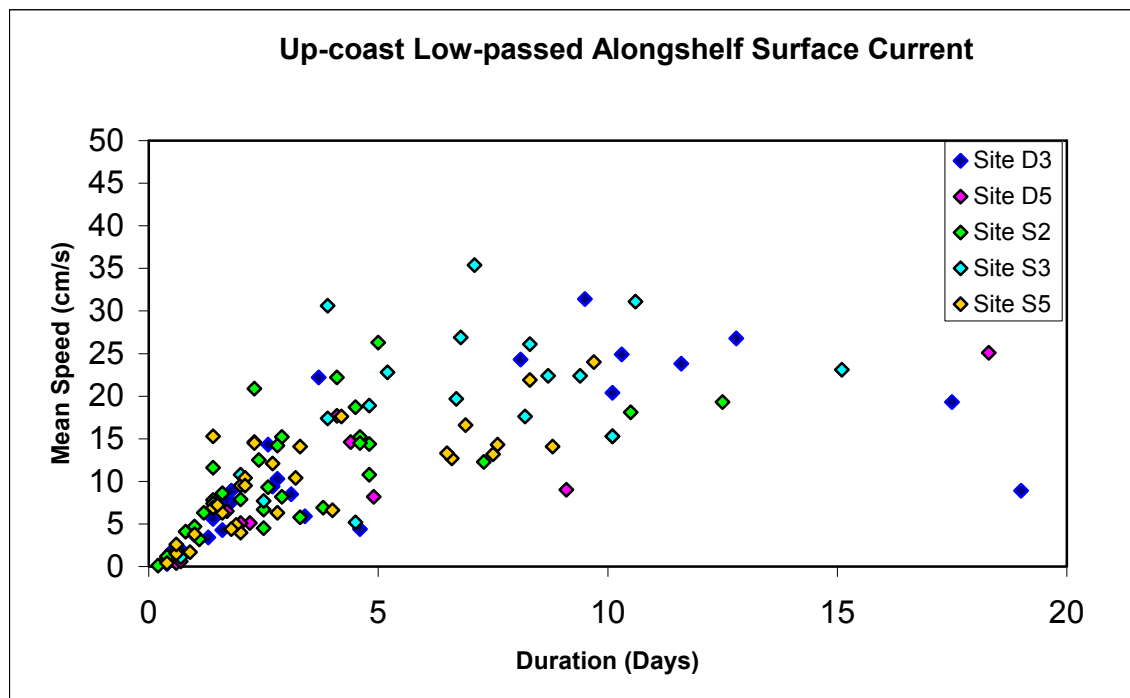


FIG. 43. Low-passed alongshelf mid-depth currents at site D3 (from April of 2000 through May of 2001). A positive speed indicates upcoast flow.

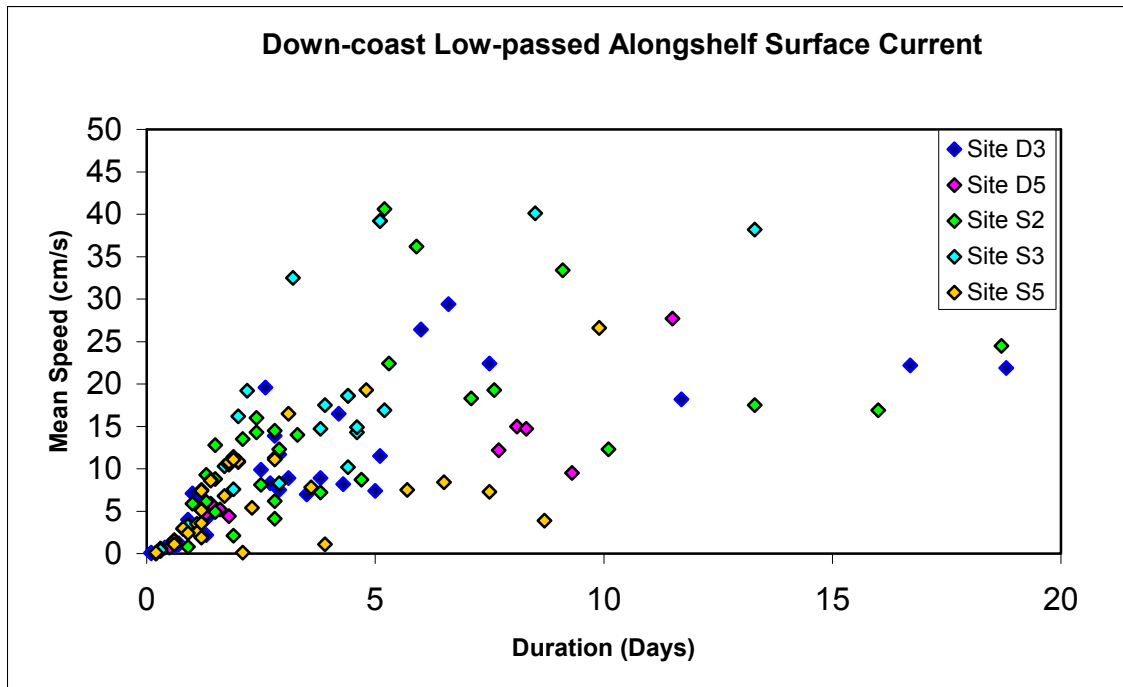
Persistence of the low-passed alongshelf surface current in one direction was examined. Fig. 44 presents plots of mean speed versus duration in both upcoast and downcoast directions. A summary of the duration times is presented as Table 5. The mean speed in a given direction was generally less than 40 cm/s, and approximately 60% of the observations had mean speeds less than 10 cm/s. At all sites the durations in a specific direction are concentrated between 0 and 5 days, with 58- to 88% of the windows or observations lasting no longer than 5 days. In addition, the duration for both upcoast and downcoast flow rarely lasted more than 10 days, with only 5-27 % of the observed duration times lasting longer than 10 days and only 1 lasting longer than 20 days. (One point missing from Fig. 44a; site D3 had one period of upcoast flow for 41 days with mean speed of 30 cm/s, the longest duration time recorded by a factor of 2.)

The compass plots in Section 6a showed low-passed currents with no strongly preferred direction; this is quantitatively reinforced below by Table 5. The percentage of time the current flowed in either direction was nearly equal except at sites S3 and D3 where the current showed a slight preference for the upcoast direction.



(a)

FIG. 44. Mean speed of 40-hr low-passed alongshelf current at site D3. Speed shown flowing up coast or downcoast versus the duration of flow in that direction for all ADCP locations that recorded data during more than 1 deployment. One point is missing for a duration of 41 days and mean speed of 30 cm/s in the upcoast direction at site D3.



(b)

FIG. 44. Continued.

Table 5. Summary of duration times for 40-hr low-passed alongshelf currents.

		D3	D5	S2	S3	S5
Up-Coast	Total Observations	26	19	34	19	30
	% > 5 days	42	16	12	63	27
	% > 10 days	27	11	9	16	0
Down-Coast	Total Observations	32	19	34	21	32
	% > 5 days	21	32	32	19	16
	% > 10 days	9	11	12	5	0
% of time current flows up-coast		59	48	42	61	55
% of time current flows down-coast		41	52	58	39	45

c. Vertical Current Structures

1) Empirical Orthogonal Function Analysis

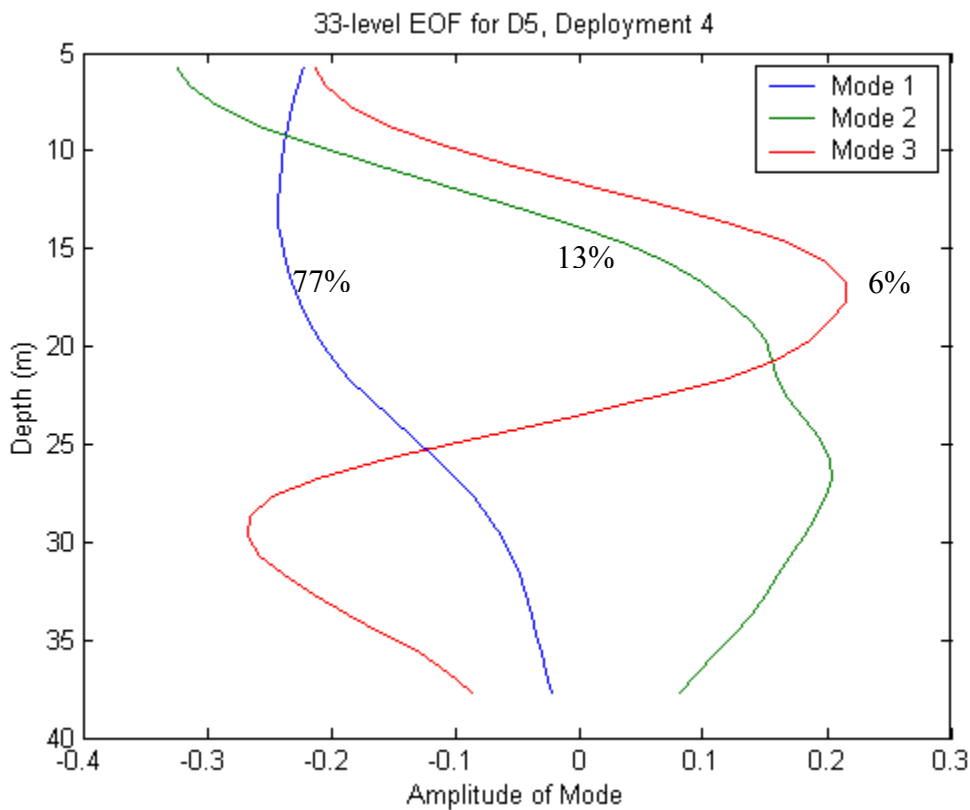
Empirical Orthogonal Functions (EOFs) were calculated at each ADCP site using measured currents at every meter in depth. The vertical structure identified by the EOF analysis was very consistent throughout the study area and throughout the study period. Fig. 45a shows the first three vertical modes typical of one deployment at a deep ADCP site, and Fig. 45b shows the first three vertical modes representing the shallow sites. In Fig. 45a, the first three modes represent 77%, 13% and 6% of the total variance, respectively. The variance of mode 1 for deep sites D3 and D5 ranged between 60 and 80% depending on deployment. For site S2, the first three modes represent 91%, 8% and 1% of the total variance (modes 4 and above had only fractional variance). Mode 1 had between 70 and 90% of the total variance at shallow sites S2, S3, S4 and S5. Fig. 45c illustrates the similarity in vertical structure seen at different deep sites throughout the region by showing the first three modes for combined deployments at deep sites D3 and D5. Compare Fig. 45c with Fig. 45a for one deployment at a deep site. In all cases, the vertical structure is dominated by Modes 1 and 2, together containing between 80 and 99 % of the total variance. At the shallow sites Mode 1 accounts for slightly more of the variance than at the deep sites (as will be explained in the following paragraphs) and Mode 3 has quite small variance. The vertical structures of the modes are very similar at shallow and deep sites.

Mode 1 is surface intensified, representing the highest amount of energy by 3 to 10 fold. Mode 1 is essentially barotropic in the upper 15 m of water, meaning Mode 1 is barotropic at the shallow ADCP locations. Below the 15-m water depth, mode 1 decays with depth to an amplitude of approximately zero near the bottom of the deep sites.

Mode 2 has the largest amplitudes at the surface and near bottom with similar vertical structures at shallow and deep sites. As the amplitude of Mode 1 decreases to zero at the deep sites, the amplitude of Mode 2 increases making the variance represented by Mode 2 an important contribution to the vertical structure near the seafloor.

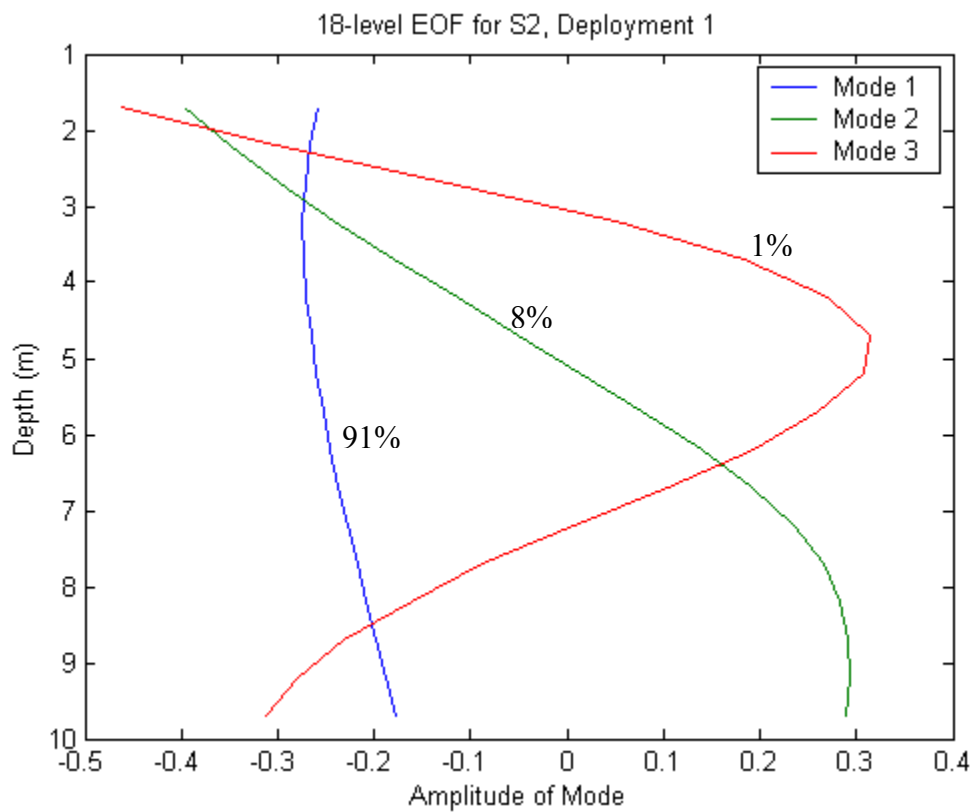
Mode 3 contains less than 10% of the total variance at deep ADCP locations and a negligible amount of variance at the shallow ADCP locations. Mode 4 and above contain negligible amounts of variance at both shallow and deep ADCP locations.

The structure of the first three EOF modes is remarkably uniform across the study area, as illustrated in Fig. 45. This spatial uniformity of the EOF vertical structures indicates there should be horizontal coherence between the currents as was shown in Section 6b-1. That mode 1 dominates from the surface to a depth of about 15 m indicates that there should also be vertical coherence within the surface waters as will be shown in the following section.



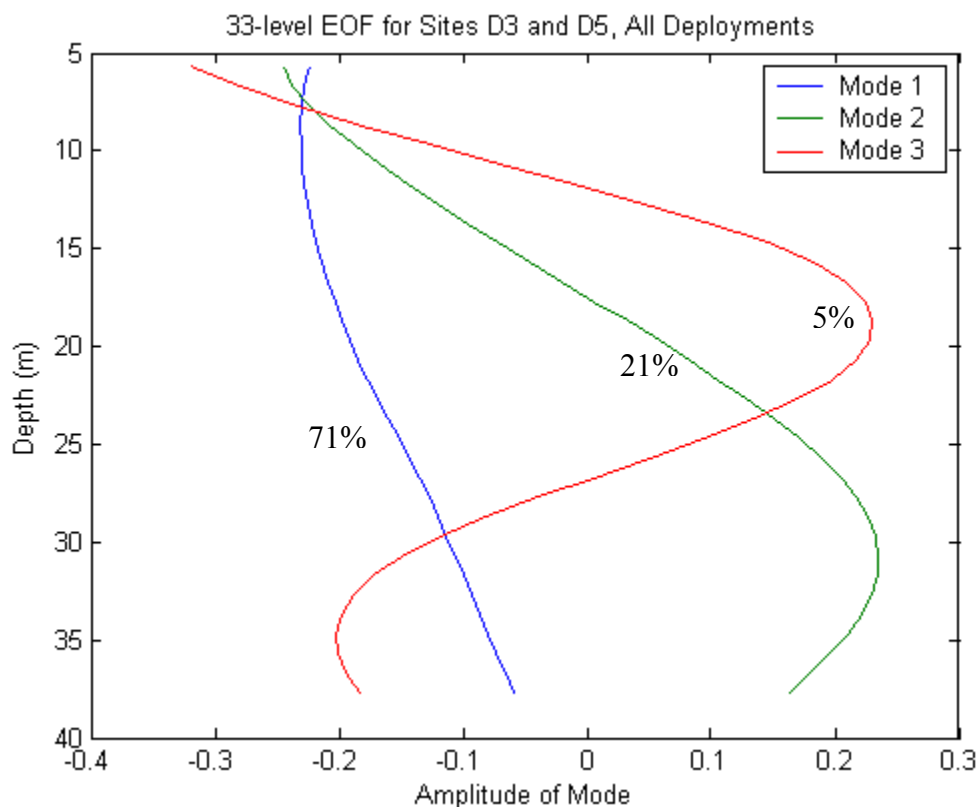
(a)

FIG. 45. (a) – (c) First three vertical modes of empirical orthogonal functions (EOFs) at Sites D5, S2 and D3 and D5 combined. (a) is calculated using 18 levels, (b) is calculated using 33 levels and (c) is calculated using 33 levels. Percentages indicate percent variance represented by each mode.



(b)

FIG. 45. Continued.



(c)

FIG. 45. Continued.

2) Vertical Coherence

Vertical coherence was calculated at the deep ADCP sites between the surface, middle and bottom depths and between the surface and bottom depths at the shallow sites.

a) Sites S2, S3, S4 and S5

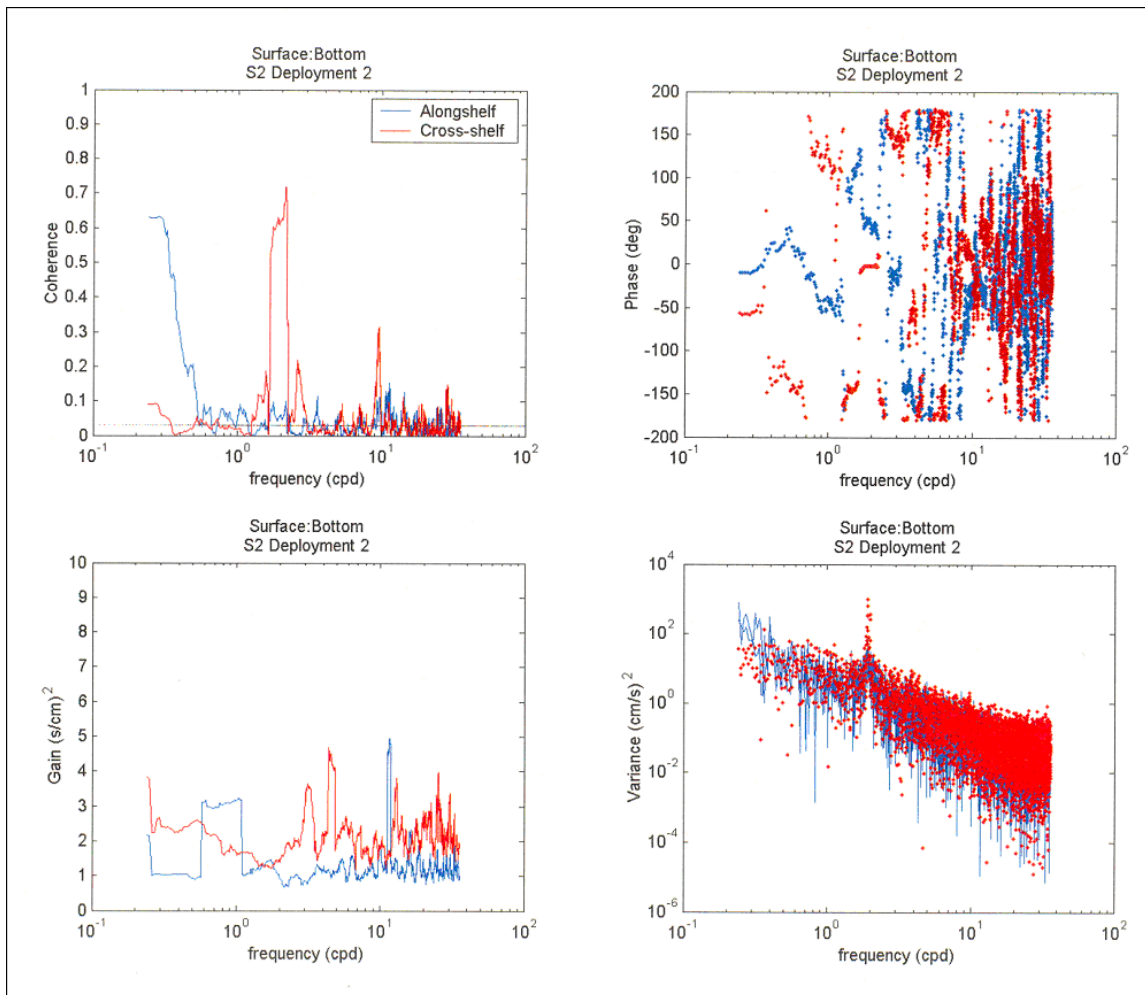
Results for deployments 1 and 2 at site S2 (deployment 2 shown as example in Fig. 46a) give high correlation with essentially zero phase difference between cross-shelf components of surface and bottom currents the semidiurnal period. Correlations are significant for periods greater than 1 day in the alongshelf direction, increasing with

increasing period for deployment 1. For deployment 2, coherence between alongshelf currents is significant for periods greater than 2 days, again with coherence increasing with increasing period. For periods of 3-4 days, phase difference is approximately -5° for alongshelf components, meaning the bottom is leading the surface by about 1 hour.

Deployments 1 and 4 at site S3 (deployment 4 shown as example in Fig. 46b) showed results very similar to deployments 1 and 2 at site S2 except site S3 showed a strong coherence in both components at semidiurnal frequency and phase difference at the 3-4 day period is $+5^\circ$ for alongshelf components during both deployments, meaning the surface is leading the bottom by about 1 hour.

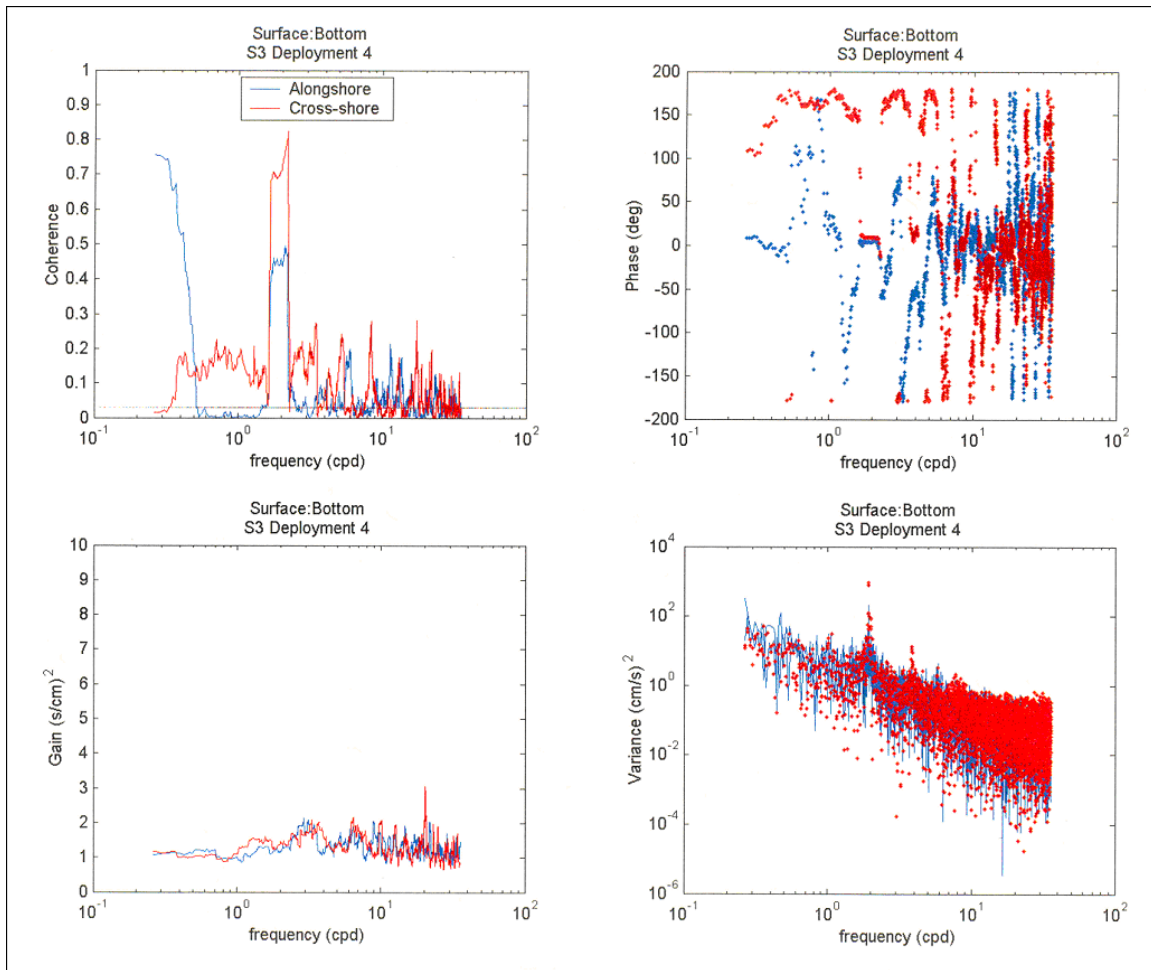
Deployment 3 at sites S2 and S4 gave quite different results for vertical coherence, as represented by site S4 in Fig. 46c. For this deployment, these two sites showed significant coherence between cross-shelf components over essentially all periods greater than about 2 hr. Alongshelf components were coherent for periods greater than about 2 day and were slightly coherent at the diurnal and semidiurnal signals. Phase differences were zero near semidiurnal period, approximately 175° for neighboring periods between 6 hr and 17 d and between -125° and 175° for longer periods. Coherence for cross-shelf currents near semidiurnal period also were significant, but with a phase difference of about -40° . Deployments 1 through 4 at site S5 all gave very similar results and are represented by results for deployment 3 shown in Fig. 46d. The cross-shelf and alongshelf components were coherent over the semidiurnal period for all deployments; cross-shelf currents at surface and bottom were essentially in phase, but again alongshelf components showed a negative phase difference, of about -30° . The cross-shelf components between about 2 hr and the semidiurnal band also appeared coherent, but with widely varying phases. For periods longer than the semidiurnal band, both current components appeared coherent between surface and bottom, much more so in the cross-shelf direction. Deployments 1 and 4 show increasing coherence with increasing period, while deployments 2 and 3 do not. For periods between diurnal and about 2 d the phase difference for cross-shelf currents was between 100° and 175° , generally increasing. For longer periods the phase difference was near -150° to -175° , at periods of 3 to 4 days This would indicate that the bottom current was leading the surface current by about 30 hours.

The phase differences between surface and bottom alongshelf currents at these longer periods were quite unstable.



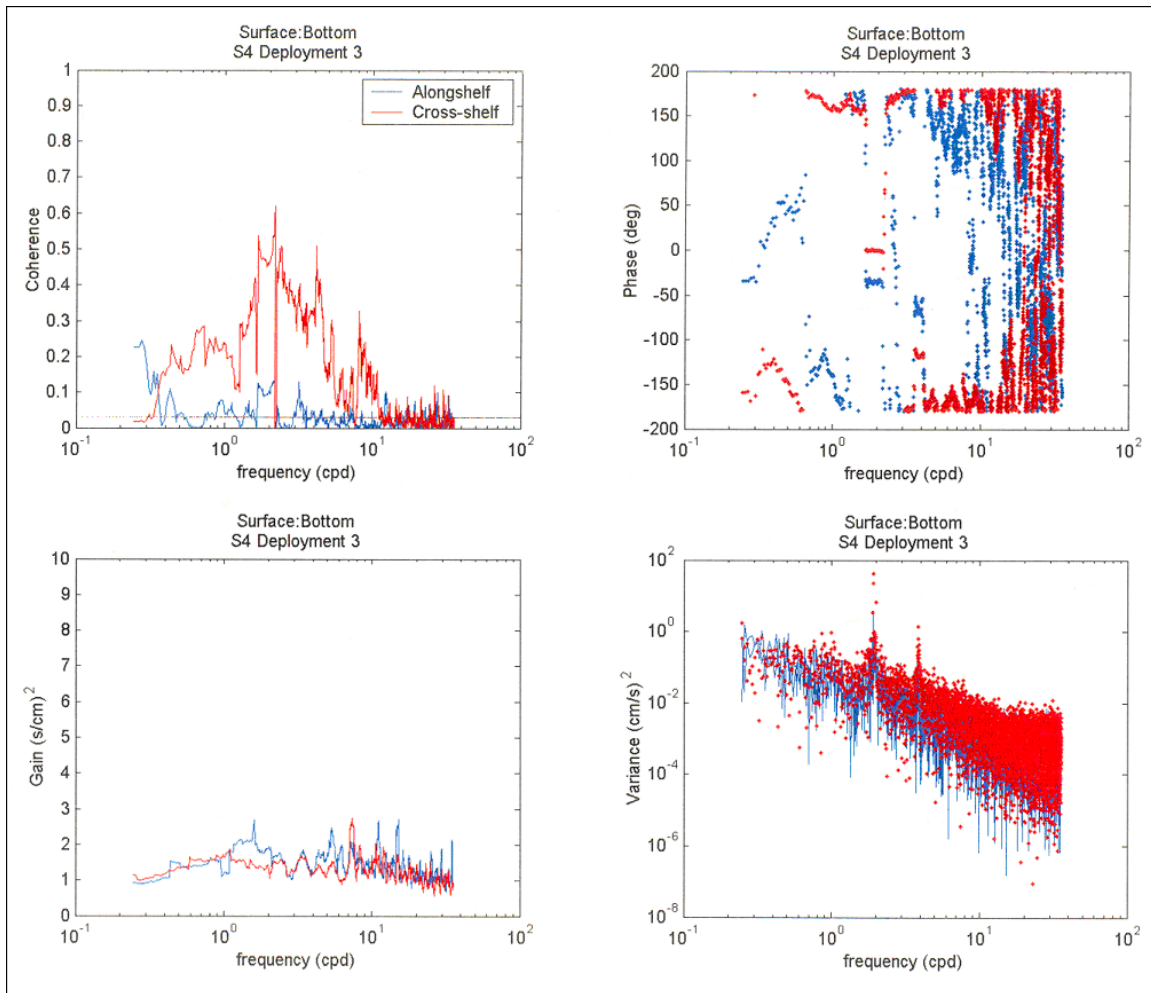
(a)

FIG. 46. (a) – (d). Examples of vertical coherence, phase, gain and variance between the surface and bottom currents at shallow ADCP sites in the study area. The horizontal line on coherence spectrum represents the significance level at the 95% confidence interval. Red represents the cross-shelf current component and blue represents the alongshelf current component.



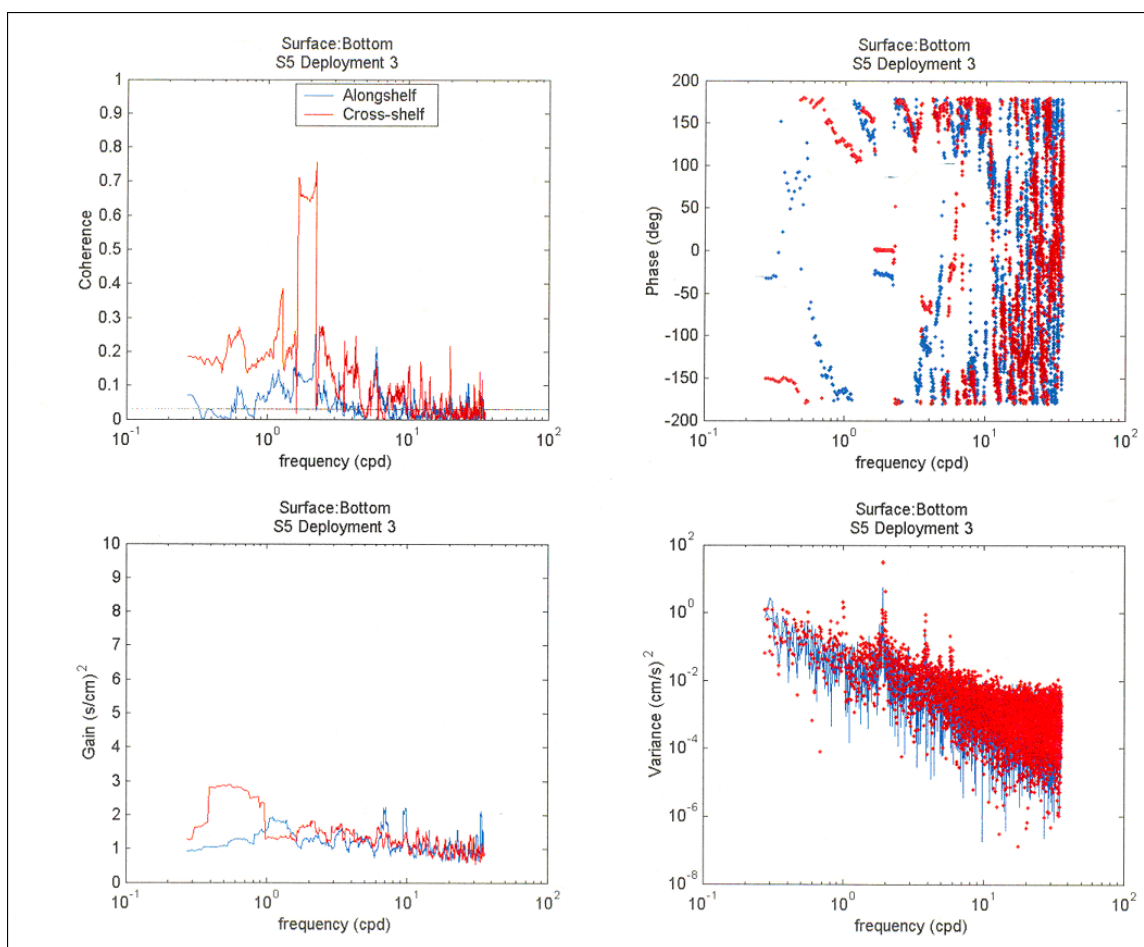
(b)

FIG. 46. Continued.



(c)

FIG. 46. Continued.



(d)

FIG. 46. Continued.

b) Site D3

At site D3, coherence was calculated between surface and mid-depth currents, mid-depth and bottom currents and surface and bottom currents. Each depth comparison yielded a distinct coherence spectra which was comparable between deployments. The following paragraphs describe each of the three unique coherence spectra. Fig. 47 provides an example during one deployment period.

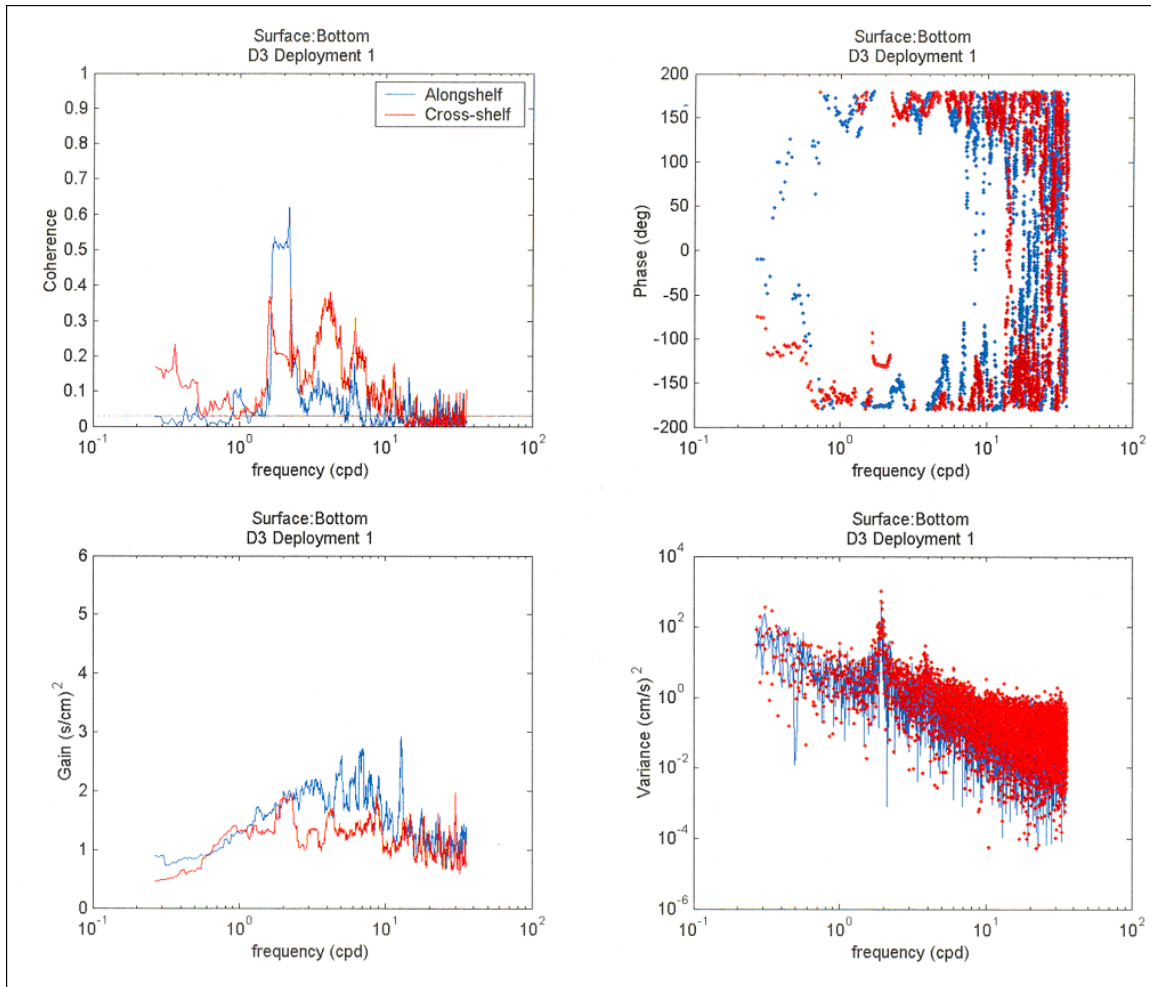
The surface to mid-depth coherence spectrum (Fig. 47c) showed highly significant semi-diurnal coherence in the cross-shelf direction. The coherence for cross-shelf

currents also was significant overmuch of the higher frequency range (greater than 4 cpd). Coherence was also significant at periods longer than about 2 days, where coherence in the alongshelf direction increased with increasing period during deployments 1, 2 and 4 with phases of -5° , $+10^\circ$ and 0° at the 3-4 day period, respectively. During deployment 3, the cross-shelf component is more significant than the alongshelf component at the diurnal frequency and at the 2-3 day period with no consistent phase. The alongshelf component is significant only at the 2-day period with a phase of approximately -40° .

The coherence between mid-depth and bottom cross-shelf currents (Fig. 47b shows an example) was significantly coherent over much of the spectrum of frequencies. The coherence near the semidiurnal period had phases of 0° during deployments 2 and 3 and -75° during deployments 1 and 4. At periods greater than 2 days the coherence for both components slowly increased with increasing period. The coherence between the surface and bottom currents differed from the two coherence spectra described above. Fig. 46a shows an example for deployment 1 from site D3. There was higher coherence between alongshelf components at the semidiurnal period, as compared to the cross-shelf components, with steady phases of about $+140^\circ$ during deployments 2, 3 and 4. Again there was significant coherence at high frequencies, mostly in the cross-shelf direction. At periods greater than 2-day, the coherence increases between: cross-shelf components during deployment 1, alongshelf components during deployment 2, both components during deployment 3 and not at all during deployment 4.

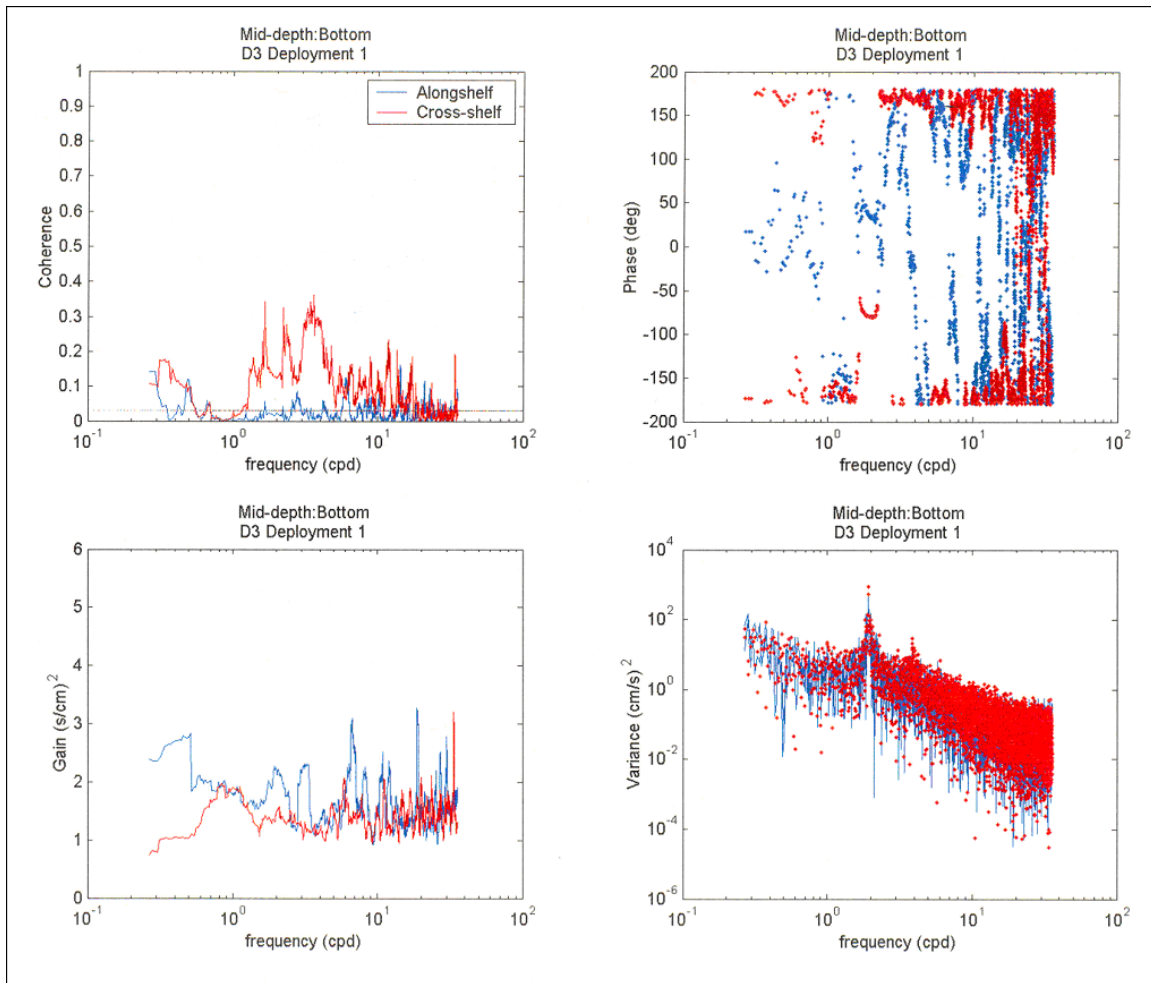
c) Site D5

At site D5, coherence was calculated between surface and mid-depth currents, mid-depth and bottom currents and surface and bottom currents. Results were all similar. Fig. 48 shows examples. In both deployments (3 and 4) there was high coherence (relative to the 95% significance level) between the cross-shelf semidiurnal currents, and lower, though still significant, coherence between the alongshelf components (See Fig 48a for example). The cross-shelf semidiurnal current had zero phase lag during deployment 3 and zero phase lag between the surface and mid-depth currents during deployment 4. There was a phase of $+50^\circ$ between the middle and bottom current and



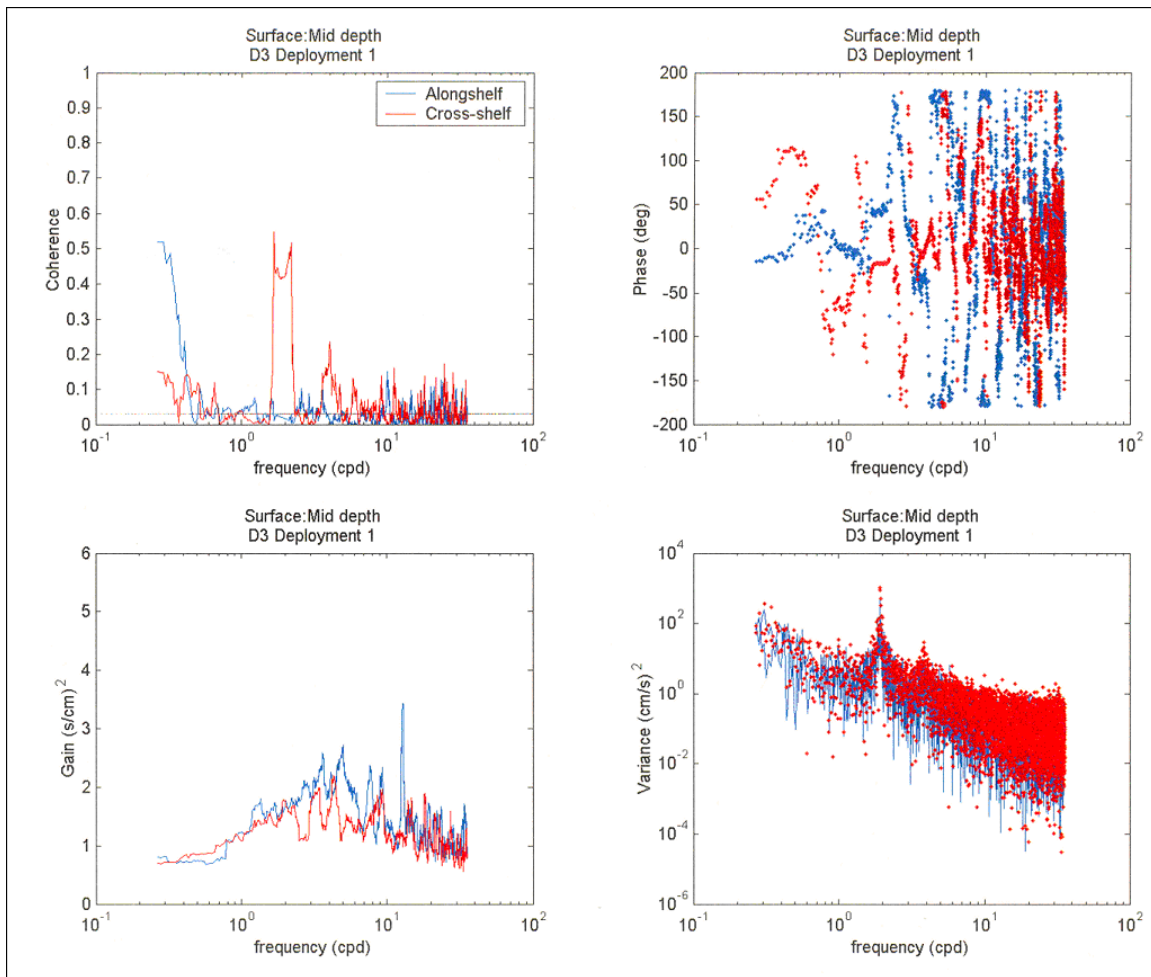
(a)

FIG. 47. (a) – (c). Examples of vertical coherence, phase, gain and variance from deployment 1 at site D3. (a) through (c) show the coherence between the surface and mid-depth currents, the mid-depth and bottom current and the surface and bottom currents, respectively. The horizontal line on the coherence plot represents the significance level of the 95% confidence interval. Red represents the cross-shelf current component and blue represents the alongshelf current component.



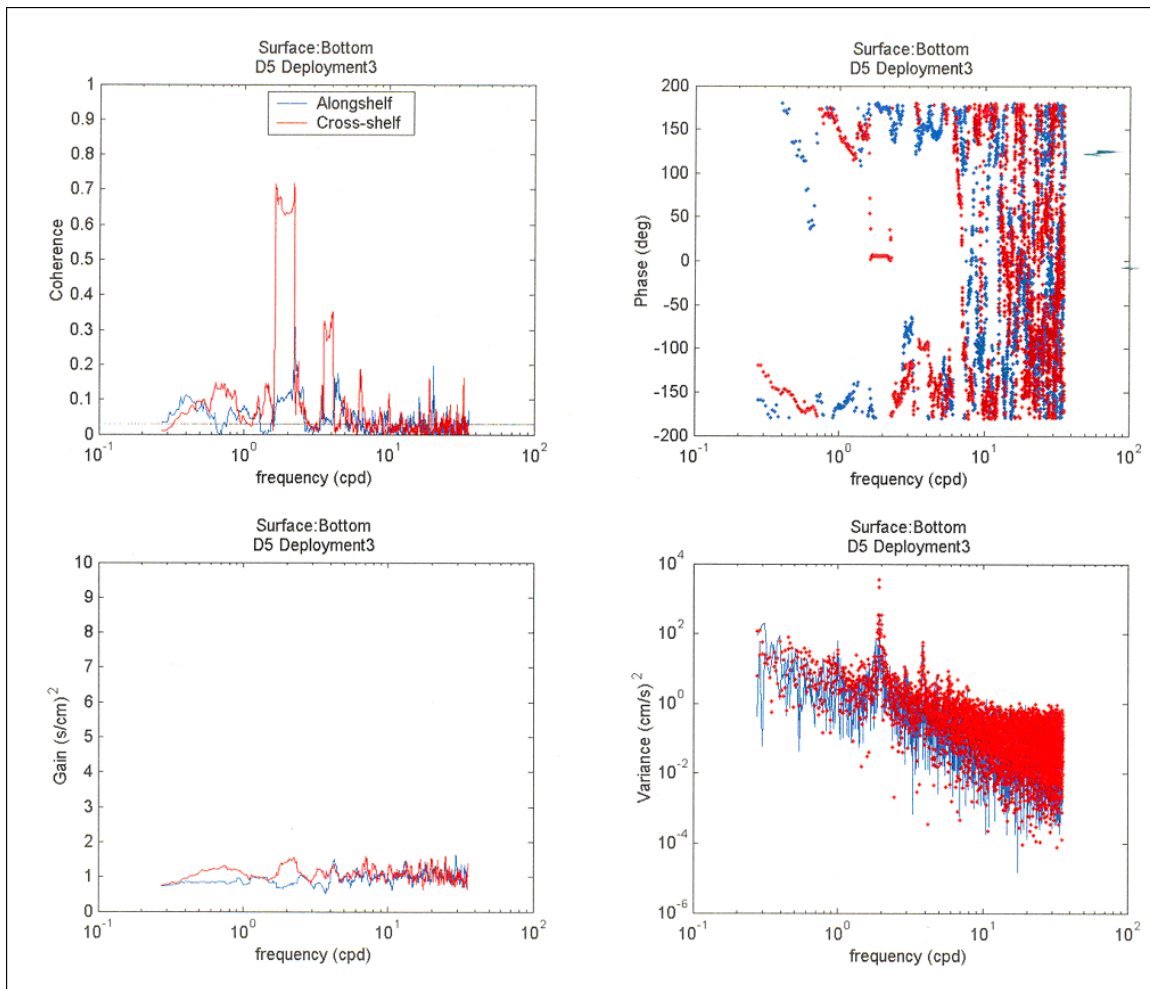
(b)

FIG. 47. Continued.



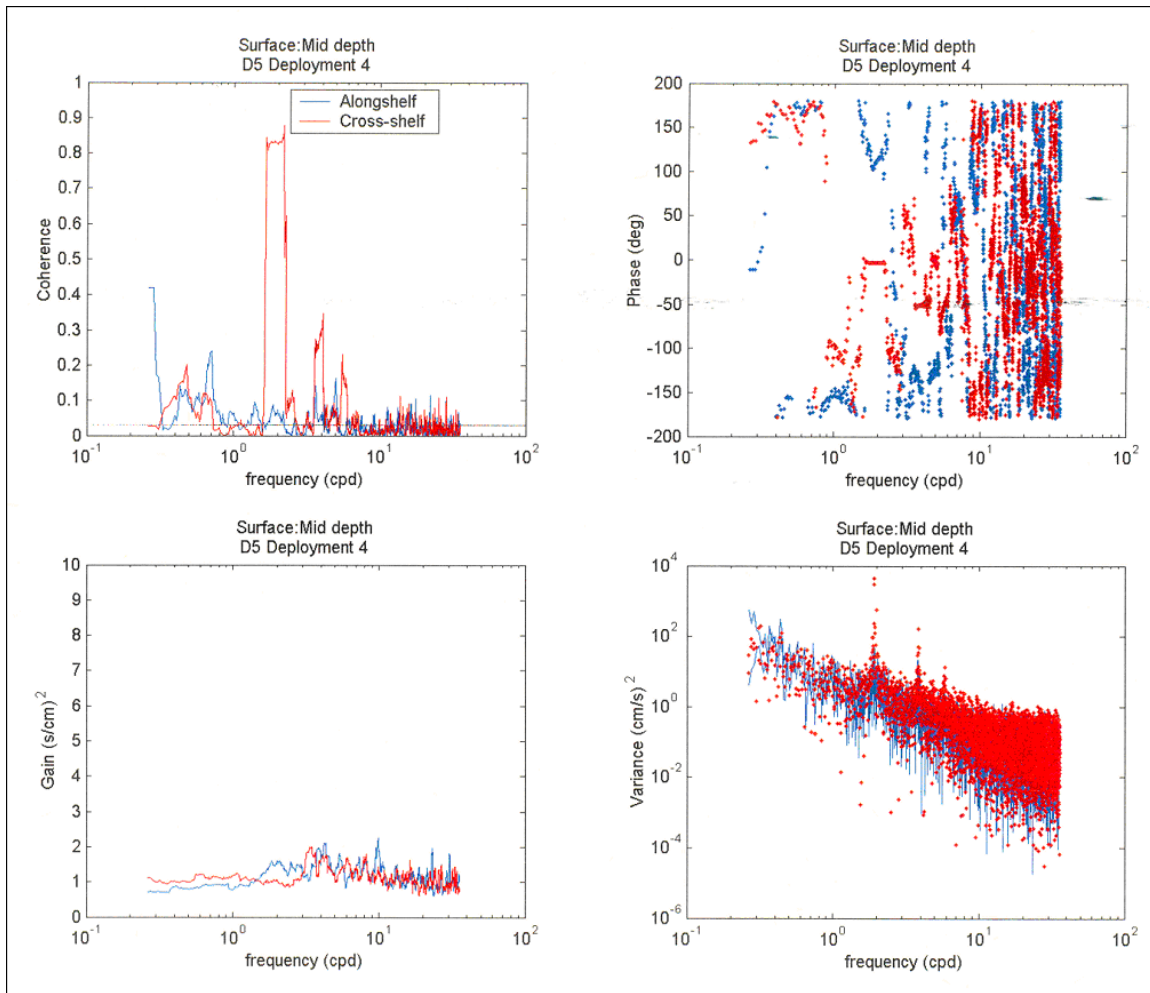
(c)

FIG. 47. Continued.



(a)

FIG. 48. (a) – (b). Examples of vertical coherence, phase, gain and variance at site D5. (a) and (b) show the coherence between the surface and bottom currents during deployment 3 and between the surface and mid-depth currents during deployment 4. The horizontal line on the coherence plot represents the significance level of the 95% confidence interval. Red represents the cross-shelf current component and blue represents the alongshelf current component.



(b)

FIG. 48. Continued.

between the surface and bottom current of deployment 4, with the surface and middle currents leading the bottom current by about 1 ½ hours. Coherence remained significant in the high frequency range as well as in periods greater than 1 day. A spike occurred in coherence at the 3-4 day period during deployment 4, seen in Fig. 48b, which existed between the surface and mid-depth currents and between the mid-depth and bottom currents, with phases of -5° and 0° , respectively.

d) Summary of Vertical Coherence

Vertical coherence is found between currents at both shallow and deep ADCP locations. Relative to the 95% confidence limit, coherence is generally higher in the cross-shelf direction as compared to the alongshelf direction. Coherence is strongest at the semi-diurnal tidal frequency signifying the strong influence of the cross-shelf semi-diurnal tide to the currents in this region, as shown in Section 4. In many cases, coherence between the alongshelf surface and bottom depths at shallow ADCP locations and between alongshelf surface and mid-depths at deep ADCP locations increased with increasing period at periods larger than 2 days. This provides an indication that there should be large vertical coherence (at periods larger than 2 days) in the surface waters of this region.

7. EVIDENCE OF UPWELLING AND PRESENCE OF FORTNIGHTLY WAVE

a. Upwelling

1) Evidence from Vertical Hydrographic Sections

Based on literature, the upwelling season for the northern Gulf of Guinea shelf begins in late June and persists through September (Picaut and Verstraete, 1979; Houghton, 1976).

On examination of the vertical profiles of temperature and salinity, presented in Sections 5a-1 to 5a-5, an upwelling event can be distinguished during the expected upwelling season, throughout the study area. At all lines, the water cools significantly from April to July: about 4°C within the top 30 m and of order 2°C for deeper shelf waters. The 17° isotherm, which is not present in April, is seen in the deeper part of all sections by July. The waters then warm up slightly by October and continue to warm throughout the year. It should be noted that the isotherms rise in the water column remaining almost horizontal along the vertical sections. This is unusual because during an upwelling event isotherms typically rise more toward shore as deeper water is moved shoreward. This peculiarity is a defining characteristic of the atypical upwelling seen elsewhere along the northern coast of the Gulf of Guinea.

The vertical sections of salinity are not clearly indicative of upwelling throughout the study area. At line 1, the water becomes very saline and homogenous between April and July, consistent with upwelling. However, this high salinity signal weakens eastwards. At lines 2 and 3, the water mass becomes only slightly more saline in July. Along line 5, the water is actually fresher in July than it was in April. The salinity profiles seem to mask the upwelling event, as was also seen by Houghton's (1976) circulation study off Ghana. It should be noted that the forcing for upwelling differs from causal mechanisms for low salinity surface waters in this region, so that salinity may not be expected to be a good indicator of upwelling in these shallow waters.

On all lines (but on line 1 to a lesser extent) the thermocline intensifies from April to July at depths of 20-30 m. In addition the surface waters are very fresh with salinities

generally decreasing shoreward, indicating high rainfall and river discharge. It has already been shown in Sections 4c and 5a that the eastern edge of the study area receives the highest volume of fresh water during the study period, first impacting line 5 and then spreading westward. As discussed above, the surface waters cooled 2° more than the deeper waters. Considering the high rainfall and river discharge beginning in June and July and the intensified thermocline at the base of the fresher surface layer, it seems possible that the enhanced cooling of the surface water could have been due to fresh water inflow, occurring concurrently with the upwelling season. This also might explain why the upwelling was less obvious in the salinity profiles, as mentioned above.

2) Evidence from Temperature Time Series

Temperature time series (Fig. 49) from the bottom-mounted ADCPs were plotted in an attempt to confirm the upwelling event identified in the hydrographic data. Mooring sites S2, S5 and D3 successfully recorded data during the season of upwelling, June to early October. At moorings S2 and S5 (at depths of 15 to 20 m), there was a temperature drop of approximately 3°C from June to October; the temperature then gradually warmed for the remainder of record shown. Mooring D3 also shows an upwelling event. The temperature drops about 3°C from June to mid-August. At that time a warming trend began which lasted until November. This warming trend was coincident with strengthened shorter period temperature oscillations of approximate fortnightly period. The fortnightly wave described by Picaut and Verstraete (1979) is capable of producing large (amplitude up to 2.5°C) vertical oscillations in the thermal structure. Although always existent, this wave is more noticeable (in the hydrography) during periods of upwelling when the thermocline surfaces. This feature is seen in Fig. 48a where the effect of the possible wave is quite pronounced. That the depth of the temperature measurement was within the thermocline probably explains why such large oscillations were recorded (refer to Fig. 19c). Small vertical movements at this depth can produce the large changes in temperature seen in Fig. 49a. If the ADCP had not been located directly in the thermocline, the pattern of bottom temperature at site D3 might look similar to those at S5 and S2.

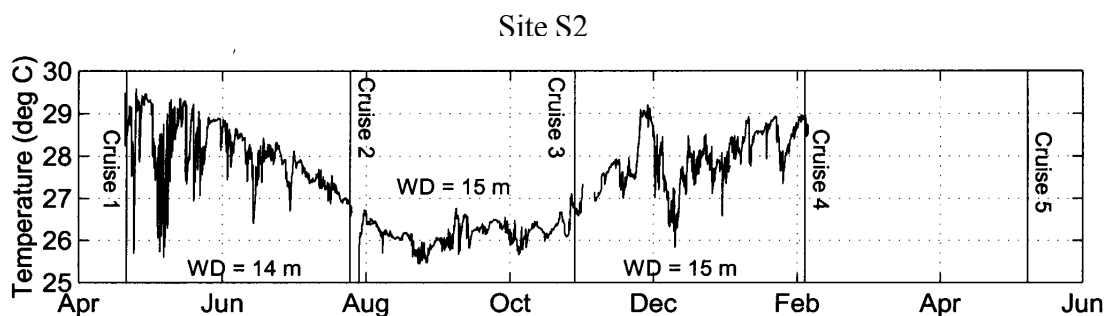
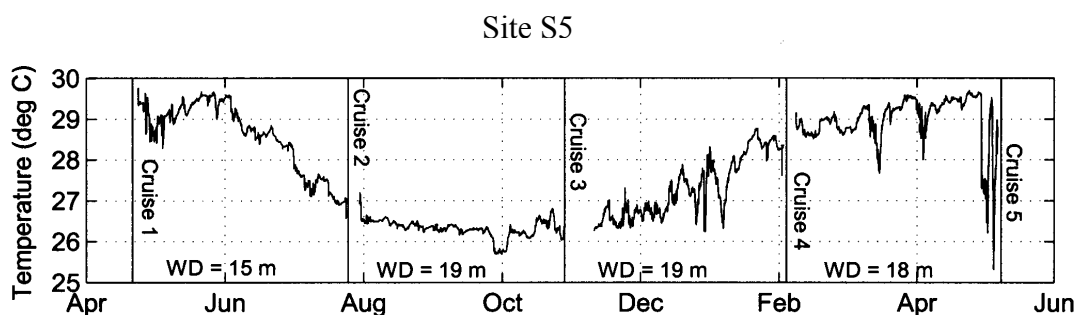
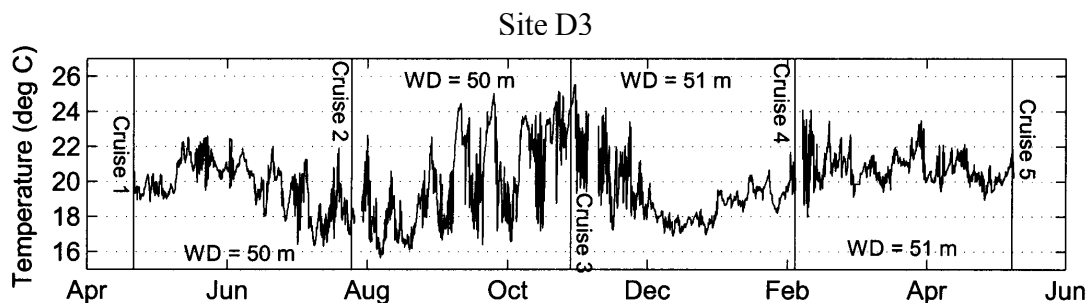


FIG. 49. Temperature records from bottom-mounted ADCPs (approximately 1.3 m above the sea floor at (a) deep-water mooring site D3, (b) shallow-water mooring site S5 and (c) shallow-water mooring site S2). The times of the five cruises when CTD measurements were made are indicated by vertical lines. WD = Total water depth. No data are available for the fourth deployment at site S2.

3) Coherence between Alongshelf Winds and Surface Currents

As shown in Section 4b, winds over the study region are consistently from the southwest with mean speeds of about 6 m/s. There was no sudden intensification or change in direction during the early summer that would force an upwelling event. Additionally, there is no apparent correlation between the winds and the currents and therefore no indication that the winds could be forcing the upwelling event. Fig. 50 presents a typical example of the independence between the currents and the local wind fields.

Coherence, phase, gain and variance between wind and surface current components were calculated for sites S2 and D3 (Fig. 51). The eastern end of the study area had too many gaps in wind data for such an analysis. All deployments at sites S2 and D3 generally produced results of low coherence below the 95% confidence level, indicating that the observed upwelling is most likely not wind-induced. This is in agreement with previous studies of upwelling along West Africa's northern coastline.

There were a few exceptions where coherence was significant between alongshelf winds and surface currents. There were several peaks in coherence within the weather band at both sites, but no steady phase. There was also a peak at about the 40-day period at site S2 with phase lag of 2.2 days and coherence at periods greater than 40-days at site D3 with phase lag from 30-50° between the alongshelf wind and surface current. Wind data were only available on a daily basis, so comparisons for higher frequencies are not possible.

The phase lag of alongshelf current to alongshelf wind may be inversely proportional to the Coriolis parameter (f). Knowing that the response time of coastal currents to the wind over the Louisiana-Texas (LATEX) shelf is 12 hours at latitude 29°N, the response time off Nigeria can therefore be estimated by multiplying the 12-hour response time by the ratio of f_{29° to f_5° . Using this information, the response time of the coastal current to the winds off Nigeria should be about 2.7 days. This corresponds to the 40-day period phase lag seen at site S2.

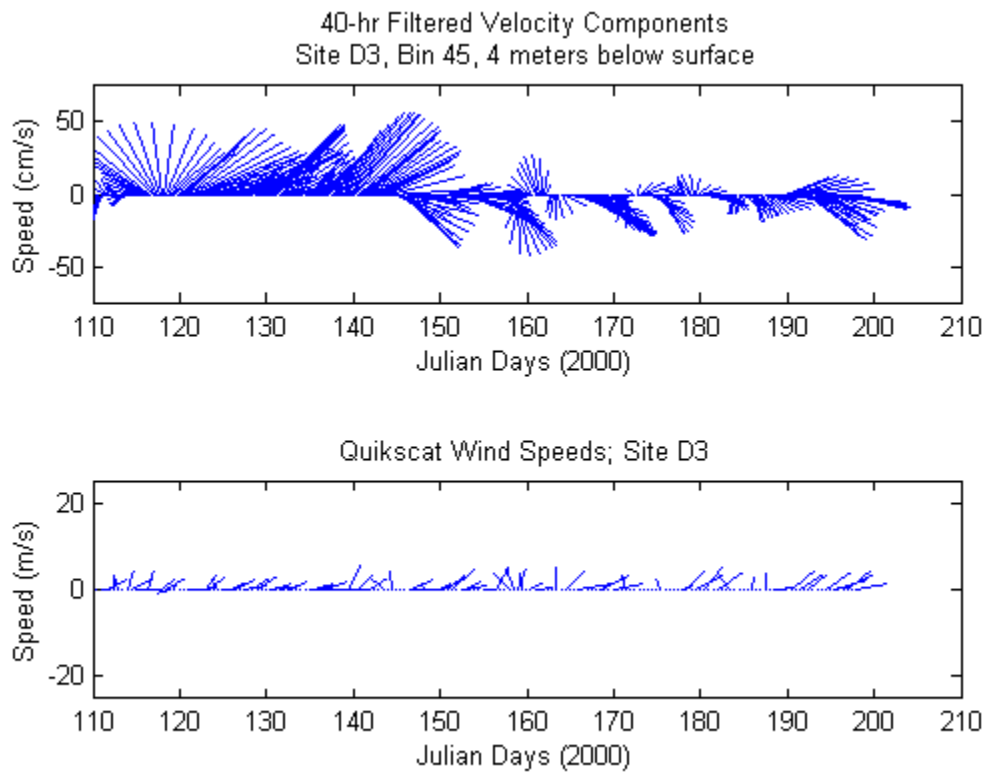


FIG. 50. Comparison of current magnitude and direction to QuikSCAT winds (for a single deployment at site D3).

Site S2 Filtered Surface Current : Winds

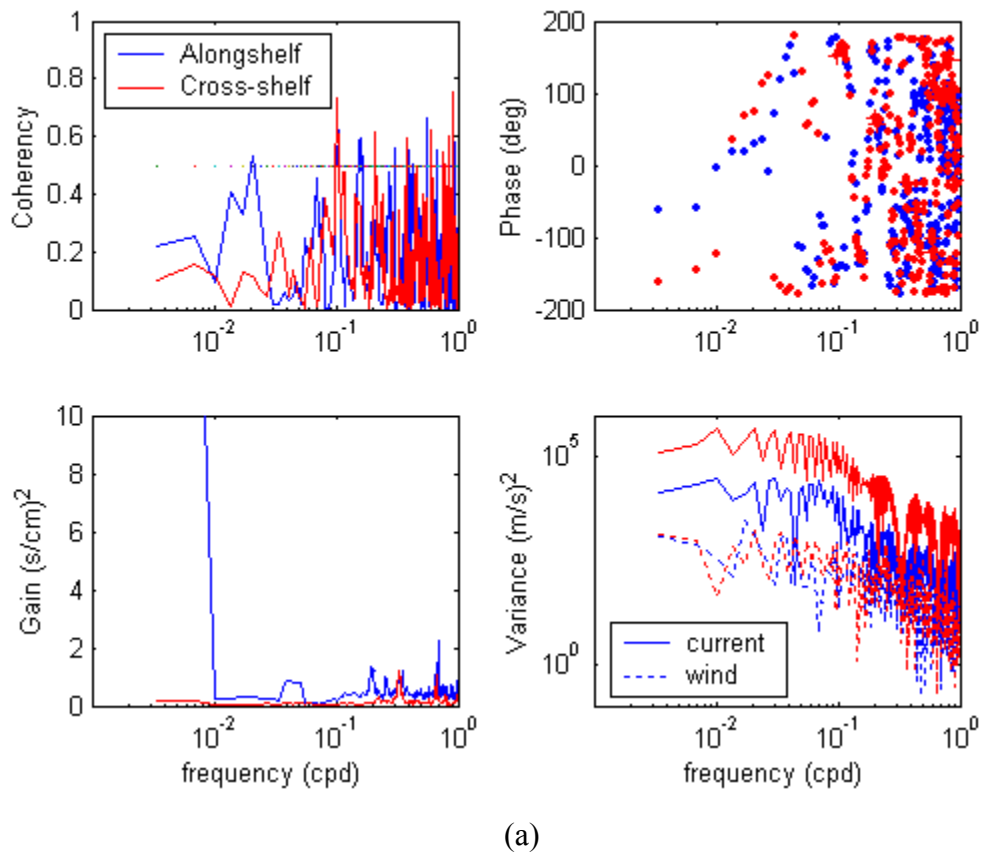


FIG. 51. (a) and (b). Coherence, phase, gain and variance between the ADCP surface current and the QuikSCAT wind data at sites S2 (a) and D3 (b). The horizontal line on the coherence plot represents the significance level. Red represents the cross-shelf current component and blue represents the alongshelf current component in each of the four plots. Here negative phase means the winds are leading the currents.

Site D3 Filtered Surface Current : Winds

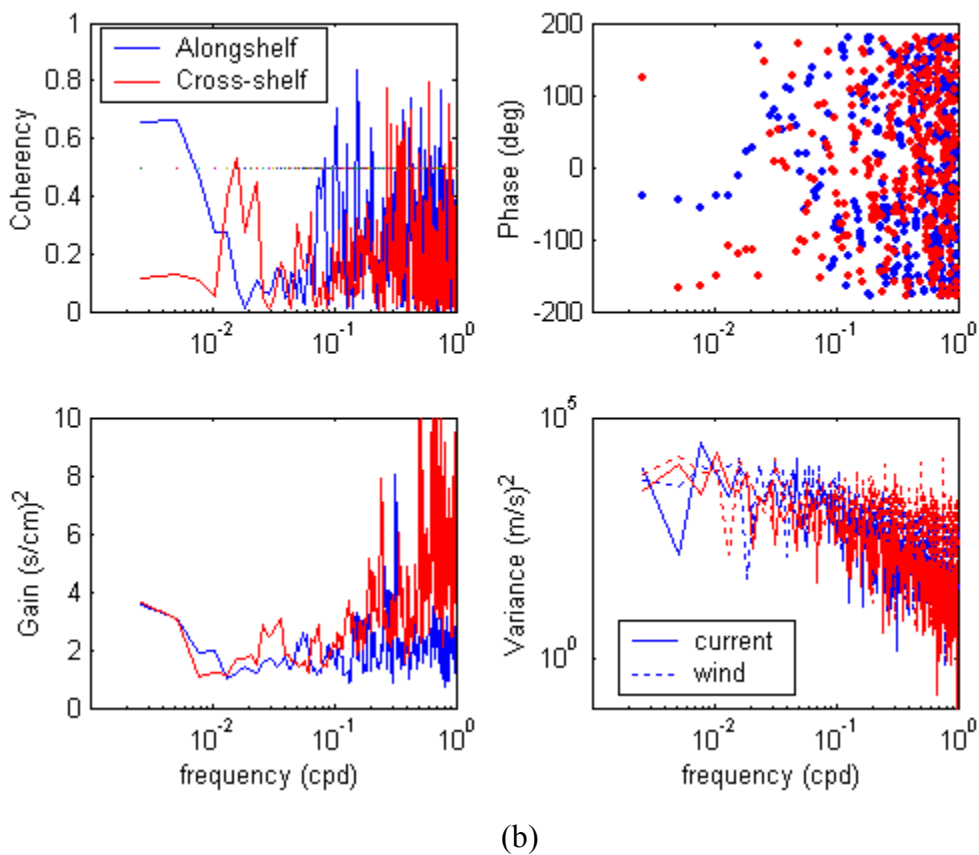


FIG. 51. Continued.

b. Fortnightly Wave Propagation

1) Current Spectra

Unfortunately the current spectra provide little information on the 14.7-day wave seen west of the Nigerian coastline. The power spectrum for each site shows a peak at approximately 14 days (See Fig. 39 for example) but no confidence can be placed on the peak due to the short length of the current records.

2) Temperature Time Series

The temperature time series, presented above in Section 7a-1 is the most obvious clue that a fortnightly wave could be present along Nigeria's coast. An oscillation (with an approximate fortnightly frequency) in temperature can be seen strongly in D3, during deployments 1 and 2 (refer to Fig. 49 for D3 and S2 records) and also seen during deployment 1 at sites S2 and S3. This temperature oscillation is not seen in the bottom temperature records at sites S4, S5 or D5. This does not seem to reflect the strength of the upwelling as upwelling was seen just as strongly in site S5 as it was in site S2. That the temperature oscillation was only seen off the Niger Delta and to the west of the delta, provides an indication that the fortnightly wave could be originating in the waters off the eastern Nigerian coast as suggested by Clarke and Battisti (1983).

The spectra of the temperature time series were also examined. Although peaks were evident at approximately the fortnightly frequency, they are not significant due to the short length of the record. Spectra of the temperature time series did however indicate a semi-diurnal heating cycle, illustrating just how influential the tides are in the dynamics of near-shore Nigerian circulation (See Fig. 52 for example).

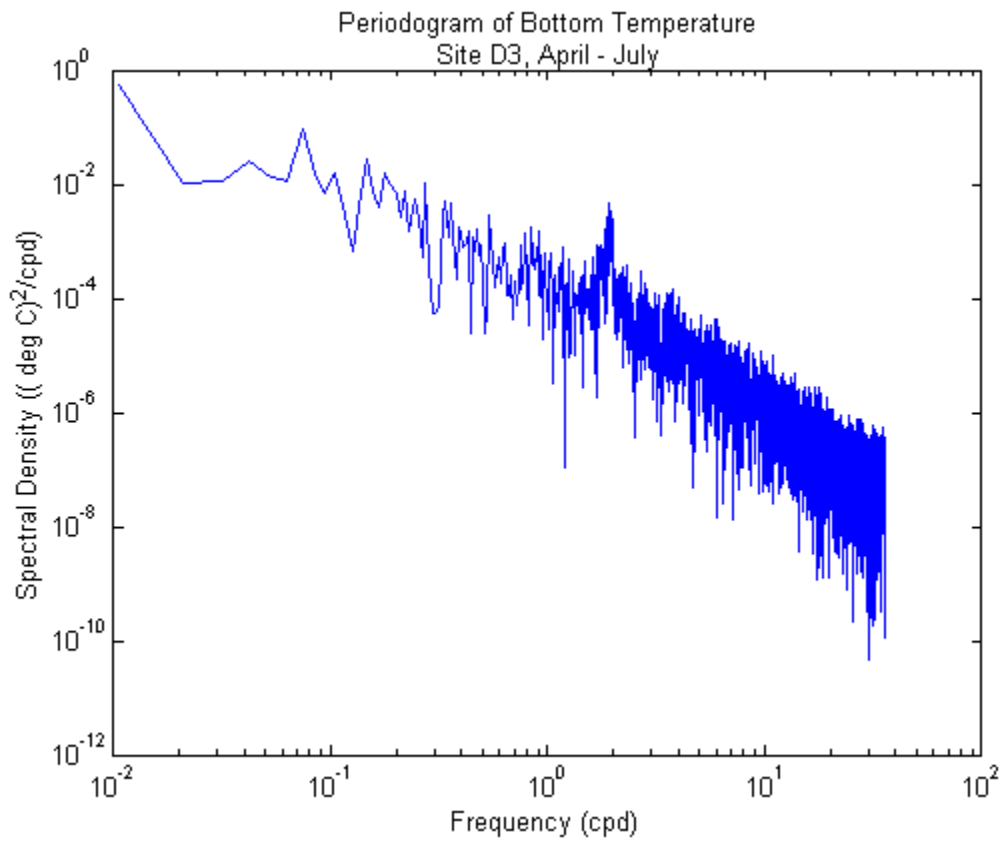


FIG. 52. Periodogram of bottom temperature time series. Time series recorded by ADCP during deployment 1 at site D3 showing the regional semi-diurnal heating cycle.

8. CONCLUSIONS AND RECOMMENDATIONS

a. Major Findings

1) Tides

The most energetic currents over this shelf are semi-diurnal tides. The semi-diurnal signals account for 90% of the total tidal variance averaged over both shallow and deep sites; shallow sites contain slightly more diurnal energy than the deeper sites. The tidal ellipses are narrow and oriented strongly across the shelf. The tides are essentially barotropic in the eastern study area. Tidal energy accounts for 25-50% of the energy of surface currents and 30-80% of that of the bottom currents. The percentage increased eastward across the study area, as the shelf widens and tides are amplified. There the tides are also more bottom intensified.

2) Weather Band Versus Mesoscale Band Energy

Events occurring within the weather band (2- to 10-day periods) and mesoscale band (10- to 100-day periods) account for 50-75% of energy in the surface currents and 20-50% of the energy in the bottom currents. On the average there is nearly about twice as much energy in the mesoscale band as in the weather band. The ratio of weather band to mesoscale energy increases toward the eastern end of the study area. The implication is that, although events within both frequency bands influence the current regime, larger scale events such as seasonal weather changes, river discharge and eddies have more influence on the current regime than shorter scale weather events.

3) Low-passed Alongshelf Currents

The 40-hr low-passed currents showed bi-directional along-isobath flow. Reversals occurred on timescales from 1 to 40 days; no preference is seen for upcoast or downcoast flow. The duration of flow in one direction was generally from 1 to 10 days (most less

than 5 days), with only 9% of alongshelf flows remaining directionally constant for 10 to 40 days. Associated mean current speeds ranged from 1 to 40 cm/s.

4) Vertical Current Structure

The vertical structure of 40-hr low pass filtered currents, as indicated by EOF analysis, shows a remarkably uniform structure for different locations and deployment periods. The vertical structure is strongly dominated by a surface intensified mode 1, carrying 60-90% of the total variance; higher percentages are found at the shallow locations. This is because mode 1 is surface intensified and decreases in amplitude with depth to about zero near the seafloor at the deep ADCP locations. At the shallow locations, mode 1 has only begun to decay near the bottom and therefore the currents at shallow water locations are dominated by first EOF mode, which is essentially barotropic indicating the currents should be vertically coherent. Because the dominant mode is surface intensified and decays with depth, the bottom currents at the deeper ADCP locations are dominated by the structure of mode 2 (carrying from 10-25 % total variance) with both surface and bottom intensification. This implies that there would be little vertical coherence between the surface and bottom currents at the deep ADCP locations as the surface currents are strongly forced by mode 1 and the bottom currents are strongly forced by mode 2.

5) Horizontal Coherence of Low-Passed Currents

Significant coherence at selected frequencies exists between low-passed currents for separations both along and across the shelf. Coherence between low-passed currents in the alongshelf direction is much higher between sites located across the shelf with the shallow sites leading the deeper site by a few hours. Coherence among the low-passed alongshelf currents between neighboring alongshelf sites is still significant but the values are low. The associated phase between sites separated both along and across the shelf provide no useful indication of a propagation direction.

6) Winds

The winds over this region are generally southwesterly with speeds of 4-7 m/s and mean directions toward 40° to 60°. They are strongest from July to September, due to movement of the intertropical convergence zone, which causes a gradual increase in southwest winds during the northern summer months and frequent rainfall. From September through December, winds decrease in magnitude and rotate 20-30° clockwise due to the influence of the Harmattan Wind blowing off the desert and opposing the consistent southwesterly winds. The Harmattan Winds are known to cause reversals in the wind direction during December. However, the southwesterlies were particularly strong during the study period (compared with published values of mean wind speeds); therefore, only slight rotation in wind direction was seen.

7) Supply of Fresh Water and Vertical Stratification

The vertical stratification is strongly affected by the discharge of fresh waters directly onto this shelf and likely by the northwestward movement into the area of discharge from the Congo River. More frequent rain contributes to the generally lower surface salinities found in the eastern end of the study region. Although there are no available records of river discharge onto the study region, a proxy time series measured on the Benue River, rather far from the coast, shows very low flow during the period January through May. There is a tenfold increase in flow rates between June and September, when the maximum occurs. Significant flow continues through November. This is consistent with rainfall rates at coastal cities in the region, which show that the rainfall normally is largest in the summer season, beginning in June and decreasing after September. This is also consistent with the hydrographic data, which show an increase of low-salinity water within the study region in July followed by a drastic increase of low-salinity water present across the study area by October.

8) Upwelling and Fortnightly Wave

The bottom temperature recorded on ADCP units as well as the CTD sections show indications of upwelling in this region corresponding to the times at which upwelling has been observed in other west African coastal regions. Coherence is not significant between alongshelf winds and alongshelf currents, so upwelling does not appear driven by the local alongshelf winds. This is consistent with findings for coastal regions west of the study area. There is some evidence at one ADCP location that the upwelling event might be accompanied by a fortnightly wave as observed along the shelves west of the study area; however, this data set cannot quantitatively support this observation.

b. Recommendations for Future Work

Several recommendations resulted from this work and from general considerations of oil spill cleanup and need for timely operational data.

1) Obtain Wind and Current Data from Local Platforms

It would be beneficial to obtain long-term current and wind data from additional platforms within the study area. This would aid in establishing quantitative information on interannual variability in current and wind strength and other climatological information.

2) Study of River Outflow off Niger Delta

Accurate river outflow data from the Niger River's major constituents would allow quantitative estimates of the effects of local river discharge on the near-shore circulation.

3) Study of Congo River and West Africa

It was shown throughout this report that the eastern end of the study area receives a much higher volume of river discharge than the western end. This does not seem to be related to an eastward transport of river discharge and indicates that water from the Congo River could be entering the study area. A study of the Congo River and its drift via the Benguela and Angola currents would aid in determining the precise source of the freshwater and therefore increase the confidence in the inferences made from the coastal hydrography towards future predictions. Once the destination of the Congo River's discharge is established it would then be useful to obtain flow rate data if the Congo does in fact enter the eastern end of the study area.

4) Continuous Measurements in Areas of Operation

It is highly recommended to obtain a continuous record of currents, water level and wind speed at all active platform locations. This would enable reasonably accurate prediction of an oil spill drift should it occur again. This also could result in estimation of interannual variability. This new information would be useful to both the oil industry and the scientific community.

5) Extended CTD Lines

Although the CTD lines provided useful information about the very nearshore hydrography, they would have been more useful had they been continued further off the shelf so that the extent of the river discharge could be seen. In the vertical sections of salinity, sharp vertical salinity gradients are seen from the shore to the seaward ends of the lines. To obtain a clear picture of the river effects on the study area, to determine possible causes of upwelling and to obtain meaningful estimates of alongshelf geostrophic currents, the CTD lines would have to extend past the front likely to exist at the seaward edge of the low-salinity regime.

REFERENCES

- Adegbei, S., E.A. Ajao, A. Ajavon, A. Armah et al., 1996: Report on the International Workshop on Continental Shelf Fluxes of Carbon, Nitrogen and Phosphorous, Section 3.4: Gulf of Guinea. JGOFS-LOICZ Workshop 96.15, www.ncor.ntu.edu.tw/cmtt/Reports/lagos-rep.PDF.
- Ajao, E.A. and R.W. Houghton, 1998: Coastal Ocean of Equatorial West Africa from 10°N to 10°S, Coastal Segment (17,E). *The Sea*, Vol 2, A. R. Robinson and K. H. Brink, Eds, John Wiley and Sons, Inc., 605-631.
- Arnault, S., 1987: Tropical Atlantic Geostrophic Currents and Ship Drifts. *J. Geophys. Res.*, **92**, 5076-5088.
- Awosika, L. and A. Ibe, 1994: Geomorphic Features of the Gulf of Guinea Shelf and Littoral Drift Dynamics. Workshop on the Results of the First IOCEA Cruise, www.unesdoc.unesco.org.
- Bloomfield, 1976: *Fourier Analysis of Time Series: An Introduction*. John Wiley & Sons, 22-41.
- ChannelMaster H- ADCP Series, 2003: RD Instruments, San Diego, CA, www.rdinstruments.com.
- Clarke, A.J., 1979: On the Generation of the Seasonal Coastal Upwelling in the Gulf of Guinea. *J. Geophys. Res.*, **84**, 3743-3751.
- , and D.S. Battisti, 1983: Identification of the Fortnightly Wave Observed along the Northern Coast of the Gulf of Guinea. *J. Phys. Oceanogr.*, **13**, 2192-2200.
- CSIRO Seawater Toolkit, 1998, <http://sea-mat.whoi.edu> (accessed September, 2001).
- The Dictionary of Earth Sciences*. 1st ed., 1999, Oxford: Oxford University Press. Harmattan Wind; www.xrefer.com.
- DiMarco, S.F., 1997: Stickplt.m (MATLAB code), Associate Research Scientist, Texas A&M University.
- Dublin-Green, C.O., L.F. Awosika, and R. Folorunsho, 1999: Climate Variability Research Activities in Nigeria. National Statements: Nigeria, Nigerian Institute for Oceanography and Marine Research, Lagos, Nigeria.

- Emery, W.J. and R.E. Thompson, 2001: *Data Analysis Methods in Physical Oceanography*. Elsevier, 536-543.
- Grodsky, S.A., and J.A. Carton, 2002: Effect of the Intraseasonal Wind Fluctuations in the West African Monsoon on Air-Sea Fluxes. University of Maryland, College Park, MD.
- Houghton, R.W., 1976: Circulation and Hydrographic Structure over the Ghana Continental Shelf during the 1974 Upwelling. *J. Phys. Oceanogr.*, **6**, 909-924.
- Ingham, M.C., 1970: Coastal Upwelling in the Northwestern Gulf of Guinea. *Bull. Mar. Sci.*, **20**, No. 1, 1-34.
- Janicot, S., and B. Sultan, 2001: Intra-seasonal Modulation of Convection in the West African Monsoon. *Geophys. Res. Lett.*, **28**, 523-526.
- Mittelstaedt, E., 1983: The Upwelling Area Off Northwest Africa – A Description of Phenomena Related to Coastal Upwelling. *Prog. Oceanogr.*, **12**, 307-331.
- Seawinds on QuickSCAT, 2001, NASA, <http://podaac.jpl.nasa.gov> (accessed August 2002).
- Picaut, J., 1983: Propagation of the Seasonal Upwelling in the Eastern Equatorial Atlantic. *J. Phys. Oceanogr.*, **13**, 18-37.
- , and J.M. Verstraete, 1979: Propagation of a 14.7-day Wave along the Northern Coast of Guinea Gulf. *J. Phys. Oceanogr.*, **9**, 136-169.
- River Systems of the World, Rev.net, 2002. Technologies, Inc., Roanoke, VA, <http://www.rev.net/~aloe/river/.Rev.Net>.
- Rudnick, D., 1996: Stickplt.m (MATLAB code). Assistant Professor of Physical Oceanography, Scripps Institution of Oceanography, University of California, San Diego.
- Viltard, A., P. de Felice, and J. Oubuin, 1997: Comparison of the African and 6-9 Day Wave-Like Disturbance Pattern over West-Africa and the Tropical Atlantic during 1985, *Meteorol. Atmos. Phys.*, **62**, 91-99.
- Wang, O., 2002: Diagnostic Calculations of Circulation over the Northeastern Gulf of Mexico, Ph.D. dissertation, Texas A&M University, College Station.

Welch, P.D., 1967: The Use of Fast Fourier Transform for the Estimation of Power Spectra: A Method Based on Time Averaging over Short, Modified Periodograms, *IEEE Trans. Audio Electroacoust.*, **AU-15**, 70-73.

Workhorse ADCP Series. RD Instruments, San Diego, CA, www.rdinstruments.com.

VITA

Kelly Elizabeth Rider

Permanent Address:

4142 Sarong Drive
Houston, TX 77025

Educational Background:

1999 B.S. in Civil Engineering, The University of Texas at Austin
2004 M.S. in Oceanography, Texas A&M University, College Station, TX